SAPIENZA
University of Rome

Faculty of "Medicina e Odontoiatria"
Department of "Medicina interna e Specialità mediche"

Ph. D. Program in

Innovative Biomedical Technologies in Clinical Medicine

XXXII cycle

(a. y. 2018/2019)

Ph. D. Thesis

Targeting Hedgehog pathway in medulloblastoma: identification of SALL4A as a new activator and isoflavone c22 as multitarget inhibitor

Candidate

Ludovica Lospinoso Severini

Tutors:

Prof. Giuseppe **Giannini**

Prof.ssa Lucia **Di Marcotullio**

Coordinator:

Prof. Marcello **Arca**

A mio padre e a mia madre.

A Giulia, a Elisa, a Marianna.

INDEX

PUBLICATIONS

1. **SALL4A is a new positive regulator of Hedgehog signalling involved in medulloblastoma tumorigenesis.**
   Lospinoso Severini L, Loricchio E, Infante P, Bufalieri F, Caimano M, Di Marcotullio L.
   Manuscript in preparation.

2. **The RNA-binding ubiquitin ligase MEX3A affects glioblastoma tumorigenesis by inducing ubiquitylation and degradation of RIG-I.**
   Bufalieri F, Caimano M, **Lospinoso Severini L**, Basili I, Paglia F, Sampirisi L, Loricchio E, Petroni M, Canettieri G, Santoro A, D'Angelo L, Infante P, Di Marcotullio L.
   Cancers (Basel). 2020 Jan 30;12, 321; doi:10.3390/cancers12020321.

3. **A Smo/Gli Multitarget Hedgehog Pathway Inhibitor Impairs Tumor Growth.**
   Lospinoso Severini L, Quaglio D, Basili I, Ghirga F, Bufalieri F, Caimano M, Balducci S, Moretti M, Romeo I, Loricchio E, Maroder M, Botta B, Mori M, Infante P, Di Marcotullio L.
   Cancers (Basel). 2019 Oct 9;11(10). pii: E1518. doi: 10.3390/cancers11101518.

4. **ERAP1 promotes Hedgehog-dependent tumorigenesis by controlling USP47-mediated degradation of βTrCP.**
   Bufalieri F, Infante P, Bernardi F, Caimano M, Romania P, Moretti M, **Lospinoso Severini L**, Talbot J, Melaiu O, Tanori M, Di Magno L, Bellavia D, Capalbo C, Puget S, De Smaele E, Canettieri G, Guardavaccaro D, Busino L, Peschiaroli A, Pazzaglia S, Giannini G, Melino G, Locatelli F, Gulino A, Ayrault O, Fruci D, Di Marcotullio L.
   Nat Commun. 2019 Jul 24;10(1):3304. doi: 10.1038/s41467-019-11093-0.

5. **Targeting Hedgehog Signalling through the Ubiquitylation Process: The Multiple Roles of the HECT-E3-ligase Itch.**
   Infante P*, **Lospinoso Severini L***, Bernardi F, Bufalieri F, Di Marcotullio L.
   Cells. 2019 Jan 29;8(2). pii: E98. doi: 10.3390/cells8020098. *Review*.
   *These authors equally contributed to the work.

6. **Itch/β-arrestin2-dependent non-proteolytic ubiquitylation of SuFu controls Hedgehog signalling and medulloblastoma tumorigenesis.**
   Infante P, Faedda R, Bernardi F, Bufalieri F, **Lospinoso Severini L**, Alfonsi R, Mazzà D, Siler M, Coni S, Po A, Petroni M, Ferretti E, Mori M, De Smaele E,

Canettieri G, Capalbo C, Maroder M, Screpanti I, Kool M, Pfister SM, Guardavaccaro D, Gulino A, Di Marcotullio L.
Nat Commun. 2018 Mar 7;9(1):976. doi: 10.1038/s41467-018-03339-0.

7. **Chemical, computational and functional insights into the chemical stability of the Hedgehog pathway inhibitor GANT61.**
   Calcaterra A, Iovine V, Botta B, Quaglio D, D'Acquarica I, Ciogli A, Iazzetti A, Alfonsi R, **Lospinoso Severini L**, Infante P, Di Marcotullio L, Mori M, Ghirga F.
   J Enzyme Inhib Med Chem. 2018 Dec;33(1):349-358. doi: 10.1080/14756366.2017.1419221.

SUMMARY

The Hedgehog (Hh) pathway is essential during embryonic development and its aberrant activation leads to tumorigenesis. Hh signalling activation is orchestrated by extracellular ligands (Hh ligands) and two transmembrane receptors (Patched, with inhibitory function, and Smoothened, acting as activator). The presence of Hh ligand triggers the intracellular signalling cascade removing the inhibitory effect that Patched (PTCH) exerts on Smoothened (SMO) and culminates with the activation of zinc-finger transcription factors of the GLI family; this event in turn induces the expression of genes involved in the most important biological processes (i.e. proliferation, survival, differentiation, stemness). Because of its crucial role in tumorigenesis, the regulation of the Hh pathway and the identification of new Hh modulators emerged as a field of great interest in tumor biology.

My Ph. D. project was focused on two main goals:

Aim 1 | Identification of new molecular mechanisms involved in Hedgehog signalling pathway regulation and medulloblastoma tumorigenesis. To address this aim, we elucidated the molecular mechanisms that involve key components of Hh signalling and whose deregulations are associated to aberrant pathway activation, leading to tumorigenesis. To this regard we focused on tumor suppressor SuFu, a well known negative regulator of Hh signalling, and we elucidated the role of ubiquitylation processes underlying its regulation. In particular, our studies demonstrated that the Itch-dependent non-proteolytic ubiquitylation of SuFu represents a novel mechanism that inhibits the Hh signalling pathway, and indicated that alterations of this process (caused by SuFu mutations that make it insensitive to Itch-mediated ubiquitylation) contribute to the pathogenesis of medulloblastoma, a childhood brain tumour often related to Hh signalling aberrations (Infante et al., 2018).

A second important focus in the field of Hh pathway regulation is the identification of new molecular players; interestingly, we found a new role for the aminopeptidase ERAP1 and for the transcription factor SALL4A in Hh context.

The endoplasmic reticulum aminopeptidase 1 (ERAP1) is a key regulator of innate and adaptive antitumor immune responses. Our findings unveiled the oncogenic role of ERAP1 that, binding the deubiquitylase enzyme USP47, displaces the USP47-associated βTrCP (the substrate-receptor subunit of the $SCF^{\beta TrCP}$ ubiquitin ligase complex) and promotes βTrCP degradation. This event results in GLI factors modulation and in the enhancement of Hh activity. Remarkably, genetic or pharmacological inhibition of ERAP1 suppresses Hh-dependent tumor growth *in vitro* and *in vivo*. Our study shows an unexpected role for ERAP1 in cancer biology and indicates ERAP1 as promising therapeutic target for Hh-driven tumors (Bufalieri et al., 2019).

For the realization of these projects, I was directly involved in the generation of SuFu mutants, biochemical *in vitro* assays, animal experiments, IHC and data analysis.

Moreover, my research activity was mainly focused on the identification of new interactors of the known Hh negative regulator and tumor suppressor REN^{KCTD11}. Through mass spectrometry analysis, we identified and focused our attention on the transcription factor SALL4A.

SALL4A plays a key role in maintaining pluripotency and self-renewal of embryonic stem cells, regulating different signalling pathway. SALL4A expression is inhibited in the post-natal period in many adult tissues, but it is reactivated in different tumors and is often related to worse prognosis and lower survival rate.

We observed that SALL4A is a substrate of REN^{KCTD11}, that induces its poly-ubiquitylation and its consequent proteasome-mediated degradation. In order to investigate its biological role in Hh signalling, we demonstrated that SALL4A enhances GLI1 activity working in complex with HDAC1, a well known Hh activator. Of note, we observed that the proliferation ability of human MB cell lines increases in presence of SALL4A, whereas

their migration rate is reduced after its genetic depletion; *in vivo*, SALL4A genetic depletion shows a reduction in Hh-dependent tumor growth.

Our findings identify SALL4A as a previously unknown regulator of Hh pathway able to promote, in complex with HDAC1, GLI1 activity and to contribute to Hh-dependent tumorigenesis. Hence, SALL4A stands as a new molecular target involved in the onset and progression of Hh-dependent tumors and represents an interesting focus in cancer research.

Aim 2 | Pharmacological targeting of Hedgehog pathway. Given the primary role of Hh signalling in tumorigenesis and in the maintenance of cancer stem cell niches, this pathway is now considered an attractive therapeutic target in cancer. In recent years, many efforts have focused on the development of drugs that can block the activating effect of SMO receptor. Among these, Vismodegib (GDC-0449/Eridevige®) was the first FDA-approved Hh inhibitor in 2012 for the treatment of advanced and metastatic basal cell carcinoma. However, several studies underlined some limitations of the inhibitors identified so far, linked in particular to the poor selectivity, the onset of drug resistance events and the activation of GLI1 mediated by other oncogenic pathways. These evidences raise the need to identify new and more effective Hh inhibitors able to overcome drug resistance and to counteract tumor growth.

To this end, my research activity was aimed at identifying, characterizing and optimizing new molecules able to block the oncogenic potential of Hh.

In particular, by combining the most profitable pharmacophores for targeting SMO and GLI1 by synthetic isoflavones, we designed and synthesized the isoflavone 22, a small molecule that acts as a multitarget Hh inhibitor blocking both SMO and GLI1 activity at the same time. Compound 22 is able to inhibit Hh-dependent tumor growth in human and murine MB cells at sub-micromolar concentration, as a consequence of the reduction in GLI1 expression levels. Isoflavone 22 remarkably shows a strong anti-tumor effect also

in vivo by suppressing cell proliferation and promoting apoptosis. Molecular modeling further corroborated the multitarget mechanism of action of compound 22, showing that the drug is able to fit the ligand binding site in both SMO and GLI1 (Lospinoso Severini et al., 2019).

Overall, these results reveal a valuable form of targeted therapy to increase the efficacy and to decrease the toxicity of individual anticancer agents. Our findings discover the first multitarget Hh inhibitor that impinges Hh-dependent tumor growth and stands as new potential weapons against Hh-driven tumors.

1 | INTRODUCTION

One never notices what has been done;
one can only see what remains to be done.
[Marie Curie, Nobel Prize in Physics and Chemistry]

1.1 | Hedgehog pathway

1.1.1 | Hedgehog signalling in human

Hedgehog (Hh) signalling was first elucidated by the developmental biologists Eric Wieschaus and Christiane Nüsslein-Volhard in the common fruit fly (*Drosophila Melanogaster*) while studying the fly body plan (Varjosalo and Taipale, 2008). Humans share many of the core components of the Hh pathway with *Drosophila* and mechanism of signal transduction is also conserved to some extent (Lee et al., 2016). The Hh pathway plays an essential role during embryonic development controlling cell proliferation, differentiation and maintaining tissue polarity; in adults, it is involved in stem cell renewal, organ homeostasis, tissue repair and oncogenesis (Ruiz i Altaba et al., 2007; Ruiz i Altaba et al., 2002; Zhang et al., 2018).

In humans, the Hh ligands have evolved into three homologues (Sonic, Indian and Desert Hh) contrasting a single Hh protein in *Drosophila*; all the three proteins bind to the receptors with equal affinity, but they are expressed in different tissues and induce different biological responses (Ingham and McMahon, 2001).

During pathway activation, Hh ligand binds to Patched1 (PTCH1) receptor; this event relieves PTCH1 repression on Smoothened (SMO) co-receptor which is critical for activating the downstream signalling cascade. This ultimately results in the activation of zinc finger Glioma-associated oncogene (GLI) transcription factors (Ingham et al., 2011), the mammalian counterpart of the final effector *Cubitus Interruptus* (Ci) in *Drosophila* (**Figure I**).

GLI has three homologues (GLI1, GLI2 and GLI3): GLI2 and GLI3 are bifunctional transcription factors with both C-terminal activation and N-terminal repression domains, and can function both as transcription activators or repressors, whereas GLI1, which lacks the N-terminal repressor domain, functions exclusively as transcription activator (Ingham et al., 2011). Activator forms of GLIs translocate into the nucleus promoting transcription of target genes, including those involved in Hh pathway feedback (such as GLI1 itself and PTCH1), proliferation-promoting genes (Cyclin-D1 and MYC), cell cycle

regulators (Cyclin-D2 and Cyclin-E1), apoptotic regulator (BCL2), genes involved in angiogenesis (ANG1/2), epithelial-to-mesenchymal transition (SNAIL) and factors involved in stem cell self-renewal (NANOG and SOX2) (Gonnissen et al., 2015; Skoda et al., 2018). The ultimate outcome of the pathway depends on the balance between activator and repressor forms of GLI proteins.

The exact molecular mechanism of signal transduction cascade from SMO to GLI proteins is not yet fully elucidated, but different studies suggested that mammalian Hh signalling requires the presence of primary *cilium* to which SMO, and other downstream pathway components, must translocate to accomplish the activation of GLI factors (Oro, 2007). In mammals, PTCH1 is present into and around the primary *cilium*; after ligand binding, this receptor dissipate to be replaced by SMO (Rohatgi et al., 2007). Then SMO is phosphorylated by protein kinase A (PKA) and Casein kinase Iα (CkIα) and moves to the *cilium*. The localization of SMO to the primary *cilium* is a necessary step in response to which the GLI factors, complexed with Suppressor of Fused (SuFu), are transported to the tip of the primary *cilium* (Haycraft et al., 2005). This translocation appears to be essential for GLI-SuFu complex dissociation, and hence for GLIs activation, promoting the translocation of their full-length forms into the nucleus where they can enhance transcription of target genes (**Figure I**).

In the absence of Hh ligand, SMO translocation to primary *cilium* is inhibited by PTCH1 receptor. Under these conditions, the kinesin protein KIF7 primarily localizes to the basal body of the primary *cilium*, a structure rich in proteasomes. Here, GLI2 and GLI3 are phosphorylated by PKA, Glycogen synthase kinase 3β (GSK3β) and KIF7. This results in the conversion of GLI2 and GLI3 into their repressor forms via proteolytic processing, thus blocking transcription (Nozawa et al., 2013).

SuFu is a strong negative regulator of the Hh pathway: it directly binds GLI proteins preventing their translocation into the nucleus (Méthot and Basler, 2000), but it can also enter the nucleus and recognize specific GLI-binding sequences in the DNA, inhibiting gene transcription (Chen et al., 2009). Hedgehog interacting protein (HHIP) is another

important transmembrane factor that attenuates Hh signalling; it binds to Hh ligands and promotes their uptake by endocytosis for lysosomal degradation (Chuang and McMahon, 1999).

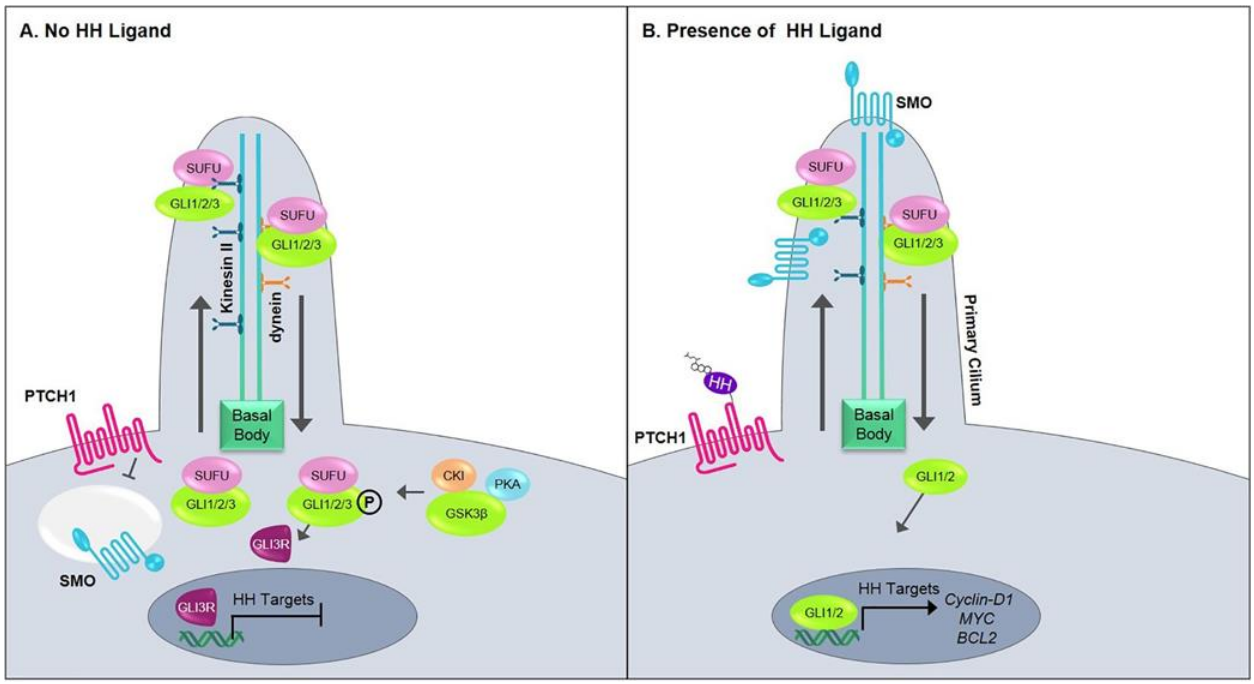

Figure I | *Model of Hh signalling.* (**A**) In the absence of Hh ligand, PTCH1 inhibits the surface localization of SMO and GLI proteins are phosphorylated by protein kinases, leading to the production of N-terminal truncated forms that repress Hh target-gene transcription. SuFu regulates the pathway by binding GLIs, thereby preventing Hh target-gene transcription. (**B**) In the presence of Hh ligand, PTCH1 inactivation allows SMO relocation to the tip of the *cilium*, promoting downstream signalling events and GLI proteins activation, thus increasing Hh target-gene expression (Cortes et al., 2019).

1.1.2 | *Hedgehog signalling and cerebellum development*

The central nervous system (CNS) is composed of the brain and the spinal cord; the brain is divided into three major components: the brainstem, the cerebrum and the cerebellum; although the cerebellum represents only 10% of the brain volume, it bears more than half of the total amount of neurons (**Figure II**).

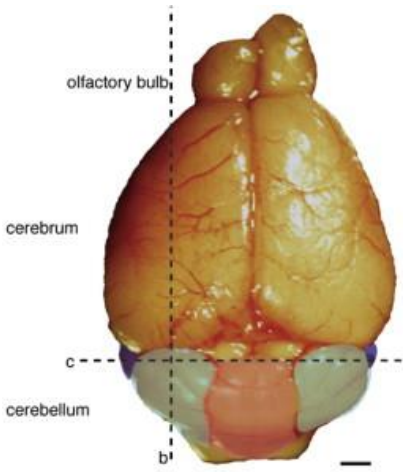

Figure II | *Anatomical subdivision of mouse brain.*

The anatomical organization and connectivity of the cerebellum allows it to efficiently function as a byway for processing a myriad of sensory modalities and cognitive tasks that require rapid communication between distinct brain units; it is also involved in cognitive functions including feed-forward sensory-motor learning, speech and spatial memory (Ito, 2008; Schmahmann, 2004; Schmahmann and Caplan, 2006; Strick et al., 2009; Timmann et al., 2010).

The cerebellum sits inferior to the cerebrum and posterior to the brainstem, comprising the dorsal wall of the fourth ventricle (**Figure II**). In mammals, it consists of a central vermis and two lateral hemispheres, each with its own sets of fissures (**Figure III**). The complexity of the foliation pattern varies between species, depending on the proprioceptive input to the organ. For example, the cerebellar vermis of many inbred mouse strains consists of eight major lobules with few sub-lobules, whereas the rat vermis consists of ten lobules and contains more sub-lobules. Although the basic ten

lobules present in the rat are conserved in human, each human cerebellar lobule is extensively subdivided into many sub-lobules. The conservation of morphology within and across species suggests that patterning of cerebellar *folia* is genetically regulated.

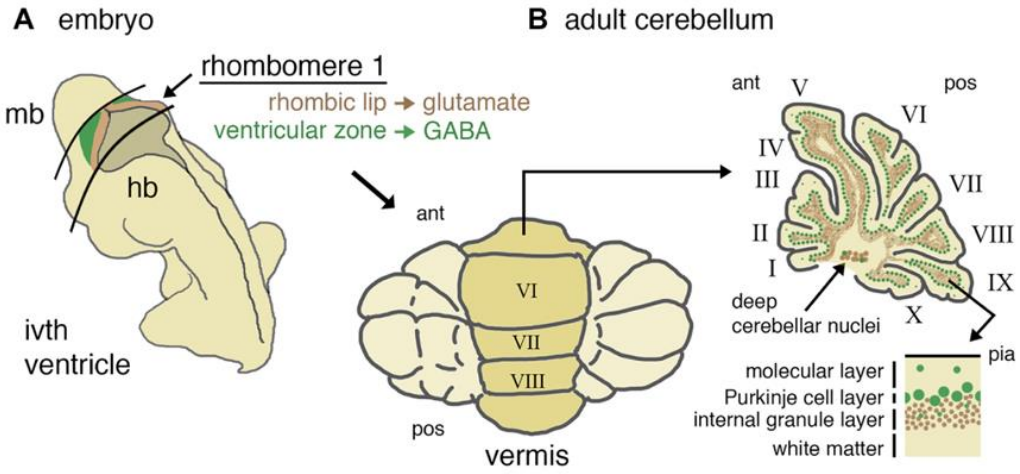

Figure III | *Representation of mouse cerebellum development.* (**A**) Schematic representation of a mid-gestation embryo showing the location of derivatives of rhombomere 1. mb: midbrain; hb: hindbrain; ivth ventricle: fourth ventricle. (**B**) In a dorsal (posterior) view, the adult cerebellum is characterized by a central (darker shaded) vermis running anterior (ant) to posterior (pos); schematic parasagittal section on the right (Basson and Wingate, 2013).

In human, the development of the cerebellum extends from the early embryonic phase (around week 4), with the development of the cerebellar primordium, to more than one post-natal year. In mouse, the cerebellum originates from the dorsal rhombomere 1 of the hindbrain at embryonic day 9 (E9). By E17, four fissures divide the cerebellum into five folds. At birth, the development of the cerebellum is not yet finalized, and it is only at postnatal day 21 (P21) that the organ becomes fully organized and mature (**Figure IV**).

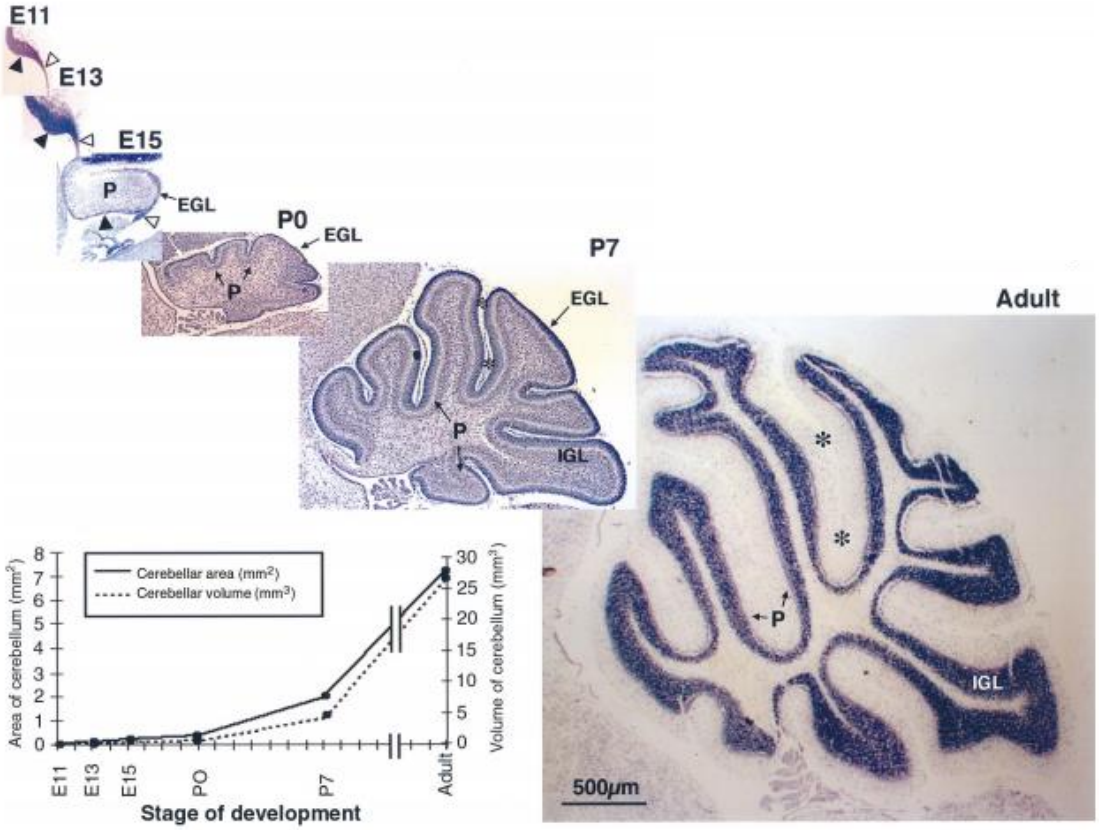

Figure IV | *The cerebellum undergoes a dramatic increase in size from its initial specification to its adult form.* Sagittal sections of mouse cerebellum from embryonic days E11, E13 and E15, postnatal days P0 (day of birth), P7 and adulthood are shown from left to right. In the photomicrographs, asterisks denote the primary fissure, P (with accompanying small arrows) points to the Purkinje cell layer, IGL labels the internal granule cell layer and EGL demarcates the external granular layer. In the three embryonic pictures, the filled arrowheads point to the ventricular neuroepithelium and the unfilled arrowheads point to the germinal trigone. The scale bar for all photomicrographs is the same. The graph in the lower inset further emphasizes the change in cerebellar size (Goldowitz and Hamre, 1998).

At cellular level, the cerebellum is organised into distinct neuronal layers: the outermost molecular layer (ML), the Purkinje cell monolayer (PCL), the densely populated internal granule layer (IGL) and the innermost white matter (WM). The different cell types that make up these layers originate from two distinct germinal centres in the early cerebellum: the upper rhombic lip and the ventricular zone (**Figure V**).

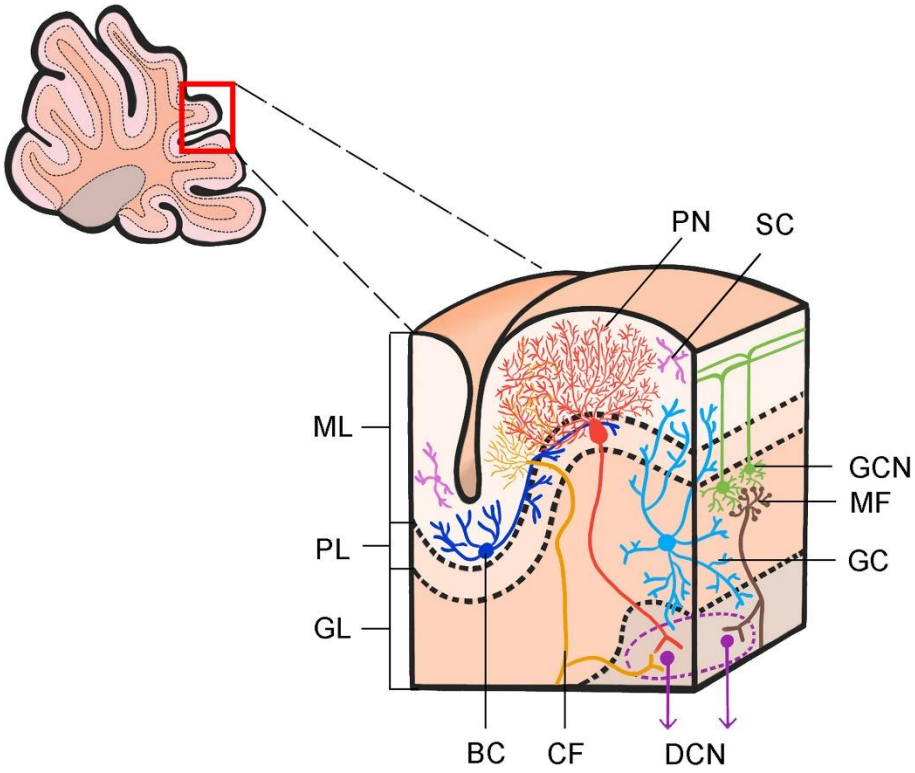

Figure V | *Scheme of the microarchitecture of the cerebellar cortex circuitry*. The main excitatory neuronal connections involve the mossy fibers (MFs), climbing fibers (CFs), granule cell neurons (GCNs) and parallel fibers (PFs). The principal inhibitory connections involve Purkinje neurons (PN) and a diversity of interneurons types including stellate cells (SCs), basket cells (BCs), and Golgi cell (GC) interneurons. (Iulianella et al., 2019).

The upper rhombic lip (localized at the caudal edge of the cerebellar primordium) expresses specifically the transcription factor ATOH1 and gives rise to the glutamatergic neurons, whereas the ventricular zone (located at the roof of the fourth ventricle) is characterized by the expression of the proneural gene *Ptf1a* and gives rise to the GABAergic neurons (Hoshino et al., 2005; Machold and Fishell, 2005; Wang et al., 2005). Each type of cerebellar neuron is produced at specific times.

Among the glutamatergic neurons, the granule neuron progenitors (GNPs) are produced from the upper rhombic lip starting at E12.5 and tangentially migrate from the cerebellar rhombic lip to the surface of the cerebellum to form the external granule layer (EGL). During the postnatal stage, GNPs undergo a rapid and massive proliferation in the EGL

starting from P2 until around P15. This massive proliferation is due principally to the soluble mitogen SHH that is released from the Purkinje cells (**Figure VI**).

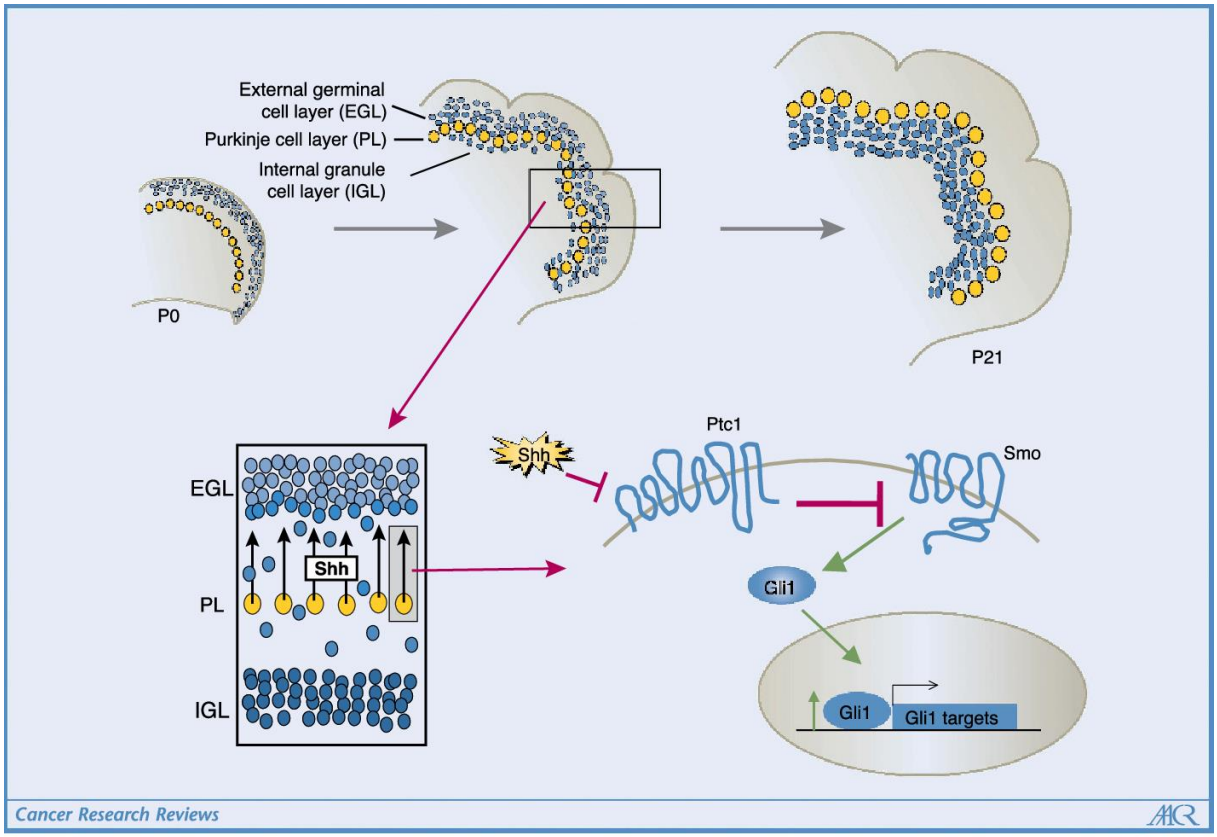

Figure VI | *The Hh pathway is critical for the normal development of the cerebellum.* SHH, released from the Purkinje cells, acts on overlying GNPs in the EGL, leading them to proliferation. After this period of SHH-dependent proliferation, GNPs exit the cell cycle, begin to differentiate and migrate inwards, pass the Purkinje cell layer, to reside in the IGL in the mature cerebellum (Romer and Curran, 2005).

Cerebellar development is tightly regulated and dysfunction in this process could lead to cancer as well as neurological disorders.

1.1.3 | *Multiple levels of Hedgehog pathway regulation*

Given the great physiological and clinical importance of Hh pathway, it is critical to understand how it is regulated. Many levels of regulation that control release, reception and interpretation of the Hh signal exist.

The first control mechanism is mediated by the inhibitory function of PTCH1 receptor on the activator co-receptor SMO. PTCH1 receptor maintains in an inactive state the seven-pass transmembrane receptor SMO, which is a member of the G protein-coupled receptor (GPCR) superfamily. The binding of Hh ligand to PTCH1 triggers the intracellular signalling cascade releasing the inhibitory effect that PTCH1 exerts on SMO (Ramsbottom and Pownall, 2016).

A second regulatory mechanism includes acetylation/deacetylation events of histone and non-histone proteins that regulate the transcription of target genes. These modifications are mediated by histone acetyltransferase (HAT) and histone deacetylase (HDAC) enzymes, which are able to add or remove acetyl groups to lysine residues, respectively. These enzymes can target both histones and other regulatory proteins, playing a crucial role in the control of transcription. On the other hand, modifications made to histone proteins can directly impact gene expression by altering chromatin conformation and its accessibility to coactivators and to the basal transcription machinery (Shahbazian and Grunstein, 2007; Yang and Seto, 2007).

HDACs have recently been discovered as regulators of the Hh pathway. In particular, in our laboratory it has been demonstrated that HDAC1 binds and deacetylate the transcription factor GLI1, leading to Hh pathway activation (Canettieri et al., 2010; Coni et al., 2013a).

A further level in Hh pathway control is mediated by ubiquitylation processes. Ubiquitylation events are carried out by major components of the transduction pathway such as SMO, SuFu and GLI factors. These events modulate the stability of proteins, resulting in their degradation through the proteasomal or lysosomal machinery, with important consequences for the activation/inhibition of Hh signalling. Nevertheless, the

ubiquitylation is also implicated in the regulation of non-proteolytic events such as the modulation of signal transduction, transcription, protein-protein interaction and DNA repair.

1.1.3.1 | *Ubiquitylation processes*

Ubiquitylation is a fine molecular mechanism responsible for regulation of the most important cellular functions such as DNA replication and repair, transcription, proliferation and differentiation, apoptosis, immune response, endocytosis and translation of signal (Scheffner et al., 1990).

This post-translational modification involves the formation of a covalent bond between ubiquitin (Ub), a 76 amino acid polypeptide highly conserved in evolution, and a specific protein substrate. Through the ubiquitylation reaction, Ub is conjugated to the accepting proteins through the formation of an isopeptidic bond between the C-terminal end of the Ub (glycine residue 76) and the ε-amino group of a lysine residue on the target (Harper and Tan, 2012; Pickart and Eddins, 2004). This constitutes a clear signal that indicates the fate of proteins (Hershko and Ciechanover, 1998).

Ubiquitylation occurs through the sequential action of three classes of protein: ubiquitin-activating enzymes (E1), ubiquitin-conjugating enzymes (E2, also referred as ubiquitin carrier proteins or UBCs) and ubiquitin-protein ligases (E3s). The C-terminal carboxyl group of Ub is activated in an ATP-dependent process, which results in a high-energy thioester linkage with the active-site cysteine of E1; the small protein is trans-thiolated from the E1 to the active-site cysteine of one of ~40 E2s (in mammals). Finally, Ub is generally transferred from the E2 to the ε-amino group of a substrate lysine in an E3-dependent manner. This last step occurs differently depending on the type of E3-ligase involved, but it gives substrate specificity (**Figure VII**).

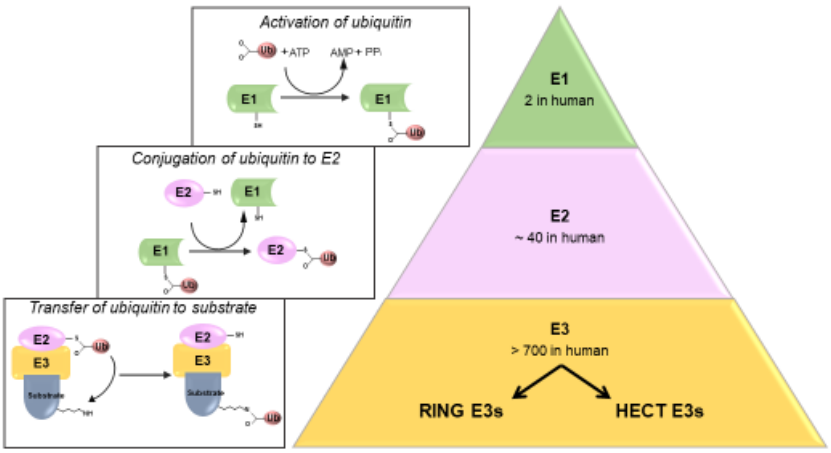

Figure VII | *Ubiquitylation process.* Ub is attached to substrates by a cascade of reactions involving three enzymes. An E1 enzyme activates Ub in an ATP-dependent way. An E2 enzyme binds and then transfers the activated Ub to a substrate specifically bound to an E3-ligase. E3 enzymes can be divided into two main families: the RING and the HECT E3-ligases. Although, the ubiquitylation process usually leads to the degradation of the substrate, it can also drive regulative events (Infante et al., 2019).

Ubiquitylation occurs with exquisite spatial, temporal and substrate specificity, most of which is dictated by more than 600 E3-ligases that are estimated to be encoded by the mammalian genome; E3 is the main substrate recognition factor. A given E3-ligase usually binds its cognate substrate(s) through a structural motif known as a ubiquitylation signal (degron): it consists of a specific primary sequence that may be subject to post-translational modifications, such as phosphorylation and dephosphorylation, which modulate its interaction ability with the E3-ligase (Skaar et al., 2013).

Based on the modality of interaction with E2, two classes of E3-ligases have been classified: the RING finger E3-ligases and the HECT E3-ligases.

HECT domain E3-ligases

HECT is the acronym of "Homologous E6-AP Carboxy Terminus" because E6-AP is an E3-ligase present in human cells whose study provided important information on the structure of the HECT domain (Scheffner et al., 1990).

Among the E3-ligases, HECTs are the only ones with intrinsic catalytic activity (Bernassola et al., 2008). The HECT domain consists of a large N-terminal lobe, containing the E2-binding site, and a smaller C-terminal lobe of ~350 amino acids originally characterized in E6-AP and including the active-site Cys residues (C830) (**Figure VIII**). Structural studies have revealed that these two lobes are connected by a flexible hinge region, which is critical for juxtaposing the catalytic Cys residues of the E2 and E3 (the HECT domain) during Ub transfer (**Figure VIII**). A conformational change involving an alteration in the relative orientation of the two lobes is thought to facilitate the transthiolation reaction.

The substrate specificity of the HECT E3-ligases is dictated by protein-protein interaction domains, which account for their classification into three further subfamilies: HECTs containing an RCC1-like domain (RLD), HECTs with WW domains (WW-HECT) and HECTs lacking either RLDs or WW domains. WW-HECTs represents the most well-defined subgroup and consists of monomeric proteins with a common general modular architecture; WW domains mediate ligase-substrate associations (**Figure VIII**).

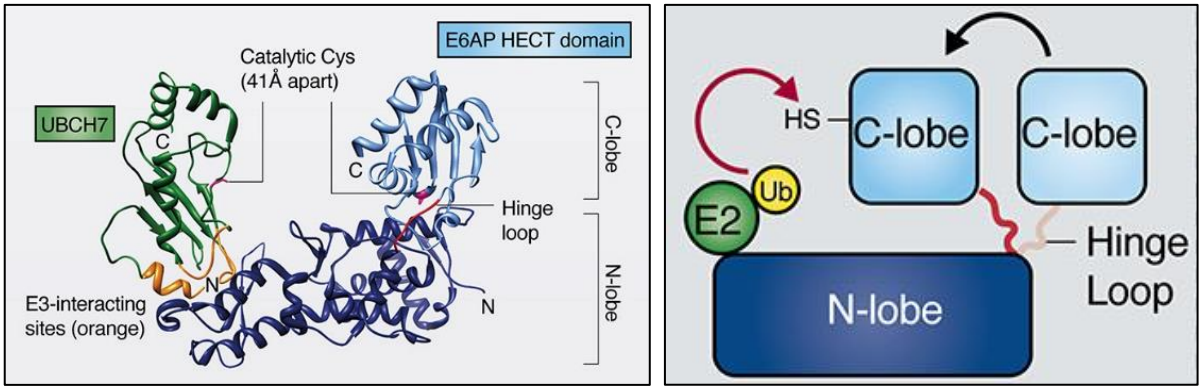

Figure VIII | *Main features of HECT E3-ligases.* (Left panel) The HECT domain consists of an N-terminal N-lobe, which interacts with the E2, and a C-terminal C-lobe, that contains the active site cysteine. (Right panel) Movement of the flexible hinge loop may bring the C-lobe active site Cyc close to that of the E2 for Ub transfer (Metzger et al., 2012).

RING finger E3-ligases

RING (Really Interesting New Gene) E3-ligases present a zinc-finger domain which includes a sequence of histidine and arginine residues able to bind two zinc ions (Pickart, 2001) (**Figure IX**). The E3-ligases of this family are further distinguished in two classes: RINGs "single subunit", which bind both E2 and substrate directly (through a domain different from the RING one), and RINGs "with multiple subunits" which are included in complexes that involve other proteins essential for substrate recruitment (**Figure IX**). A representative example of the latter group is the SCF complex (Skp1, Cul1, F-box) composed by Cullin 1 (belonging to the Cullin family), the RING Rbx1/Roc1, the adaptor protein Skp1 and one F-box protein responsible for binding to the substrate (Lorick et al., 1999) (**Figure IX**).

All eukaryotic species show a wide variety of proteins that contain a BTB/Poz (Bric-a-brack, Tram-track, Broad complex) domain, including several transcription factors, proteins involved in the regulation of apoptosis and cell cycle. These proteins are able to interact specifically with Cullin 3 (Cul3) forming a complex called SCF-like; in this complex, the BTB/Poz-containing protein alone is able to mediate the interaction between Cul3 and the substrate of ubiquitylation.

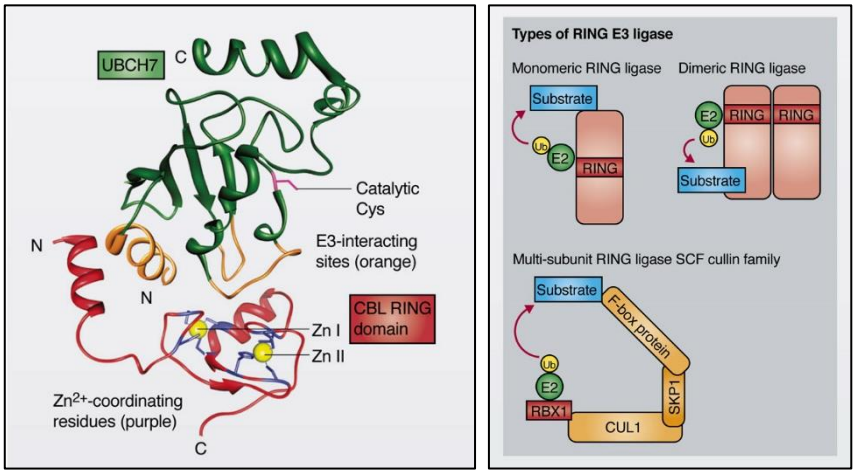

Figure IX | *Main features of RING E3-ligases.* A RING finger domain coordinates Zn^{2+} through specifically spaced cysteine and histidine residues. The RING brings E2 and substrate together, and mediates Ub transfer from E2 to the substrate (Metzger et al., 2012).

1.1.4 | *Ubiquitylation processes in the control of proteins fate*

Ubiquitylation is best-known for targeting proteins for degradation mediated by the 26S proteasome: the proteasome recognizes a chain of at least four molecules of Ub, bonded to each other through the lysine 48 residue of the Ub itself (K48-linkage poly-ubiquitylation), as a degradative signal.

E3-ligases choose the substrate, but they do not always determine the outcome of the tagging; the fate of ubiquitylated proteins is determined by the nature of Ub attachment and the type of isopeptide linkage forming the poly-Ub chain. Ub molecule has seven different lysines (Lys6, Lys11, Lys27, Lys29, Lys33, Lys48 and Lys63) and each of them can be involved in the formation of Ub chains. The way by which Ub is bound to protein substrates determines the fate of target proteins; a given protein can be modified on single or on several lysine residues (**Figure X**).

In the simplest ubiquitylation process, a single molecule of Ub is attached to the substrate (mono-ubiquitylation); alternatively, single molecules of Ub can be attached to different lysine residues (multi-mono-ubiquitylation) (Haglund et al., 2003). With few exceptions, single or multiple mono-ubiquitylation of cell surface receptors triggers receptor internalization and trafficking to the endosomal-lysosomal degradation pathway. The third, and most well-known, ubiquitylation mechanism involves the formation of long chains of Ub (poly-ubiquitylation). Poly-ubiquitylation may mediate different biochemical functions, depending on the lysine of the Ub molecule involved in the formation of the chain; for example, K48 Ub chains of at least four molecules length lead to the recognition of the target protein by the proteasome and subsequent degradation. In a different way, K63-dependent poly-ubiquitylation is associated with the regulation of various cellular processes such as DNA repair, protein localization, stabilization of protein-protein interaction (Lee et al., 2008; Scialpi et al., 2008). Occasionally, K6 and K11-mediated Ub chains have been observed to target protein for a proteasome-dependent degradation and their accumulation correlates with the pathogenesis of neurodegenerative disorders (Bennett et al., 2007; Cripps et al., 2006).

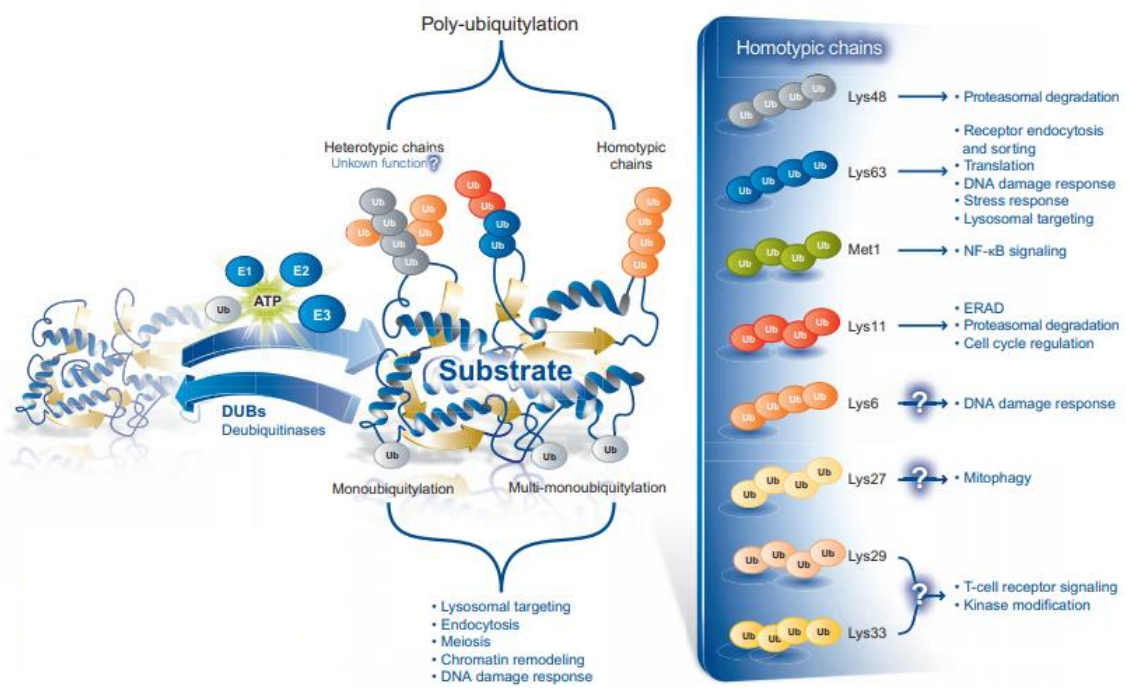

Figure X | *Schematic representation of Ub modifications and their cellular functions.* [This image was created by Abcam in association with David Komander (LMB, Cambridge, UK) and Yaron Galanty (Gurdon Institute, Cambridge, UK)].

Ubiquitylation is therefore a complex post-translational modification that can influence and control different cellular processes. Understanding how this mechanism is involved in the control of cellular pathways can help to understand how its deregulation leads to a pathological condition.

1.1.5 | *Ubiquitin-dependent regulation of Hedgehog signalling*

Ubiquitylation of Hh pathway key components represents an important mechanism for the regulation of the Hh signalling (**Figure XI**).

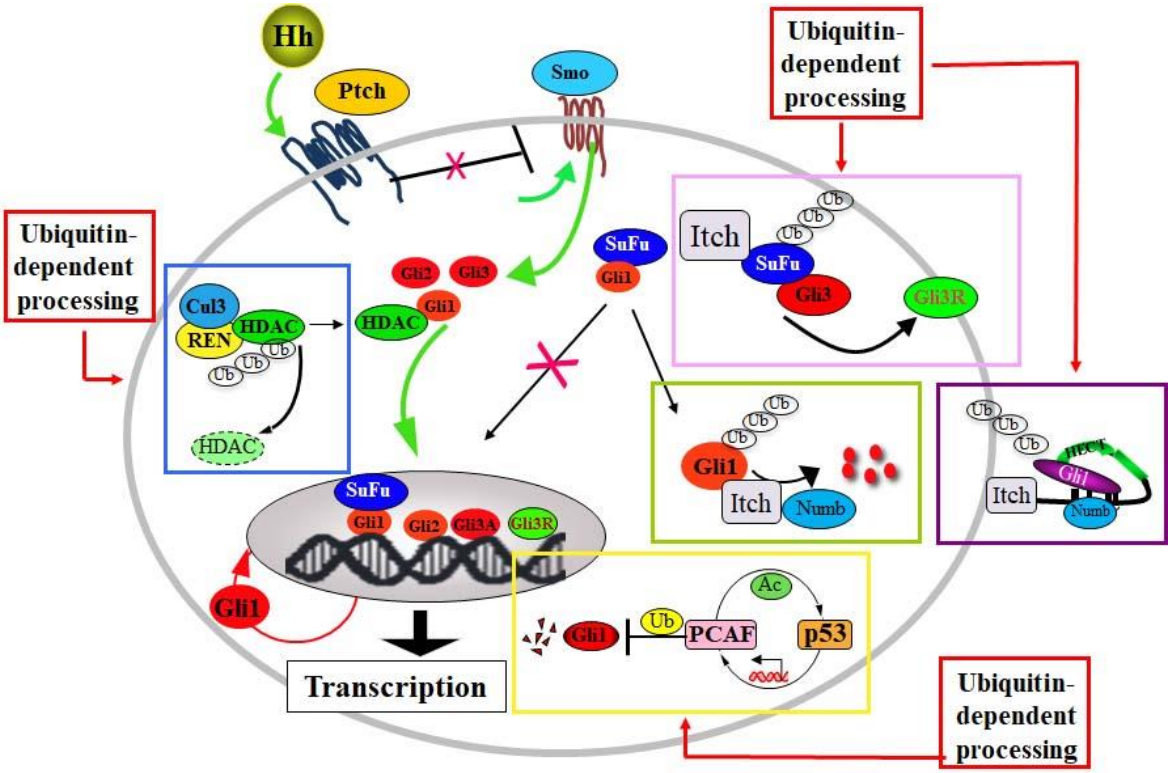

Figure XI | *Hh pathway regulation through ubiquitylation processes.*

The regulation of the Hh signalling through ubiquitylation processes was first identified in *Drosophila* (Nüsslein-Volhard and Wieschaus, 1980). So far, two mechanisms of Ci ubiquitylation have been identified in *Drosophila*, both based on the activity of E3-ligases belonging to the RING E3-ligase family with multiple subunits.

The first studied mechanism is mediated by the SCF complex; the RING Skip1-Cul1-F-box E3-ligase complex targets Ci in *Drosophila* for partial proteolytic degradation to generate the C-terminally truncated repressor forms. In the absence of Hh, the kinases PKA, GSK3β and CK1 phosphorylate the full-length Ci (Ci155), leading it to an SCF complex-mediated ubiquitylation and inducing its proteolytic cleavage in the repressor form (Ci75R) (Smelkinson et al., 2007). In presence of Hh, this event does not occur, and full-length Ci is transformed into its activator form (Ci155A) (Humke et al., 2010).

A similar mechanism is found in vertebrates: in the absence of Hh signal, a phosphorylation-dependent mechanism involving PKA, GSK3β and CK1 targets GLI proteins, which are in turn ubiquitylated by the SCF complex composed of F-box βTrCP. Full-length GLI3 (190 KDa) and, to a lesser extent, full-length GLI2 (185 KDa) are converted into repressor fragments (GLI3R of 83kDa and GLI2R of 78kDa); otherwise, GLI1 ubiquitylation results in complete degradation (Gulino et al., 2012).

The second mechanism of ubiquitylation identified in the regulation of the Hh signalling involves a protein from the Cullin family, Cul3, able to interact with proteins containing a BTB/Poz domain (Pintard et al., 2004). When the Hh pathway is off, the E3-ubiquitin ligase HIB (in *Drosophila*)/SPOP (in vertebrates) mediates the ubiquitylation and proteasome degradation of full-length Ci and full-length GLI2 and GLI3 respectively, but not GLI1; this process does not require the phosphorylation of the downstream transcription factors. These mechanisms may represent a Hh-induced negative feedback loop to modulate the signalling response (Di Marcotullio et al., 2007).

Two novel ubiquitylation mechanisms involved in GLI1 degradation have been identified by our team. The first is mediated by the HECT E3-ligase Itch: Di Marcotullio and colleagues have shown that Itch, assisted by Numb, is able to interact with GLI1 and promote its ubiquitylation, leading it to a proteasome-dependent degradation. This event results in a reduction of Hh-target genes expression (**Figure XI**) (Di Marcotullio et al., 2011b). The second ubiquitylation process identified is mediated by the acetyltransferase p300/CREB-binding protein (CBP)-associated factor (PCAF): upon genotoxic stress, p53 triggers the transcription of PCAF and promotes its accumulation; the intrinsic E3-ligase activity of PCAF is then responsible for the Ub-dependent degradation of GLI1 (**Figure XI**) (Mazzà et al., 2013).

Ubiquitylation events that regulate Hh pathway do not involve only GLI factors; recent studies described ubiquitylation events on the receptor SMO which result in SMO endocytic internalization and subsequent degradation. SMO undergoes both mono-ubiquitylation and poly-ubiquitylation processes, suggesting that its degradation occurs

in both lysosomal and proteasome machinery. The link of Ub molecules occurs at the level of the C-terminal portion of SMO, particularly at the SMO Auto Inhibitor Domain (SAID). The Hh signal induces SMO phosphorylation simultaneously inhibiting ubiquitylation of the receptor and allowing its membrane accumulation (Jia et al., 2004).

Among the most important Hh signalling regulators an important role is played by the tumor-suppressor SuFu. SuFu is required for mouse embryonic development (Cooper et al., 2005; Svärd et al., 2006). Its genetic inactivation, leading to constitutive activation of the Hh pathway in a ligand-independent manner, causes early embryonic lethality at E9.5 with neural tube defects. SuFu is in turn regulated by ubiquitylation events on K257 that lead it to degradation through the proteasome machinery (Yue et al., 2009).

Since ubiquitylation processes finely regulate Hh activity affecting the stability of key components of the signalling, a deeper knowledge of the players involved in these regulatory processes represents an appealing goal in the biology of Hh-driven tumors.

1.2 | The tumor suppressor REN^{KCTD11}

Deregulation of Hh signalling is considered to play a crucial oncogenic role and commonly occurs in medulloblastoma (MB), a childhood brain tumour often associated with Hh signalling aberrations. Germ-line and somatic mutations in components of the Hh pathway (i. e. PTCH1, SMO and SuFu), which lead to the activation of ligand-independent signals, have been reported in MB and are suggested to be responsible for tumorigenesis (Ellison, 2002; Rubin and Rowitch, 2002; Ruiz i Altaba et al., 2002). However, genetic lesions in components of this pathway are observed in a minority of cases; among them, the most frequent one is represented by allelic deletion on chromosome 17p, occurring in up to 50% of tumors with a loss of heterozygosity (LOH) sometimes restricted to a common region at 17p13.2–13.3 (Ellison, 2002).

To this regard, our team identified REN (also named KCTD11 according to HUGO Gene Nomenclature Committee, HGNC) mapping on human chromosome 17p13.2 and indicated its function as a specific checkpoint for Hh signalling activity (Di Marcotullio et al., 2004; Gallo et al., 2002).

1.2.1 | *REN^{KCTD11} gene and protein structure*

REN^{KCTD11} gene maps on chromosome 17p in region 13.2 and is deleted in 30% of the sporadic MBs (Di Marcotullio et al., 2004). REN^{KCTD11} is also named KCASH1 because it is a member of the recently identified KCASH family (**K**CTD containing, **C**ullin3 **A**daptors, **S**uppressors of **H**h), which also includes the two homologs KCASH2 (or KCTD21, for Potassium – K – Channel Tetramerization Domain containing 21) and KCASH3 (also known as KCTD6); all these proteins share high homology, specific expression in brain and cerebellum, suppressor activity on acetylation-dependent Hh/GLI1 signalling, genetic loss or silencing in human primary MBs and growth-inhibitory activity on MB cells; moreover, they have a common BTB/Poz domain (**Figure XII**) (De Smaele et al., 2011) necessary for Cul3 binding. All BTB/Poz-Cul complexes contain a single monomeric BTB/Poz domain interacting with a single Cul molecule (1:1 stoichiometry)

(Correale et al., 2011). Despite the similarity of the N-terminal regions among KCTD proteins, their C-terminus is highly variable (Dementieva et al., 2009).

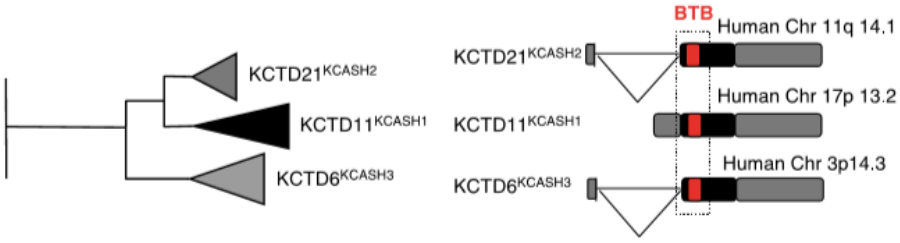

Figure XII | *Identification of KCASH family members.* Phylogenetic tree of KCTD11, KCTD21 and KCTD6 (left panel) and schematic representation of their human genetic locus (right panel) (De Smaele et al., 2011).

The characterization of REN^{KCTD11} in solution indicates that the protein works as tetramer (Correale et al., 2011); protein oligomerization is driven by BTB/Poz domain, being ΔBTB monomeric. The tetrameric state of the protein is fully compatible with the binding of Cul3; analysis of the structure indicates that a single Cul3 molecule interacts with two subunits of REN^{KCTD11} BTB/Poz (**Figure XIII**) (Correale et al., 2011).

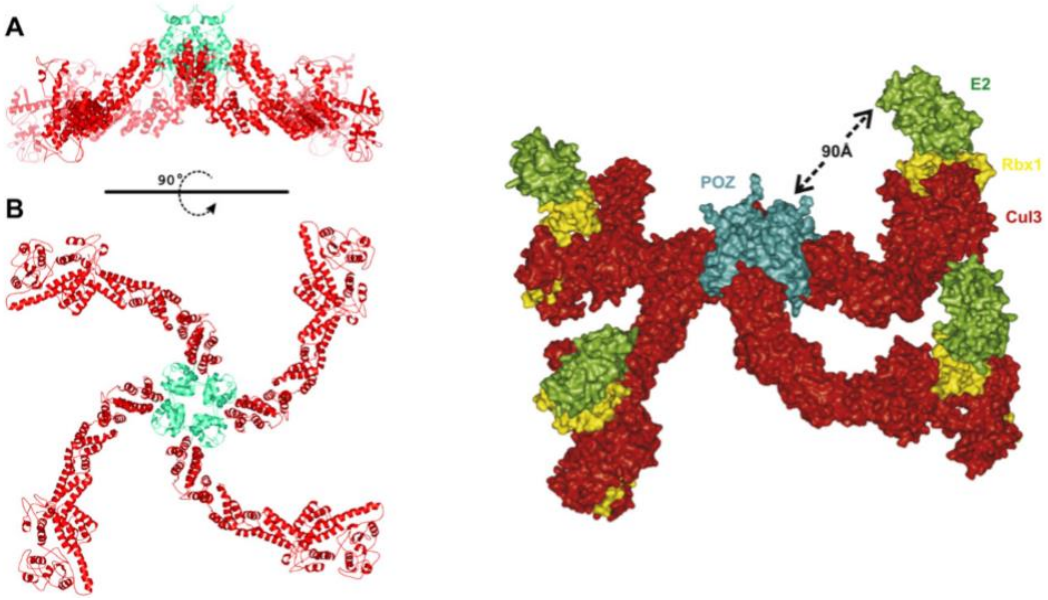

Figure XIII | *Complex of REN^{KTCD11} BTB/Poz with Cul3.* (Left panel) Two different views of the complex between the REN^{KTCD11} BTB/Poz tetramer with four molecules of Cul3 (in red). (Right panel) Complex between the REN^{KTCD11} BTB/Poz tetramer with Cul3 (in red), Rbx1 (in yellow) and E2 (in green) (Correale et al., 2011).

1.2.2 | *REN^{KCTD11} expression in the transition from proliferating to differentiating neuronal cells*

The analysis of REN^{KCTD11} expression during different stages of mouse embryonic development has shown its close involvement with the neurogenetic processes in early developmental stages; its expression is developmentally regulated. REN^{KCTD11} is expressed at higher concentrations in the non-proliferating granules of the internal EGL (inner EGL) and IGL, rather than in highly proliferating cells of the external EGL (outer EGL) (**Figure XIV**) (Argenti et al., 2005).

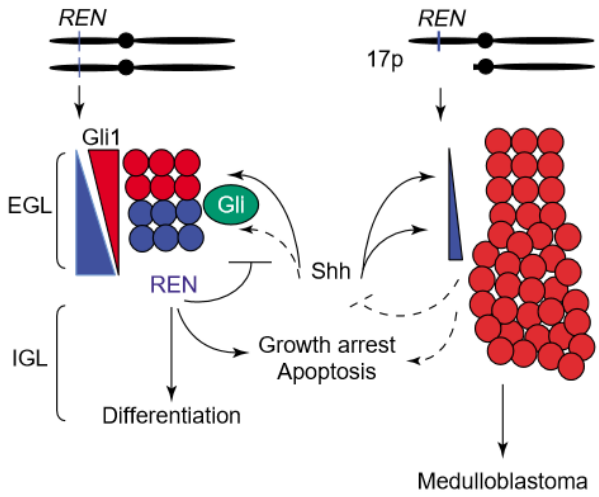

Figure XIV | *Expression of REN^{KCTD11} in cerebellar GCPs development and tumorigenesis.* REN^{KCTD11} expression (in blue) increases along the transition from outer to inner EGL GCPs, thus lowering the Hh-GLI1 signalling (in red) activated in the outer EGL. In this way, REN^{KCTD11} enables granule cells to differentiate and migrate into the internal granule layer (IGL). The number of developing granule cells is also limited by REN^{KCTD11}-induced apoptosis. Chromosome 17p deletion-dependent loss of REN^{KCTD11} removes the constraints from Hh-induced immature cell expansion, thus favouring tumorigenesis (Ferretti et al., 2005).

Accordingly, the increased expression of REN^{KCTD11} leads to GCPs differentiation *in vitro*, reduces the transcription of GLI2-dependent genes and GLI1 target genes, thus antagonizing the effects induced by SHH on GCPs proliferation and differentiation (Argenti et al., 2005). These evidences suggest that REN^{KCTD11} represents an antagonist of the Hh pathway and that its loss, due to chromosomic deletion, may alter the regulation of this signalling promoting MB onset.

1.2.3 | *REN^{KCTD11} as negative regulator of Hedgehog signalling*

Human REN^{KCTD11} mRNA levels are higher in the cerebellum than in the whole brain and significantly lower in MB cells. REN^{KCTD11} hemizygosity was found in 30% of human MBs and it is expected to result in REN^{KCTD11} impaired function; indeed, although the retained allele is unaffected by somatic mutation, REN^{KCTD11} transcript levels are 5-fold lower in hemizygous MB cell lines and primary tumors compared with normal cerebellar tissue. Interestingly, a 50% decrease of REN^{KCTD11} mRNA levels is also observed in REN$^{KCTD11+/+}$ primary tumor samples and cell lines suggesting that, in addition to allelic loss, MB displays a down-regulated REN^{KCTD11} expression occurring by mechanisms that need to be further elucidated.

Deletion of REN^{KCTD11} N-terminus BTB/Poz domain (ΔPoz), involved in protein–protein interactions (Bardwell and Treisman, 1994), abrogates almost completely REN^{KCTD11} ability to block cell proliferation whereas deletion of the C-terminus (ΔC) is much less effective, suggesting that the BTB/Poz domain is responsible for REN^{KCTD11} growth suppressor function.

GLI1 has cytoplasmic or nuclear localization, depending on cell context (Ding et al., 1999; Kogerman et al., 1999; Ruiz i Altaba, 1999) and the major mechanism controlling its activity is represented by the regulation of its cytoplasmic-nuclear shuttling. In presence of REN^{KCTD11}, a significant amount of GLI1 is retained into the cytoplasm, whereas the inactive REN^{KCTD11} ΔPoz mutant is not able to modify GLI1 nuclear localization. Although REN^{KCTD11} is mostly cytoplasmic under basal conditions and colocalizes with co-transfected GLI1 into the cytoplasm, the two proteins do not bind directly suggesting that REN^{KCTD11} abrogate GLI1 function by means of an indirect mechanism.

REN^{KCTD11}-mediated antagonism of the Hh signalling has been recently discovered. It is known that HDACs play a pivotal role in developmental processes and tumorigenesis, regulating gene expression through the modulation of the acetylation status of histone and non-histone proteins. HDACs have been recently uncovered as Hh activity modulators; in particular HDAC1 deacetylates the transcription factors GLI1 and GLI2

enhancing their activity (Canettieri et al., 2010). Although few endogenous cell signals have been described to regulate HDACs function through post-translational modifications (e.g. phosphorylation, sumoylation, acetylation and ubiquitylation), the role of these regulatory events in cancer is not yet defined and growing evidences indicate the relevance of ubiquitylation-dependent control of HDACs.

REN^{KCTD11} functions as an adaptor protein able to recruit specific protein substrates to Cul3 thus promoting their ubiquitylation; in particular, HDAC1 is a substrate recognized by REN^{KCTD11} that undergoes ubiquitylation and degradation (Canettieri et al., 2010). HDAC1 is upregulated by Hh signalling itself and is highly expressed in MBs, thus providing a constitutive auto-maintenance loop of the pathway (Canettieri et al., 2010); notably, its expression is mutually exclusive to REN^{KCTD11} expression in developing GCPs *in vivo* (Canettieri et al., 2010). In agreement with its E3-ligase function, ectopic expression of REN^{KCTD11} in MB cells reduces HDAC1 levels, leading to GLI1 deacetylation and consequent impairment of its transcriptional activity (**Figure XV**) (Canettieri et al., 2010).

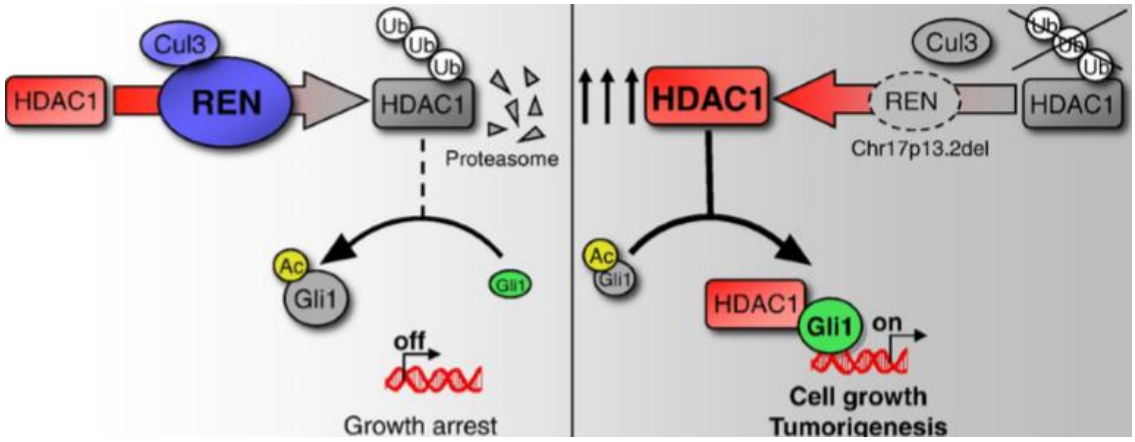

Figure XV | *Model showing REN^{KCTD11} mechanism of action as inhibitor of Hh signalling.* During cerebellar development, REN^{KCTD11} binds and downregulates HDAC1 by inducing its ubiquitylation and degradation, thus inhibiting GLI1 activity and transcription of its target genes. Loss of REN^{KCTD11}, frequently observed in MB and caused by chromosome 17p deletion and methylation-dependent silencing, allows HDAC1 accumulation that determines GLI1 deacetylation. This confers to GLI1 increased transcriptional activity, thereby enhancing Hh/GLI1 signalling and sustaining cell growth (Di Marcotullio et al., 2011a).

These observations suggest that REN^{KCTD11} suppresses Hh signalling via the negative regulation of HDAC1, providing a novel mechanism of regulation of GLI1 activation. However, given the complex molecular organization of REN^{KCTD11}, its relevance in MB onset and its activity as Cul3-adaptor protein, it cannot be excluded that REN^{KCTD11} may mediate the regulation of other substrates through molecular mechanisms that are still unknown.

1.3 | SALL4 stem cell factor

In order to deepen REN^{KCTD11} function in Hh signalling and in the pathogenesis of MB, our study was mainly focused on the identification of new interactors able to regulate or be regulated by REN^{KCTD11} itself. Mass spectrometry analysis showed different REN^{KCTD11} interactors; among them we focused on SALL4.

SALL4 is one of four human homologues (SALL1, 2, 3 and 4) of the *Drosophila* region-specific homeotic gene *spalt* (*sal*) (de Celis and Barrio, 2009; Eildermann et al., 2012; Kohlhase et al., 1996; Sweetman and Münsterberg, 2006). *Sall4* gene encodes multiple Cys2His2 zinc finger (C2H2-ZF) domain-containing transcription factor that either activates or represses gene transcription depending on cell context. This protein is required for embryonic stem cells (ESCs) pluripotency and early embryonic development.

In humans, heterozygous SALL4 mutation has been linked to Okihiro syndrome, Holt-Oram syndrome, acro-renal-ocular syndrome and IVIC syndrome, all diseases characterized by multiple organ malformations (Al-Baradie et al., 2002; Kohlhase et al., 2003; Paradisi and Arias, 2007). While normally downregulated or no longer expressed in fully differentiated somatic cells, abnormal reactivation of SALL4 in adult cells may lead to malignancy. To date, aberrant SALL4 expression has been detected in over 10 types of human solid tumors and in several types of leukemia and the transcription factor is now considered a useful biomarker and therapeutic target for these diseases (Wang et al., 2014; Xiong, 2014; Zhang et al., 2015).

1.3.1 | SALL4 gene and protein structure

In humans, *Sall4* gene is located on chromosome 20q13.2 and consists of four coding exons with a 3162bp long coding sequence (Wong et al., 2008). Two alternative splicing products exist in addition to the full length Sall4A mRNA: the isoform B consists of exons 1-3-4 and is 1020bp long, whereas in isoform C exon 2 is spliced out (Kohlhase et al., 2005); SALL4C is the isoform less studied so far (**Figure XVI**).

Human SALL4 contains a single C2H2 zinc finger near the N-terminus, two C2H2 zinc finger clusters in the middle portion and one at the C-terminus of the protein (de Celis and Barrio, 2009) (**Figure XVI**). SALL4A presents all zinc finger clusters, while SALL4B lacks ZF2 and ZF3. The most C-terminal ZF4 cluster of SALL4 is both necessary and sufficient for its localization to the heterochromatin (Sakaki-Yumoto et al., 2006). In addition, SALL4 also contains a glutamine (Q)-rich region that is highly conserved in all invertebrate and vertebrate SALL family members; this domain is necessary for interactions between Spalt family proteins (Sweetman et al., 2003). SALL4A and B isoforms are able to form homodimers and heterodimers (Rao et al., 2010), possibly through their Q-rich regions.

SALL4 is a nuclear protein, and its subcellular localization is mediated through at least one conserved nuclear localization signal (NLS); a single mutation in lysine 64 residue which belongs to this region is sufficient to disrupt its subcellular distribution and compromises its function *in vivo* (Wu et al., 2014).

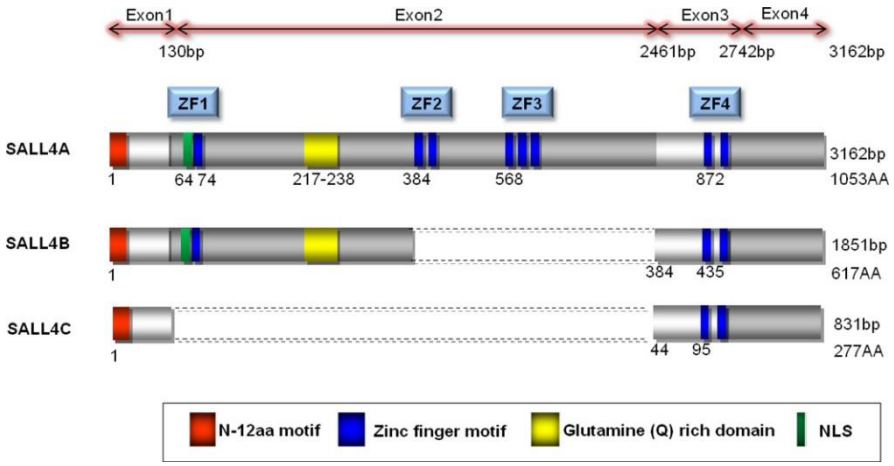

Figure XVI | *Human Sall4 gene structure and isoforms.* Alternative splicing generates 3 forms of Sall4 mRNA. SALL4A (encoding 1053 amino acids) has all 4 exons and contains 4 zinc finger domains (ZF1–4, indicated by blue bars). SALL4B (encoding 617 amino acids) is generated via an alternative splice donor site that results in the deletion of large portion of exon 2 and a protein that contains only ZF1 and ZF4. SALL4C (encoding 277 amino acids) does not have exon 2 and results in a protein that only has ZF1. The conserved N-terminal 12 amino acid (N-12aa, red bars) motif is required for recruiting the nucleosome remodeling and histone deacetylase (NuRD) complex and mediates transcription repression; glutamine (Q)-rich region (yellow bars) is necessary in protein interactions between Spalt family proteins; the conserved nuclear localization signal (NLS) is indicated by green bars (Tatetsu et al., 2016).

1.3.2 | *SALL4 expression in development*

SALL4 is an essential component of the "stemness" regulatory machinery involving OCT4, SOX2, NANOG in maintaining ESCs self-renewal and pluripotency (Elling et al., 2006; Tan et al., 2013; Zhang et al., 2006) (**Figure XVII**). In ESCs, a well-controlled SALL4/OCT4 transcription regulatory loop balances proper expression dosage of SALL4 and OCT4 and, like OCT4, SALL4 reduction results in re-specification of ESCs to the trophoblast lineage (Yang et al., 2010). In mouse ESCs, studies of chromatin immunoprecipitation coupled to microarray hybridization (ChIP-on-chip) revealed that SALL4 binds to about twice as many gene promoters as NANOG and about four times more genes than OCT4; the three factors were found to form heteromeric protein complex involved in the regulation of stem cell pluripotency. SALL4 is also a critical regulator in reprogramming of somatic cells to pluripotency (**Figure XVII**).

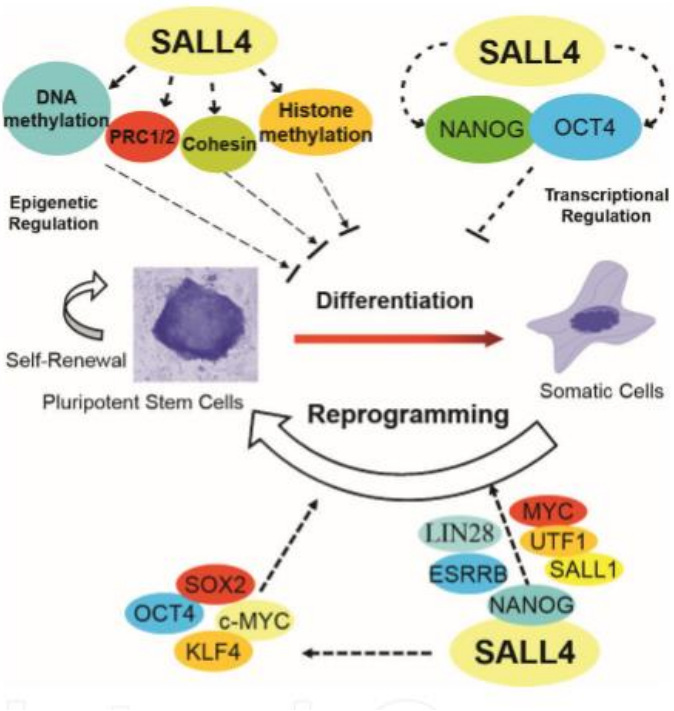

Figure XVII | *SALL4 plays different regulatory functions in maintaining and/or reprogramming cells to pluripotency.* (PRC: polycomb-repressive complex) (Yang, 2018).

In murine development, SALL4 protein expression is first observed at the two-cell stage due to maternal contribution, and later in some cells of the 8- to 16-cell-stage mouse embryo after zygotic transcription has initiated (Elling et al., 2006). In late blastocysts, Sall4 RNA and SALL4 protein become enriched in the inner cell mass (ICM) and the trophectoderm. Finally, by E11.5, SALL4 expression is observed in the midbrain, the rostral edge of the forebrain, maxillary arch, genital tubercle, limb buds, tail and left ventricular myocardium (**Figure XVIII**) (Kohlhase et al., 2002a; Koshiba-Takeuchi et al., 2006). In adult mice, SALL4 expression is mostly restricted to germ cells, wherein it is highly expressed in undifferentiated spermatogonia and oocytes in primordial, primary and secondary follicles (Cao et al., 2009). Similarly, expression of SALL4 in adult human tissue is restricted to the testis and ovary (Kohlhase et al., 2002b) (**Figure XVIII**).

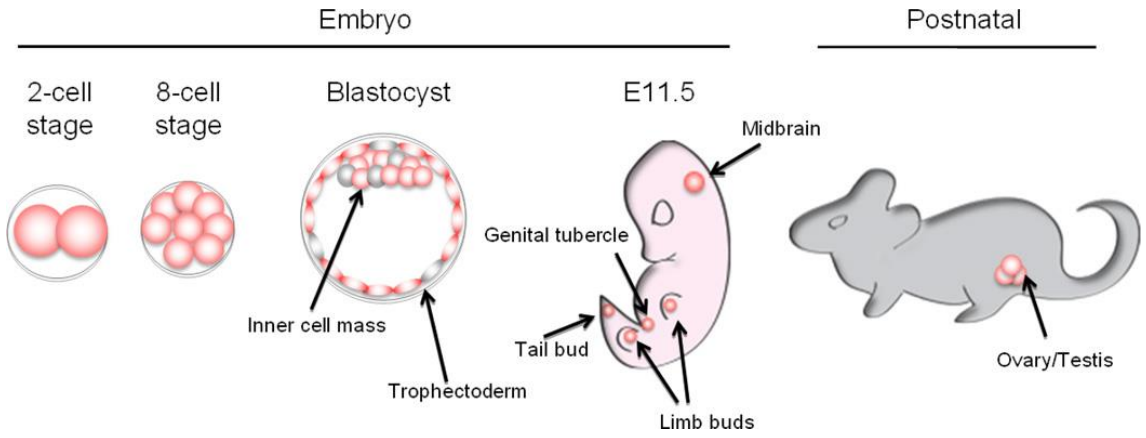

Figure XVIII | *SALL4 expression during development.* SALL4 protein expression is represented by red circles (Tatetsu et al., 2016).

Reduction of SALL4 in oocytes and ESCs results in early embryo defects, and disruption of both Sall4 alleles causes embryonic lethality during peri-implantation (Warren et al., 2007).

1.3.3 | *SALL4 regulates stem cell self-renewal and pluripotency through multiple layers*

The regulation of stem cell self-renewal and pluripotency mediated by SALL4 is first related to the activation of several important signalling pathways in stem cells.

Activation of WNT/β-catenin signalling maintains the pluripotency of human and mouse ESCs (Sato et al., 2004); it has been shown that SALL4 binds β-catenin, thus up-regulating the expression of its target genes (Ma et al., 2006b). Furthermore, STAT3 activation mediates the self-renewal and pluripotency of embryonic stem cells (Niwa et al., 1998) and it is known that SALL4 may interact with STAT3. Also the Hh signalling pathway plays a pivotal role in organogenesis and differentiation during development (Choudhry et al., 2014) and genome-wide analysis reveals that SALL4 regulates Hh pathway (Yang et al., 2008a) preventing the differentiation of embryonic stem cells.

In a second layer of regulation, SALL4 modulates the transcription of key stemness factors including OCT4, NANOG, SOX2 and c-MYC (Wu et al., 2006; Yang et al., 2010). Compared to wild type ESCs, the expression of these 4 genes is remarkably down-regulated in SALL4$^{+/-}$ ESCs (Yang et al., 2008a).

Finally, SALL4 may regulate the expression of key genes associated with stem cell self-renewal and differentiation through epigenetic modulation; indeed this transcription factor induces the activation of Bmi-1, an important regulator of stem cell self-renewal, by mediating H3K4 tri-methylation and H3K79 di-methylation at the promoter region (Yang et al., 2007).

In summary, these findings indicate that SALL4 is involved in regulating self-renewal and pluripotency of stem cells working on different signalling pathways and collaborating with many transcription factors and epigenetic modulators. The great variety of interactors and target genes whose expression is controlled by SALL4 makes the regulation of this transcription factor very fine and, unavoidably, its aberrant expression is associated to tumorigenesis.

1.3.4 | *SALL4 activity in tumor cells*

SALL4 is overexpressed in cancer and affects multiple cellular processes involved in tumorigenesis, tumor growth and progression of different types of cancer.

For example, during normal haematopoiesis SALL4 is expressed in the $CD34^+$ (a marker for pluripotent stem cells) hematopoietic stem cells (HSCs)/hematopoietic progenitor cells (HPCs) population, and its expression is downregulated or silenced in mature blood cells. Conversely, SALL4 is constitutively expressed in human primary acute myeloid leukemia (AML) and myeloid leukemia cell lines. The potential target pathways that SALL4 may affect in leukemogenesis include the activation of WNT/β-catenin signalling. Constitutive expression of SALL4 in AML may enable leukemic blasts to gain stem cell properties thus becoming leukemic stem cells (LSCs). In addition, Bmi-1 (a putative oncogene that modulates stem cell pluripotency and plays a role in leukemogenesis) is identified as a target gene for SALL4 in both hematopoietic and leukemic cells (Yang et al., 2007).

SALL4 acts also as a key regulator of cell proliferation and apoptosis in cancer cells; its knockdown induces massive apoptosis and significant growth arrest in human leukemic cells (Yang et al., 2008b). It has also an important role in the proliferation and survival of chronic myeloid leukemia (CML) cells and its expression is associated with an advanced stage of the disease: SALL4 downregulation leads to cell cycle arrest and apoptosis in CML cells (Lu et al., 2011). Furthermore, SALL4 knockdown leads to growth inhibition of lung, breast cancer and gastric cells as a result of cell cycle arrest (Kobayashi et al., 2011a; Kobayashi et al., 2011b; Zhang et al., 2014). Conversely, SALL4-overexpressing liver cancer cells exhibit enhanced cell proliferation due to the reduction of cell population in G1 consequent to the up-regulation of cyclin D1 and D2 (Oikawa et al., 2013).

SALL4 affects also invasion and migration of cancer cells; its enforced expression up-regulates the levels of Twist1 and N-cadherin, while down-regulates those of E-cadherin promoting the migration of human gastric cancer cells (Zhang et al., 2014).

In addition to its control of transcription, SALL4 regulates gene expression also through epigenetic mechanisms; DNA methylation, histone modification, chromatin remodelling and non-coding RNAs are the four major molecular mechanisms responsible for epigenetic modification. Yang et al. suggest that SALL4 protein directly interacts with DNA methyltransferases (DNMTs), thus repressing transcription (Yang et al., 2012b). In addition, SALL4 co-occupies target gene regulatory regions together with polycomb repressive complex (PRC) (Yang et al., 2008a), thus repressing transcription though the induction of PRC components. Moreover, SALL4 interacts with histone lysine-specific demethylase1 (LSD1) to repress gene transcription in stem cells.

SALL4 does not induce exclusively transcription repression of its target genes, but it also enhances gene expression through the interaction with the histone methyltransferase MLL (Li et al., 2013) and the Mi-2/nucleosome remodeling and deacetylase (NuRD) complex (Lu et al., 2009). Existing data suggest that SALL4 may recruit multiple epigenetic modifiers to synergistically remodel local chromatin structure and coordinately regulate gene transcription (**Figure XIX**).

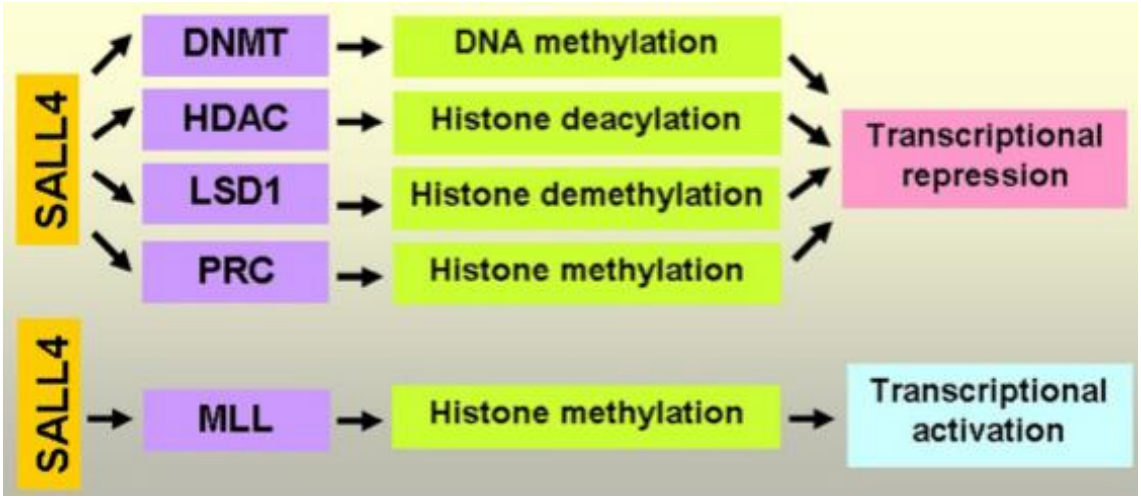

Figure XIX | *SALL4 and epigenetic machinery.* SALL4 represses or activates gene transcription through the interaction with distinct epigenetic modifiers (Zhang et al., 2015).

1.3.5 | SALL4 regulation in cancer

A variety of transcription factors closely linked with tumor development and progression are implicated in SALL4 regulation. For example, multiple STAT3-binding sites have been identified in SALL4 gene promoter region and STAT3 down-regulation remarkably decreases the expression of SALL4 (Bard et al., 2009); this mechanism of regulation is critical for the survival of breast cancer cells. Moreover, SALL4 is a direct transcription target of canonical WNT signalling and it is finely regulated by it (Böhm et al., 2006).

Furthermore, microRNAs modulate SALL4 expression in glioma cells (He et al., 2013); miR-107 overexpression inhibits cell proliferation and induces apoptosis in glioma cells, effects that are reversed by SALL4 reintroduction.

Finally, post-translational modifications regulate SALL4 expression. For example, SALL4B can be modified by both ubiquitylation and sumoylation. It is known so far that only SALL4 sumoylation is functionally important (Yang et al., 2012a): a constitutive sumoylation of SALL4B is readily detectable in teratocarcinoma cells. SUMO-deficiency compromises the trans-activation or trans-repression activities of SALL4B, suggesting that this post-translational modification is tightly important for SALL4 activity.

This synthetic overview of the mechanisms that modulate SALL4 expression and their involvement in different tumor contexts highlights the importance of the regulation of this transcription factor also in tumor contexts in which its role has not yet been elucidated. This was one of the main focus of my Ph. D. project that will be widely discussed below.

1.4 | Aberrant Hedgehog signalling activations are involved in tumorigenesis

The Hh pathway is mostly inactive or poorly active in the adult organism; it can be activated if necessary, for example, in wound healing (Le et al., 2008). Dysfunction or aberrant activation of the Hh signalling is associated with developmental anomalies and cancer; according to the latest estimates, the Hh signalling pathway contributes to the development of ⅓ of all malignant tumors.

There are three mechanisms of aberrant Hh signalling activation identified in different cancer types (**Table I**) (Rubin and de Sauvage, 2006):

- Type I - autonomous and ligand-independent;
- Type II - ligand-dependent in autocrine/juxtacrine manner;
- Type IIIa/b - ligand-dependent in paracrine or reverse paracrine manner.

1.4.1 | Type I – Ligand independent

The first evidence of a link between aberrant Hh signalling and cancer is the rare Gorlin syndrome condition (also known as Naevoid Basal Cell Carcinoma Syndrome or Basal Cell Naevus Syndrome), which is caused by activating mutations in *Ptch* gene. Gorlin syndrome is characterized by developmental anomalies and a distinct post-natal occurrence of cancers, known to be caused also by the aberrant activation of Hh signalling (Johnson et al., 1996; Lo Muzio, 2008). Cancers that arise in patients with Gorlin syndrome include basal cell carcinomas (BCCs) (Dahmane et al., 1997; Johnson et al., 1996), the most common cancer in the Western world, MB (Goodrich et al., 1997; Raffel et al., 1997) and rhabdomyosarcoma (RMS), the most common type of soft tissue cancer in children (Tostar et al., 2006). The tumorigenesis is ligand independent among all these cases: Hh pathway is constitutively activated in the absence of Hh ligand through mutations in its components, including activating mutations in SMO co-receptor and inactivating mutations in PTCH1 (Reifenberger et al., 1998). Mutations in SuFu and GLI2 amplifications were found in children with MB (Ellison et al., 2011; Raffel et al., 1997;

Taylor et al., 2002; Kool et al., 2014). Besides mentioned diseases, LOH or somatic mutations in *Ptch* gene are observed in invasive transitional cell carcinoma of the bladder (McGarvey et al., 1998), esophageal squamous cell carcinoma (Maesawa et al., 1998) and trichoepitheliomas (Vorechovský et al., 1997).

1.4.2 | Type II – Ligand-dependent autocrine/juxtacrine signalling

Hh signalling could also be ligand-dependent autocrine/juxtacrine-activated, a condition that occurs when Hh ligand is profusely released and taken up thus activating the same or surrounding tumor cells. In addition to Hh ligand overexpression, tumors that arise from this condition may display high levels of PTCH1 and GLI1 expression. The use of Hh-neutralizing antibodies (Berman et al., 2003) or Cyclopamine, a known Hh pathway inhibitor, enhances the apoptosis and suppresses the proliferation of tumor cells as well as xenografts tumor growth after treatment, data that strengthen the hypothesis that the Hh pathway could be activated via Hh ligands released by the same or surrounding tumor cells (Mukherjee et al., 2006; Thayer et al., 2003; Varnat et al., 2009).

1.4.3 | Type III – Ligand-dependent paracrine signalling

Hh pathway can be activated through a paracrine secretion in stromal cells as well. In this activation mechanism, Hh ligands released by cancer cells will bind to PTCH1 receptor and switch on the Hh signalling in stromal cells; these cells will secrete paracrine growth signals such as vascular endothelial growth factor (VEGF), insulin-like growth factor (IGF), interleukin-6 (IL-6), WNT, platelet-derived growth factor (PDGF) and bone morphogenetic proteins (BMP) to induce tumor growth (Amakye et al., 2013). For instance, in prostate cancer specimens, the expression of SHH is also detected in the tumor epithelium while GLI1 expression is found in the tumor stromal cells, suggesting that Hh signalling is induced in stromal cells by tumor cells through secreting paracrine signals (Fan et al., 2004). Similarly, the SHH transcript is localized to tumor tissue whereas GLI1 and PTCH1 are detected in both the tumor and the stroma, confirming the

hypothesis that SHH and its target genes act in a paracrine manner to regulate the development of esophageal cancer subsets (Ma et al., 2006a). Moreover, this type of Hh signalling pathway could also work in a reverse paracrine manner, in which cancer cells take up the Hh ligands released by stromal cells; for example, Hh ligands released by bone-marrow, nodal and splenic stroma could activate Hh signalling and maintain the survival of B and plasma cell malignancies (Dierks et al., 2007). Interestingly, it was also demonstrated that intact SHH-producing microenvironment is required for GLI activation in gliomas (Becher et al., 2008).

Table I | *Hh signalling activation in cancer* (Sari et al., 2018).

Type	*Characteristics*	*Cancer Type*
Type I	Ligand independent	Basal cell carcinoma Medulloblastoma (MB) Pediatric brain tumor & Rhabdomyosarcoma
Type II	Ligand-dependent autocrine/juxtacrine signalling	Colorectal Prostate Liver Breast Ovarian Brain Melanoma
Type III	Ligand-dependent paracrine signalling	Pancreatic Leukemia (reverse paracrine)

1.5 | Medulloblastoma

Deregulations of Hh signalling are frequently associated to medulloblastoma onset. Medulloblastoma (MB) is among the most common malignant childhood brain tumors (World Health Organization – WHO – grade IV). The peak age of diagnosis is ~6–8 years, although MB can occur during the first year of life or during adulthood in some individuals.

Initial descriptions of MB date back to Harvey Cushing, who initially depicted MB as a subset of gliomas (**Figure XX**) (Rutka and Hoffman, 1996); he listed many key features of these tumors, like the tendency to arise from the cerebellar vermis and to exhibit leptomeningeal metastasis. Along with neuropathologist Percival Bailey, Cushing described MB histopathologically as containing numerous mitoses, small round nuclei and minimal cytoplasm. The two recognized that MB cells look alike undifferentiated cells present in embryonal stages and defined that MB arise from "medulloblasts," multipotent stem cells thought to be present in the neural tube (Rutka and Hoffman, 1996). Cushing and Percival's foundational work in defining the clinical characteristics and histopathology of this tumor formed our basic understanding of MB (Rutka and Hoffman, 1996).

Some early MB patients were treated with radiation sporadically, but the first landmark change in the management of these tumors came in 1953, when a study of 27 MB patients demonstrated significantly improved survival (approximately 60%) after receiving craniospinal radiation (Rutka and Hoffman, 1996). The addition of cytotoxic chemotherapy regimens as standard of care, starting with trials in the '70s, improved the 5-year survival risk to 70%–80% for average-risk disease, and to 60%–65% for high-risk disease (Bautista et al., 2017).

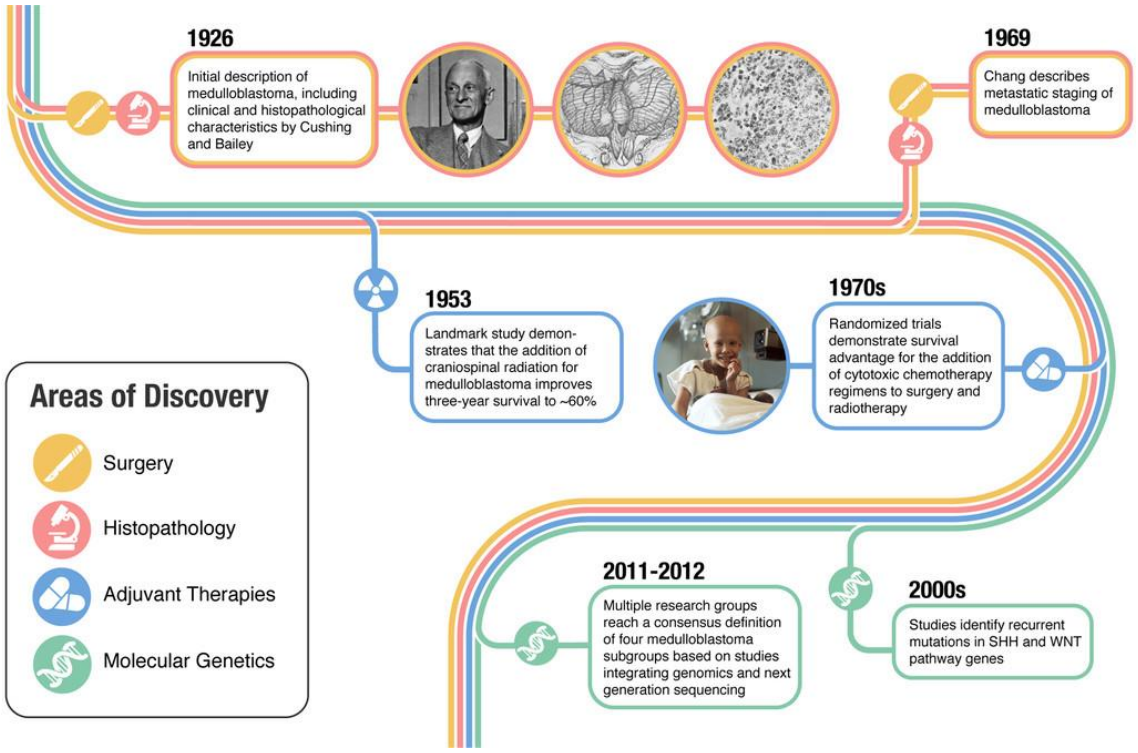

Figure XX | *Timeline of key discoveries in MB*, culminating in the definition of the four molecular subgroups (Juraschka and Taylor, 2019).

Rapid developments in molecular genetics over the past two decades have provided significant advancements in our understanding of MB. Starting with gene expression array studies, this tumor is now considered as a distinct entity from other embryonal central nervous system cancers (Robinson et al., 2012).

Different independent research groups performed transcriptional profiling on MB samples and, in 2012, a consensus (Taylor et al., 2012) on MB subgroups proposed the following designation: Wingless (WNT-MB), Sonic Hedgehog (SHH-MB), Group 3 MB and Group 4 MB (**Figure XXI**). These consensus subgroup definitions have been adopted by both the basic and clinical research communities, changing the way in which MB is diagnosed and managed in the clinic. In 2016, the WHO incorporated consensus MB subgroups into the updated edition of the *Classification of Tumors of the Central Nervous System* (Louis et al., 2016).

	Subgroup	WNT	SHH	Group 3	Group 4
Clinical Characteristics	% of Cases	10	30	25	35
	Age at Diagnosis				
	Gender Ratio (M:F)	1:1	1:1	2:1	3:1
	Anatomic Location				
	Histology	Classic, Rarely LCA	Desmoplastic, Classic, LCA	Classic, LCA	Classic, LCA
	Metastasis at Diagnosis (%)	5-10	15-20	40-45	35-40
	Recurrence Pattern	Rare; Local or metastatic	Local	Metastatic	Metastatic
	Prognosis	Very good	Infants good, others intermediate	Poor	Intermediate
Molecular Characteristics	Proposed Cell of Origin	Progenitor cells in the lower rhombic lip	Granule precursors of the external granule layer	Neural stem cells	Unipolar brush cells
	Recurrent Gene Amplifications	-	*MYCN* *GLI1* or *GLI2*	*MYC* *MYCN* *OTX2*	*SNCAIP* *MYCN* *OTX2* *CDK6*
	Recurrent SNVs	*CTNNB1* *DDX3X* *SMARCA4* *TP53*	*PTCH1* *TERT* *SUFU* *SMO* *TP53*	*SMARCA4* *KBTBD4* *CTDNEP1* *KMT2D*	*KDM6A* *ZMYM3* *KTM2C* *KBTBD4*
	Cytogenetic Events ■ Gain ■ Loss	6	3q, 9p 9q, 10q, 17p	1q, 7, 18 8, 10q, 11, 16q i17q	7, 18q 8, 11p, X i17q
	Other Recurrent Genetic Events	-	-	*GFI1* and *GFI1B* enhancer hijacking	*PRDM6*, *GFI1*, and *GFI1B* enhancer hijacking

Age:  Infant Child Adult

Figure XXI | *The molecular subgroups of MB* (Juraschka and Taylor, 2019).

1.5.1 | *Medulloblastoma subgroups*

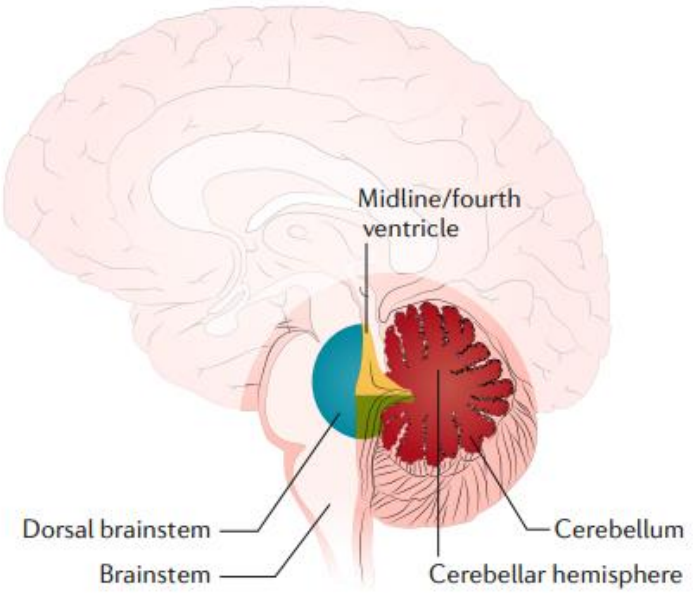

Figure XXII | *Location of MBs*. Sagittal section of the cerebellum and brainstem, with common diagnostic locations of MB indicated on the basis of MRI. WNT-MB location is in blue, SHH-MB in red, Group 3 MB in yellow and Group 4 MB in green (Northcott et al., 2019).

1.5.1.1 | *WNT-MB*

WNT-MBs account for approximately 10% of all MBs (Taylor et al., 2012). These tumors typically occur in children over the age of 4 and adolescents and affect an equal number of males and females (Taylor et al., 2012). The WNT subgroup is associated with an excellent prognosis (> 95% survival at 5 years in pediatric patients), is rarely metastatic at diagnosis (5%–10% of cases) and rarely recurs (Taylor et al., 2012). WNT-MB is thought to arise from progenitor cells in the lower rhombic lip of the developing brainstem (**Figure XXII**) (Veneroni et al., 2017).

Approximately 90% of WNT tumors presents a mutation in CTNNB1, which encodes β-catenin (Northcott et al., 2017). This mutation enhances WNT signalling constitutive activation, driving the expression of target genes that promote tumor proliferation (Taylor et al., 2012). Mutations in the APC tumor suppressor gene account for the majority of WNT tumors lacking CTNNB1 mutations (Taylor et al., 2012). Monosomy 6 is also characteristic of WNT tumors (80%–85% of cases) and typically ovelaps with

CTNNB1 mutations (Northcott et al., 2017); aside from monosomy 6, WNT tumors have balanced genomes and rarely contain copy number aberrations (Northcott et al., 2011).

Recent integrated analysis of DNA methylation, gene expression, copy number alterations and clinical data suggested the existence of further subtypes of MB within each subgroup (Cavalli et al., 2017). Using gene expression and methylation array data, Cavalli et al. suggested the existence of two WNT subtypes: WNT α and WNT β. The WNT α subtype primarily occurs in children and 98% of these cases has monosomy 6, whereas the WNT β subtype occurs in older children and adults and infrequently (29%) has monosomy 6 (**Figure XXIII**) (Cavalli et al., 2017).

1.5.1.2 | SHH-MB

Genetically, the SHH-MB subgroup is among the best understood, with the majority of patients harbouring either germline or somatic mutations and copy-number alterations in critical genes of the Hh signalling pathway. The SHH subgroup has a balanced sex ratio and a bimodal peak age incidence, most often occurring in infants and adults, accounting for ⅔ of MB cases in these age groups; approximately 30% of MBs are classified as SHH tumors (Taylor et al., 2012). They characteristically arise in the cerebellar hemispheres, rather than the midline location characteristic of other subgroups (**Figure XXII**). Outcomes in this subgroup vary according to clinical (age and metastatic status) and molecular (MYCN amplification and TP53 mutation status) characteristics (Ramaswamy et al., 2016). SHH tumors are thought to arise from granule cell precursors of the external granule layer (Vladoiu et al., 2019). The majority of these tumors shows germline or somatic mutations or copy number alterations in the Hh pathway components; these alterations include loss-of-function mutations or deletions in PTCH1 (43% of patients), loss-of-function mutations or deletions in SuFu (10%), activating mutations in SMO (9%), GLI1 or GLI2 amplifications (9%) and MYCN amplifications (7%) (Kool et al., 2014). deregulations of these factors and their related genes lead to the constitutive, ligand-independent, activation of Hh signalling.

Unlike WNT-MB, which is generally considered to be molecularly homogeneous, SHH-MB exhibits biologically and clinically relevant heterogeneity in the form of molecular subtypes (Taylor et al., 2012). These subtypes have different cytogenetics, demographics and overall survival. Recently, four SHH subtypes were described by Cavalli et al. using DNA methylation and gene expression array data sets: SHH α, SHH β, SHH γ and SHH δ. SHH α occurs in childhood and is characterized by frequent TP53 mutations and MYCN/GLI2 amplifications; SHH β occurs in infants, is frequently metastatic and is associated with a poor outcome compared to SHH γ, which also occurs in infants and is associated with MB with extensive nodularity (MBEN) histology. Finally, the SHH δ subtype occurs in adults and is enriched for TERT promoter mutations (**Figure XXII**) (Cavalli et al., 2017).

1.5.1.3 | *Group 3 MB*

High-level MYC amplification is a defining feature of Group 3 MBs; this deregulation occurs in ~17% of patients and is exceedingly rare in other MB subgroups. Group 3 MB has a male predominance and occurs nearly exclusively in infants and young children (Taylor et al., 2012). This subgroup accounts for approximately 25% of all MB cases and is associated with high rates of metastasis at diagnosis (40%–45%) and the worst survival outcomes of any subgroup (under 60% at 5 years) (Taylor et al., 2012). Radiographically, these tumors typically demonstrate a midline vermian location adjacent to the fourth ventricle (**Figure XXII**) (Perreault et al., 2014). Group 3 tumors likely arise from a neural stem cell population (Vladoiu et al., 2019).

Unlike WNT and SHH subgroups, integrated molecular analyses have not identified a common driver pathway that defines the Group 3 and Group 4 subgroups. Recurrent somatic mutations are rare in Group 3 tumors, with only four genes mutated in over 5% of cases (SMARC4, KBTBD4, CTDNEP1 and KMT2D) (Northcott et al., 2017); cytogenetic events are abundant: isochromosome 17q is present in 40%–50% of cases, and other

common events are loss of chromosomes 8, 10q and 16q, gain of 1q, 7 and 18 (Northcott et al., 2017).

Several subgroups classifications for Group 3 MB have emerged; one study outlined high-risk and low-risk subtypes using methylation data, in which the high-risk subgroup featured frequent MYC amplifications in infants and a hypomethylation phenotype (Schwalbe et al., 2017). Cavalli et al. defined three subtypes for Group 3 MB: 3α occurs in infants and is frequently metastatic but associated with a better outcome, 3β occurs in older children and is associated to OTX2 gain, DDX31 loss and high GFI1/GFI1B expression, and 3γ occurs in infants and is associated with high rates of metastasis and MYC amplification (**Figure XXIII**) (Cavalli et al., 2017).

1.5.1.4 | *Group 4 MB*

Group 4 MB accounts for 35%–40% of all MB diagnoses; it typically occurs in childhood and adolescents and more frequently in males (3:1 sex ratio) (Taylor et al., 2012). Anatomically, these tumors typically have a midline vermian location (**Figure XXII**) (Perreault et al., 2014). Although this subgroup is also frequently metastatic (35%–40% at diagnosis), survival outcomes are intermediate and recurrences tend to occur late (Taylor et al., 2012). The cell of origin of Group 4 MB has not been definitively established; however, these tumors appear to have transcription similarities to unipolar brush cells (Vladoiu et al., 2019). Common somatic mutations are also rare in this subgroup, while cytogenetic events include isochromosome 17q, gain of chromosomes 7 and 18q and loss of 8q, 8p, 11p and X (Taylor et al., 2012). High-risk and low-risk subtypes were characterized by Schwalbe et al., in which the high-risk group is enriched for isochromosome 17q and has a 36% 10-year survival, whereas the low-risk group shows chromosome 11 loss and a 72% 10-year survival (Schwalbe et al., 2017). Cavalli et al. divided Group 4 MBs into three subtypes; molecular features associated with these subgroups include MYCN and CDK6 amplifications in Group 4α, SNCAIP duplication in Group 4β and CDK6 amplification in Group 4γ (**Figure XXIII**) (Cavalli et al., 2017).

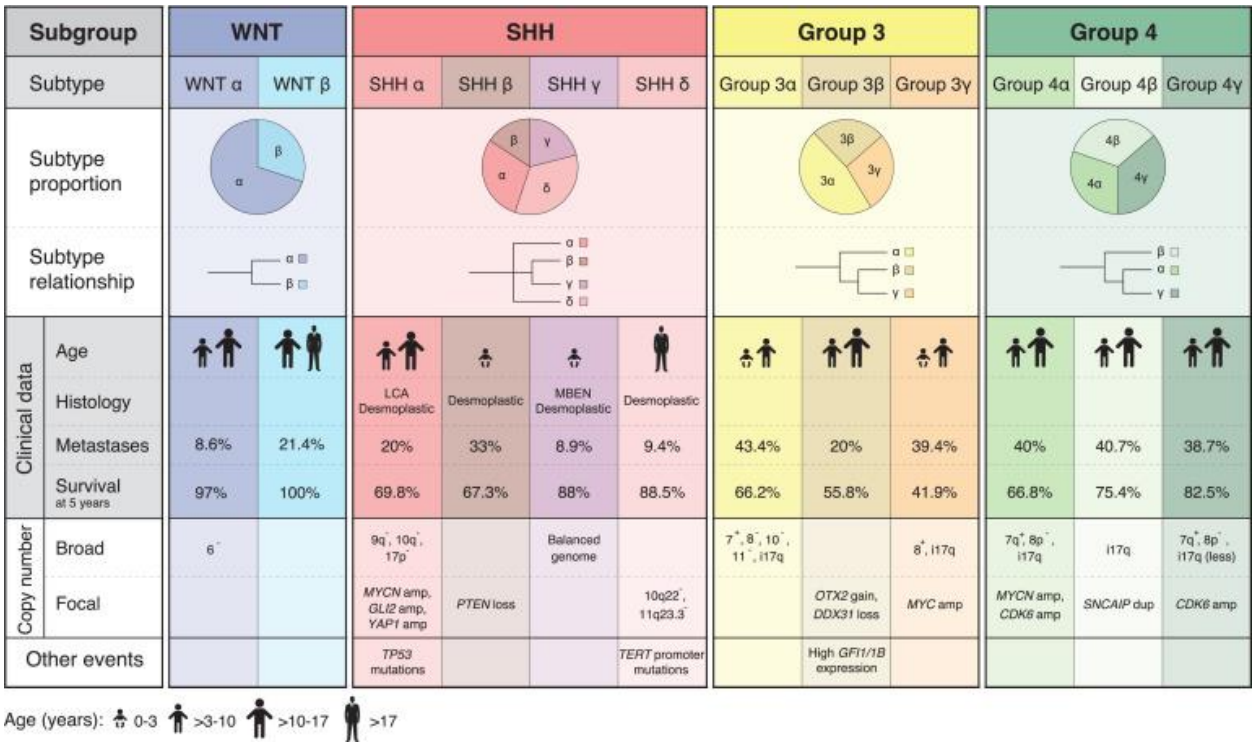

Figure XXIII | *Graphical summary of the 12 MB subtypes.* Schematic representation of key clinical data, copy-number events and relationship between the subtypes inside each of the four MB subgroups. The percentages of patients presenting metastases and the 5-year survival percentages are mentioned. The age groups are: infant 0–3 years, child > 3–10 years, adolescent > 10–17 years and adult > 17 years (Cavalli et al., 2017).

1.5.2 | *Medulloblastoma treatment*

MB is currently treated with maximal safe surgical resection, chemotherapy and craniospinal radiation. Despite such aggressive multimodal therapy, approximately 30% of patients eventually succumb to this disease, and survivors cope with the long-term side effects of treatment that have significant impacts on their quality of life.

Post-operatively radiated patients, in whom a gross total or near total resection is achieved, show a better overall survival compared to patients who undergo biopsy alone (del Charco et al., 1998). Beyond surgical resection, current standards of radiation therapy and medical management vary by extent of disease and age of the patient, based on the risks of recurrence and neurocognitive effects of radiation therapy, respectively.

Despite marked improvements in overall survival for MB patients over the past decades, considerable work remains to be done in order to improve survival within specific patient subgroups as well as to attenuate treatment-related morbidities and to improve quality of life for survivors. In the last decades, a striking increase in our understanding of MB biology, achieved through molecular subgrouping, allowed researchers to better characterize MBs and to improve both prognostic and therapeutic significance. As increased attention is given to post-therapy quality of life and the risk of long-term treatment-related side effects, a substantial goal in oncology research is now focused on the improvement of treatment intensity and the development of novel, less toxic and more efficient agents.

Incorporating targeted therapy into multimodal treatment planning may allow further reduction of radiation dose and cytotoxic chemotherapy with subsequent mitigation of the negative consequences of treatment and improvement of quality of life for MB survivors.

1.5.3 | *Targeting the Hedgehog signalling pathway for medulloblastoma treatment*

Given the increasing evidences supporting the crucial role of the Hh pathway in cancer initiation, progression, metastasis, chemoresistance and in the survival of CSCs (Coni et al., 2013b; Ruiz i Altaba et al., 2002), its components represent attractive druggable targets for anticancer therapy. The first Hh inhibitor discovered was Cyclopamine, a naturally occurring alkaloid isolated from *Veratrum californicum* (Chen et al., 2002) which inactivates SMO by directly binding to its heptahelical bundle. Nevertheless, Cyclopamine has shown several limitations as a drug candidate (such as toxicity and teratogenicity) poor oral bioavailability and suboptimal pharmacokinetics with relatively short elimination half-life (Lipinski et al., 2008).

In recent years, drug discovery efforts directed against the Hh pathway have been focused predominantly on the development of SMO antagonists and a remarkable number of small molecules of natural, semisynthetic or synthetic origin have been developed and extensively reviewed in recent reports (Hadden, 2013; Ruat et al., 2014). Several SMO antagonists have demonstrated efficacy in mouse xenograft models and, most notably, have been investigated in clinical trials against a large range of metastatic and advanced cancers (**Table II**) (Amakye et al., 2013; Ng and Curran, 2011). Among them, Vismodegib (GDC-0449/Erivedge) became the first Hh inhibitor to receive approval from the USA Food and Drug Administration (FDA) in January 2012 for the treatment of locally advanced or metastatic BCC (Dlugosz et al., 2012). Despite the initial enthusiasm, clinical development of SMO antagonists has ultimately proved disappointing due to poor pharmacokinetics, low selectivity on CSCs, severe side effects and the emergence of drug resistance. Indeed, after an initial clinical response to treatment with Vismodegib, a patient with metastatic MB showed tumor regrowth within 3 months due to D473H point mutation in SMO receptor that makes it insensitive to the drug (Yauch et al., 2009). Recently, genomic analysis of SMO resistance to Vismodegib in BCC patients has revealed a number of additional SMO mutations and variants that confer constitutive activity and drug resistance (Atwood et al., 2015; Sharpe et al., 2015).

Several lines of evidence also suggest that cancer cells can acquire resistance to SMO antagonists via SMO-independent hyperactivation of the powerful downstream GLI1 factor, or mutations at different nodal points of the Hh pathway. Moreover, the onset and progression of some types of Hh-driven cancers are related to Hh pathway-activating mutations downstream of SMO, such as loss of SuFu or GLI1 amplification, thus rendering SMO antagonists ineffective in these scenarios. Not least, studies investigating systemic treatments with SMO antagonists have revealed several side effects including dysgeusia, alopecia, fatigue, nausea, diarrhea, decreased appetite, hyponatremia, weight loss and especially muscle cramping due to non-canonical SMO signalling (SMO–AMP-activated protein kinase axis) and Ca^{2+} influx (Tang et al., 2012; Teperino et al., 2012).

Table II | *Overview of SMO antagonists in clinical trials, including the most advanced clinical phase per therapeutic indication.* Data sourced from https://clinicaltrials.gov. *Drugs are considered either alone or in combination with other therapeutic agents (Ghirga et al., 2018).

*Drug name**	*Therapeutic indications*	*Most advanced phase per indication (August 2018)*	*Status*	*Clinicaltrials.gov identifier*
Vismodegib (GDC-0449)	BCC	Phase IV	Recruiting	NCT02436408
	MB	Phase II	Recruiting	NCT01878617
	Keratocystic Odontogenic Tumor	Phase II	Active	NCT02366312
	Locally Advanced BCC; Skin Cancer; Cutaneous Malignancy	Phase II	Recruiting	NCT01835626
	Stomach Neoplasms	Phase II	Recruiting	NCT03052478
	Breast Cancer	Phase II	Recruiting	NCT02694224
	Acute Myeloid Leukemia	Phase II	Recruiting	NCT02073838
	Neoplasms	Phase II	Recruiting	NCT02091141
	Glioblastoma	Phase II	Recruiting	NCT03158389
	Lymphoma, Non-Hodgkin; Multiple Myeloma; Advanced Solid Tumors	Phase II	Recruiting	NCT03297606
Sonidegib (LDE225)	BCC	Phase II	Not yet recruiting	NCT03534947
	Esophageal Cancer	Phase I	Active	NCT02138929

	Recurrent/Refractory Plasma Cell Myeloma	Phase II	Active	NCT02086552
	Pancreatic Cancer	Phase I	Active	NCT01485744
	Resectable Pancreatic Adenocarcinoma	Phase II	Active	NCT01431794
	Hepatocellular Carcinoma; Cirrhosis	Phase I	Active	NCT02151864
Glasdegib (PF04449913)	Glioblastoma	Phase II	Recruiting	NCT03466450
	Acute Myeloid Leukemia	Phase III	Recruiting	NCT03416179
Vitamin D3	BCC; Basal Cell Nevus Syndrome	Phase I	Not yet recruiting	NCT03483441
	Pancreas Cancer	Phase III	Recruiting	NCT03472833
	Acute Myeloid Leukemia	Phase II	Recruiting	NCT02341495
	Chronic Lymphocytic Leukemia; Non-Hodgkin Lymphoma	Phase I	Recruiting	NCT02553447
	Follicular/Small Lymphocytic/Marginal Zone/Mucosal-Associated Lymphoid Tissue Lymphoma	Phase III	Recruiting	NCT03078855
Taladegib (LY2940680)	Esophageal Cancer	Phase II	Active	NCT02530437
	Solid Tumor; Breast Cancer; Colon Cancer; Cholangiocarcinoma; Soft Tissue Sarcoma	Phase I	Recruiting	NCT02784795
LEQ-506	Advanced Solid Tumors; Recurrent/Refractory MB; Locally Advanced/Metastatic BCC	Phase I	Completed	NCT01106508
Itraconazole	BCC	Phase II	Active	NCT02354261
	Advanced/Inoperable Non-Small Cell Lung Cancer	Phase I	Active	NCT02157883
	Prostate Adenocarcinoma	Phase II	Active	NCT01787331
	Neoplasms	Phase I	Active	NCT01772563
	Glioblastoma	Phase I	Active	NCT02770378

Consequently, the development of Hh inhibitors that modulate targets acting downstream of SMO or independently by it, such as molecules acting on GLI1, has recently emerged as a more promising therapeutic strategy for the treatment of Hh-dependent tumor. This approach would allow overcoming anti-SMO resistance and adverse effects, which are responsible for >50% dropouts rates in SMO antagonists clinical trials (**Figure XXIV**).

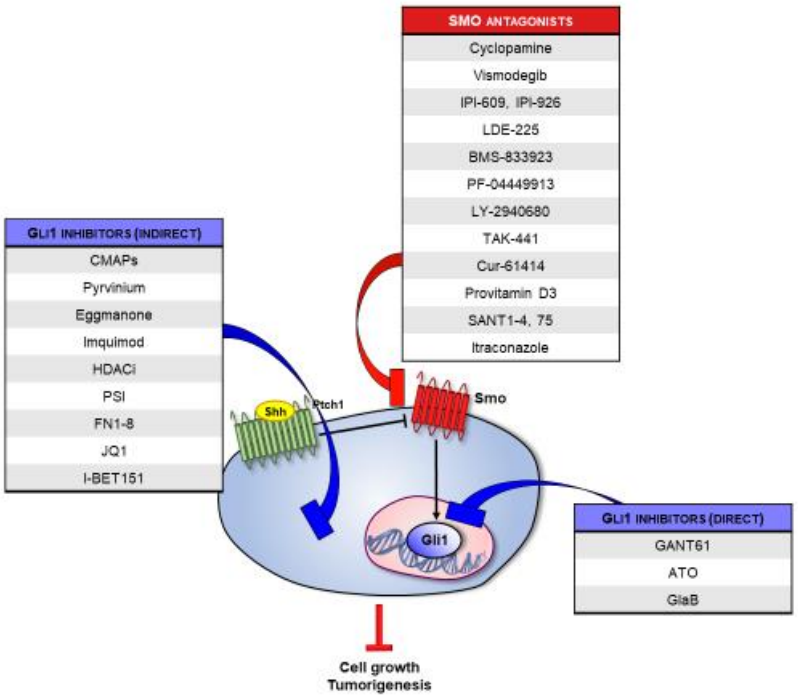

Figure XXIV | *Small molecule as Hh pathway inhibitors and their targets.*

A significant contribution to the discovery of novel Hh inhibitors is given by natural compounds (Bao et al., 2018; Infante et al., 2016; Infante et al., 2015b). Of particular interest is the case of isoflavones, a class of natural compounds mainly occurring in plants of the *Leguminosae* family. The isoflavone nucleus consists of two phenyl rings linked by a propane bridge to form an oxygenated heterocyclic ring, resulting in the typical 15 carbon atoms (C6-C3-C6) skeleton with three rings, labelled A, B and C (**Figure XXV**). Isoflavones have long received attention due to their interesting biological activity and multiple benefits to human health (Ko, 2014). Furthermore, isoflavones emerged as

privileged structures for Hh inhibition in multiple and independent works: the phytoestrogen Genistein (**Figure XXV**) has been first shown in 2010 to inhibit Hh signalling in prostate cancer cells *in vitro* and *in vivo*. In contrast, Daidzein (**Figure XXV**) has been found to suppress GLI1 activation in human breast cancer cells by inhibiting the tumor necrosis factor-α (TNF-α), which is known to activate Hh signalling by enhancing GLI1 nuclear translocation and transcriptional activity (Bao et al., 2014). Recently, by screening a library of natural compounds, our team identified the prenylated isoflavone Glabrescione B (GlaB, **Figure XXV**) as direct inhibitor of GLI1/DNA interaction endowed with significant anticancer efficacy *in vitro* and *in vivo* against Hh-dependent MB and BCC (Infante et al., 2015b) cancers. The mechanism of action of GlaB has been deeply characterized at molecular level, thus pointing to the druggability of GLI1/DNA interaction in the treatment of the Hh-dependent tumors. Moreover, chemical modifications at the ring B of GlaB (**Figure XXV**) proved not effective in Hh inhibition, a data which highlights preliminary structure-activity relationships (SAR) of GlaB and identifies the relevant molecular determinants for the inhibition of GLI1 binding to DNA.

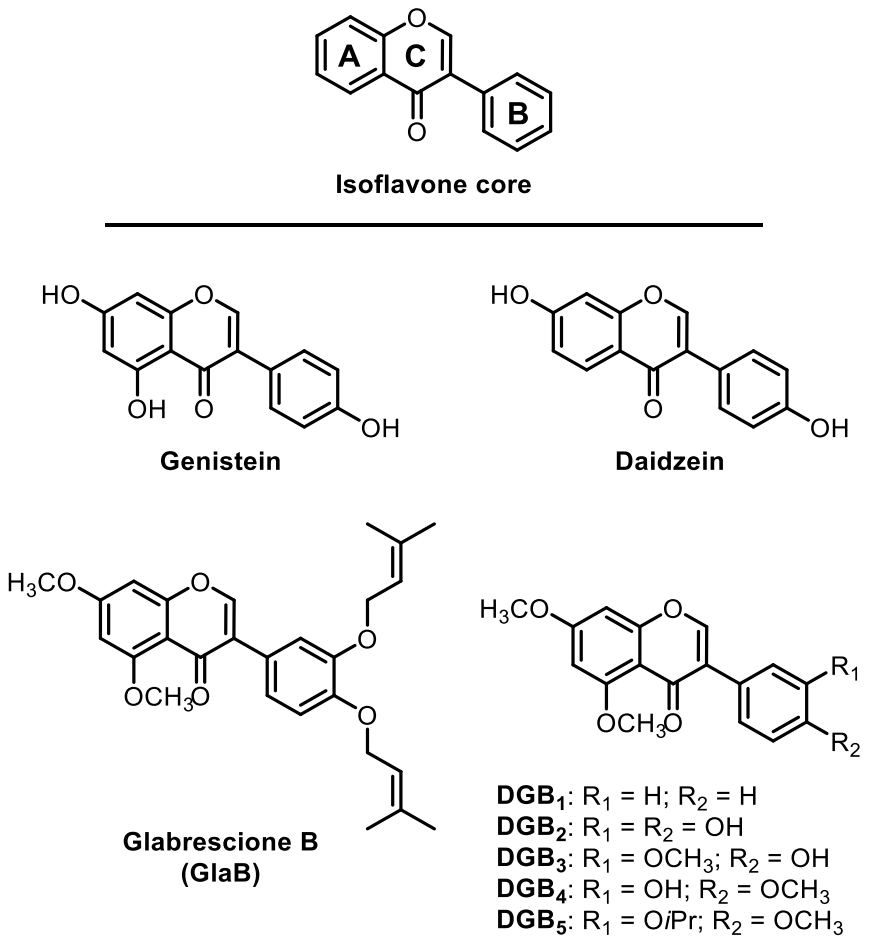

Figure XXV | *Chemical structure of isoflavones that have been previously investigated as Hh inhibitors.* (Berardozzi et al., 2018).

Based on the versatility of the isoflavone scaffold as well as its affinity for the Hh signalling pathway, and taking inspiration from current clinical studies on Hh inhibitors designed to test a combination between a FDA-approved SMO antagonist and cytotoxic anticancer agents (i.e. Sonidegib in combination with Etoposide and Cisplatin, clinicalTrial.gov identifier: NCT01579929), the design of multitarget Hh inhibitors (in particular isoflavones that act both at SMO and GLI1 level according to the fashionable poly-pharmacology principles) could provide synergistic Hh pathway inhibition which might become relevant to overcome drug resistance, particularly at the level of SMO receptor.

2 | AIMS OF THE THESIS

If you know you are on the right track,
if you have this inner knowledge,
then nobody can turn you off.
No matter what they say.
[Barbara McClintock, Nobel Prize in Physiology or Medicine]

Aim 1 | Identification of new molecular mechanisms involved in Hedgehog signalling pathway regulation and medulloblastoma tumorigenesis

The Hh signalling plays a crucial role during organogenesis and stem cells maintenance; its deregulation is responsible for the onset of several human cancers (Briscoe and Thérond, 2013; Caro and Low, 2010; Ramaswamy and Taylor, 2017). Due to its crucial role in tumorigenesis, Hh pathway has emerged as an attractive druggable target and a number of pathway-specific inhibitors are moving into the clinic (Rimkus et al., 2016). However, therapeutic strategies aiming at blocking Hh pathway activation are complicated by the development of resistance and side effects, thus prompting the development of alternative treatment approaches.

The discovery of new molecular routes involved in Hh activation would provide the possibility to target this pathway at multiple layers of regulation, in order to develop multitargeting therapeutic approaches more effective for cancer treatment (Amakye et al., 2013; Di Magno et al., 2015; Infante et al., 2015a). For this reason, the identification of molecular players involve in the control of Hh activity is of clinical importance and represents a dramatic challenge in tumor biology.

To this regard, the first aim of my Ph. D. project can be structured as follows:

- Investigation of the molecular mechanisms that involve Hh signalling key components and whose alterations are implicated in the onset of MB (please refer to Results section ***3.1.1*** **|** ***Itch/β-arrestin2-dependent non-proteolytic ubiquitylation of SuFu controls Hedgehog signalling and medulloblastoma tumorigenesis***);
- Elucidation of the role of two proteins that we identified as new Hh pathway positive regulators, giving them new functions in Hh signalling context: the non-immunological role of the aminopeptidase ERAP1 and the adaptor function of the transcription factor SALL4A in the SALL4A/HDAC1/GLI1 axis (please refer to Results sections ***3.1.2*** **|** ***ERAP1 promotes Hedgehog-dependent tumorigenesis by***

controlling USP47-mediated degradation of βTrCP and **3.1.3** | ***SALL4A/HDAC1/GLI1 axis as a new positive mechanism in Hedgehog signalling regulation***).

Aim 2 | **Pharmacological targeting of Hedgehog pathway**

Pharmacological inhibition of the Hh pathway has been proposed as a therapeutic strategy first in typical Hh-dependent tumors such as advanced BCCs and MBs (Sekulic et al., 2012) and, subsequently, as a potential therapeutic approach in combinatorial treatments for other tumor types (Nowacka-Zawisza and Krajewska, 2013). Although, many Hh-driven human cancers involve upstream pathway activation (i.e. either loss-of-function PTCH1 mutations, gain-of-function SMO mutations or ligand overproduction) (Amakye et al., 2013; Briscoe and Thérond, 2013; Yang et al., 2008c), several tumors harbour SMO-independent increased function of the downstream GLI effectors, due to high protein levels or activating mechanisms, such as *Gli* gene amplification (6-8), *Gli1* chromosomal translocation (Dahlén et al., 2004), GLI2 protein stabilization (Bhatia et al., 2006), mutations in or LOH of the tumor suppressor gene SuFu found in MB (Infante et al., 2018; Kool et al., 2014).

The first-in-class drug in the Hh inhibitors was the SMO antagonist Vismodegib (Erivedge; Genentech) approved for metastatic and advanced BCC (Basset-Seguin et al., 2015); later on, a new drug Sonidegib has also been added in this category. Both drugs targeting the SMO receptor have proven effective in Hh-dependent cancer treatment and phase I/II trials are being conducted in MB and other malignancies (Burness, 2015). Unfortunately, the clinical development of SMO antagonists has failed due to different issues including pharmacokinetics, low selectivity on cancer stem cells or the onset of drug resistance, raising the need for new drugs.

Small molecules have been reported to represent helpful tools to modulate Hh/GLI axis. GLI transcription factors are the final effectors of the Hh pathway and share common

structural features; nevertheless, GLI proteins exert different functions *in vivo*: GLI1 acts only as a transcription activator, whereas GLI2 and GLI3 can act both as transcription activators and as repressors, depending on the specific cell context and on the activation state of Hh signalling. Albeit several aspects of GLI regulation remain unclear, it is evident the key role of GLI in embryogenesis and adult homeostasis, as well as the importance of its deregulation that could clearly lead to unfavourable developmental and pathological consequences, such as oncogenesis. It is important to consider that, whatever alteration leads to aberrant Hh pathway activation, all trigger the downstream effector GLI1. For this reason, GLI factors are emerging as attractive targets for the development of novel anticancer drugs. However only a few GLI antagonists have been identified, most likely due to the lack of structural details related to GLI activity.

To this regard, the second aim of my Ph. D. project can be structured as follows:

- Explanation of the mechanism and kinetics of GANT61 (Gli-ANTagonist 61, the first small molecule identified as GLI1 inhibitor) hydrolysis in order to complement the knowledge about the mechanism of action of this reference Hh signalling inhibitor (please refer to Results section ***3.2.1*** | ***Chemical, computational and functional insights into the chemical stability of the Hedgehog pathway inhibitor GANT61***);
- Deepening, in collaboration with Prof. Bruno Botta team (Department of Chemistry and Technology of Drugs, Sapienza University), of GlaB structure (the first small molecule that works as Hh inhibitor binding directly GLI1 and inhibiting its interaction with DNA) in order to modify its isoflavonic backbone by adding specific substituents in the ring B that make the molecule more suitable for SMO and GLI1 interaction. We synthesized an individual molecule able to bind and to inhibit the activity of both SMO receptor and GLI1 transcription factor simultaneously, targeting and impairing the activity of Hh pathway acting both at upstream and downstream level (please refer to Results section ***3.2.2*** | ***A Smo/Gli Multitarget Hedgehog Pathway Inhibitor Impairs Tumor Growth***).

3 | RESULTS

I am among those who think that science has great beauty.
A scientist in his laboratory is not only a technician:
he is also a child placed before natural phenomena which impress him like a fairy tale.
[Marie Curie, Nobel Prize in Physics and Chemistry]

3.1 | Aim 1: Identification of new molecular mechanisms involved in Hedgehog pathway regulation and medulloblastoma tumorigenesis

3.1.1 | Itch/β-arrestin2-dependent non-proteolytic ubiquitylation of SuFu controls Hedgehog signalling and medulloblastoma tumorigenesis

The tumor suppressor SuFu is a negative regulator of Hh signalling (Aberger and Ruiz I Altaba, 2014; Briscoe and Thérond, 2013; Ingham and McMahon, 2001); it is required for mouse embryonic development (Cooper et al., 2005; Svärd et al., 2006) and its genetic inactivation causes early embryonic lethality at E9.5 with neural tube defects. In humans, SuFu mutations are associated with Gorlin's syndrome, a hereditary condition characterised by increased risk of developing different forms of tumors, such as BCC and MB (Kijima et al., 2012; Pastorino et al., 2009). Moreover, SuFu is mutated either in the germline or somatically in patients with SHH-MB (Brugières et al., 2010; Pastorino et al., 2009). Despite the central role of SuFu in controlling Hh pathway and its relevance for Hh-dependent tumorigenesis, little information regarding the mechanisms that control its activity are available. Moreover, in the last years SuFu-GLI3 complex has emerged as a major control node in Hh signalling, but how the integrity of this complex is maintained is still poorly understood.

Post-translational modifications, such as phosphorylation and ubiquitylation, affect SuFu stability; in particular, ubiquitin-dependent events have emerged as crucial mechanisms by which stability, activity or localisation of GLI proteins are controlled (Gulino et al., 2012). Ubiquitylation is a relevant mechanism to regulate protein degradation (Ciechanover et al., 2000), but it is also required for a variety of non-proteolytic functions.

During my Ph. D., I contributed to the identification of a new mechanism involved in SuFu regulation; our data show that the HECT E3-ubiquitin ligase Itch ubiquitylates SuFu through K63-mediated linkages. Itch/β-arrestin2-dependent K63-linked poly-ubiquitylation of SuFu on K321 and K457 does not lead SuFu to degradation, but increases the association of SuFu with GLI3 thus driving the generation of GLI3R, which in turn inhibits Hh signal transduction.

Interestingly, we show that the Itch-induced non-proteolytic ubiquitylation of SuFu is regulated by the adaptor β-arrestin2, a member of the arrestin protein family involved in numerous key physiological processes and in tumor progression (Hu et al., 2013; Kohout and Lefkowitz, 2003; Philipp et al., 2013). β-Arrestins have been described to have signalling functions, serve as scaffolds by regulating the internalisation of various types of receptors or allow E3-ubiquitin ligase recruitment (Kovacs et al., 2008). We demonstrated that expression of β-arrestin2 increases Itch/SuFu interaction and enhances Itch-dependent ubiquitylation of SuFu. Biochemical data also demonstrate that βarrestin2, Itch and SuFu form a trimeric complex that is promptly dissociated in response to Hh activation.

Germline and somatic mutations in SuFu are a feature of the SHH-MB subgroup and alter SuFu repressor functions. Kool et al. recently reported the genome sequencing of the largest series to date of SHH-MBs. Interestingly, this group identified two novel non-sense SuFu mutations (Y424X and W430X, Kool et al., 2014), both lacking lysine 457, a residue that we identify as required for the Itch-dependent ubiquitylation of SuFu. These mutations encode truncated proteins that maintain GLI consensus, but are unable to be ubiquitylated by Itch, thus hampering SuFu ability to inhibit MB cell growth.

These findings support our model in which the impairment of SuFu ubiquitylation is implicated in MB oncogenesis. In conclusion, the Itch-dependent non-proteolytic ubiquitylation of SuFu identified in our study represents a novel mechanism that inhibits the Hh signalling pathway and indicates that alterations of this process, caused by SuFu mutations that make it insensitive to Itch-mediated ubiquitylation, contribute to the pathogenesis of MB.

Since this work has been published, I only provided a brief outline of obtained results. Please refer to the paper attached below[1] for more detailed evaluation.

[1]Infante, P.*, Faedda, R.*, Bernardi, F.*, Bufalieri, F., **Lospinoso Severini, L.**, Alfonsi, R., ... & Petroni, M. (**2018**). Itch/β-arrestin2-dependent non-proteolytic ubiquitylation of SuFu controls Hedgehog signalling and medulloblastoma tumorigenesis. **Nature communications**, 9(1), 976.

nature COMMUNICATIONS

ARTICLE

DOI: 10.1038/s41467-018-03339-0 OPEN

Itch/β-arrestin2-dependent non-proteolytic ubiquitylation of SuFu controls Hedgehog signalling and medulloblastoma tumorigenesis

Paola Infante[1], Roberta Faedda[2], Flavia Bernardi[2], Francesca Bufalieri[2], Ludovica Lospinoso Severini[2], Romina Alfonsi[2], Daniela Mazzà[2], Mariangela Siler[2], Sonia Coni[2], Agnese Po[2], Marialaura Petroni[1], Elisabetta Ferretti[3], Mattia Mori[1], Enrico De Smaele[3], Gianluca Canettieri[2,4], Carlo Capalbo[2], Marella Maroder[5], Isabella Screpanti[2], Marcel Kool[6,7], Stefan M. Pfister[6,7,8], Daniele Guardavaccaro[9], Alberto Gulino[2] & Lucia Di Marcotullio[2,4]

Suppressor of Fused (SuFu), a tumour suppressor mutated in medulloblastoma, is a central player of Hh signalling, a pathway crucial for development and deregulated in cancer. Although the control of Gli transcription factors by SuFu is critical in Hh signalling, our understanding of the mechanism regulating this key event remains limited. Here, we show that the Itch/β-arrestin2 complex binds SuFu and induces its Lys63-linked polyubiquitylation without affecting its stability. This process increases the association of SuFu with Gli3, promoting the conversion of Gli3 into a repressor, which keeps Hh signalling off. Activation of Hh signalling antagonises the Itch-dependent polyubiquitylation of SuFu. Notably, different SuFu mutations occurring in medulloblastoma patients are insensitive to Itch activity, thus leading to deregulated Hh signalling and enhancing medulloblastoma cell growth. Our findings uncover mechanisms controlling the tumour suppressive functions of SuFu and reveal that their alterations are implicated in medulloblastoma tumorigenesis.

[1] Center for Life NanoScience@Sapienza, Istituto Italiano di Tecnologia, 00161 Rome, Italy. [2] Department of Molecular Medicine, University La Sapienza, 00161 Rome, Italy. [3] Department of Experimental Medicine, University La Sapienza, 00161 Rome, Italy. [4] Istituto Pasteur-Fondazione Cenci Bolognetti, University La Sapienza, 00161 Rome, Italy. [5] Department of Medico-Surgical Sciences and Biotechnologies, University La Sapienza, 00161 Rome, Italy. [6] Hopp Children's Cancer Center at the NCT (KiTZ), 69120 Heidelberg, Germany. [7] Division of Pediatric Neurooncology, German Cancer Research Center (DKFZ) and German Cancer Consortium (DKTK), 69120 Heidelberg, Germany. [8] Department of Pediatric Hematology and Oncology, Heidelberg University Hospital, 69120 Heidelberg, Germany. [9] Hubrecht Institute-KNAW and University Medical Center Utrecht, 3584CT Utrecht, The Netherlands. These authors contributed equally: Paola Infante, Roberta Faedda, Flavia Bernardi. Correspondence and requests for materials should be addressed to L.D.M. (email: lucia.dimarcotullio@uniroma1.it)

Suppressor of Fused *(SuFu)* is a tumour suppressor gene and negative regulator of Hedgehog (Hh) signalling, a conserved developmental pathway crucial for tissue patterning, stem cell maintenance, and tumorigenesis[1–3]. The SuFu protein is localised to both the nucleus and the cytoplasm and controls the Hh pathway by binding directly to Gli transcription factors, the final effectors of Hh signalling[4,5]. Three Gli proteins have been identified in mammals: Gli1 functions exclusively as a transcriptional activator, whereas Gli2 and Gli3 exist in both full-length (FL) activator and truncated repressor (R) forms. Recently, SuFu has emerged as essential for the stabilisation of Gli2FL and Gli3FL[6], protecting them from degradation by the E3 ubiquitin ligase SPOP. In this context, SuFu regulates the formation of either the repressor or activator forms of Gli3. In the absence of Hh signalling, SuFu restrains Gli3 in the cytoplasm, promoting its processing into the repressor form (Gli3R). Initiation of signalling induces the dissociation of SuFu from Gli3, preventing the formation of Gli3R. This event allows Gli3 to enter the nucleus, where it is converted into a labile transcriptional activator[7]. However, the mechanism by which the SuFu–Gli interaction is controlled remains poorly understood.

SuFu is required for mouse embryonic development[8,9]. Its genetic inactivation leading to constitutive activation of the Hh pathway in a ligand-independent manner causes early embryonic lethality at E9.5 with neural tube defects. In humans, SuFu mutations are associated with Gorlin's syndrome, a hereditary condition characterised by increased risk of developing various forms of tumours, such as basal cell carcinoma and medulloblastoma (MB)[10–12]. Moreover, SuFu is mutated either in the germline or somatically in patients with Sonic hedgehog medulloblastoma (Shh-MB)[10,12–17], a childhood brain tumour associated with Hh signalling aberrations. Despite the central role of SuFu in controlling Hh pathway and its relevance for Hh-dependent tumorigenesis, little information regarding the mechanisms that control its activity is available.

Post-translational modifications, such as phosphorylation and ubiquitylation, affect SuFu stability. Indeed, Shh signalling promotes ubiquitylation of SuFu leading to its proteasomal degradation[18]. This process is opposed by SuFu phosphorylation by glycogen synthase kinase-3β (GSK3β) and cyclic adenosine monophosphate (cAMP)-dependent protein kinase A (PKA) that induce SuFu stabilisation[19]. By means of an enzymatic cascade involving an activating enzyme (E1), a conjugating enzyme (E2), and a ligase (E3) that determines substrate selectivity, ubiquitin is transferred to substrate proteins, generally inducing their degradation by the 26S proteasome[20,21]. Ubiquitin-dependent events have emerged as crucial mechanisms by which stability, activity, or localisation of Gli proteins are controlled[3,22,23]. Gli ubiquitylation is mediated by E3 ligases belonging to the RING-Cullin family, such as Cullin1-Slimb/βTrCP and Cullin3-HIB/Roadkill/SPOP[24–26], and the HECT family, such as Itch[27,28], as well as by PCAF (P300/CBP-associated factor), a histone acetyltransferase protein with E3 ubiquitin ligase activity[29,30]. Ubiquitylation promoted by these E3 ligases lead to either proteasome-dependent proteolytic cleavage of the Gli2 and Gli3 factors[25,26] or degradation of Gli1[24,27,28]. Although ubiquitylation is a relevant mechanism to control protein degradation[21], it is also required for a variety of non-proteolytic functions.

Here, we identify a new mechanism of regulation of SuFu. We show that the HECT E3 ubiquitin ligase Itch, in complex with the adaptor protein β-arrestin2, binds SuFu and promotes its K63-linked ubiquitylation. This event does not affect SuFu stability. Rather, Itch-mediated ubiquitylation of SuFu facilitates the formation of the SuFu/Gli3 complex, increasing the stability of Gli3FL and, consequently, the amount of Gli3R, thus keeping the Hh pathway off. Moreover, we demonstrate that the Itch-dependent ubiquitylation of SuFu has a key protective role in MB oncogenesis.

Results

The E3 ubiquitin ligase Itch promotes SuFu ubiquitylation. To identify the molecular mechanisms controlling SuFu activity, we set out to investigate the role of ubiquitylation in the regulation of SuFu. First, we tested whether SuFu can be targeted for ubiquitylation by E3 ubiquitin ligases known to modulate Hh signalling, namely Itch, Nedd4 (HECT E3s), $SCF^{\beta TrCP}$, $CRL3^{SPOP}$, $CRL3^{REN}$, and $CRL3^{KCTD21}$ (Cullin-RING E3s). We found that only Itch was able to ubiquitylate SuFu (Fig. 1a and Supplementary Fig. 1a, b) in cultured cells. Accordingly, increasing amounts of Itch induced a progressive increase in the ubiquitylation of endogenous SuFu (Fig. 1b), while no effect was observed with other HECT E3 ligases (Supplementary Fig. 1a, b). To determine whether SuFu interacts with Itch, we carried out co-immunoprecipitation experiments and demonstrated that Itch interacts with both exogenous (Fig. 1c) and endogenous SuFu (Fig. 1d) in cultured cells. Direct interaction between GST-Itch and in vitro translated [^{35}S]-labelled SuFu, as well as between recombinant Itch and GST-SuFu, was also demonstrated by in vitro pull-down assays (Fig. 1e, f). The modular structural organisation of Itch consists of an N-terminal Ca^{2+}-dependent phospholipid-binding C2 domain, four WW domains implicated in multiple protein–protein interactions, and a C-terminal catalytic HECT domain (Fig. 1g). To identify the specific domains of Itch involved in the interaction with SuFu, we performed glutathione *S*-transferase (GST) pull-down assays using in vitro transcribed/translated SuFu and different GST-Itch proteins containing only the HECT catalytic domain, the four WW domains, or single WW domains (WW1, WW2, WW3, WW4). We found that the WW1 and WW2 domains of Itch, but not WW3, WW4, or the HECT domain, directly bind to SuFu (Fig. 1h–j).

Itch ubiquitylates SuFu by K63 linkage. We next investigated the ability of Itch to ubiquitylate SuFu both in vivo and in vitro. In cultured cells, ectopic expression of Itch, but not of the catalytically inactive ItchC830A mutant, induced the ubiquitylation of endogenous SuFu (Fig. 2a). Moreover, $Itch^{-/-}$ mouse embryonic fibroblasts (MEFs) displayed decreased ubiquitylation of endogenous SuFu when compared to wild-type MEFs (Fig. 2b). SuFu ubiquitylation was rescued by wild-type Itch, but not by its catalytically inactive mutant (ItchC830A) (Fig. 2b).

The Itch-dependent ubiquitylation of SuFu was confirmed in vitro. We used purified recombinant Itch in a reconstituted in vitro ubiquitylation system containing ubiquitin, E1, E2 (UbcH7), adenosine triphosphate (ATP), and in vitro synthesised radiolabelled [^{35}S] SuFu as substrate. High levels of SuFu ubiquitylation were observed in the presence of recombinant Itch (Fig. 2c), whereas a SuFu mutant in which all lysine residues were mutated to arginine (SuFu K-less) was not ubiquitylated (Fig. 2d).

To identify the specific lysine residues of SuFu that are ubiquitylated by Itch, we assessed the Itch-dependent ubiquitylation of SuFu mutated in lysine 257, 321, or 457, previously described as direct (K257) or potential (K321 and K457) SuFu ubiquitylation sites[18,31] (Fig. 2e). We observed a significant reduction in the ubiquitylation of SuFuK321R and SuFuK457R mutants, as well as the SuFuK321/457R mutant, when compared to ubiquitylation of wild-type SuFu (Fig. 2f, g and Supplementary Fig. 2). No decrease was observed in the Itch-mediated ubiquitylation of SuFu when lysine 257, previously identified as a ubiquitin acceptor site that induces SuFu proteasomal

degradation[18], was replaced by arginine (K257R) (Supplementary Fig. 2). Overall, these results indicate that Itch ubiquitylates SuFu on lysines 321 and 457.

To determine if Itch-induced ubiquitylation of SuFu primes it for proteasomal degradation, we examined the effect of the proteasome inhibitor MG132 on this event. As shown in Fig. 2h, proteasome inhibition did not cause accumulation of the Itch-dependent ubiquitylation of SuFu. Accordingly, ectopic expression of increasing amounts of Itch or its depletion by RNA interference did not result in any change in the exogenous or endogenous SuFu protein levels, indicating that the Itch-dependent ubiquitylation of SuFu does not lead to SuFu degradation (Fig. 2i–k). Similarly, no changes in the half-life of SuFu were observed in Itch$^{-/-}$ MEFs compared to wild-type MEFs (Fig. 2l).

Next, we analysed the molecular mechanism by which Itch ligates ubiquitin to SuFu. An in vitro ubiquitylation assay performed in the presence of in vitro transcribed/translated SuFu, GST-Itch, and ubiquitin (wild type or mutant) showed that Itch polyubiquitylates SuFu through lysine 63- but not lysine 48-

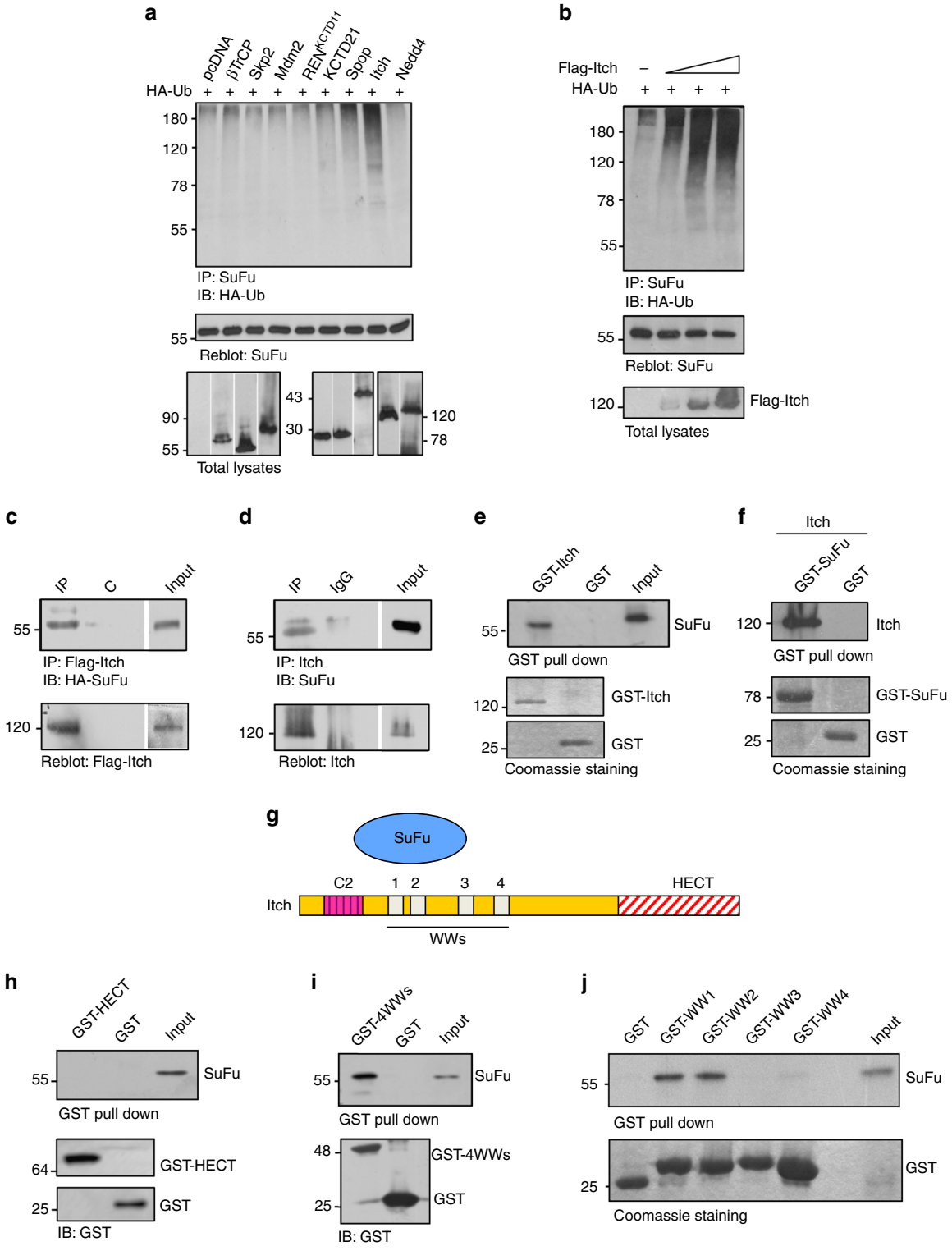

mediated linkages. Indeed, while a ubiquitin mutant in which K48 is replaced by arginine (K48R) was efficiently ligated to SuFu by Itch, a ubiquitin mutant in which K63 is replaced by arginine (K63R) was not linked to SuFu and showed a reduced formation of high polyubiquitin chains and a pattern similar to the one observed in the presence of the K-less ubiquitin mutant, in which all lysine residues are mutated. Accordingly, the ubiquitin mutant containing only lysine 63 (K63O), but not the ubiquitin mutant containing only lysine 48 (K48O), was efficiently ligated to SuFu by Itch, similarly to wild-type ubiquitin (Fig. 2m). Similar results were obtained in in vivo ubiquitylation assays in which the ectopic expression of K63R ubiquitin, but not of the K48R ubiquitin mutant, strongly reduced the Itch-dependent ubiquitylation of SuFu (Supplementary Fig. 3). Taken together, these results indicate that Itch catalyzes the assembly of K63-linked polyubiquitin chains on SuFu and does not target SuFu for degradation.

Itch-mediated SuFu ubiquitylation affects SuFu–Gli3 interaction. K63-linked polyubiquitin chains are thought to serve a scaffolding function for signalling proteins and positively regulate protein complex formation[32]. We hypothesised that the Itch-mediated K63-linked polyubiquitylation could regulate the interaction of SuFu with Gli factors, the final effectors of the Hh pathway. SuFu is known to bind and protect Gli3 from SPOP-mediated degradation, favouring the generation of a cleaved form (Gli3R) that has nuclear repressor activity on Hh-dependent gene expression[7,33].

To determine whether the Itch-dependent ubiquitylation of SuFu increases the association between SuFu and Gli3, we examined the ability of the SuFuK321/457R mutant to interact with Gli3. To this regard we carried out a NanoLucR Binary Technology (NanoBiT) assay, a two-subunit system based on NanoLucR luciferase used for intracellular detection of protein–protein interactions[34,35]. We fused Gli3 and SuFu WT or the SuFuK321/457R mutant protein to Small BiT (SmBiT) or Large BiT (LgBiT) subunits, respectively. The interaction of fusion partners leads to structural complementation of LgBiT with SmBiT, generating a luminescent signal that is a read-out of binding strength. As shown in Fig. 3a, we observed a significant reduction of luminescence when we overexpressed Gli3-SmBiT and SuFuK321/457R-LgBiT mutant compared to wild-type SuFu-LgBiT, demonstrating a decreased association of Gli3 with SuFuK321/457R mutant. Of note, the expression of Itch was able to increase the interaction of Gli3-SmBiT with wild-type SuFu-LgBiT, but not with the SuFuK321/457R-LgBiT mutant.

The effect of Itch-dependent ubiquitylation of SuFu on the formation of the SuFu/Gli3 complex was then tested by immunoprecipitation. Endogenous Gli3 was immunoprecipitated from cells expressing wild-type SuFu or the SuFuK321/457R mutant. The SuFuK321/457R mutant displayed a decreased ability to bind Gli3 when compared to wild-type SuFu, as measured by the absolute levels of SuFu coimmunoprecipitated with Gli3 and by the SuFu/Gli3 ratio (Fig. 3b, c). In agreement with this result, the formation of the SuFu/Gli3 complex was affected by Itch modulation. While Itch depletion by RNA interference caused a reduction of the SuFu/Gli3 interaction (Fig. 3d, e), expression of Itch in Itch$^{-/-}$ MEFs led to increased formation of the SuFu/Gli3 complex (Fig. 3f, g).

To monitor the possible structural consequence of the K321/457R mutation in SuFu, as well as its impact on Gli3 binding affinity, we performed computational studies based on molecular dynamics (MD) simulations and free energy of binding calculations. To this aim, we used the available crystallographic structure of SuFu in complex with a Gli3 peptide (PDB ID: 4BLD) that well represents a static snapshot of the SuFu/Gli3 interaction at high resolution (2.8 Å). The results from this study indicate that the interaction between Gli3 and SuFu is not expected to be impaired by the K321/457R mutation of SuFu at either the structural or thermodynamic level (Supplementary Fig. 4).

We also demonstrated by immunoprecipitation followed by re-immunoprecipitation experiments that SuFu co-purifying with Gli3 is ubiquitylated (Fig. 3h) and that the strong ubiquitylation of SuFu observed in the presence of both Gli3 and Itch was associated with an increased interaction of SuFu with Gli3 (Fig. 3i).

Next, we addressed the role of the Itch-dependent ubiquitylation of SuFu in the regulation of Gli3. As shown in Fig. 3j, in SuFu$^{-/-}$ MEFs the steady-state levels of Gli3FL and Gli3R were higher after the expression of wild-type SuFu than after the expression of the SuFuK321/457R mutant or in control cells. Moreover, in SuFu$^{-/-}$ MEFs the half-life of Gli3FL was significantly shorter after expression of the SuFuK321/457R mutant than after expression of wild-type SuFu (Fig. 3k). In agreement with the finding that SuFu potentiates the formation of Gli3R by controlling the rate of Gli3R production and not the rate of its degradation[7], we found that the half-life of Gli3R remained unchanged. Accordingly, the expression of the SuFuK321/457R mutant resulted in a reduction of Gli3FL and of the Gli3R nuclear fraction when compared to Gli3FL and of the Gli3R nuclear fraction present after the expression of wild-type SuFu (Fig. 3l). The stability of Gli3 was also investigated in response to modulation of Itch. As shown in Fig. 3m, the steady-state levels of Gli3FL and Gli3R were lower after the knockdown of Itch when compared to the ones in control cells. In agreement with this result, the expression of Itch, but not of the ItchC830A mutant, in Itch$^{-/-}$ MEFs led to an increase of Gli3FL stability (Fig. 3n). These data strongly suggest the role of Itch-mediated ubiquitylation of SuFu in

Fig. 1 Itch ubiquitylates and binds SuFu. **a**, **b** HEK293T cells were transfected with plasmids expressing HA-ubiquitin (HA-Ub) in the presence of different E3 ubiquitin ligases (**a**) or increasing amount of Flag-Itch (**b**). Cell lysates were immunoprecipitated with an anti-SuFu antibody, and ubiquitylated forms were revealed with an anti-HA antibody. **c** HEK293T cells were co-transfected with Flag-Itch and HA-SuFu as indicated. Interaction between Itch and SuFu was detected by immunoprecipitation (IP) followed by immunoblot (IB) analysis with the indicated antibodies. **d** Interaction between endogenous Itch and SuFu was detected in HEK293T cells by immunoprecipitation followed by immunoblot analysis with the indicated antibodies. **e** GST-Itch was bound to glutathione-sepharose beads and used for in vitro pull-down assay. In vitro translated ^{35}S-labelled SuFu was incubated with free GST control or GST-Itch. After GST pull-down, the protein complex was detected by fluorography. Coomassie blue staining shows the expression levels of recombinant proteins GST-Itch or GST only. **f** GST-SuFu was bound to glutathione-sepharose beads and used for in vitro pull-down assay. Untagged Itch recombinant protein was incubated with free GST control or GST-SuFu. After GST pull-down, the protein–protein interaction was detected by IB with an anti-Itch antibody. Coomassie blue staining shows the expression levels of recombinant proteins GST-SuFu or GST only. **g** Schematic representation of Itch and its interaction with SuFu. **h**, **i** GST-HECT (**h**) or GST-4WWs (**i**) were bound to glutathione-sepharose beads and used for in vitro pull-down assay with in vitro translated ^{35}S-labelled SuFu. After GST pull-down, protein complexes were analysed by IB. **j** A GST pull-down assay with GST-WW1, -WW2, -WW3, or -WW4 and in vitro translated ^{35}S-labelled SuFu was carried out as described in **e**

the formation of SuFu/Gli3 complex leading to an increase of Gli3FL stability, and consequently of the Gli3R amount.

Next, we tested whether SuFu ubiquitylation is involved in the negative regulation of Hh-dependent gene expression. Figure 3o shows that overexpression of Gli3 and wild-type SuFu in SuFu$^{-/-}$ MEFs caused a significant reduction of the messenger RNA (mRNA) levels of Hh target genes. This effect was rescued in the presence of SuFuK321/457R mutant, indicating that Itch-dependent SuFu ubiquitylation is relevant for the suppressive function of SuFu in Hh signalling.

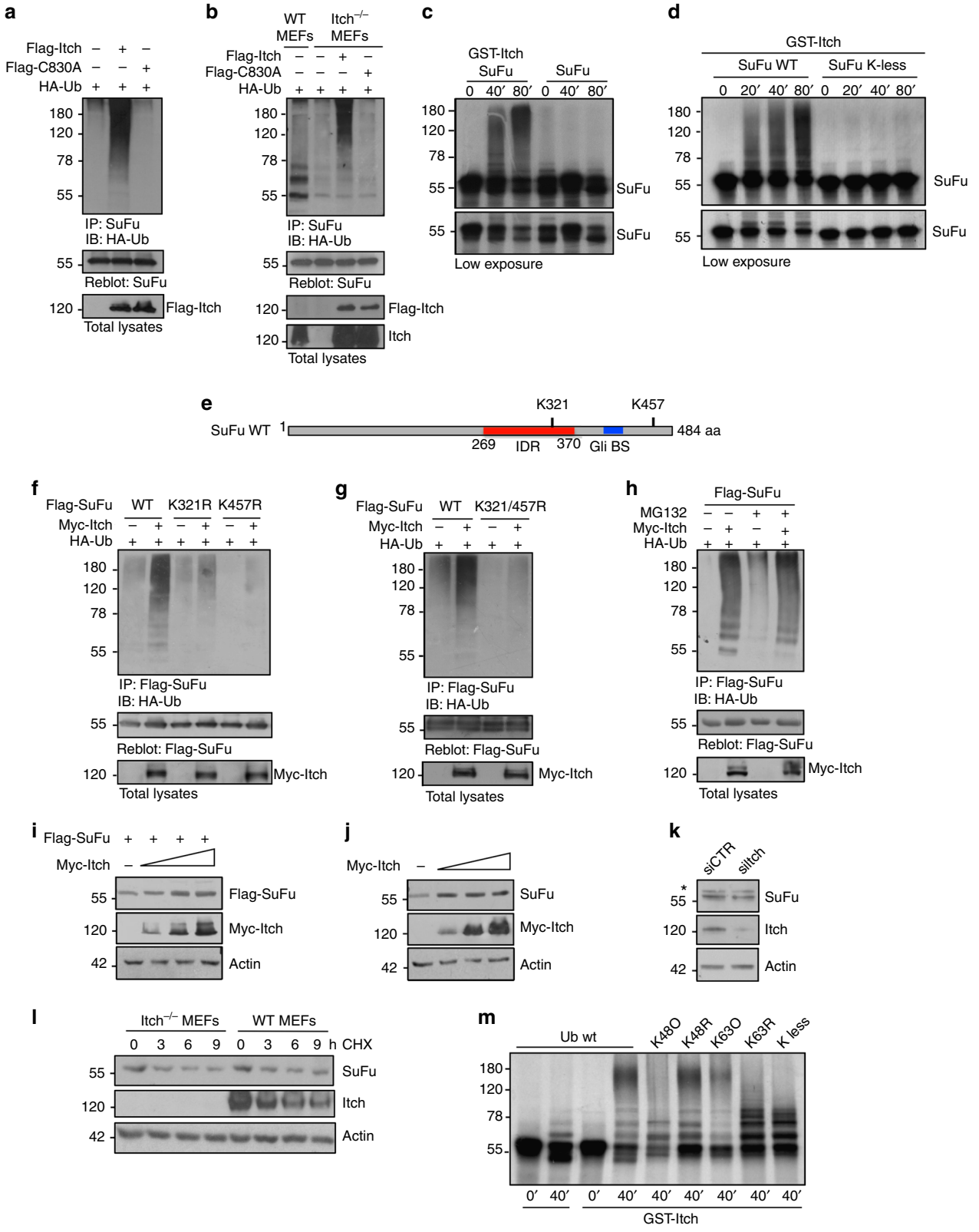

Hh activation inhibits the Itch-mediated ubiquitylation of SuFu. To clarify the correlation between SuFu ubiquitylation and the activity of Hh signalling, we first evaluated SuFu ubiquitylation levels during cerebellar development in mice. It is known that Hh signalling regulates cerebellar development by controlling the proliferation of granule cell progenitors (GCPs). During the first week of postnatal development, the cerebellum is formed by an external cortical germinal layer populated by high-proliferating GCPs, which are sustained by high Hh signalling as a result of Purkinje cell-derived Shh stimuli. After the first postnatal week, the physiologic withdrawal of Hh signal causes GCPs growth arrest, their migration in the internal granule layer, and differentiation into mature granules[36,37]. We analysed the ubiquitylation of SuFu and the interaction of SuFu with Gli3 in the postnatal cerebellum tissues of P2- up to P15-old mice and found that SuFu ubiquitylation, as well as the SuFu/Gli3 complex, increased as the pathway is progressively switched off, as indicated by the reduction of the mRNA and protein levels of Gli1, a major read-out of Hh signalling (Fig. 4a–c). These data suggest that SuFu ubiquitylation is functionally related to the activity of Hh signalling. To support this finding, we analysed SuFu ubiquitylation, in the presence or absence of Itch, in NIH3T3 cells treated with Smoothened agonist (SAG), a known small-molecule agonist of the Hh pathway. In agreement with the in vivo results, we observed a reduction of the Itch-dependent ubiquitylation of SuFu in response to Hh signalling activation induced by SAG (Fig. 4d).

Overall, these data support a negative role of the Itch-mediated ubiquitylation of SuFu in the regulation of Hh signalling.

β-Arrestin2 increases the Itch-mediated ubiquitylation of SuFu. Itch is an E3 ubiquitin ligase whose activity is regulated by post-translational events such as phosphorylation[38] as well as by proteins that induce its catalytic activity[28,39] and by the interaction with adaptor proteins that mediate the recruitment of specific substrates[40–43]. Of note, among these, the multifunctional adaptor proteins β-arrestins (β-arrestin1 and β-arrestin2) have emerged as important mediators of the Hh pathway[44,45]. Therefore, we tested whether the Itch-dependent ubiquitylation of SuFu was affected by the presence of β-arrestins. We observed that ectopic expression of β-arrestin2, but not β-arrestin1, promoted the ubiquitylation of endogenous SuFu (Fig. 5a). Moreover, expression of β-arrestin2 resulted in increased Itch-mediated ubiquitylation of SuFu as assessed by both in vivo and in vitro ubiquitylation assays (Fig. 5b, c and Supplementary Fig. 5). Accordingly, small interfering RNA (siRNA)-mediated depletion of β-arrestin2 inhibited SuFu ubiquitylation (Fig. 5d). We also found that β-arrestin2 binds SuFu and that this interaction requires Itch (Fig. 5e).

We then expressed tagged SuFu, Itch, and β-arrestin2 in wild-type MEFs in different combinations. As expected, Flag-tagged Itch co-immunopurified both haemagglutinin (HA)-tagged SuFu and GFP-tagged β-arrestin2. Parallel anti-Flag immunoprecipitates were eluted with Flag peptide and re-immunoprecipitated with an anti-HA antibody. Again, all three proteins were detected by immunoblotting of the second immunoprecipitation indicating that the three proteins, SuFu, Itch, and β-arrestin2, are assembled in a ternary complex (Fig. 5f). Further, this result shows that the presence of β-arrestin2 increases the interaction of SuFu with Itch, as also confirmed by re-expressing β-arrestin2 in $\beta arr2^{-/-}$ MEFs (Fig. 5g).

Moreover, in agreement with our previous data indicating that SuFu ubiquitylation correlates with the activity of the Hh signalling pathway (Fig. 4), the formation of the SuFu/Itch/β-arrestin2 complex increased as the pathway is progressively switched off, as shown in postnatal mouse cerebellum tissues (Fig. 5h), and was significantly reduced when the pathway was either activated in response to SAG treatment (Fig. 5i, j) or in MB tumour cells in which the Hh pathway is hyperactivated by deletion of Ptch repressor[46] (Fig. 5k).

Itch-mediated ubiquitylation of SuFu counteracts MB formation. Several germline and somatic mutations of SuFu have been identified in MB patients[10,12–17]. Recently, whole genome sequencing of a large cohort of Shh-MBs revealed a high frequency of mutations of Hh pathway genes, including new SuFu genetic alterations[47]. Notably, many mutations described so far occur in the C-terminal region of SuFu thus affecting the K321 and K457 residues, suggesting that alterations in Itch-mediated SuFu ubiquitylation might play a key role in MB development.

To address the biological role of the Itch-dependent ubiquitylation of SuFu in the regulation of tumour cell growth, we used human MB Daoy cells belonging to the Shh-MBs subgroup[48–50]. We first compared the proliferation of human MB Daoy cells expressing wild-type SuFu, the SuFuK321/457R mutant, or a control vector. As evaluated by BrdU incorporation and colony-formation assay, wild-type SuFu, but not the SuFuK321/457R mutant, was able to inhibit the proliferation of human MB Daoy cells or decrease the number of colonies (Supplementary Fig. 6a–c). As expected, the SuFuK321/457R mutant retained its inability to block cell growth of Daoy cells following Itch or SuFu modulation (Supplementary Fig. 6e, f). Moreover, we carried out wound healing assays to determine the effect of the Itch-mediated ubiquitylation of SuFu on the migration of MB cells. Daoy cells

Fig. 2 Itch ubiquitylates SuFu through K63 linkage. **a** HEK293T cells were co-transfected with HA-Ub in the presence or absence of Flag-Itch or Flag-C830A. Cell lysates were immunoprecipitated with an anti-SuFu antibody, followed by immunoblotting with an anti-HA antibody to detect ubiquitylated forms. **b** $Itch^{-/-}$ MEFs were transfected with HA-Ub in the presence or absence of Flag-Itch or Flag-C830A. The assay was carried out as described in **a**. Wild-type (WT) MEFs were used as control to evaluate the basal ubiquitylation of endogenous SuFu. **c**, **d** In vitro translated ^{35}S-labelled SuFu WT (**c**, **d**) or SuFu K-less (**d**) was incubated alone or in combination with GST-Itch for the indicated times. The ubiquitylated forms were detected by fluorography. **e** Schematic representation of SuFu protein showing its lysine residues involved in Itch-dependent ubiquitylation. **f**, **g** Flag-SuFu WT or Flag-SuFu mutants were co-transfected in HEK293T cells with HA-Ub in the presence or absence of Myc-Itch. The assay was carried out as described in **a**. **h** HEK293T cells were transfected with HA-Ub and Flag-SuFu in the presence or absence of Myc-Itch. Transfected cells were treated with MG132 (50 μM for 4 h) to enrich for ubiquitylated proteins. The assay was carried out as described in **a**. **i** HEK293T cells were transfected with Flag-SuFu in the presence or absence of increasing amount of Myc-Itch. Total protein levels were analysed by immunoblotting. **j** HEK293T cells were transfected in the presence or absence of increasing amount of Myc-Itch. Total protein levels were analysed by immunoblotting. **k** Immunoblotting analysis of SuFu and Itch proteins in HEK293T cells transfected with control (siCTR) or Itch siRNAs (siItch). β-Actin is shown as a control for loading (*non-specific bands). **l** SuFu protein levels in WT MEF or $Itch^{-/-}$ MEF cells treated with cycloheximide (CHX, 100 μg/ml) at different time points. **m** Purified recombinant proteins wild-type Ub or Ub mutants K48 only (K48O), K48R, K63 only (K63O), K63R, or K-less were incubated with GST-Itch and in vitro translated ^{35}S-labelled SuFu for the indicated times. Ubiquitylated SuFu was detected by fluorography

expressing the SuFuK321/457R mutant displayed an increased motility when compared to cells expressing wild-type SuFu (Supplementary Fig. 6d).

The effect of the SuFuK321/457R mutant on MB cell growth was also tested in vivo. To this end, we xenografted human MB Daoy cells previously infected with control lentiviruses or lentiviruses carrying wild-type SuFu or the SuFuK321/457R mutant into NOD/SCID mice. Non-invasiveness T2-weighted magnetic resonance imaging (MRI) at 41 days after transplantation showed, as expected, the ability of wild-type SuFu to decrease the tumour volume. Strikingly, this effect was not observed with the SuFuK321/457R mutant (Supplementary Fig. 7a, b).

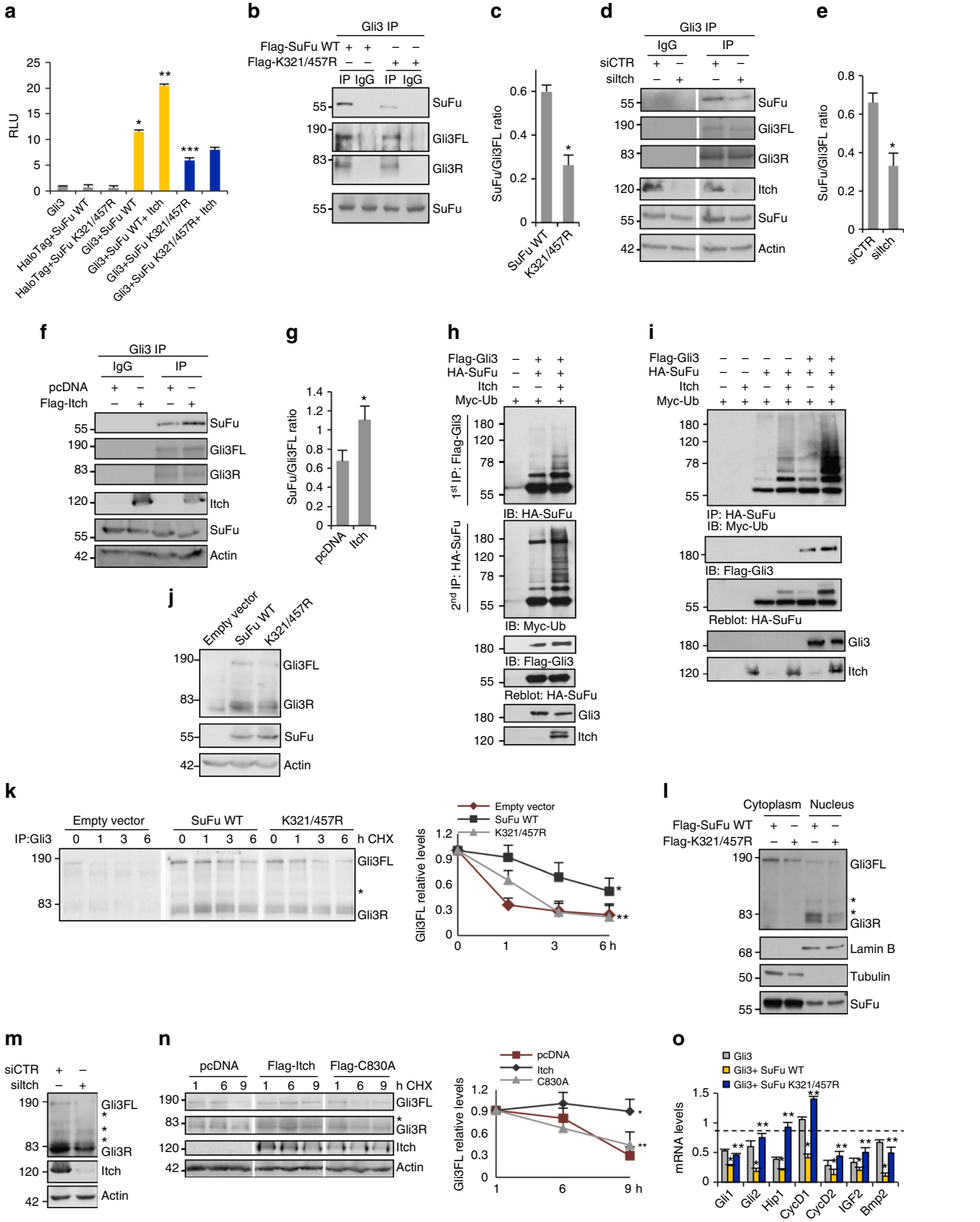

Moreover, a significant decrease of ^{18}F-fludeoxyglucose (FDG) uptake in mice engrafted with cells expressing wild-type SuFu, but not in mice engrafted with cells expressing SuFuK321/457 R mutant, was observed by PET/SPECT/CT imaging (Fig. 6a) and PET quantification (Fig. 6b). Consistently, compared to mice engrafted with empty lentiviruses, mice engrafted with wild-type SuFu showed a reduced tumour growth rate, a reduced tumour volume (at the end point of experiment) (Fig. 6c–e), a decreased labelling of Ki67 and Gli1 (the final downstream target of Hh signalling) (Fig. 6f, g), and an increased expression of the Gli3 repressor form (Fig. 6h). Notably, all these effects were not observed in mice engrafted with the SuFuK321/457R mutant.

The effect of the SuFuK321/457R mutant on MB cell growth in vivo was confirmed in an MB orthotopic xenograft animal model. Human Daoy cells, previously infected with control lentiviral particles or lentiviral particles expressing wild-type SuFu or the SuFuK321/457R mutant, were implanted into the cerebellum of immunocompromised mice. Assessment of the tumour volume (calculated along serial histologic brain sections) demonstrated the failure of the SuFuK321/457R mutant to decrease the tumour mass as instead observed in wild-type SuFu mice (Fig. 7a, b). Such an effect was likely caused by the inability of the SuFuK321/457R mutant to suppress the tumour cell proliferation as suggested by increased expression of Ki67 and Gli1 observed in mice engrafted with the SuFuK321/457R mutant compared to mice engrafted with wild-type SuFu (Fig. 7c, d).

The relevance of Itch-dependent ubiquitylation of SuFu in the control of tumour growth was also validated in primary MB cells derived from Ptch$^{+/-}$ mice[46]. In this mouse model, MB formation results from the deletion of the *Ptch* gene that leads to constitutive activation of the Hh pathway[46]. Primary MB cells freshly isolated from Ptch$^{+/-}$ mice were transduced with control lentiviruses or lentiviruses expressing wild-type SuFu or the SuFuK321/457R mutant. The proliferation of MB cells was impaired by expression of wild-type SuFu, but not by expression of the SuFuK321/457R mutant (Supplementary Fig. 8). Of note, this result was also confirmed in vivo in primary mouse Ptch$^{+/-}$ allografts. As expected, compared to mice engrafted with control lentiviruses, mice engrafted with wild-type SuFu showed a reduced tumour growth rate, a reduced tumour volume (at the end point of the experiment), and a decreased Ki67 and Gli1 labelling. Remarkably, these effects were not observed in mice engrafted with the SuFuK321/457R mutant (Fig. 8a–e).

Collectively, these findings demonstrate that the Itch-mediated ubiquitylation of SuFu plays a crucial role for the negative regulation of Hh signalling and explain how alterations of this process, caused by SuFu mutations, contribute to MB oncogenesis.

Discussion

In the last years, SuFu-Gli3 complex has emerged as a major control node in Hh signalling. However, how the integrity of SuFu–Gli3 complex is maintained and how SuFu is regulated by Hh signalling is still poorly understood.

In the present study, we demonstrate that the HECT E3 ligase Itch in complex with β-arrestin2 ubiquitylates SuFu through K63-mediated linkages. Itch/β-arrestin2-dependent K63-linked poly-ubiquitylation of SuFu on lysines 321 and 457 does not trigger degradation of SuFu; instead, it increases the association of the SuFu-Gli3 complex driving the synthesis of Gli3R, which in turn inhibits signal transduction.

Our findings add further complexity to the regulation of the Hh pathway by ubiquitylation. Indeed, following phosphorylation by PKA, GSK3β, and CK1, which generates binding sites for the SCF$^{\beta TrCP}$ ubiquitin ligase, Gli1 is completely degraded, whereas Gli3 and, to a lesser extent, Gli2, undergo partial proteasomal degradation, leading to the formation of repressor forms that translocate into the nucleus and inhibit the transcription of Hh target genes[51,52]. Downregulation of βTrCP-dependent degradation of Gli proteins is part of an Hh-induced activation signal by which Hh maintains a low degradation mode to enable Gli function[24]. Conversely, HIB/SPOP, the substrate-receptor subunit of the CRL3$^{HIB/SPOP}$ ubiquitin ligase, is upregulated by Hh, and promotes Gli2 and Gli3 degradation thus representing an Hh-induced negative feedback loop that modulates signalling activity[6,33,53]. Further, we have recently reported that PCAF induces the proteasome-dependent degradation of Gli1 in response to genotoxic stress[29], and described the ubiquitin-dependent proteolysis of Gli1 mediated by Itch and Numb[27,28]. Itch was also found to regulate the basal turnover of Ptch1[54], thus linking this HECT E3 ligase to different aspects of Hh signalling.

Interestingly, we show that the Itch-induced non-proteolytic ubiquitylation of SuFu is regulated by the adaptor β-arrestin2, a member of the arrestin family of proteins involved in numerous key physiological processes and in cancer progression[55–57]. β-Arrestins have been described to have signalling functions, serve as scaffolds by regulating the internalisation of various types of

Fig. 3 Itch-dependent K63-linked ubiquitylation of SuFu leads to Gli3R formation. **a** Gli3/SuFu proteins interaction by NanoBiT technology. Itch$^{-/-}$ MEFs were transfected with indicated plasmids. *$P < 0.05$, Gli3+SuFu WT versus Gli3; **$P < 0.05$, Gli3+SuFu WT+Itch versus Gli3+SuFu WT; ***$P < 0.05$, Gli3+SuFuK321/457R versus Gli3+SuFu WT. **b**, **c** Association between endogenous Gli3 and Flag-SuFu WT or Flag-SuFuK321/457R assayed by determining the amount of SuFu that co-precipitated with anti-Gli3 antibody or control goat antisera (IgG) from MEFs lysates (**b**). The ratio of the SuFu signal to the Gli3FL signal from **b** was plotted (**c**). *$P < 0.05$. **d**–**g** Gli3/SuFu, interaction, assessed as in (**b**), in WT MEFs transfected with siltch or siCTR (**d**) or in Itch$^{-/-}$ MEFs transfected with the indicated plasmids (**f**). The ratio of the SuFu signal to the Gli3FL signal from (**d**) and (**f**) was plotted (respectively (**e**) and (**g**)). *$P < 0.05$. **h** WT MEFs were co-transfected with indicated plasmids in the presence or absence of Itch. Cell lysates were immunoprecipitated with anti-Flag agarose beads (1st IP). After two elutions with Flag peptide, cell lysates were re-immunoprecipitated with anti-HA agarose beads (2nd IP), followed by immunoblotting as indicated. **i** WT MEFs were co-transfected with the indicated plasmids. Cell lysates were immunoprecipitated with anti-HA antibody followed by immunoblotting as indicated. **j** Gli3FL and Gli3R protein levels in SuFu$^{-/-}$ MEFs before and after expression of SuFu WT or SuFuK321/457R. **k** Gli3 half-life in SuFu$^{-/-}$ MEFs after cycloheximide treatment. Gli3FL and Gli3R protein levels were analysed by immunoprecipitation from whole-cell lysates. The graph shows densitometric analysis. *$P < 0.05$, SuFu WT versus empty vector; **$P < 0.05$, SuFuK321/457R versus SuFu WT. **l** Subcellular fractions generated from WT MEFs transfected with Flag-SuFu WT or Flag-K321/457R. Lamin B and Tubulin were used as nuclear and cytoplasmic markers, respectively. **m** Gli3FL and Gli3R protein levels in WT MEFs transfected with siCTR or siltch. **n** Gli3 half-life in Itch$^{-/-}$ MEFs transfected as indicated and then treated with cycloheximide for the indicated times. The graph shows densitometric analysis. *$P < 0.05$, Itch versus pcDNA; **$P < 0.05$, C830A versus Itch. **o** The graphs show the mRNA levels of the indicated Hh target genes in SuFu$^{-/-}$ MEFs transfected with Gli3 alone or in combination with Flag-SuFu WT or Flag-K321/457R. *$P < 0.05$, Gli3+SuFu WT versus Gli3; **$P < 0.05$, Gli3+SuFuK321/457R versus Gli3+SuFu WT. *Non-specific band. Each experiment was performed three times independently. Error bars indicate SD. *P*-values were determined using Student's *t*-test

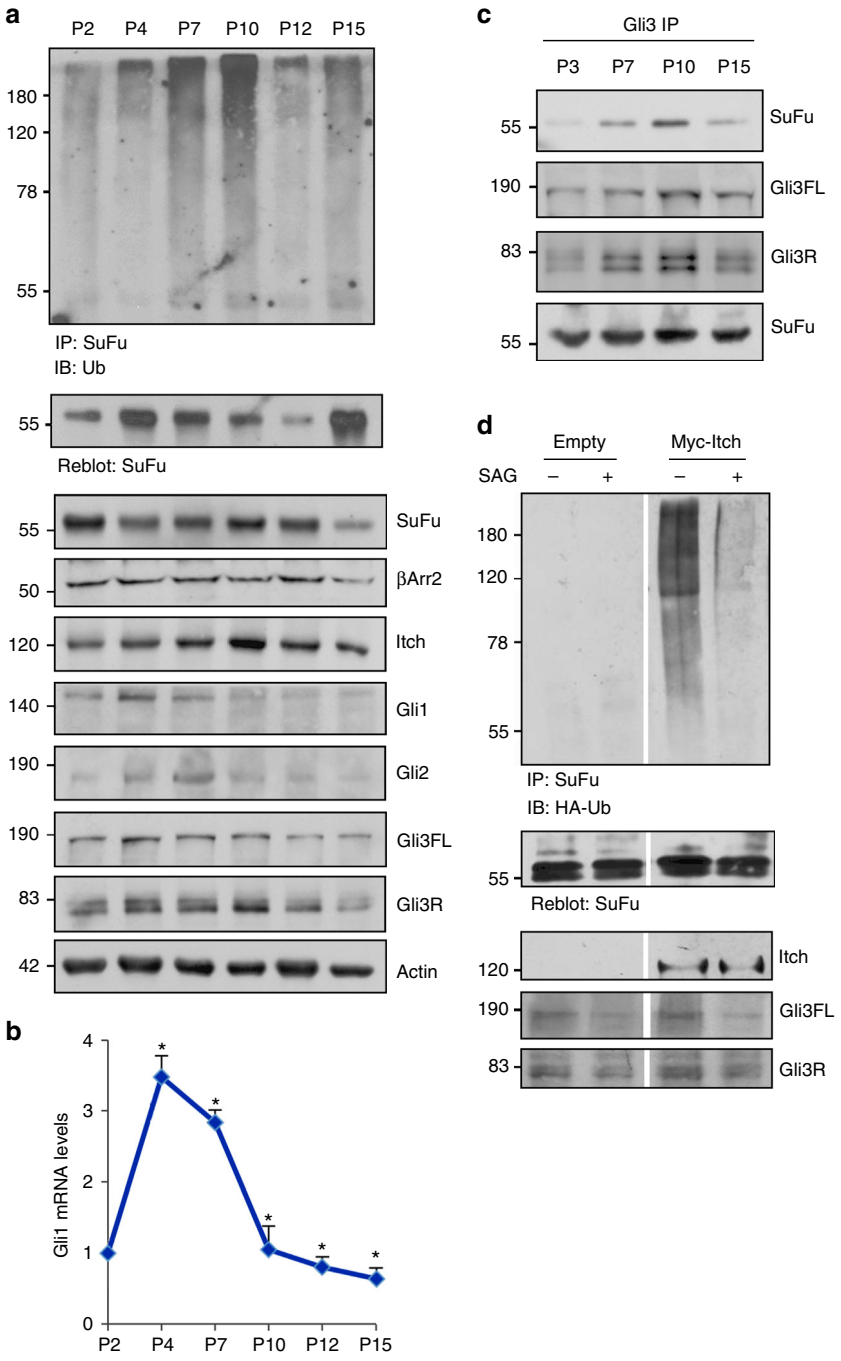

Fig. 4 Itch-dependent ubiquitylation of SuFu is reverted by Hh pathway activation. **a** Cerebellum lysates from CD1 mice killed at 2d, 4d, 7d, 10d, 12d, and 15d postpartum (P2, P4, P7, P10, P12, P15) were immunoprecipitated with an anti-SuFu antibody and immunoblotted with an anti-Ub antibody. Gli3 proteins were only detected after enriching its levels by immunoprecipitation with an anti-Gli3 antibody. **b** The graph shows the mRNA levels of *Gli1* gene, as a control of pathway activation, in the cerebella described in **a**. Error bars indicate SD from three independent experiments. *$P < 0.05$ (Student's *t*-test). **c** Association between endogenous Gli3 and SuFu from cell lysates of CD1 mice cerebellum (P3, P7, P10, P15) immunoprecipitated with an anti-Gli3 antibody. **d** Itch-dependent SuFu ubiquitylation is inhibited by activation of the Hh pathway. NIH3T3 cells were transfected with HA-Ub in the presence or absence of Myc-Itch and treated with SAG (200 nM for 6 h). Cell lysates were immunoprecipitated with an anti-SuFu antibody and immunoblotted with an anti-HA antibody

receptors, or allow E3 ubiquitin ligase recruitment[58]. Here, we show that expression of β-arrestin2 increases the Itch/SuFu interaction and enhances the Itch-dependent ubiquitylation of SuFu and that, conversely, knockdown of β-arrestin2 inhibits these processes. Biochemical data also demonstrate that β-arrestin2, Itch, and SuFu form a trimeric complex that is promptly dissociated in response to Hh activation. These observations support a new additional role of β-arrestin2 in Hh signalling. β-Arrestin2 has been identified as an important regulator of the Hh pathway that activates signalling by promoting Smo movement to the primary cilium[44,45]. This potential dual role of β-arrestin2 would be similar to that of the type-II kinesin motor protein Kif3a, which, in the absence of Shh, promotes conversion of Gli3 into a truncated repressor form[59], and in the

presence of Shh and in association with β-arrestin2 promotes Gli activator formation by transporting Smo into cilia[45]. We speculate that β-arrestin2 might regulate the switch between pathway OFF, promoting Itch-dependent SuFu ubiquitylation and Gli3R formation, and pathway ON, triggering the formation of the Smo/β-arrestin2/Kif3a complex.

Mutations in SuFu are a feature of the Shh-MB subgroup. Germline and somatic mutations of SuFu described in patients with medulloblastoma alter SuFu repressor functions. Indeed,

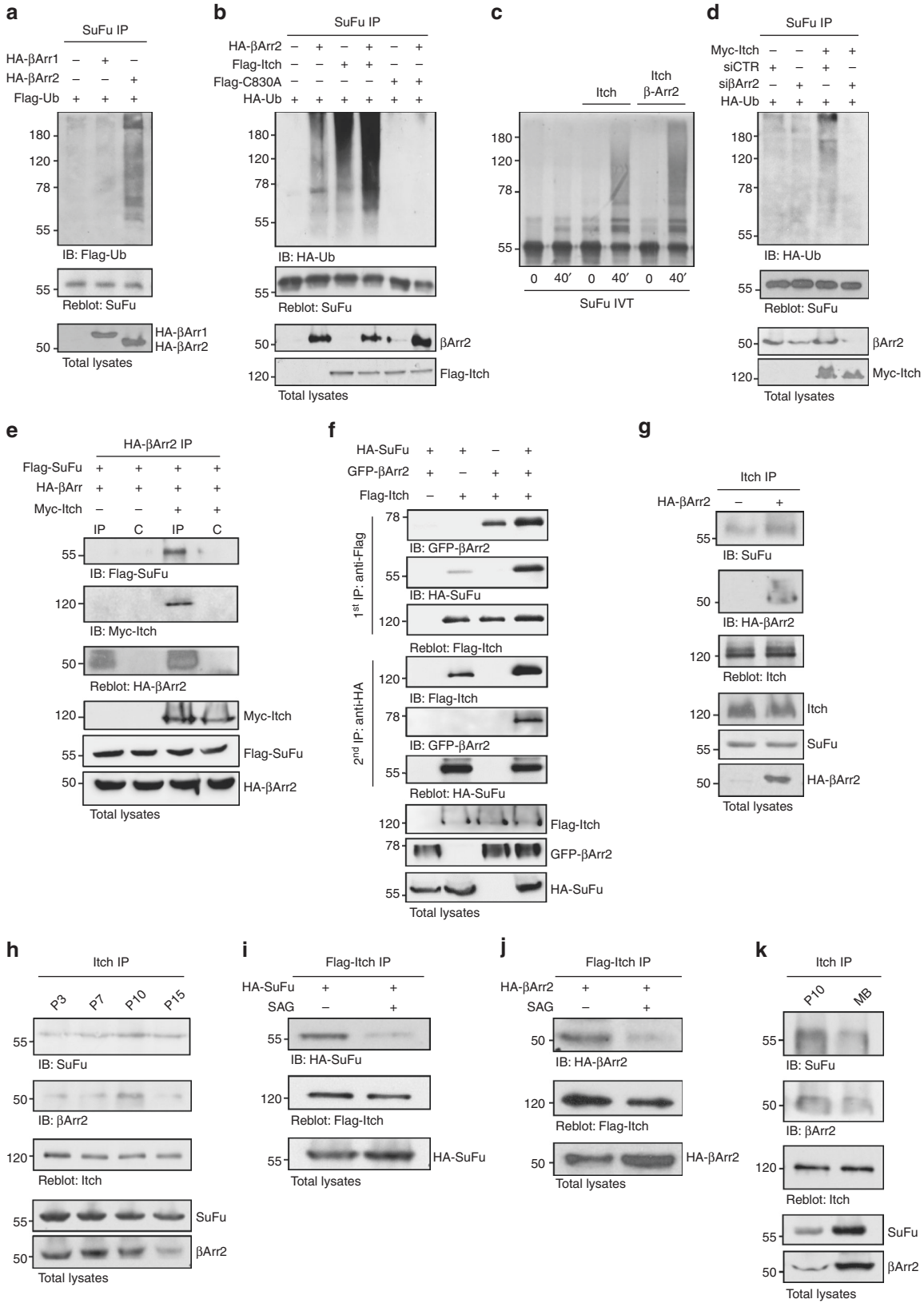

some of these mutations generate truncated proteins that are unable to bind Gli factors[17], thus leading to aberrant activation of Hh signalling. Kool et al.[47] recently reported the genome sequencing of the largest series to date of Shh-related MBs. Interestingly, this group identified two novel non-sense SuFu mutations, Y424X and W430X, both lacking lysine 457 here identified as required for the Itch-dependent ubiquitylation of SuFu (Supplementary Fig. 9a). We have now shown that these mutations encode truncated proteins that conserve Gli consensus, but are unable to be ubiquitylated by Itch (Supplementary Fig. 9b). Accordingly, SuFuY424X or SuFuW430X display a reduced ability to bind Gli3 (Supplementary Fig. 9c), cause a decrease in the abundance of nuclear Gli3R when compared to wild-type SuFu (Supplementary Fig. 9d), and hamper the ability of SuFu to inhibit MB cell growth (Supplementary Fig. 9e). These findings support our model (Fig. 9) that the impairment of SuFu ubiquitylation is implicated in MB oncogenesis.

In conclusion, the Itch-dependent non-proteolytic ubiquitylation of SuFu identified in our study represents a novel mechanism that inhibits the Hh signalling pathway and indicates that alterations of this process, caused by SuFu mutations that make it insensitive to Itch-mediated ubiquitylation, contribute to the pathogenesis of MB.

Methods

Plasmids. pcDNA-Flag-Gli3, pCXN-Flag-REN^{KCTD11}, pCXN-Flag-KCTD21, pcDNA-Itch, GST-SuFu, pCHN3HA-SuFu, pCHN3HA-SuFu-W430X and -Y424X constructs were generated in our lab with standard cloning techniques and verified by sequencing. SuFu mutants (SuFuK321/457R, SuFuK321R, SuFuK257R, SuFuK457R) were generated using the QuickChange II site-directed mutagenesis kit (Agilent Technologies, Santa Clara, CA, USA) and verified by sequencing. The following plasmids were kindly provided by other labs: pcDNA-Myc-Itch, pcDNA-Myc-Nedd4, pcDNA-Myc-Ubiquitin (M. Alimandi), pCMV2-Flag-Itch, -Flag-C830A (A. Angers), GST-Itch, GST-HECT, GST-4WWs, GST-WW1, GST-WW2, GST-WW3, GST-WW4, pcDNA-Flag-WWP1 (G. Melino), HA-Ubiquitin constructs (I. Dikic), pRK5-Flag-SuFu (M. Merchant), pcDNA3.1-Flag-SPOP (Wang B), pcDNA-Flag-βTrCP, and pcDNA-Flag-Skp2 (M. Pagano). pcDNA3-HA-β-arrestin1, pcDNA3-HA-β-arrestin2, pEGFP-N1-β-arrestin2, and pRK-Myc-Smurf were purchased from Addgene (Cambridge, MA, USA), and pLenti-GIII-CMV-SuFu-GFP-2A-PURO and pLenti-GIII-CMV-GFP-2A-PURO-Blank were purchased from Applied Biological Materials (Richmond, BC, CA).

Antibodies and reagents. Rabbit anti-SuFu C81H7 (#2522S, 1:3000), rabbit anti-β-arrestin2 C16D9 (#3857S, 1:1000), and mouse anti-Gli1 L42B10 (#2643S, 1:500) were from Cell Signalling (Beverly, MA, USA); goat anti-SuFu C-15 (sc-10933 2 µg), mouse anti-GST B-14 (sc-138, 1:10,000), goat anti-Actin I-19 (sc-1616, 1:1000), goat anti-Lamin B M-20 (sc-6217, 1:1000), mouse anti-α Tubulin TU-02 (sc-8035, 1:1000), mouse anti-Ub P4D1 (sc-8017, 1:500), rabbit anti-Gli1 H300 (sc-20687, 1:100), mouse anti-HA-probe F-7 horseradish peroxidase (HRP) (sc-7392 HRP, 1:1000), mouse anti-c-Myc 9E10 HRP (sc-40 HRP, 1:500), mouse anti-GFP (B-2) HRP (sc-9996 HRP, 1:1000), and HRP-conjugated secondary antibodies were purchased from Santa Cruz Biotechnology (Santa Cruz, CA, USA); anti-Flag M2 HRP (A8592, 1:1000), anti-Flag M2 agarose (A2220, 1–2 µg), and anti-HA agarose (A2095, 1–2 µg) were from Sigma Aldrich (St Louis, MO, USA); goat anti-Gli3 (AF3690, 1:1000 or 2–4 µg) and goat anti-Gli2 (AF3635, 1:1000) were from R&D Systems (Minneapolis, MN, USA); mouse anti-Itch (611199, 1:2000) antibody was purchased from BD Bioscience (Heidelberg, Germany); rabbit anti-Ki67 SP6 (MA5-14520, 1:100) was from Thermo Fisher Scientific (Waltham, MA, USA); mouse anti-MDM2 OP46 (Ab-1, 1:500) was from Calbiochem (Darmstadt, Germany). Where indicated, cells were treated with SAG (200 nM, Alexis Biochemicals Farmingdale, NY, USA) for 6 h, MG132 (50 µM; Calbiochem, Nottingham, UK) for 4 h, or Cycloheximide (CHX 100 µg/ml, Sigma Aldrich).

Cell culture and transfection and lentiviral infection. HEK293T cells, wild-type MEFs, SuFu$^{-/-}$, Itch$^{-/-}$, and βArr2$^{-/-}$ MEFs were cultured in Dulbecco's modified Eagle's medium plus 10% fetal bovine serum (FBS) or 10% bovine serum (BS) for NIH3T3 cells. Daoy cells were maintained in Eagle's minimum essential medium (MEM) plus 10% FBS. All media contained L-glutamine and antibiotics.

Primary MB cells were freshly isolated from Ptch$^{+/-}$ mice as previously described[60]. Cells were cultured in Neurobasal Media-A with B27 supplement minus vitamin A[61]. HEK293T (CRL-3216™), NIH3T3 (CRL-1658™), and Daoy (HTB-186™) cells were obtained from ATCC. Itch$^{-/-}$ MEFs were a gift from Dr C. Brou (Institut Pasteur), SuFu$^{-/-}$ MEFs were a gift from Dr R. Toftgård (Karolinska Institutet), and βArr2$^{-/-}$ MEFs were a gift from Dr R.J. Lefkowitz (Howard Hughes Medical Institute).

Mycoplasma contamination in cell cultures was routinely detected by using PCR detection kit (Applied Biological Materials, Richmond, BC, Canada).

Transient transfections were performed using DreamFect^{TM}Gold transfection reagent (Oz Biosciences SAS, Marseille, FR) or Lipofectamine® with Plus™ Reagent (Thermo Fisher Scientific, Waltham, MA, USA) in accordance with the manufacturer's protocols. For lentiviral infection, HEK293 cells were transfected with lentiviral constructs and the packaging plasmids pMD.G and pCMVR8.74 using Calcium/Phosphate precipitation. Culture medium containing the lentivirus was collected 48 and 72 h after transfection. Daoy cells were infected with purified lentiviruses for 48 h in the presence of 4 µg/ml polybrene (Sigma Aldrich, St Louis, MO), primary MB cells were infected with purified lentiviruses for 48 h, and SuFu$^{-/-}$ MEFs were infected with lentiviruses in the presence of 8 µg/ml polybrene for 72 h.

For RNA interference, scrambled (Cat no: D-001810-10-05), Itch (Cat no: L-007196-00-0005), SuFu (Cat no: E-015382-00), or β-arrestin2 (Cat no: J-041022-11 and J-041022-10) short interfering RNA oligos (Dharmacon, Inc., Lafayette, CO, USA) were transfected for 48 h using Lipofectamine 2000® (Thermo Fisher Scientific) or HiPerFect Transfection Reagent (Qiagen, Milan, IT).

GST pull-down assay. Recombinant GST-fusion proteins were expressed in *Escherichia coli* BL21, and purified as previously described[62]. GST, GST-SuFu, and GST-Itch recombinant proteins were bound to glutathione beads (GE Healthcare, Pittsburgh, PA, USA) and incubated for 2 h with in vitro translated protein in binding buffer (4-(2-hydroxyethyl)-1-piperazineethanesulfonic acid 20 mM, $MgCl_2$ 2 mM, KCl 100 mM, 20% glycerol, EDTA 0.2 mM, 0.05% NP-40) and analysed by immunoblotting or fluorography. As an alternative, GST or GST-SuFu recombinant proteins bound to glutathione beads were incubated for 2 h with untagged

Fig. 5 β-arrestin2 increases the Itch-dependent SuFu ubiquitylation. **a** WT MEFs were transfected with Flag-Ub in the presence or absence of HA-β-arrestin1 (HA-βArr1) or HA-β-arrestin2 (HA-βArr2). Cell lysates were immunoprecipitated with an anti-SuFu antibody and ubiquitylated forms were revealed with an anti-Flag antibody. **b** HEK293T cells transfected with the indicated plasmids were immunoprecipitated with an anti-SuFu antibody. Ubiquitylated forms were revealed with an anti-HA antibody. **c** In vitro translated ^{35}S-labelled SuFu was incubated alone or in combination with untagged recombinant Itch protein in the presence or absence of recombinant β-arrestin2 protein for the indicated times. Levels of ubiquitylated ^{35}S-labelled SuFu were detected by fluorography. **d** SuFu ubiquitylation in WT MEFs transfected with HA-Ub in the presence or absence of Myc-Itch and with specific siRNA for β-arrestin2 (siβArr2) or non-specific control (siCTR). Immunoprecipitation and immunoblotting were performed as in (**b**). **e** HEK293T cells were co-transfected with the indicated plasmids. Interaction of β-arrestin2 with SuFu and Itch was detected by immunoprecipitation followed by immunoblot analysis with the indicated antibodies. **f** SuFu, Itch, and β-arrestin2 form a trimeric complex. WT MEFs were transfected with different combinations of Flag-Itch, GFP-β-arrestin2, and HA-SuFu constructs. Protein lysates were immunoprecipitated with anti-Flag agarose beads. One-third of immunocomplexes was probed with antibodies to the indicated proteins (1st IP), whereas two-thirds were subjected to two elutions with Flag peptide and re-immunoprecipitated with HA-agarose beads followed by immunoblotting as indicated (2nd IP). **g** β-Arrestin2$^{-/-}$ MEF cells were transfected with HA-β-arrestin2 plasmid. Interaction of Itch with SuFu and β-arrestin2 was detected by immunoprecipitation followed by immunoblot analysis with the indicated antibodies. **h** Association of endogenous Itch with SuFu and β-arrestin2 from cell lysates of CD1 mice cerebellum (P3, P7, P10, P15) immunoprecipitated with an anti-Itch antibody. **i**, **j** NIH3T3 cells transfected with the indicated plasmids were treated with SAG (200 nM for 6 h) or vehicle only. Interaction between Flag-Itch and HA-SuFu (**i**) or HA-β-arrestin2 (**j**) was detected by anti-Flag immunoprecipitation, followed by immunoblot analysis with the indicated antibodies. **k** Association of endogenous Itch with SuFu and β-arrestin2 from cell lysates of CD1 mice cerebellum (P10) and from MB Ptch$^{+/-}$ tissue both immunoprecipitated with an anti-Itch antibody

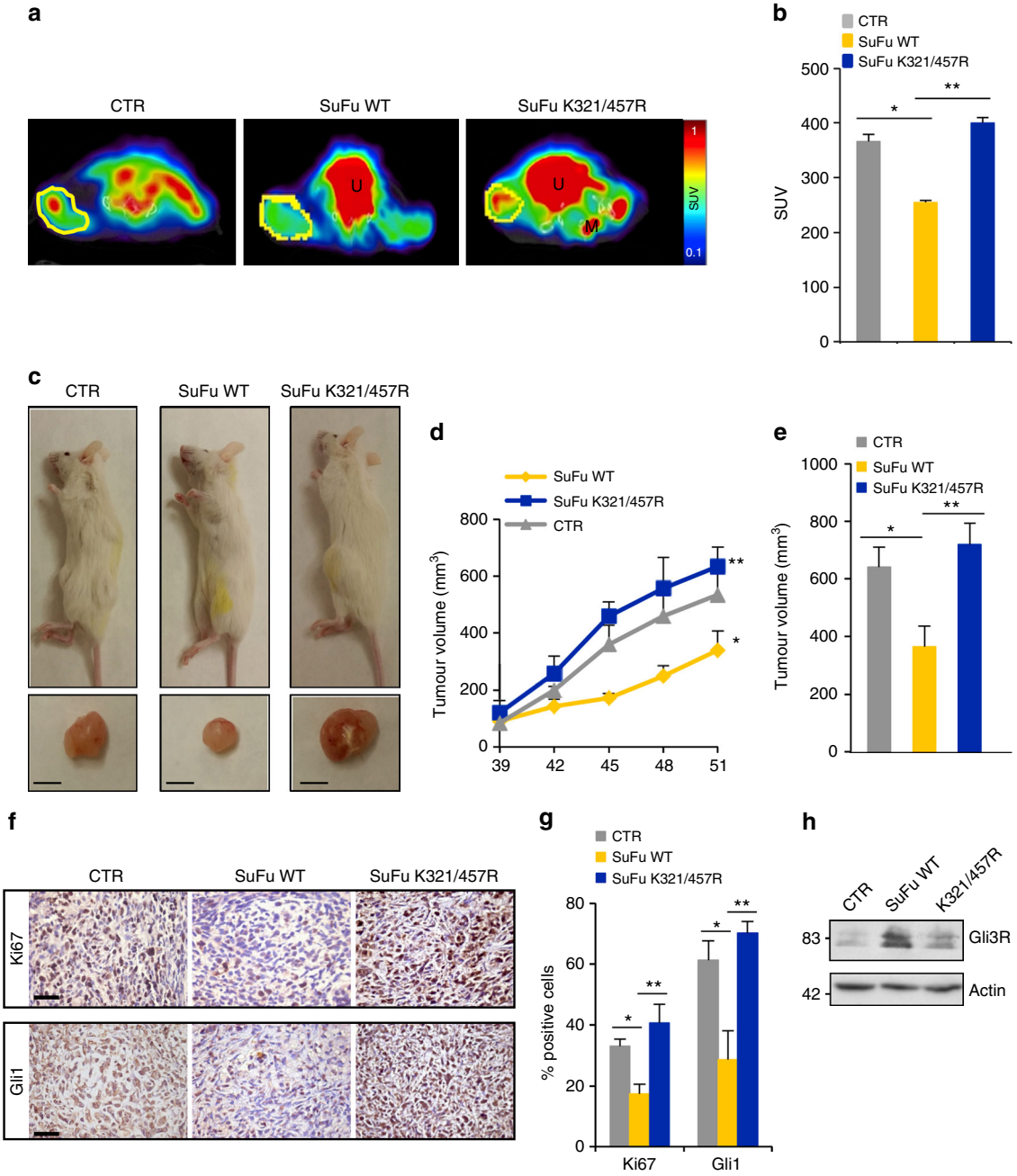

Fig. 6 Human Daoy MB xenografts. **a** PET/CT images of representative CTR ($n = 6$), SuFu WT ($n = 6$), and SuFu K321/457R ($n = 8$) mice showing tumour FDG (F-18-fluorodeoxyglucose) uptake at 41 days after implantation. ROI (region of interest) drafts the tumour mass. Significant differences were observed between SuFu WT and SuFu K321/457R mutant mice. U urinary bladder, M femoral muscle. **b** Graphic representation of SUV (standard uptake value). For each tumour, the SUV as mean tumour FDG uptake normalised for animal body weight was calculated. Significant difference in tumour FDG uptake was observed between SuFu K321/457R and SuFu WT mice. $^{*}P < 0.05$, SuFu WT versus CTR; $^{**}P < 0.05$, SuFu K321/457R versus SuFu WT. **c** Images of xenografted NOD/SCID mice with bilateral MB xenograft tumours. Tumour volume in SuFu K321/457R mutant mice is visually bigger than SuFu WT (scale bars = 5 mm). **d** Tumour volumes were monitored over time by caliper measurements at the indicated times. $^{*}P < 0.01$, SuFu WT versus CTR; $^{**}P < 0.01$, SuFu K321/457R versus SuFu WT. **e** Tumour volumes were measured post explantation. $^{*}P < 0.01$, SuFu WT versus CTR; $^{**}P < 0.01$, SuFu K321/457R versus SuFu WT. **f** Immunohistochemistry of Ki67 and Gli1 stainings. Scale bars indicate 50 µm. **g** Quantification of Ki67 and Gli1 stainings from immunohistochemistry. $^{*}P < 0.01$, SuFu WT versus CTR and $^{**}P < 0.01$, SuFu K321/457R versus SuFu WT. **h** Western blot analysis shows protein expression levels. Error bars indicate SD. *P*-values were determined using Mann–Whitney *U*-test

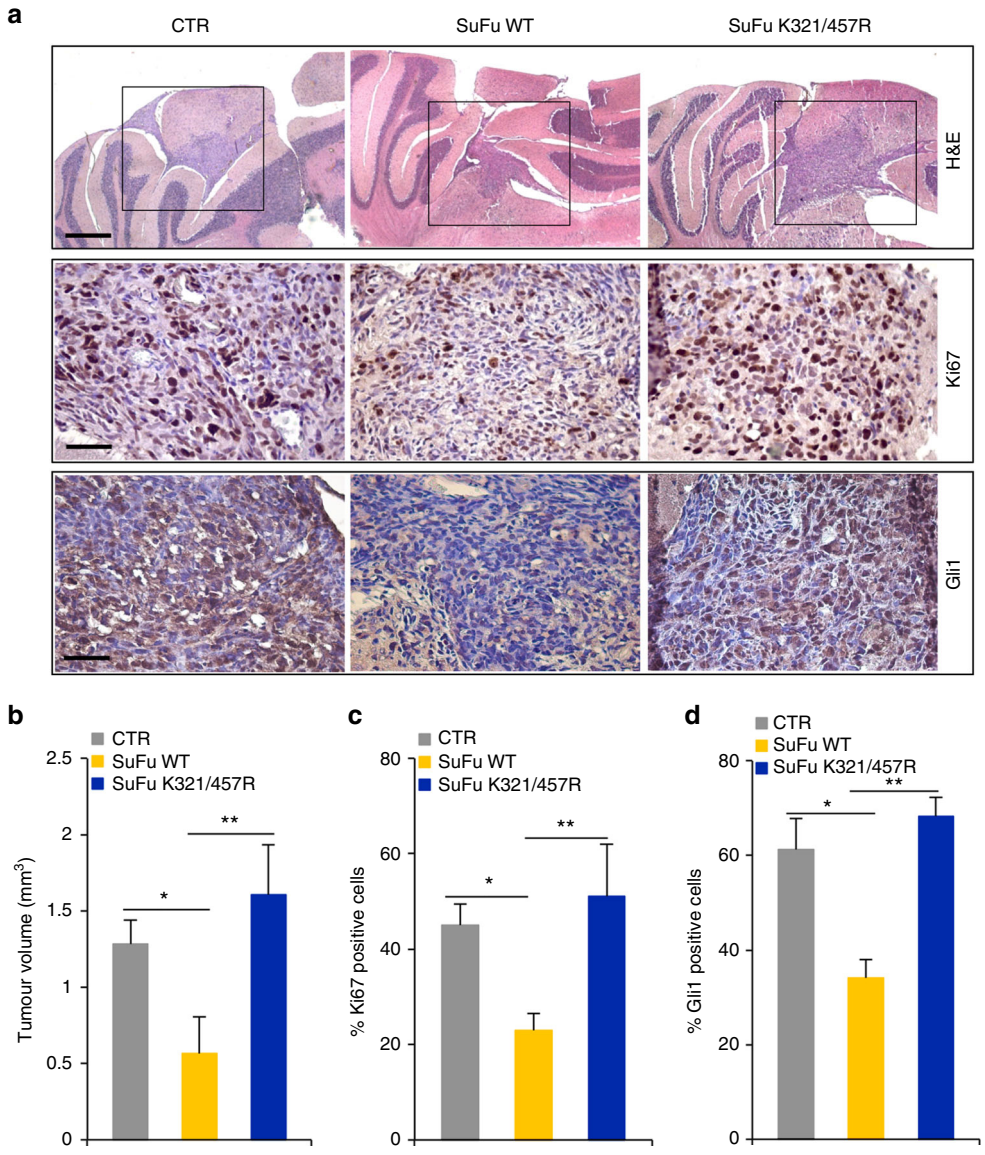

Fig. 7 Human Daoy orthotopic MB xenografts. **a** Representative images of haematoxylin and eosin (H&E), Ki67, and Gli1 immunohistochemical stainings of a human Daoy MB cell-derived orthotopic tumour in NOD/SCID mice ($n = 6$ mice for each group, CTR, SuFu WT, and SuFu K321/457R). Scale bars represent 500 µm for H&E staining and 50 µm for Ki67 and Gli1 stainings. **b** Representative tumour average volumes after explantation. **c**, **d** Quantification of Ki67 (**c**) and Gli1 (**d**) stainings from immunohistochemistry shown in (**a**). *$P < 0.01$, SuFu WT versus CTR; **$P < 0.01$, SuFu K321/457R versus SuFu WT. Error bars indicate SD. *P*-values were determined using Mann–Whitney *U*-test

recombinant protein Itch (Boston Biochem Cambridge, MA, USA) in binding buffer and analysed by immunoblotting.

Immunoblot analysis and immunoprecipitation. Transfected cells were lysed in a solution containing 50 mM Tris at pH 7.4, 300 mM NaCl, 2% NP-40, 0.25% deoxycholic acid sodium, 1 mM dithiothreitol (DTT), and protease inhibitors or in RIPA buffer (50 mM Tris at pH 7.6, 150 mM NaCl,0.5% deoxycholic acid sodium, 5 mM EDTA, 0.1% SDS,100 mM NaF, 2 mM NaPPi, 1% NP-40). The lysates were centrifuged at 13,000×*g* for 30 min and the resulting supernatants were subjected to immunoblot analysis or immunoprecipitation. For immunoprecipitation, cell lysates were immunoprecipitated with specific antibodies: anti-Flag and anti-HA agarose or anti-Gli3, anti-SuFu, and anti-Itch antibodies from 2 h to overnight at 4 °C with rotation. Flag- or HA-peptide (0,1 mg/ml, Sigma Aldrich) or IgG (1–2 µg, Santa Cruz Biotechnology) were used as a control. The immunoprecipitations performed by the use of primary antibodies not conjugated to agarose beads were followed by incubation with Protein G- or Protein A-agarose beads (Santa Cruz Biotechnology) for 1 h with rotation[63]. The immunoprecipitates were then washed five times with the lysis buffer described above, resuspended in sample loading buffer, boiled for 5 min, resolved in sodium dodecyl sulphate–polyacrylamide gel electrophoresis (SDS-PAGE), and then subjected to immunoblot analysis. Uncropped images of the most important blots were shown in the Supplementary Figures.

Subcellular fractionation. Subcellular fractionation experiments were performed as previously described[7]. Briefly, freshly collected cells were washed twice with phosphate-buffered saline (PBS) and twice with 10 mM HEPES (pH 7.4) and then were incubated for 10 min in 10 mM HEPES (pH 7.4). Subsequently, the cells were lysed in SEAT Buffer (10 mM triethanolamine/acetic acid at pH 7.4, 250 mM sucrose, 1× EDTA protease inhibitor cocktail) by 15 passages through a 25-G needle. The lysates were centrifuged at 900×*g* for 5 min and the resulting supernatants were brought to 1× buffer A (50 mM Tris at pH 7.4, 300 mM NaCl, 2% NP-40, 0.25% deoxycholic acid sodium, 1 mM DTT, and protease inhibitors), extracted for 1 h, and clarified by centrifugation at 20,000×*g* for 1 h to obtain the citoplasmatic fraction. On the other side, the nuclear pellets were washed once in SEAT buffer. The nuclei were extracted for 1 h with 20 mM HEPES at pH 7.9, 1 mM $MgCl_2$, 0.5 M NaCl, 0.2 mM EDTA, 20% glycerol, 1% Triton X-100, 1 mM DTT, benzonase, and a protease inhibitor cocktail and clarified by centrifugation at 20,000×*g* for 1 h. An equal percentage of nuclear and cytoplasmic fractions were loaded for lane to ensure that equal amounts of each fraction were loaded on the gel.

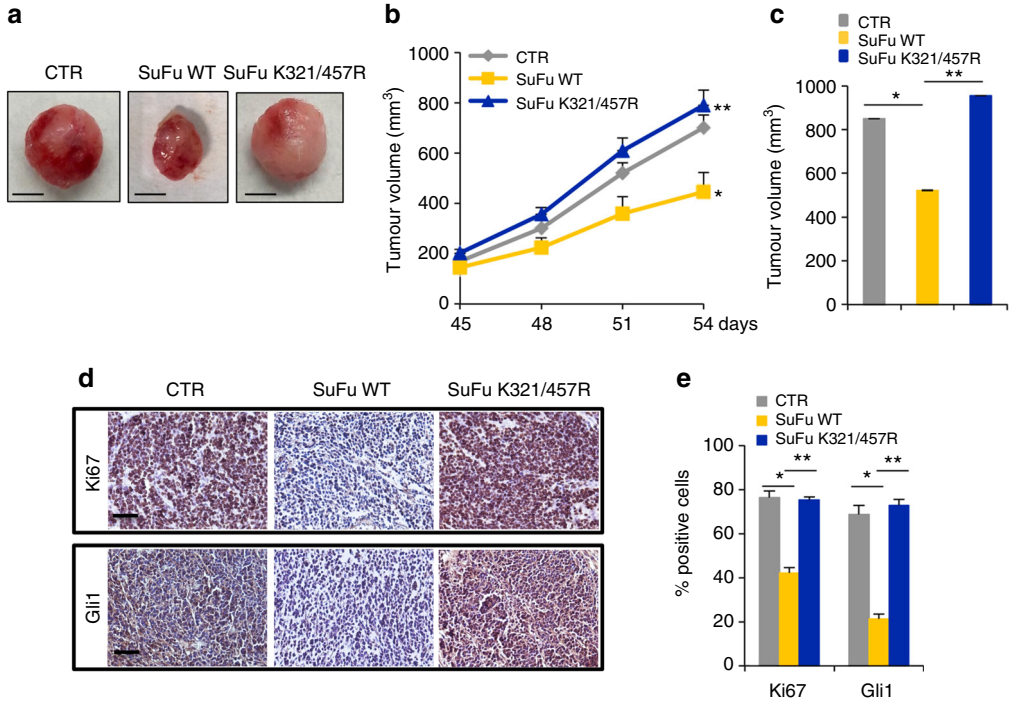

Fig. 8 Mouse Ptch1$^{+/-}$ MB allografts. **a** Images of representative CTR, SuFu WT, and SuFu K321/457R flank allograft masses ($n = 6$ mice for each group) (scale bars = 5 mm). **b** Tumour volumes were monitored over time by caliper measurements at the indicated times. *$P < 0.05$, SuFu WT versus CTR; **$P < 0.05$, SuFu K321/457R mutant versus SuFu WT. **c** Tumour volumes were measured post explantation. *$P < 0.05$, SuFu WT versus CTR; **$P < 0.05$, SuFu K321/457R mutant versus SuFu WT. **d** Immunohistochemistry of Ki67 and Gli1 stainings. Scale bars indicate 50 µm. **e** Quantification of Ki67 and Gli1 stainings from immunohistochemistry. *$P < 0.05$, SuFu WT versus CTR and **$P < 0.05$, SuFu K321/457R mutant versus SuFu WT, for Ki67 staining quantification. *$P < 0.05$, SuFu WT versus CTR and **$P < 0.01$, SuFu K321/457R versus SuFu WT, for Gli1 staining quantification. Error bars indicate SD. *P*-values were determined using Mann–Whitney *U*-test

In vivo ubiquitylation assay. In vivo ubiquitylation experiments were performed as previously described[29]. MEFs or HEK293T cells transfected with various plasmids were lysed with denaturing buffer (1% SDS, 50 mM Tris at pH 7.5, 0.5 mM EDTA, 1 mM DTT) to disrupt protein–protein interactions and then lysates were diluted 10 times with lysis buffer and subjected to immunoprecipitation with antibodies indicated in figures from 2 h to overnight at 4 °C. The immunoprecipitated proteins were then washed five times with the lysis buffer described above, resuspended in sample loading buffer, boiled for 5 min, resolved in SDS-PAGE, and then subjected to immunoblot analysis. Polyubiquitylated forms were detected using anti-HA, anti-Flag, anti-Myc, or anti-Ubiquitin antibodies.

In vitro ubiquitylation assay. In vitro ubiquitylation was performed as previously described[64,65]. In vitro translated protein SuFu, produced using TnT® Coupled Wheat Germ Extract System (Promega, Madison, WI, USA), was incubated at 30 °C with GST or Itch-GST or Itch-GST and βarr2-GST 400ng (Abnova, Heidelberg, Germany), 50 mM Tris-HCl at pH 7.5, 5 mM $MgCl_2$, 200 µM okadaic acid, 2 mM ATP, 0.6 mM DTT, 1 mM ubiquitin aldehyde, E1, UbcH7, and either wild-type or mutant ubiquitin (Boston Biochem). Polyubiquitylated products were subjected to SDS-PAGE and detected by fluorography.

NanoLuc Binary Technology assay. Gli3, SuFu WT, and SuFuK321/457R were cloned into vectors compatible with the Flexi Vector System (NanoBiT™, Promega) in accordance with the manufacturer's protocols. For our assay we used Gli3 protein fused to the SmBiT subunit and SuFu WT or SuFuK321/457R mutant protein fused to LgBiT subunit. Itch$^{-/-}$ MEFs cells were seeded in 96-well plates and transfected with the plasmids or with the NanoBiT Negative Control Vector, which encodes HaloTag-SmBiT used in combination with SuFu WT-LgBiT or SuFu K321/457R-LgBiT. At 24 h post transfection, the Nano-Glo Live Cell Reagent was added to a 1× concentration and luminescence was measured using the Glo-Max Multi+Detection System (Promega).

mRNA expression analysis. Total RNA was isolated with TRIzol (Thermo Fisher Scientific) and reverse-transcribed with SensiFASTcDNA Synthesis Kit (Bioline Reagents Limited, London, UK). Quantitative real-time PCR (Q-PCR) analysis of *Gli1*, *Gli2*, *Hip1*, *CyclinD1*, *CyclinD2*, *Igf2*, and *Bmp2* mRNA expression was performed on each complementary DNA (cDNA) sample using the ViiA™ 7 Real-Time PCR System (Life Technologies, Foster City, CA, USA). A reaction mixture containing cDNA template, SensiFAST™ Probe Lo-ROX mix (Bioline Reagents Limited), and primer probe mixture was amplified using standard Q-PCR thermal cycler parameters. Each amplification reaction was performed in triplicate and the average of the three threshold cycles was used to calculate the amount of transcript in the sample (using SDS version 2.3 software). mRNA quantification was expressed, in arbitrary units, as the ratio of the sample quantity to the calibrator. All values were normalized with two endogenous controls, *β-2 microglobulin* and *HPRT*, which yielded similar results.

Cell proliferation and wound healing assays. Cell proliferation was evaluated by BrdU detection (Roche, Welwyn Garden City, UK). Briefly, after the BrdU pulse cells were fixed with 4% paraformaldehyde and permeabilized with 0.2% Triton X-100, and BrdU detection was performed according to the manufacturer's instructions. Nuclei were counterstained with Hoechst reagent. At least 500 nuclei were counted in triplicate, and the number of BrdU-positive nuclei was recorded. For colony-formation assays, 1×10^4 Daoy cells, infected with lentiviral particles, were plated in 10-cm-diameter dishes, and after 2 weeks of puromycin (Sigma Aldrich) selection, cell colonies were counted in triplicate after staining in 20% methanol and crystal violet. Cells were counted in triplicate. For wound healing assay Daoy cells, were infected with lentiviral particles and then seeded at high density into 12-multiwell plates. The following day, a linear scratch in the confluent cell monolayer was made with a sterile pipette tip. Cells were washed three times with PBS with Ca^{2+} and Mg^{2+} and incubated in regular media. For each well, three pictures were taken along the scratch area at the indicated times, and the wound areas were calculated using ImageJ. Cell migration was defined as the reduction of the wound area in each photographed field during the course of the treatment.

Animal studies. For xenograft models, 4×10^6 Daoy cells infected with lentiviral particles were resuspended in an equal volume of MEM medium and Matrigel (BD Biosciences, Heidelberg, Germany) and injected subcutaneously (s.c.) at the posterior flank of 6-week-old female NOD/SCID mice ($n = 6$ CTR, $n = 6$ SuFu WT, $n = 8$ SuFuK321/457R) (Charles River Laboratories, Lecco, Italy). After 40 days following tumour cells injection, animals were imaged using a dedicated whole body mouse coil in a 1T MRI scanner (Bruker, Icon, Germany). Mice were anaesthetised with 1–2% isofluorane in air and O_2. During measurements,

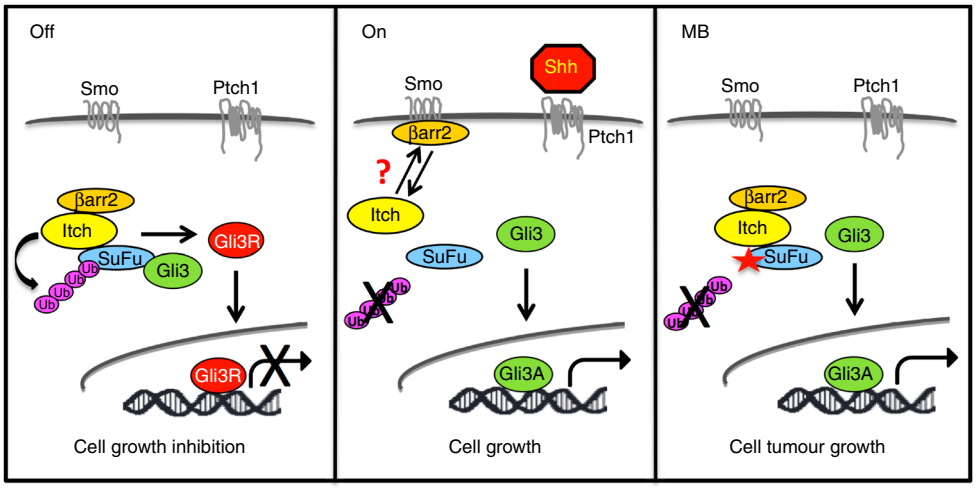

Fig. 9 Model of the Itch/β-arrestin2-dependent regulation of the SuFu/Gli3 complex function. When Hh pathway is OFF, Itch, coadjuvated by the protein adaptor β-arrestin2, ubiquitylates SuFu. This event does not lead to SuFu degradation, but increases the association between SuFu and Gli3. In this way Gli3 is protected from SPOP-dependent degradation and is cleaved into a repressor form (Gli3R) that inhibits Hh target gene transcription and cell growth. When Hh pathway is switched ON, β-arrestin2 dissociates from the SuFu/Itch complex, thus abrogating Itch-dependent SuFu ubiquitylation. This process induces the dissociation of the Gli3-SuFu complex and impairs Gli3R formation, thereby leading to Hh pathway activation and sustained cell growth. Alterations in this mechanism, caused by SuFu mutations that make it insensitive to Itch-dependent ubiquitylation, are responsible for MB tumorigenesis

respiration was monitored with a sensor connected to an ECG/respiratory unit. T2-weighted MR scans with Fast Spin-Echo RARE sequence (TR/TE = 2500/35 ms, number of average (NA = 2)), were acquired for the tumour volume evaluation. Animals were imaged with a PET/SPECT/CT scanner (Trifoil Imaging, USA) equipped with gas anaesthesia, respiratory monitoring, and heated bed. Mice were injected with 9.43 MBq (SD 1.26; range 7.43–11.61 MBq) of 18F-FDG (AAA, Italy). PET imaging started 45 min after FDG injection and lasted 30 min. Positron emission tomography (PET) images were corrected for decay, randoms, dead time, and computed tomography (CT) attenuation, and reconstructed using an OSEM algorithm with 8 subsets and 30 iterations. PET quantitative data were obtained by an investigator blinded to the group identity by outlining the tumours directly on the anatomical CT images. At the end of PET experiment, animal were killed with an overdose of anaesthetic, the tumours were collected, and the volume (mm^3) of each tumour measured with a caliper and calculated by the formula ($length^2 \times width$) / 2 where length refers to the smaller dimension.

For orthotopic xenografts model, Daoy cells (prepared from fresh culture to ensure optimal viability of cells during tumour inoculation) infected with lentiviruses particles were stereotaxically implanted (2×10^5) into the cerebellum of 6-week-old female NOD/SCID mice ($n = 6$ animals per group) (Charles River Laboratories) as previously described[66]. Brain tumour volume calculation was performed as described in ref. [66].

For allograft models, spontaneous MB from $Ptch1^{+/-}$ mice was isolated, minced, and pipetted to obtain a single-cell suspension, as previously described[67] and then infected with lentiviral particles. Equal volumes of cells (2×10^6) were injected s.c. at the posterior flank of 6-week-old female BALB/c nude mice (nu/nu) ($n = 6$ animals per group) (Charles River Laboratories). Tumour growth was monitored by measuring the size by caliper and calculated as above describe. All animal experiments were approved by local ethic authorities and conducted in accordance with Italian Governing Law (D.lgs 26/2014; Prot. no. 03/2013). Animals were housed in the Institute's Animal Care Facilities, which meet international standards and were checked regularly by a certified veterinarian responsible for health monitoring, animal welfare supervision, and revision of experimental protocols and procedures.

Immunohistochemistry. The 4 µm thick sections were prepared from paraffin-embedded tissues and immunostained with anti-Gli1 or anti-Ki67 antibodies. After washes, secondary biotinylated antibodies were applied. Binding of antibodies was detected with the Mouse to Mouse HRP (DAB) Staining System (Scytek Laboratories, Inc., Logan, UT, USA) according to the manufacturer's protocol.

Molecular dynamics. The crystallographic structure of SuFuWT/Gli3 complex coded by PDB ID: 4BLD[68] was used as starting point in MD simulations. Particularly, chain A was selected, and structural gaps were filled. For larger portions such as the IDR disordered region, a preliminary folding experiment was performed starting from a linear sequence of residues. WT and mutant SuFu/Gli3 complexes were solvated in a rectilinear box of TIP3P water molecules buffering 12 Å from the protein. MD simulations were performed according to the procedure described previously[66,69], but in this case unrestrained trajectories were initially equilibrated for 50 ns and then produced for 200 ns. Free energy of binding of Gli3 to SuFu WT and K321457R double mutant was estimated by the Molecular Mechanics Generalised Born Surface Area (MM-GBSA) approach[70].

Statistical analysis. Statistical analysis was performed using the StatView 4.1 software (Abacus Concepts, Berkeley, CA, USA). Statistical tests were appropriately chosen for each experiment. For in vivo studies statistical differences were analysed by Mann–Whitney *U*-test for non-parametric values and a $P < 0.05$ was considered significant. For all other experiments, *P*-values were determined using Student's *t*-test and statistical significance was set at $P < 0.05$. Results are expressed as mean ± SD from an appropriate number of experiments (at least three biological replicas).

Data availability. All data supporting the findings of this study are within the Article and Supplementary Files, or available from the authors upon request.

Received: 19 May 2016 Accepted: 6 February 2018
Published online: 07 March 2018

References

1. Ingham, P. W. & McMahon, A. P. Hedgehog signaling in animal development: paradigms and principles. *Genes Dev.* **15**, 3059–3087 (2001).
2. Briscoe, J. & Therond, P. P. The mechanisms of Hedgehog signalling and its roles in development and disease. *Nat. Rev. Mol. Cell Biol.* **14**, 416–429 (2013).
3. Aberger, F. & Ruiz I Altaba, A. Context-dependent signal integration by the GLI code: the oncogenic load, pathways, modifiers and implications for cancer therapy. *Semin. Cell Dev. Biol.* **33**, 93–104 (2014).
4. Pearse, R. V. 2nd, Collier, L. S., Scott, M. P. & Tabin, C. J. Vertebrate homologs of Drosophila suppressor of fused interact with the gli family of transcriptional regulators. *Dev. Biol.* **212**, 323–336 (1999).
5. Stone, D. M. et al. Characterization of the human suppressor of fused, a negative regulator of the zinc-finger transcription factor Gli. *J. Cell Sci.* **112**, 4437–4448 (1999).
6. Wang, C., Pan, Y. & Wang, B. Suppressor of fused and Spop regulate the stability, processing and function of Gli2 and Gli3 full-length activators but not their repressors. *Development* **137**, 2001–2009 (2010).
7. Humke, E. W., Dorn, K. V., Milenkovic, L., Scott, M. P. & Rohatgi, R. The output of Hedgehog signaling is controlled by the dynamic association between Suppressor of Fused and the Gli proteins. *Genes Dev.* **24**, 670–682 (2010).

8. Cooper, A. F. et al. Cardiac and CNS defects in a mouse with targeted disruption of suppressor of fused. *Development* **132**, 4407–4417 (2005).
9. Svärd, J. et al. Genetic elimination of Suppressor of fused reveals an essential repressor function in the mammalian Hedgehog signaling pathway. *Dev. Cell* **10**, 187–917 (2006).
10. Pastorino, L. et al. Identification of a SUFU germline mutation in a family with Gorlin syndrome. *Am. J. Med. Genet. A* **149A**, 1539–1543 (2009).
11. Kijima, C., Miyashita, T., Suzuki, M., Oka, H. & Fujii, K. Two cases of nevoid basal cell carcinoma syndrome associated with meningioma caused by a PTCH1 or SUFU germline mutation. *Fam. Cancer* **11**, 565–570 (2012).
12. Smith, M. J. et al. Germline mutations in SUFU cause Gorlin syndrome-associated childhood medulloblastoma and redefine the risk associated with PTCH1 mutations. *J. Clin. Oncol.* **32**, 4155–4161 (2014).
13. Brugières, L. et al. High frequency of germline SUFU mutations in children with desmoplastic/nodular medulloblastoma younger than 3 years of age. *J. Clin. Oncol.* **30**, 2087–2093 (2012).
14. Slade, I. et al. Heterogeneity of familial medulloblastoma and contribution of germline PTCH1 and SUFU mutations to sporadic medulloblastoma. *Fam. Cancer* **10**, 337–342 (2011).
15. Brugières, L. et al. Incomplete penetrance of the predisposition to medulloblastoma associated with germ-line SUFU mutations. *J. Med. Genet* **47**, 142–144 (2010).
16. Ng, D. et al. Retrospective family study of childhood medulloblastoma. *Am. J. Med. Genet. A* **134**, 399–403 (2005).
17. Taylor, M. D. et al. Mutations in SUFU predispose to medulloblastoma. *Nat. Genet.* **31**, 306–310 (2002).
18. Yue, S., Chen, Y. & Cheng, S. Y. Hedgehog signaling promotes the degradation of tumor suppressor Sufu through the ubiquitin-proteasome pathway. *Oncogene* **28**, 492–499 (2009).
19. Chen, Y. et al. Dual phosphorylation of suppressor of fused (Sufu) by PKA and GSK3beta regulates its stability and localization in the primary cilium. *J. Biol. Chem.* **286**, 13502–13511 (2011).
20. Welchman, R. L., Gordon, C. & Mayer, R. J. Ubiquitin and ubiquitin-like proteins as multifunctional signals. *Nat. Rev. Mol. Cell Biol.* **6**, 599–609 (2005).
21. Ciechanover, A., Orian, A. & Schwartz, A. L. Ubiquitin-mediated proteolysis: biological regulation via destruction. *Bioessays* **22**, 442–451 (2000).
22. Gulino, A., Di Marcotullio, L., Canettieri, G., De Smaele, E. & Screpanti, I. Hedgehog/Gli control by ubiquitination/acetylation interplay. *Vitam. Horm.* **88**, 211–227 (2012).
23. Jiang, J. Regulation of Hh/Gli signaling by dual ubiquitin pathways. *Cell Cycle* **5**, 2457–2463 (2006).
24. Huntzicker, E. G. et al. Dual degradation signals control Gli protein stability and tumor formation. *Genes Dev.* **20**, 276–281 (2006).
25. Pan, Y., Bai, C. B., Joyner, A. & Wang, B. Sonic hedgehog signaling regulates Gli2 transcriptional activity by suppressing its processing and degradation. *Mol. Cell Biol.* **26**, 3365–3377 (2006).
26. Wang, B. & Li, Y. Evidence for the direct involvement of βTrCP in Gli3 protein processing. *Proc. Natl. Acad. Sci. USA* **103**, 33–38 (2006).
27. Di Marcotullio, L. et al. Numb is a suppressor of Hedgehog signalling and targets Gli1 for Itch-dependent ubiquitination. *Nat. Cell Biol.* **8**, 1415–1423 (2006).
28. Di Marcotullio, L. et al. Numb activates the E3 ligase Itch to control Gli1 function through a novel degradation signal. *Oncogene* **30**, 65–76 (2011).
29. Mazzà, D. et al. PCAF ubiquitin ligase activity inhibits Hedgehog/Gli1 signaling in p53-dependent response to genotoxic stress. *Cell Death Differ.* **20**, 1688–1697 (2013).
30. Infante, P., Canettieri, G., Gulino, A. & Di Marcotullio, L. Yin-Yang strands of PCAF/Hedgehog axis in cancer control. *Trends Mol. Med* **20**, 416–418 (2014).
31. Kim, W. et al. Systematic and quantitative assessment of the ubiquitin-modified proteome. *Mol. Cell* **44**, 325–340 (2011).
32. Deng, L. et al. Activation of the IκB kinase complex by TRAF6 requires a dimeric ubiquitin-conjugating enzyme complex and a unique polyubiquitin chain. *Cell* **103**, 351–361 (2000).
33. Chen, M. H. et al. Cilium-independent regulation of Gli protein function by Sufu in Hedgehog signaling is evolutionarily conserved. *Genes Dev.* **23**, 1910–1928 (2009).
34. Dixon, A. S. et al. NanoLuc complementation reporter optimized for accurate measurement of protein interactions in cell. *ACS Chem. Biol.* **11**, 400–408 (2016).
35. England, C. G., Ehlerding, E. B. & Cai, W. NanoLuc: a small luciferase is brightening up the field of bioluminescence. *Bioconjug. Chem.* **27**, 1175–1187 (2016).
36. Ruiz i Altaba, A., Sanchez, P. & Dahmane, N. Gli and hedgehog in cancer: tumours, embryos and stem cells. *Nat. Rev. Cancer* **2**, 361–372 (2002).
37. Wechsler-Reya, R. J. & Scott, M. P. Control of neuronal precursor proliferation in the cerebellum by Sonic Hedgehog. *Neuron* **22**, 103–114 (1999).
38. Gallagher, E., Gao, M., Liu, Y. C. & Karin, M. Activation of the E3 ubiquitin ligase Itch through a phosphorylation-induced conformational change. *Proc. Natl. Acad. Sci. USA* **103**, 1717–1722 (2006).
39. Mund, T. & Pelham, H. R. Control of the activity of WW-HECT domain E3 ubiquitin ligases by NDFIP proteins. *EMBO Rep.* **10**, 501–507 (2009).
40. McGill, M. A. & McGlade, C. J. Mammalian Numb Proteins promote Notch1 receptor ubiquitination and degradation of the Notch1 intracelllar domain. *J. Biol. Chem.* **278**, 23196–23203 (2003).
41. Bhandari, D., Trejo, J., Benovic, J. L. & Marchese, A. Arrestin-2interacts with the ubiquitin-protein isopeptide ligase atrophin-interacting protein 4 and mediates endosomal sorting of the chomokine receptor CXCR4. *J. Biol. Chem.* **282**, 36971–36979 (2007).
42. Shukla, A. K. et al. Arresting a transient receptor potential (TRP) channel: beta-arrestin 1 mediates ubiquitination and functional down-regulation of TRPV4. *J. Biol. Chem.* **285**, 30115–30125 (2010).
43. Hooper, C., Puttamadappa, S. S., Loring, Z., Shekhtman, A. & Bakowska, J. C. Spartin activates atrophin-1-interacting protein 4 (AIP4) E3 ubiquitin ligase and promotes ubiquitination of adipophilin on lipid droplets. *BMC Biol.* **8**, 72 (2010).
44. Chen, W. et al. Activity-dependent internalization of smoothened mediated by beta-arrestin 2 and GRK2. *Science* **306**, 2257–2260 (2004).
45. Kovacs, J. J. et al. Beta-arrestin-mediated localization of smoothened to the primary cilium. *Science* **20**, 1777–1781 (2008).
46. Goodrich, L., Milenkovic, L., Higgins, K. M. & Scott, M. P. Altered neural cell fates and medulloblastoma in mouse Patched mutants. *Science* **277**, 1109–1113 (1997).
47. Kool, M. et al. Genome sequencing of SHH medulloblastoma predicts genotype-related response to smoothened inhibition. *Cancer Cell* **25**, 393–405 (2014).
48. Triscott, J. et al. Personalizing the treatment of pediatric medulloblastoma: Polo-like kinase 1 as a molecular target in high-risk children. *Cancer Res.* **73**, 6734–6744 (2013).
49. Ivanov, D. P. et al. In vitro models of medulloblastoma: choosing the right tool for the job. *J. Biotechnol.* **236**, 10–25 (2016).
50. Northcott, P. A. et al. Rapid, reliable, and reproducible molecular sub-grouping of clinical medulloblastoma samples. *Acta Neuropathol.* **123**, 615–626 (2012).
51. Bhatia, N. et al. Gli2 is targeted for ubiquitination and degradation by beta-TrCP ubiquitin ligase. *J. Biol. Chem.* **281**, 19320–19326 (2006).
52. Wang, B. & Li, Y. Evidence for the direct involvement of {beta}TrCP in Gli3 protein processing. *Proc. Natl. Acad. Sci. USA* **103**, 33–38 (2006).
53. Zhang, Q. et al. A hedgehog-induced BTB protein modulates hedgehog signaling by degrading Ci/Gli transcription factor. *Dev. Cell* **10**, 719–729 (2006).
54. Chen, X. L. et al. Patched-1 proapoptotic activity is downregulated by modification of K1413 by the E3 ubiquitin-protein ligase Itchy homolog. *Mol. Cell Biol.* **34**, 3855–3866 (2014).
55. Kohout, T. A., Lin, F. S., Perry, S. J., Conner, D. A. & LefkowitzR. J. beta-Arrestin 1 and 2 differentially regulate heptahelical receptor signaling and trafficking. *Proc. Natl. Acad. Sci. USA* **98**, 1601–1606 (2001).
56. Philipp, M., Evron, T. & Caron, M. G. The role of arrestins in development. *Prog. Mol. Biol. Transl. Sci.* **118**, 225–242 (2013).
57. Hu, S. et al. Involvement of β-arrestins in cancer progression. *Mol. Biol. Rep.* **40**, 1065–1071 (2013).
58. Kovacs, J. J., Hara, M. R., Davenport, C. L., Kim, J. & Lefkowitz, R. J. Arrestin development: emerging roles for beta-arrestins in developmental signaling pathways. *Dev. Cell* **17**, 443–458 (2009).
59. Huangfu, D. & Anderson, K. V. Cilia and Hedgehog responsiveness in the mouse. *Proc. Natl. Acad. Sci. USA* **102**, 11325–11330 (2005).
60. Di Magno, L. et al. Druggable glycolytic requirement for Hedgehog-dependent neuronal and medulloblastoma growth. *Cell Cycle* **13**, 3404–3413 (2014).
61. Shi, W. et al. Itraconazole side chain analogues: structure-activity relationship studies for inhibition of endothelial cell proliferation, vascular endothelial growth factor receptor 2 (VEGFR2) glycosylation, and hedgehog signaling. *J. Med. Chem.* **54**, 7363–7374 (2011).
62. Infante, P., Alfonsi, R. & Di Marcotullio, L. Insights into Gli factors ubiquitylation methods. *Methods Mol. Biol.* **1322**, 131–146 (2015).
63. Colicchia, V. et al. PARP inhibitors enhance replication stress and cause mitotic catastrophe in MYCN-dependent neuroblastoma. *Oncogene* **36**, 4682–4691 (2017).
64. Zhao, X. et al. The HECT-domain ubiquitin ligase Huwe1 controls neural differentiation and proliferation by destabilizing the N-Myc oncoprotein. *Nat. Cell Biol.* **10**, 643–653 (2008).
65. Raducu, M. et al. SCF (Fbxl17) ubiquitylation of Sufu regulates Hedgehog signalling and medulloblastoma development. *EMBO J.* **35**, 1400–1416 (2016).
66. Infante, P. et al. Gli1/DNA interaction is a druggable target for Hedgehog-dependent tumors. *EMBO J.* **34**, 200–217 (2015).

67. Di Magno et al. The energy sensor AMPK regulates Hedgehog signalling in human cells through a unique Gli1 metabolic checkpoint. *Oncotarget* **7**, 9538–9549 (2016).
68. Cherry, A. L. et al. Structural basis of SUFU-GLI interaction in human Hedgehog signalling regulation. *Acta Crystallogr D Biol. Crystallogr* **69**, 2563–2579 (2013).
69. Infante, P. et al. Inhibition of Hedgehog-dependent tumors and cancer stem cells by a newly identified naturally occurring chemotype. *Cell Death Dis.* **7**, e2376 (2016).
70. Miller, B. R. 3nd et al. MMPBSA.py: an efficient program for end-state free energy calculations. *J. Chem. Theory Comput.* **8**, 3314–3321 (2012).

Acknowledgements

We thank C. Brou for the gift of Itch$^{-/-}$ MEFs, R.Toftgard for the gift of SuFu$^{-/-}$ MEFs, R. Lefkowitz for the gift of β-arrestin2$^{-/-}$ MEFs, and G. Giannini for the critical discussion. This work was supported by Associazione Italiana Ricerca Cancro (AIRC) Grant IG14723, IG17575 and IG20801, PRIN 2012-2013 (2012C5YJSK002), Progetti di Ricerca di Università di Roma La Sapienza, Pasteur Institute/Cenci Bolognetti Foundation, Istituto Italiano di Tecnologia (IIT), Grant 111537 by the Deutsche Krebshilfe to M.K. and S.M.P. LLS was supported by PhD Degree Program in Biotechnology in clinical medicine, University of Rome La Sapienza.

Author contributions

P.I., R.F., F.B., and L.D.M. conceived and designed the study. P.I., R.F., and F.B. performed most of the experiments. P.I., L.L.S., D.M., and M.S. generated the SuFu mutants and performed ubiquitylation in vitro or in vivo assays. P.I., F.B., R.A., M.P., and A.P. performed the animal experiments and analysis. A.G., D.G., S.C., G.C, M.M., E.D.S., E.F., C.C., M.M., I.S., M.K., and S.M.P. discussed the results, and provided critical reagents and comments. P.I., D.G., and L.D.M. wrote the manuscript.

Additional information

Supplementary Information accompanies this paper at https://doi.org/10.1038/s41467-018-03339-0.

Competing interests: The authors declare no competing interests.

Reprints and permission information is available online at http://npg.nature.com/reprintsandpermissions/

Publisher's note: Springer Nature remains neutral with regard to jurisdictional claims in published maps and institutional affiliations.

3.1.2 | *ERAP1 promotes Hedgehog-dependent tumorigenesis by controlling USP47-mediated degradation of βTrCP*

Keeping the same focus of my Ph. D. project, aimed at identifying new Hh signalling regulators and molecular mechanisms involved in MB tumorigenesis, we identified and elucidated the oncogenic role of ERAP1 in Hh signalling regulation and MB pathological context.

Endoplasmic reticulum aminopeptidase 1 (ERAP1) is crucial for the maturation of a wide spectrum of substrates involved in multiple biological processes, including antigen processing, regulation of blood pressure and inflammation (Fruci et al., 2014). Functional single nucleotide polymorphisms in ERAP1 have been associated with predisposition to several human diseases including autoimmune diseases, viral infections and virally induced cancer (Stratikos et al., 2014). In human neoplastic lesions, the expression of ERAP1 differs as compared to the normal counterparts, depending on the tumor type (Fruci et al., 2008). In general, loss of ERAP1 is frequently associated with the lack of detectable MHC class I surface expression, potentially contributing to tumor immunoescape (Fruci et al., 2006).

We identified a new role of ERAP1, independent from its immunogenic function, in MB tumorigenesis demonstrating that ERAP1 enhances Hh activity by sequestering the βTrCP-bound deubiquitylase enzyme Ubiquitin Specific Proteases 47 (USP47); we observed that USP47 strongly stabilizes βTrCP, and ERAP1 binding to USP47 hampers βTrCP/USP47 interaction inducing βTrCP degradation.

βTrCP triggers the proteasome-dependent degradation of GLI1 and GLI2 and the processing of GLI3 in its repressor form (Bhatia et al., 2006; Pan et al., 2006; Tempé et al., 2006; Wang and Li, 2006). Hence, inhibition of the βTrCP-mediated degradation of GLI proteins is part of an Hh-induced activation signal. Although βTrCP is fundamental for the regulation of Hh signalling, the mechanisms controlling its function are still largely unexplored.

We identified that βTrCP proteolysis, resulting from ERAP1-dependent USP47 sequestration, leads to an increase of GLI1 and GLI2 protein levels and a reduction of the GLI3R form, thus activating the Hh pathway and stimulating cell proliferation and tumorigenesis. Conversely, inhibition of ERAP1 function stabilizes βTrCP, which in turn induces ubiquitylation of GLI factors leading to proteolysis of GLI1 and GLI2 and generation of GLI3R, thereby suppressing tumor cell growth.

Remarkably, both genetic and pharmacological inhibition of ERAP1 (induced by the treatment with the ERAP1 inhibitor Leucinethiol, Leu-SH) suppresses Hh-dependent tumor growth *in vitro* and *in vivo*, suggesting that targeting ERAP1 could open innovative perspectives for effective therapeutic approaches in the treatment of Hh-dependent tumors.

Since this work has been published, I only provided a brief outline of obtained results. Please refer to the paper attached below[2] for more detailed evaluation.

[2]Bufalieri, F.*, Infante, P.*, Bernardi, F., Caimano, M., Romania, P., Moretti, M., **Lospinoso Severini**, L., ... Fruci, D. & Di Marcotullio, L. (**2019**). ERAP1 promotes Hedgehog-dependent tumorigenesis by controlling USP47-mediated degradation of βTrCP. **Nature communications**, 10(1), 1-15.

nature COMMUNICATIONS

ARTICLE

https://doi.org/10.1038/s41467-019-11093-0 OPEN

ERAP1 promotes Hedgehog-dependent tumorigenesis by controlling USP47-mediated degradation of βTrCP

Francesca Bufalieri[1,17], Paola Infante[2,17], Flavia Bernardi[1,3,4], Miriam Caimano[1], Paolo Romania[5], Marta Moretti[1], Ludovica Lospinoso Severini[1,3,4], Julie Talbot[3,4], Ombretta Melaiu[5,6], Mirella Tanori[7], Laura Di Magno[2], Diana Bellavia[1], Carlo Capalbo[1], Stéphanie Puget[8], Enrico De Smaele[9], Gianluca Canettieri[1,10], Daniele Guardavaccaro[11], Luca Busino[12], Angelo Peschiaroli[13], Simonetta Pazzaglia[7], Giuseppe Giannini[1,10], Gerry Melino[14,15], Franco Locatelli[5,16], Alberto Gulino[1], Olivier Ayrault[3,4], Doriana Fruci[5] & Lucia Di Marcotullio[1,10]

The Hedgehog (Hh) pathway is essential for embryonic development and tissue homeostasis. Aberrant Hh signaling may occur in a wide range of human cancers, such as medulloblastoma, the most common brain malignancy in childhood. Here, we identify endoplasmic reticulum aminopeptidase 1 (ERAP1), a key regulator of innate and adaptive antitumor immune responses, as a previously unknown player in the Hh signaling pathway. We demonstrate that ERAP1 binds the deubiquitylase enzyme USP47, displaces the USP47-associated βTrCP, the substrate-receptor subunit of the $SCF^{\beta TrCP}$ ubiquitin ligase, and promotes βTrCP degradation. These events result in the modulation of Gli transcription factors, the final effectors of the Hh pathway, and the enhancement of Hh activity. Remarkably, genetic or pharmacological inhibition of ERAP1 suppresses Hh-dependent tumor growth in vitro and in vivo. Our findings unveil an unexpected role for ERAP1 in cancer and indicate ERAP1 as a promising therapeutic target for Hh-driven tumors.

[1] Department of Molecular Medicine, University La Sapienza, 00161 Rome, Italy. [2] Center for Life NanoScience@Sapienza, Istituto Italiano di Tecnologia, 00161 Rome, Italy. [3] Institut Curie, PSL Research University, CNRS UMR, INSERM, 91405 Orsay, France. [4] Université Paris Sud, Université Paris-Saclay, CNRS UMR 3347, INSERM U1021 Orsay, France. [5] Paediatric Haematology/Oncology Department, Ospedale Pediatrico Bambino Gesù, IRCCS, 00146 Rome, Italy. [6] Department of Biology, University of Pisa, 56126 Pisa, Italy. [7] Laboratory of Biomedical Technologies, Agenzia Nazionale per le Nuove Tecnologie, l'Energia e lo Sviluppo Economico Sostenibile (ENEA), S.Maria di Galeria, 00123 Rome, Italy. [8] Department of Pediatric Neurosurgery, Necker University Hospital, University Paris Descartes, Sorbonne Paris Cité, 75015 Paris, France. [9] Department of Experimental Medicine, University La Sapienza, 00161 Rome, Italy. [10] Istituto Pasteur-Fondazione Cenci Bolognetti, University La Sapienza, 00161 Rome, Italy. [11] Department of Biotechnology, University of Verona, 37134 Verona, Italy. [12] Department of Cancer Biology, Perelman School of Medicine, University of Pennsylvania, Philadelphia 19104 PA, USA. [13] National Research Council of Italy CNR, Institute of Translational Pharmacology (IFT), 00133 Rome, Italy. [14] MRC Toxicology Unit, University of Cambridge, LE17HB Leiicester, UK. [15] Dipartimento Medicina Sperimentale e Chirurgia, Università Tor Vergata, 00133 Rome, Italy. [16] Department of Pediatrics, University La Sapienza, 00161 Rome, Italy. [17] These authors contributed equally: Francesca Bufalieri, Paola Infante. Correspondence and requests for materials should be addressed to Doriana Fruci (email: doriana.fruci@opbg.net) or to L. Di Marcotullio (email: lucia.dimarcotullio@uniroma1.it)

The Hedgehog (Hh) signaling pathway plays a crucial role during organogenesis and stem cells maintenance. Its deregulation is responsible for the onset of several human cancers[1–5]. Hh signaling is triggered by the binding of the Hh ligand to the Patched1 (Ptch1) receptor, relieving the repression on the Smoothened (Smo) co-receptor. This event leads activation of the Gli family transcription factors upon the dissociation from SuFu protein, an important negative regulator of the pathway[2,6]. In mammals, three Gli proteins have been identified: Gli1 and Gli2 with activating functions and Gli3 mainly working as repressor[7]. Ubiquitin-dependent proteolytic processing of Gli transcription factors is important for controlling the Hh pathway output. Of note, all Gli transcription factors undergo ubiquitination through β-transducin-repeat containing E3 ubiquitin protein ligase (βTrCP), an F-box protein of the Skp1–Cul1–Fbox protein (SCF) E3-ligase complex, which promotes the complete degradation of Gli1 and Gli2[8–11], and the processing of Gli3 into the repressor form Gli3R[12–14]. Deregulation of these events results in uncontrolled cell proliferation and tumorigenesis[9]. One of the most relevant Hh-dependent tumors is medulloblastoma (MB), a highly aggressive pediatric malignancy arising from cerebellar granule cell progenitors (GCPs) mainly mutated in Ptch1 or Smo receptors[15]. The non-canonical Hh/Gli activation regardless of the presence of mutated components of the pathway or overexpression of the ligand is also frequently observed in MB and other tumors. This emphasizes the importance of the mechanisms controlling Gli activity, which are impaired in disease[16,17]. Pharmacological inhibition of the Hh pathway has been proposed as a therapeutic strategy in typical Hh-dependent, tumors such as advanced basal cell carcinoma (BCC) and medulloblastoma (MB)[18,19]. Hence, to identify novel Hh antagonists we tested a number of small molecules and found leucinethiol (Leu-SH), an inhibitor of Endoplasmic reticulum aminopeptidase 1 (ERAP1)[20–28], as one of Hh inhibitors.

ERAP1 is crucial for the maturation of a wide spectrum of substrates involved in multiple biological processes, including antigen processing and regulation of blood pressure and inflammation[29]. Functional single nucleotide polymorphisms in ERAP1 have been associated with predisposition to several human diseases, including autoimmune diseases, viral infections and virally-induced cancer[30]. Reduction of ERAP1 expression by RNA interference results in a drastic change in the repertoire of antigenic peptides presented by MHC class I molecules[21,31,32]. In mouse models, the complete loss of ERAAP expression, the mouse homologous of ERAP1, inhibits surface expression of MHC class I molecules. In human neoplastic lesions, the expression of ERAP1 differs as compared to the normal counterparts, depending on the tumor type[33]. In general, loss of ERAP1 is frequently associated with the lack of detectable MHC class I surface expression, potentially contributing to tumor immunoescape[34]. Consistently, in cervical carcinoma, altered ERAP1 expression is linked to poor clinical outcome, suggesting that an aberrant antigen processing may contribute to escape the host immune surveillance[35]. Accordingly, inhibition of ERAP1 was shown to generate strong innate and adaptive anti-tumor immune responses resulting in tumor regression in two distinct tumor mouse models, thus providing evidences that modulation of ERAP1 activity may represent a promising tool for cancer immunotherapy[27,36].

Here, we identified a role of ERAP1 in tumorigenesis, acting through the activation of the Hh pathway. We demonstrate that ERAP1 induces the degradation of βTrCP by physically interacting with βTrCP-bound deubiquitylase enzyme USP47. This event protects Gli transcription factors from βTrCP-dependent degradation and stimulates Hh activity. Remarkably, both genetic and pharmacological inhibition of ERAP1 suppresses Hh-dependent tumor growth in vitro and in vivo, suggesting an innovative therapeutic approach in the treatment of Hh-dependent tumors.

Results

ERAP1 positively regulates the Hh pathway. While exploring novel Hh antagonists we found Leu-SH[27,28], an inhibitor of ERAP1[20–28], as one of Hh inhibitors. Leu-SH significantly reduced the luciferase activity of the Hh pathway-reporter in NIH Shh-Light II cells activated via SAG treatment[37] (Fig. 1a) but not the one driven by Hh-unrelated or Hh-related signaling pathway (i.e. Jun/AP1 and Wnt/β-Catenin, respectively) (Supplementary Fig. 1). To explore the role of ERAP1 in the regulation of the Hh pathway, we inhibited genetically or pharmacologically ERAP1 in in vitro models. Following silencing of the murine ER aminopeptidase ERAAP (herein referred as ERAP1) by means of short hairpin RNAs and treatment with the Hh pathway agonist SAG[38], we observed a reduced expression of Gli1, the final and most powerful effector of Hh signaling, both at mRNA and protein levels (Fig. 1b, c). Consistent with these data, treatment with Leu-SH of *Ptch*$^{-/-}$ mouse embryonic fibroblasts (MEFs), in which the pathway is constitutively active[39], induced a significant reduction in the expression of several endogenous Hh target genes (Fig. 1d, e). To investigate if ERAP1 is acting at post-receptor level, we used *SuFu*$^{-/-}$ MEFs, in which the pathway is active due to the loss of the well-known Gli inhibitor SuFu[40]. Leu-SH treatment determined a downregulation of the Hh signature gene also in this cellular context (Fig. 1f). Similar results were achieved following genetic ERAP1 depletion in both cell models (Fig. 1g, h), indicating that ERAP1 promotes the Hh signaling acting downstream of SuFu.

ERAP1 activates Hh signaling by impairing βTrCP stability. To better characterize the molecular mechanism whereby ERAP1 regulates the Hh pathway, we analyzed the protein levels of Gli transcription factors in MEFs upon expression of increasing amounts of ERAP1 (Fig. 2a). We observed that while Gli1 and Gli2 were increased, both the full length and the cleaved form of the Gli3 protein (Gli3FL and Gli3R, respectively) were reduced (Fig. 2a). The opposite effect was observed following treatment with increasing amounts of Leu-SH (Fig. 2b), which impairs the enzymatic activity of ERAP1 without affecting its protein level (Supplementary Fig. 2a). Of note, Leu-SH treatment was able to antagonize the activation of Hh signaling induced by SAG, leading to decreased expression of Gli1 and Gli2 and increased levels of Gli3FL and Gli3R (Fig. 2c). Since ERAP1 did not directly associate with Gli transcription factors (Supplementary Fig. 2b), we hypothesized that ERAP1 could regulate βTrCP, an F-box protein belonging to a Skp1/Cul1/F-box E3 ubiquitin ligase complex crucial for the degradation of Gli1[9] and Gli2[8,10], and the formation of Gli3R[14,41,42]. Dose-dependent overexpression of ERAP1 led to reduction of βTrCP protein levels (Fig. 2d), whereas its pharmacological or genetic inhibition resulted in the opposite effect (Fig. 2e, f). Importantly, the reintroduction of ERAP1 in ERAP1-knockdown cells downregulated βTrCP leading to increased Gli1, to a lesser extend and Gli2 and decreased Gli3FL and Gli3R levels (Fig. 2f). No change in βTrCP mRNA expression was detected in both assays (Supplementary Fig. 3a, b). Importantly, the modulation of ERAP1 had no effect on other E3 ligases involved in Gli ubiquitylation, such as Itch[43,44], pCAF[45], SPOP[46] or SCF ubiquitin ligase Skp2[47] (Fig. 2d–f), as well as on other βTrCP substrates[48] (Supplementary Fig. 3c,d). Notably, ERAP1 did not affect Gli1 protein levels in the absence of βTrCP, indicating that the latter is required for ERAP1-mediated regulation of the Hh pathway (Fig. 2g). Moreover, βTrCP half-life was

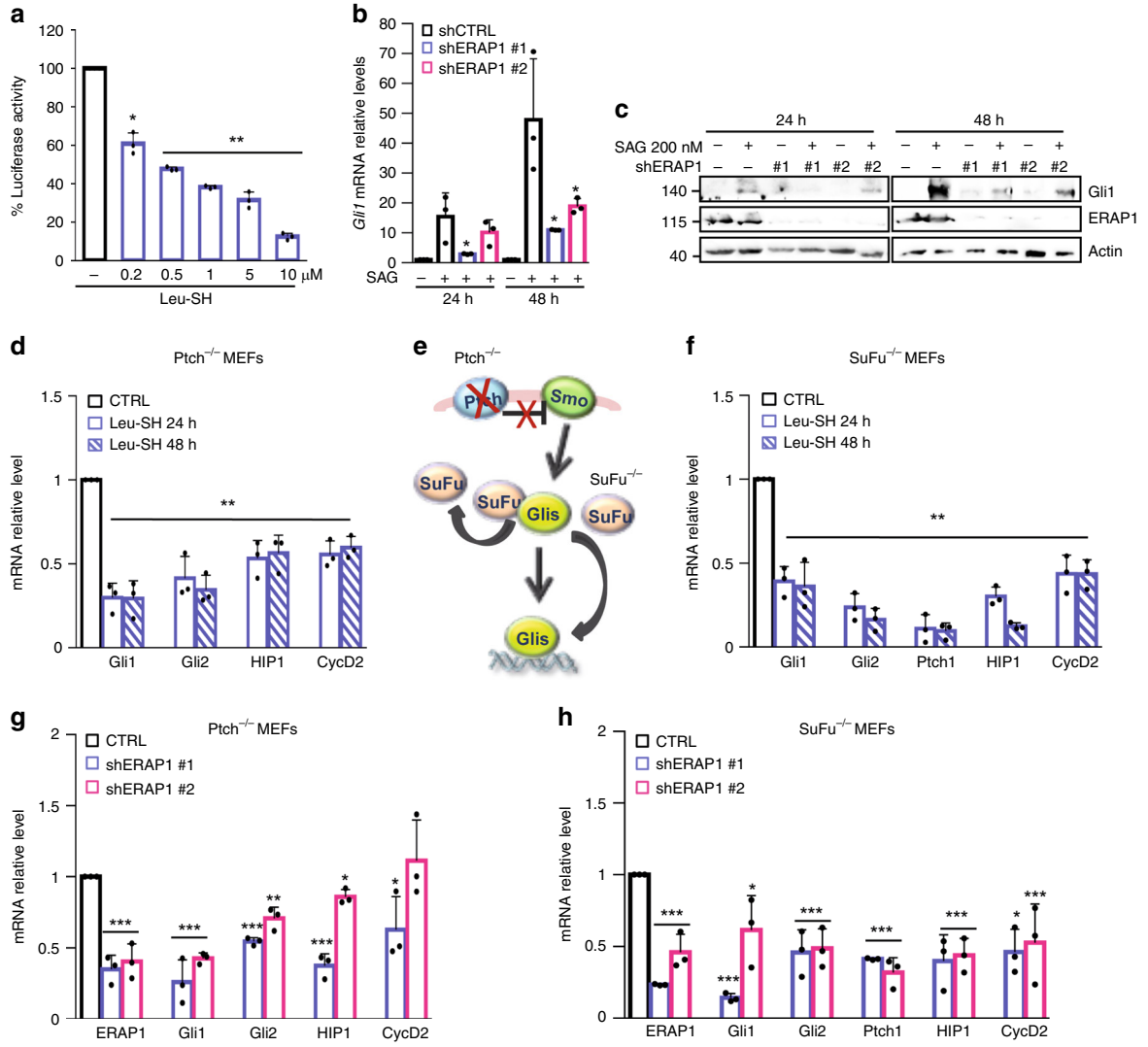

Fig. 1 ERAP1 positively regulates the Hh pathway at postreceptor level. **a** Luciferase activity of NIH3T3 Shh-Light II cells treated for 24 h with SAG and increasing amounts of Leu-SH or DTT as control. **b**, **c** Quantitative real-time PCR (qRT-PCR) (**b**) and representative immunoblotting (**c**) analyses of Gli1 expression in the NIH3T3 murine fibroblasts transduced with lentiviral vectors encoding either control shRNA (shCTRL) or ERAP1 shRNA (shERAP1#1 and shERAP1#2) and treated with SAG or DMSO for either 24 or 48 h. In **c** ERAP1 expression was also evaluated and actin was used as loading control. **d**, **f** qRT-PCR analysis of Hh target genes expression in Ptch$^{-/-}$ (**d**) and SuFu$^{-/-}$ MEFs (**f**) both treated with Leu-SH (30 μM) or DTT as control. **e** Representative model of the constitutive activation of Smo or Gli1 in Ptch$^{-/-}$ and SuFu$^{-/-}$ MEFs, respectively. **g**, **h** qRT-PCR analysis of Hh target genes expression in Ptch$^{-/-}$ (**g**) and SuFu$^{-/-}$ MEFs (**h**) transduced with shCTRL or shERAP1 constructs. Data in **b**, **d**, **f**, **g**, and **h** are normalized to endogenous *GAPDH* and *HPRT* controls and expressed as the fold change respect to the control sample value. All data represent the mean of three independent experiments. Mean ± SD; $^{*}P < 0.05$; $^{**}P < 0.01$; $^{***}P < 0.001$ calculated with two-sided Student's *t*-test

shorter following ERAP1 overexpression (Fig. 2h), suggesting that ERAP1 controls βTrCP protein stability.

Next, we evaluated whether ERAP1 controls βTrCP levels by modulating its ubiquitylation. To this purpose, we performed an in vivo ubiquitylation assay upon ectopic expression of ERAP1. High levels of ERAP1 promoted the poly-ubiquitylation of endogenous βTrCP and its subsequent degradation by the proteasome, leading to a significant accumulation of βTrCP protein and its ubiquitylated forms in cells treated with the proteasome-inhibitor MG132 (Fig. 2i). Conversely, βTrCP poly-ubiquitylation was decreased in MEFs treated with increasing amount of Leu-SH (Fig. 2j). As the phosphorylation of the Gli transcription factors within the DSG(X)$_{2+n}$S destruction motifs (degron) is required for the interaction of βTrCP[9,41,49], we evaluated if the effect of ERAP1 depended upon the presence of this motif. To this purpose, MEFs were transfected with the wild type (HA-Gli1 WT) or the mutant (HA-Gli1ΔC) form of Gli1 lacking the degron essential for βTrCP recognition[9], and then treated with increasing amount of Leu-SH. Inhibition of ERAP1 induced a reduction in the levels of the wild type, but not of the mutated form of Gli1 (Fig. 2k). The same result was obtained in MEFs transduced with shCTRL or shERAP1 (Fig. 2l). Interestingly, we also observed that Gli1 is phosphorylated in *Ptch*$^{-/-}$ MEFs by Phospho-Kinase A (PKA) (Supplementary Figure 4), the kinase that triggers the phosphorylation cascade of Gli transcription factors required for βTrCP recognition, being increased after treatment with PKA inhibitor[50,51].

Altogether these data demonstrate that ERAP1 promotes Hh pathway activity by impairing βTrCP protein levels leading to the modulation of Gli proteins.

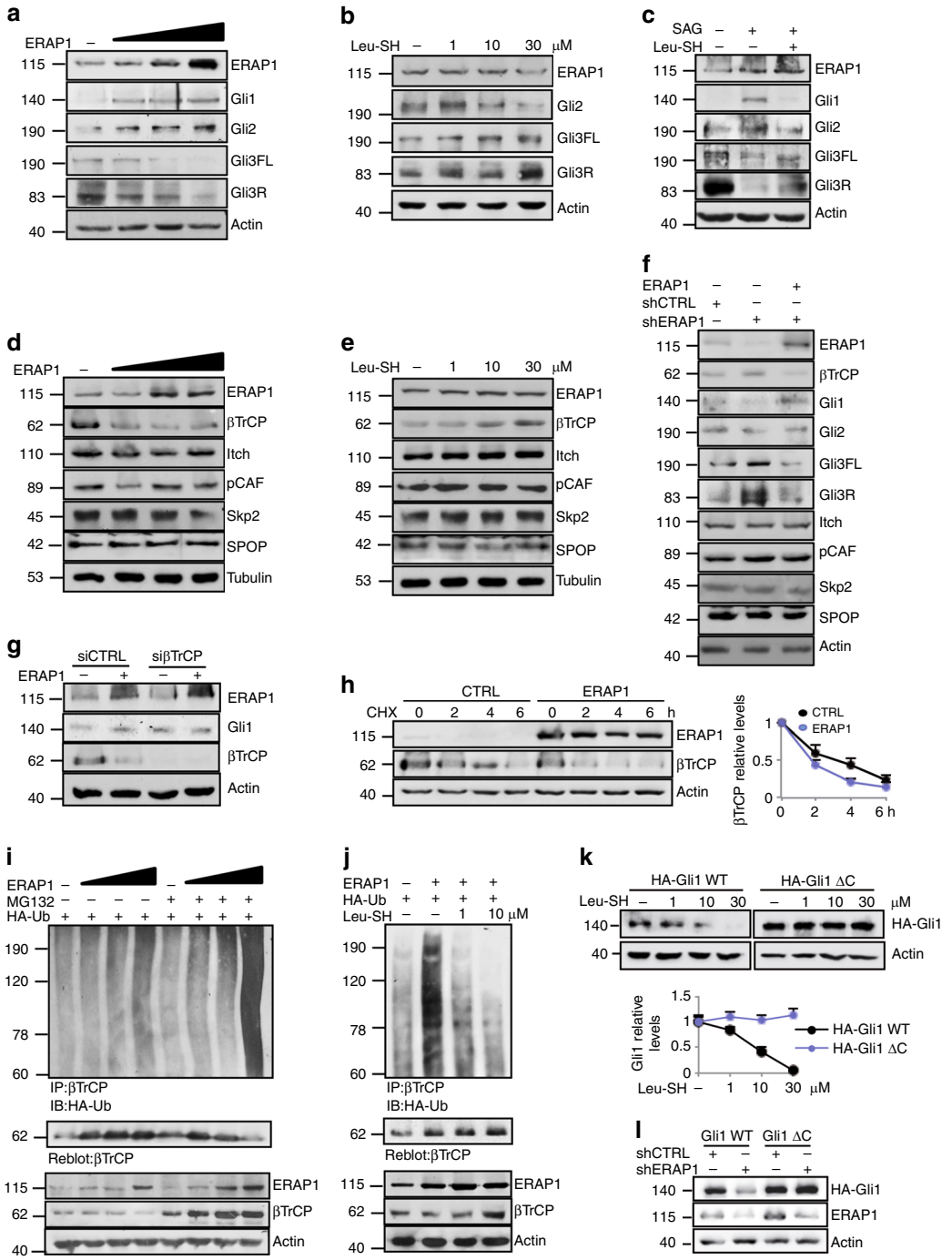

Fig. 2 ERAP1 activates Hh signaling by impairing βTrCP protein expression. **a**–**f** Representative immunoblotting analyses of the indicated proteins in MEFs transfected with increasing amounts of vector encoding ERAP1 (**a**, **d**) or treated for 24 h with Leu-SH at the indicated concentration (**b**, **e**), or SAG (200 nM) and Leu-SH (30 μM) (**c**), or DTT as control. In **f** MEFs were transduced with shCTRL or shERAP1 and transfected with a vector encoding ERAP1. Actin (**a**–**c**, **f**) and tubulin (**d**, **e**) were used as loading controls. **g** ERAP1, Gli1 and βTrCP protein levels in MEFs transfected with an empty vector or a vector encoding ERAP1 in the presence of small interfering RNAs (siRNAs) to a non-relevant mRNA (siCTRL) or murine βTrCP mRNA (siβTrCP). **h** βTrCP protein levels in MEFs transfected with an empty vector or a vector encoding ERAP1 and treated with cycloheximide (CHX, 100 μg/mL) at different time points. Densitometry analysis of actin-normalized βTrCP values of three independent experiments is shown (right panel). **i**, **j** Endogenous βTrCP was immunoprecipitated from MEFs expressing the indicated proteins and treated with MG132 (50 μM) for 4 h (**i**) or increasing doses of Leu-SH for 24 h (**j**), followed by immunoblotting with an anti-HA antibody to detect conjugated HA-Ub. Blots were both reprobed with a βTrCP antibody. Bottom ERAP1 and βTrCP protein levels in total cell lysate. Actin was used as loading control. **k** Immunoblotting (upper panel) and densitometric analysis (lower panel) of HA-Gli1 WT or HA-Gli1ΔC protein levels transfected in MEFs and treated after 24 h with increasing amount of Leu-SH for 24 h. **l** Immunoblotting analysis of HA-Gli1 WT or HA-Gli1ΔC protein levels transfected in MEFs transduced with shCTRL or shERAP1. Actin was used as loading control

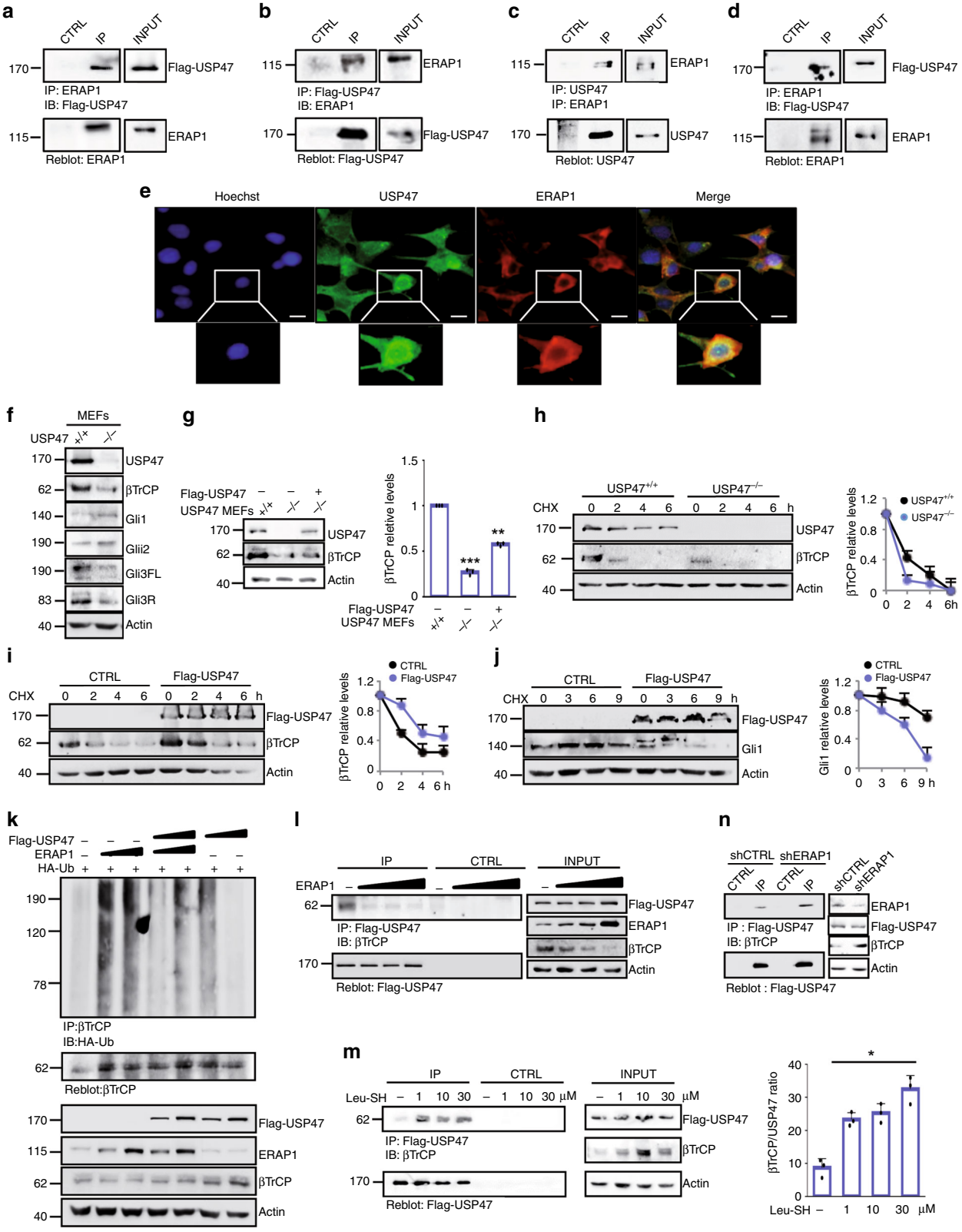

ERAP1 promotes βTrCP degradation by interacting with USP47. As ERAP1 did not appear to interact directly with βTrCP (Supplementary Figs. 5a, b), we investigated whether ERAP1 interferes with the Ubiquitin-Specific Protease 47 (USP47), a deubiquitylating enzyme known to interact with βTrCP[52]. Co-immunoprecipitation experiments demonstrated that ERAP1 binds both exogenous and endogenous USP47 in MEFs (Fig. 3a–d). Accordingly, confocal microscopy revealed that ERAP1 co-localizes with endogenous USP47 proteins in the perinuclear region, where endogenous ERAP1 is mainly localized[31] (Fig. 3e). Further, ERAP1 did not bind other Ubiquitin-Specific Proteases known to regulate the stability or activity of βTrCP, such as USP24[53] and USP22[54] (Supplementary Fig. 5c). βTrCP stability was impaired in USP47$^{-/-}$ MEFs, leading to

Fig. 3 ERAP1 promotes βTrCP ubiquitylation by interacting with USP47. **a–d** MEFs were transfected with ERAP1 and/or Flag-USP47. Interaction between USP47 and ERAP1 was detected by immunoprecipitation followed by immunoblot analysis with the indicated antibodies. **e** MEFs transfected with ERAP1 were stained with anti-ERAP1 and anti-USP47 antibodies. Green and red, USP47 and ERAP1 expressing cells, respectively. Nuclei were counter stained with Hoechst (Blue). Magnification ×60; Bars: 5 μm. Representative images from three independent experiments. **f** βTrCP and Gli steady state in USP47$^{+/+}$ and USP47$^{-/-}$ MEFs. **g** βTrCP protein level in USP47$^{+/+}$, USP47$^{-/-}$ and USP47$^{-/-}$ Flag-USP47 transfected MEFs. **h** βTrCP half-life in USP47$^{+/+}$ vs. USP47$^{-/-}$ MEFs treated with CHX (100 μg/mL) at the indicated times. **i** βTrCP protein levels in MEFs transfected with empty vector as control or Flag-USP47 and treated with CHX (100 μg/mL) at different time points. **j** Gli1 protein levels in Ptch$^{-/-}$ MEFs transfected with empty vector as control or Flag-USP47 and treated after 24 h with CHX (100 μg/mL) for different time points. In **g–j** densitometric analysis of βTrCP and Gli1 protein levels of three independent experiments are shown (right panels). **k** MEFs were transfected with HA-Ub and increasing amount of ERAP1 in the presence or absence of Flag-USP47. Endogenous βTrCP was immunoprecipitated with an anti-βTrCP antibody and the ubiquitylated forms were revealed with an anti-HA antibody (upper panel). The blot was reprobed with an anti-βTrCP antibody. Flag-USP47, ERAP1 and βTrCP total protein levels are shown (lower panel). **l** MEFs were transfected with Flag-USP47 and increasing amount of ERAP1. Interaction between Flag-USP47 and endogenous βTrCP was assessed by immunoprecipitation and immunoblotting with the indicated antibodies. Actin was used as loading control. **m** MEFs were transfected with Flag-USP47 and treated for 24 h with Leu-SH at the indicated concentration. Interaction between Flag-USP47 and endogenous βTrCP was detected as described in **l**. Densitometric analysis of the Flag-USP47/βTrCP binding ratio representative of three independent experiments is shown (right panel). **n** MEFs were transduced with shCTRL or shERAP1 and transfected with Flag-USP47. Interaction between Flag-USP47 and endogenous βTrCP was assessed as described in **l**

increased expression of Gli1 and Gli2 and decreased expression of Gli3FL and Gli3R (Fig. 3f). Consistently, the re-introduction of USP47 in USP47$^{-/-}$ MEFs restored βTrCP protein levels (Fig. 3g). Moreover, βTrCP half-life was reduced in the USP47$^{-/-}$ MEFs (Fig. 3h) and increased in the presence of USP47 as compared to control cells (Fig. 3i). Of note, USP47 overexpression decreased Gli1 half-life (Fig. 3j) in agreement with the established role of βTrCP in Gli1 regulation.

The effect of USP47 on ERAP1-mediated βTrCP ubiquitylation was studied by performing an in vivo βTrCP ubiquitylation assay in the presence of ectopic expression of ERAP1 and/or USP47. High levels of ERAP1 promoted a robust ubiquitylation of βTrCP that was counteracted by the co-expression of USP47 (Fig. 3k). Accordingly, the overexpression of USP47 alone leads to a decrease of ubiquitylated βTrCP (Fig. 3k) consistent with the enzymatic function of USP47[52]. Importantly, ERAP1 strongly impaired βTrCP/USP47 interaction (Fig. 3l), whereas its pharmacological inhibition or genetic depletion resulted in an increased association between the two proteins (Fig. 3m, n).

Overall, these findings indicate that ERAP1 promotes ubiquitylation and degradation of βTrCP by displacing its interaction with the USP47 deubiquitylase enzyme.

ERAP1 affects Hh-dependent growth of cerebellar GCPs. Hh signaling crucially regulates cerebellar development by controlling the expansion of a subset of granule cell progenitors (GCPs) and the proper development of the granule neuron lineage under Purkinje cell-derived Shh stimuli. Withdrawal of Hh signal causes physiologically GCPs growth arrest after the first post-natal week in mice inducing their differentiation into mature granules[55]. Importantly, genetic or epigenetic alterations in the Hh signaling lead to GCPs increased proliferation and their tumorigenic conversion[56,57]. To investigate the biological role of ERAP1 on Hh-dependent growth, the levels of ERAP1 expression were analyzed in GCPs at an early post-natal stage that is Hh-dependent. Similar to Gli1, ERAP1 was mainly expressed in the Hh-dependent outer external germinal layer (EGL) where highly proliferating GCPs reside, and absent in non-proliferating inner germinal layer (IGL) GCPs (Fig. 4a). Consistently, the proliferation rate and Gli1 expression levels of SAG-treated GCPs were significantly reduced in the presence of high doses of Leu-SH (Fig. 4b, c) or following the genetic inhibition of ERAP1 (Fig. 4d–f). As expected, the opposite effect was observed in SAG-treated GCPs overexpressing ERAP1 (Fig. 4g–i), suggesting a potential role of ERAP1 in controlling GCPs proliferation through Hh signaling.

ERAP1 affects Hh-dependent tumor cell growth in vitro. GCPs are considered the cells of origin of MB, the most common pediatric brain tumor genetically classified in four subgroups, of which Shh-group is the best characterized[1,58]. The relevance of ERAP1 on Hh-dependent tumor cell growth was determined by testing short-term cultures of primary MB cells freshly isolated from Math1-cre/Ptc$^{C/C}$ mice tumors, one the most used model to study the Hh-dependent tumorigenesis[39,57,59–61]. Pharmacological inhibition of ERAP1 significantly reduced the proliferation of Math1-cre/Ptc$^{C/C}$ MB cells in a dose- and time-dependent manner (Fig. 5a). This was consistent with increased cell death (Fig. 5b), increased levels of the cleaved Caspase 3 protein (Fig. 5c) and reduced BrdU uptake (Fig. 5d). Accordingly, Gli1 expression was reduced at mRNA and protein levels (Fig. 5e, f), indicating an impairment of the Hh signaling activity. Given the difficulty to obtain stable Hh-dependent MB cell lines, tumor cells from spontaneous MB of Math1-cre/Ptc$^{C/C}$ mice were propagated as neurospheres (MB Stem-Like Cells, MB-SLCs) in EGF- and bFGF-free cultured medium to retain the characteristic of in vivo Hh-subtype MB and preventing the differentiation of GCPs[62]. Similarly to cerebellar progenitors, the pharmacological inhibition of ERAP1 impaired both tumor cell proliferation in a dose- and time-dependent manner (Fig. 5g) and clonogenic self-renewal ability (Fig. 5h). Accordingly, MB neurospheres treated with increasing amounts of Leu-SH showed an impaired Hh pathway activity as evaluated by the significant reduced expression of the Hh pathway target genes Gli1, Gli2, and Ptch1, stemness markers (Oct4 and Nanog) and growth (CycD2) and oncogenic (N-Myc) related signals (Fig. 5i, j). Overall, these data demonstrate that ERAP1 affects Hh-dependent MB cell proliferation.

ERAP1 affects Hh-dependent tumor growth in vivo. Based on the in vitro studies, we hypothesized that inhibition of ERAP1 activity may reduce tumor growth in vivo. To address this critical issue NOD/SCID gamma (NSG) mice were grafted with spontaneous primary MB from Math1-cre/Ptc$^{C/C}$ mice and the obtained tumor masses were treated with Leu-SH or vehicle for about three weeks[27]. Leu-SH treatment significantly reduced tumor growth as compared to controls (Fig. 6a, b). Reduced cellularity associated with a decreased Ki67 and increased NeuN and cleaved Caspase-3 positive tumor cells was detected in Leu-SH treated tumor masses, indicating that ERAP1 inhibition impairs tumor growth by promoting cell differentiation and committing tumor cells to apoptosis (Fig. 6c, d). In agreement with the in vitro data (Fig. 5), the

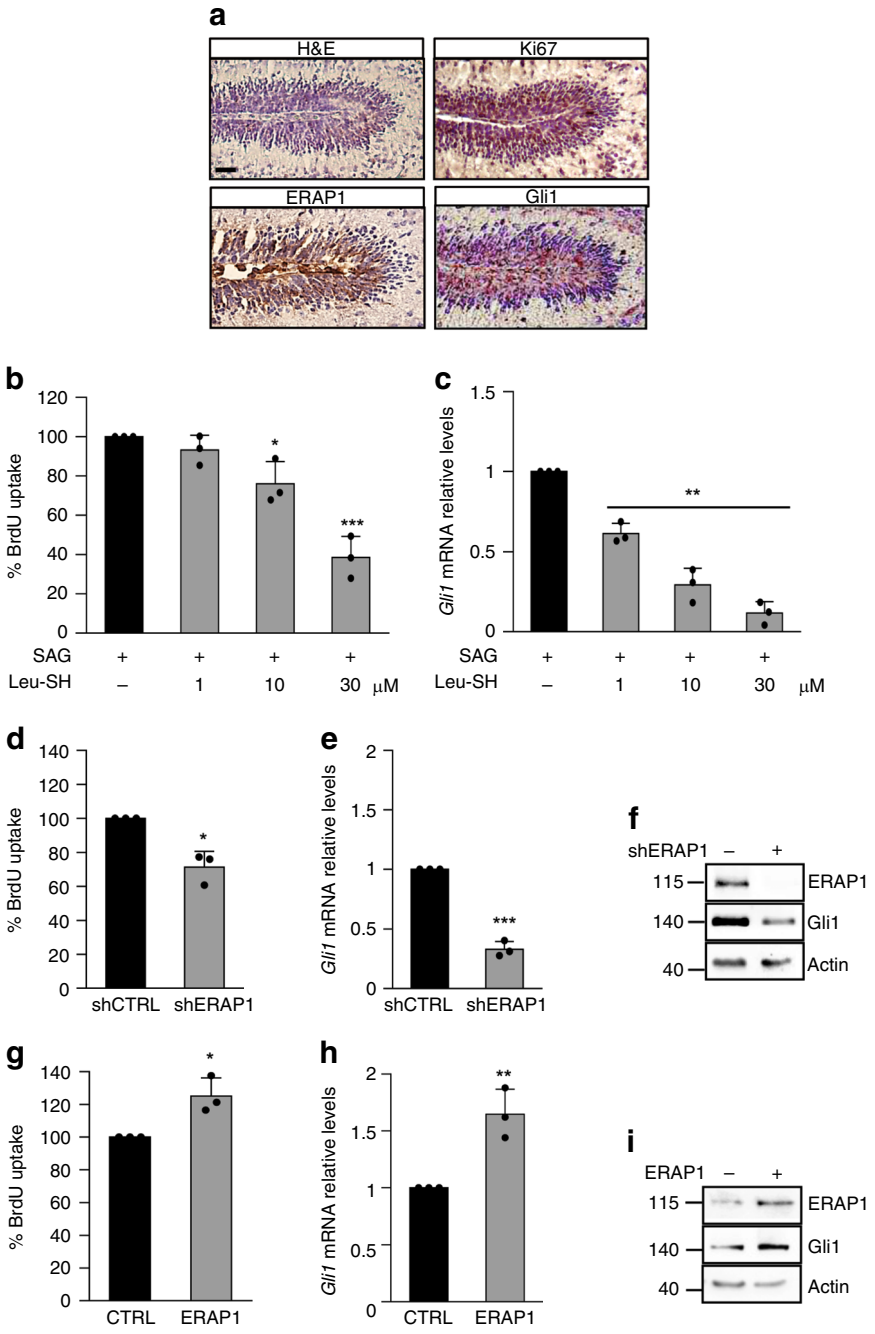

Fig. 4 ERAP1 impairs Hh-dependent growth of cerebellar granule cell progenitors. **a** H&E and immunohistochemical staining of Ki67, ERAP1 and Gli1 in the outer EGL during mouse cerebellum development. Magnification ×40. Scale bars represent 50 μm. **b**, **c** GCPs were isolated from 4-day-old mice and treated with either SAG alone or in combination with increasing doses of Leu-SH for 24 h. BrdU uptake (**b**) and mRNA levels of *Gli1* (**c**) are shown. **d**, **i** GCPs isolated from 4-day-old mice were infected with lentiviral particles encoding for shERAP1 (**d**–**f**) or ERAP1 (**g**–**i**) and the corresponding controls, respectively. The percentage of BrdU uptake (**d**, **g**), mRNA (**e**, **h**), and protein levels (**f**, **i**) of Gli1 are shown. Results in **c**, **e**, **h** were normalized to endogenous *GAPDH* and *HPRT* controls and expressed as described in Fig. 1 legend, and represent the mean of three independent experiments. In f and i, actin was used as loading control. Mean ± S.D. $^{*}P < 0.05$; $^{**}P < 0.01$ determined with two-sided Student's *t*-test

expression of endogenous Hh target genes was reduced at both mRNA and protein levels in Leu-SH-treated tumors compared to controls, whereas protein levels of NeuN, cleaved Caspase-3 and βTrCP were increased (Fig. 6e, f). An orthotopic allograft animal model in which primary MB cells isolated from Math1-cre/$Ptc^{C/C}$ mice tumors were implanted into the cerebellum of NSG mice confirmed these results. The animals treated with Leu-SH showed a significant reduction of tumor masses as compared to control (Fig. 6g, h). Accordingly, in a further allograft model all mice engrafted on the flanks with MB cells infected with control lentiviruses developed progressively enlarging tumors, whereas no palpable tumor masses were developed in most mice engrafted with MB cells infected with shERAP1 lentiviruses (Fig. 6i, j). Consistent with above data, these tumor masses showed a reduced cellularity with few MB cells dispersed in a large amount of Masson's staining-mediated blue-labeled connective tissue and reduced Hh-pathway signature, as compared to control tumors (Fig. 6k, l). A more

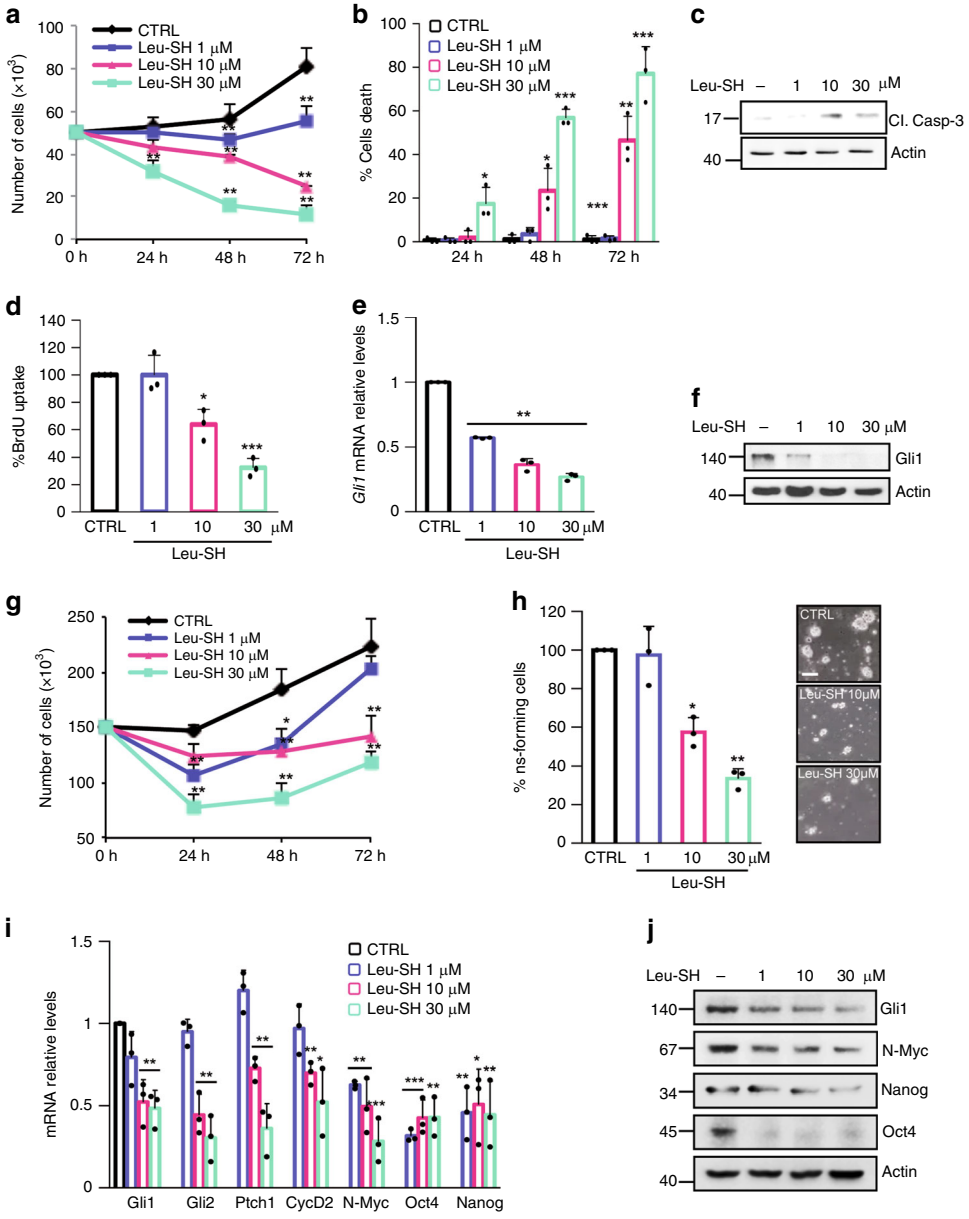

Fig. 5 ERAP1 impinges Hh-dependent tumor cell growth in vitro. **a**–**f** Primary cell cultures from Math1-cre/Ptc$^{C/C}$ mice MBs were treated with different amounts of Leu-SH. **a**, **b** Cells were counted with trypan blue at the indicated time points to evaluate the growth rate of viable cells (**a**) and the percentage of cell death (**b**). **c** Cleaved Caspase-3 protein levels in cells treated with Leu-SH at the indicated concentration for 24 h. **d**–**f** Percentage of BrdU uptake (**d**) and *Gli1* mRNA (**e**), and protein (**f**) expression in MB cells treated with Leu-SH at the indicated concentrations for 24 h. **g** MB Stem-Like Cells (MB-SLCs) from Math1-cre/Ptc$^{C/C}$ mice were treated with Leu-SH as in (a) and counted with trypan blue at the indicated time points. **h** MB-SLCs were dissociated and treated with the indicated concentrations of Leu-SH or DTT as control. After 7 days of treatment, the number of secondary neurospheres derived from a known number of single cells was evaluated. The self-renewal MB-SLCs capability is expressed as percentage of neurosphere-forming cells (right). Representative bright field images of tumor neurospheres after Leu-SH treatment are shown (left). Scale bar 100 μM. **i**, **j** mRNA and protein expression levels of Hh target genes of MB-SLCs treated with the indicated concentrations of Leu-SH for 24 h. Actin was used as loading control. Results in **e**, **i** were normalized to endogenous *GAPDH* and *HPRT* controls and expressed as described in Fig. 1 legend. All data are representative of three independent experiments. Mean ± S.D. $^{*}P < 0.05$; $^{**}P < 0.01$ calculated using two-tailed Student's *t*-test

robust effect of the ERAP1 function on the MB in vivo cell growth was observed in an orthotopic allograft model where spontaneous primary MB cells from Math1-cre/Ptc$^{C/C}$ mice genetically silenced for ERAP1 were implanted into the cerebellum of NSG mice. As shown in Fig. 6m, only the cells infected with the lentiviral particles encoding for a non-targeting sequence gave rise to detectable tumor masses. These findings demonstrate that inhibition of ERAP1 interferes with Hh-dependent MB growth processes in vivo.

To investigate the role of ERAP1 during MB development, tumor-prone GCPs from the cerebellum of five-day postnatal (P5) Math1-cre/Ptc$^{C/C}$ mice were infected with lentiviruses expressing ERAP1 and then injected into the flank of NSG recipient animals. Compared to controls, mice engrafted with GCPs overexpressing ERAP1 showed an increased tumor growth rate, tumor volume (at the end point), and expression of *Gli1* and *CyclinD2* (Fig. 6n–p), accordingly with the role of ERAP1 in promoting Hh signaling.

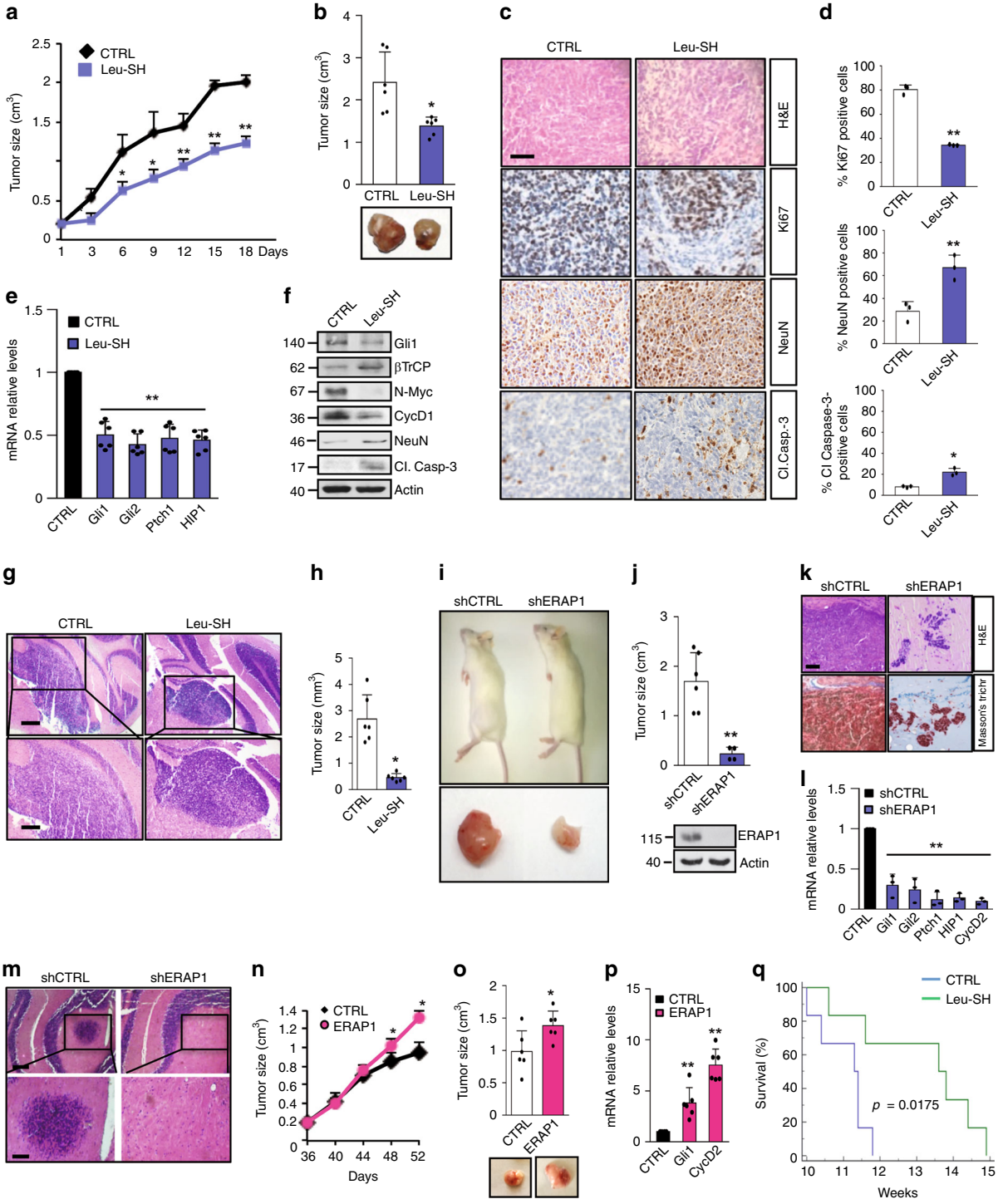

Moreover, to verify the effect of ERAP1 inhibition in a natural tumor niche for MB growth, symptomatic Gfap-cre/Ptc$^{fl/fl}$ mice were treated with Leu-SH or vehicle for two consecutive days. Treatment with Leu-SH resulted in reduced levels of the Hh pathway target genes and increased levels of βTrCP (Supplementary Figs. 6a, b). Interestingly, we found that i.p. treatment with Leu-SH significantly improved survival in the Math1-cre/Ptc$^{C/C}$ (Fig. 6q), demonstrating the potential therapeutic benefit of ERAP1 inhibition in the development of tumors in situ.

Together, these data identify a molecular mechanism in the regulation of Hh signaling and unveil the relevance of ERAP1 in the control of Hh-dependent tumor growth.

ERAP1 inhibition impairs human SHH-MB growth. Next, we investigated the effect of the inhibition of ERAP1 in human SHH-MB models. Similarly to murine tumor models, either pharmacological or genetic inhibition of ERAP1 impairs in vitro proliferation of the human Hh-dependent MB cell line Daoy (Supplementary Fig. 7a, b, d, e), leading to a decreased Hh-pathway activity (Supplementary Fig. 7c, f, g). To further evaluate the effect of ERAP1 activity in vivo, we performed a xenograft in NSG mice grafted on the flank with Daoy cells infected with lentiviral particles encoding for either shERAP1 or shCTRL. As expected, inhibition of ERAP1 significantly reduced tumor growth compared to controls, resulting in a decrease in

Fig. 6 ERAP1 inhibition impairs Hh-dependent tumor growth in vivo. **a**–**f** NSG mice were grafted with spontaneous primary MB from Math1-cre/Ptc$^{C/C}$ mice. Tumor masses (150 mm^3) were intratumorally injected with Leu-SH. **a** Tumor growth was monitored. **b** Representative flank allograft average volumes (lower panel) and quantification of tumor explants (upper panel). **c**, **d** Ki67, NeuN, and cleaved Caspase-3 (Cl.Casp-3) immunohistochemical stainings of allograft tumor samples. **d** Quantification of immunohistochemical stainings shown in **c**. Scale bar 100 µm. **e** mRNA and **f** protein expression levels of Hh targets from tumors assayed in **b**. **g** Representative H&E images (low and high magnification) of a murine MB cell-derived orthotopic tumor in NSG mice after i.p. injection of Leu-SH. Scale bars, 500 µm and 200 µm (upper and lower panels, respectively). **h** Representative average volume of orthotopic tumor. **i**–**j** NSG mice were grafted with spontaneous primary MB from Math1-cre/Ptc$^{C/C}$ mice genetically silenced for ERAP1 expression. **i** Representative images of mice and the explanted tumor masses. **j** Quantification of the flank allograft average tumor volume. ERAP1 protein expression is shown below. In **f**, **j**, actin was used as loading control. **k** H&E and representative Masson's trichrome staining of tumors. Scale bar 100 µm. **l** mRNA levels of the indicated Hh target genes. **m** Representative H&E images (low and high magnification) of a murine MB cell-derived orthotopic tumor genetically interfered for ERAP1 before the injection in NSG mice cerebella. Scale bars, 500 and 200 µm (upper and lower panels, respectively). **n**–**p** ERAP1 accelerates Hh-MB formation. **n** Tumor volume of mice subcutaneously transplanted with GCPs from tumor-prone Math1-cre/Ptc$^{C/C}$ animals overexpressing ERAP1. **o** Representative flank allograft average volumes (lower panel) and quantification of the explanted tumor masses (upper panel). **p** mRNA expression of Hh target genes from the tumor masses assayed in **o**. **q** Survival curves of Math-cre/Ptc$^{C/C}$ mice treated with Leu-SH or vehicle. Results in **e**, **l**, **p** were normalized to endogenous *GAPDH* and *HPRT* controls and expressed as in Fig. 1. All data represent the mean of three independent experiments. Mean ± S.D. of tumor ($n = 6$) for each treatment. *$P < 0.05$, **$P < 0.01$, *** $P < 0.001$ calculated by two-sided Student's *t*-test

endogenous Hh target genes at both mRNA and protein levels (Supplementary Figs. 7h–k).

Finally, we found that the pharmacological inhibition of ERAP1 affected SHH-MB Patient-Derived Xenograft (PDX)[63] cell proliferation and increased tumor cell death in a dose- and time-dependent manner leading to apoptosis, as indicated by increased cleaved Caspase-3 positive cells (Fig. 7a–e). These results were confirmed by evaluating the cellular confluence over time of the SHH-MB PDX cells treated with increased amounts of Leu-SH (Supplementary Figs. 8a–c). As expected, the genetic depletion of ERAP1 in SHH-MB PDX cells resulted in reduced cell proliferation, increased cell death and reduced levels of Gli1 protein (Supplementary Figs. 8d–g).

In agreement with the in vitro data, Leu-SH treatment reduced the growth of MB SHH-PDX cells injected into the flank of NSG mice (Fig. 7f, g). As in the allograft model performed with spontaneous murine tumor (Fig. 6a–f), tumor masses treated with Leu-SH showed a reduced cellularity associated with a decrease in Ki67-positive tumor cells and an increase in NeuN and cleaved Caspase-3 positive tumor cells (Fig. 7h, i). Moreover, mRNA and protein expression levels of the endogenous Hh target genes were reduced, unlike the βTrCP protein levels (Fig. 7j, k). Overall, these data confirm the role of ERAP1 in the regulation of Hh-dependent tumor growth.

Discussion

Hh signaling is an evolutionarily conserved pathway regulating cell fate and specification. Its tight regulation is essential for proper development and adult tissue preservation. Constitutive activation of the Hh pathway has been associated with a multitude of cancer types, including brain tumors. Hh signaling is also known to regulate stemness and drive tumor initiation and progression[64]. Due to its crucial role in tumorigenesis, Hh signaling has emerged as an attractive druggable target and a number of pathway-specific inhibitors are moving into the clinic[65,66]. However, therapeutic strategies aiming at blocking Hh signaling activation are complicated by the development of resistance and side effects, thus prompting alternative treatment approaches.

The combination of multiple drugs targeting different Hh signaling components and/or correlating Hh activating routes represents the most effective strategy for cancer treatment[67–72]. For this reason, the identification of molecular players controlling Hh activity is of clinical importance and represents a dramatic challenge in tumor biology.

In the present study, we identify and characterize an oncogenic property of ERAP1, an endoplasmic reticulum aminopeptidase. So far, ERAP1 has been well-studied for its role in the antigen processing, a mechanism resulting in the production of high affinity peptides for the binding to MHC class I molecules. Like the other components of the antigen processing machinery, ERAP1 is induced in response to IFN-γ stimulation[22], a feature that makes it particular active in counteracting antiviral and anti-tumor immune responses. In this context, ERAP1 trims the N-terminal extension of precursor peptides to generate mature antigenic peptides[21]. Loss of ERAP1 function results in the generation of a new immunopeptidome, which stimulates anti-tumor immune responses determining the tumor regression of different mouse models[27,36]. Moreover, recent genome-wide studies have strongly associated ERAP1 polymorphisms with several autoimmune diseases, such as ankylosing spondylitis[29]. The polymorphic residues map to ERAP1's catalytic and regulatory sites and alter peptide specificity and processing activity, thus suggesting that the enzymatic activity of ERAP1 is important in the link with genetic disease[30]. However, the lack of commercial availability for highly specific chemical compounds for ERAP1 has constrained the progress in this area. Given the great interest in ERAP1, many pharmaceutical companies are investing in the development of ERAP1 inhibitors for potential therapeutic intervention.

Herein, we uncovered an unexpected role of ERAP1 in regulating Hh-dependent tumorigenesis, thus providing further evidence that inhibition of ERAP1 may be exploited for cancer treatment. We demonstrated that ERAP1 enhances Hh activity by sequestering USP47 and promoting ubiquitylation and degradation of βTrCP. This event results in an increase of Gli1 and Gli2 protein levels and a reduction of the Gli3R form, thus activating the Hh pathway and stimulating cell proliferation and tumorigenesis (Fig. 8). Conversely, inhibition of ERAP1 function stabilizes βTrCP, which in turn induces ubiquitylation of Gli factors leading to proteolysis of Gli1 and Gli2 and generation of Gli3R, thereby suppressing tumor cell growth.

Gli transcription factors are crucial effectors of the Hh pathway and their activity and expression are finely regulated by several mechanisms, mainly by the ubiquitin-proteasome system. Upon phosphorylation by PKA, GSK3β, and CK1, Gli factors are recognized by the SCF^{βTrCP} ubiquitin ligase, which triggers the proteasome-dependent degradation of Gli1[9] and processing of Gli3 in its repressor form[14,41]. Gli2 is processed by both events, although the degradation one being predominant[8,10]. Hence, inhibition of the βTrCP-mediated degradation of Gli proteins is part of an Hh-induced activation signal by which Hh supports the function of Gli. Although βTrCP is fundamental for the regulation of Hh-mediated signals, the mechanisms controlling its function are still largely unexplored.

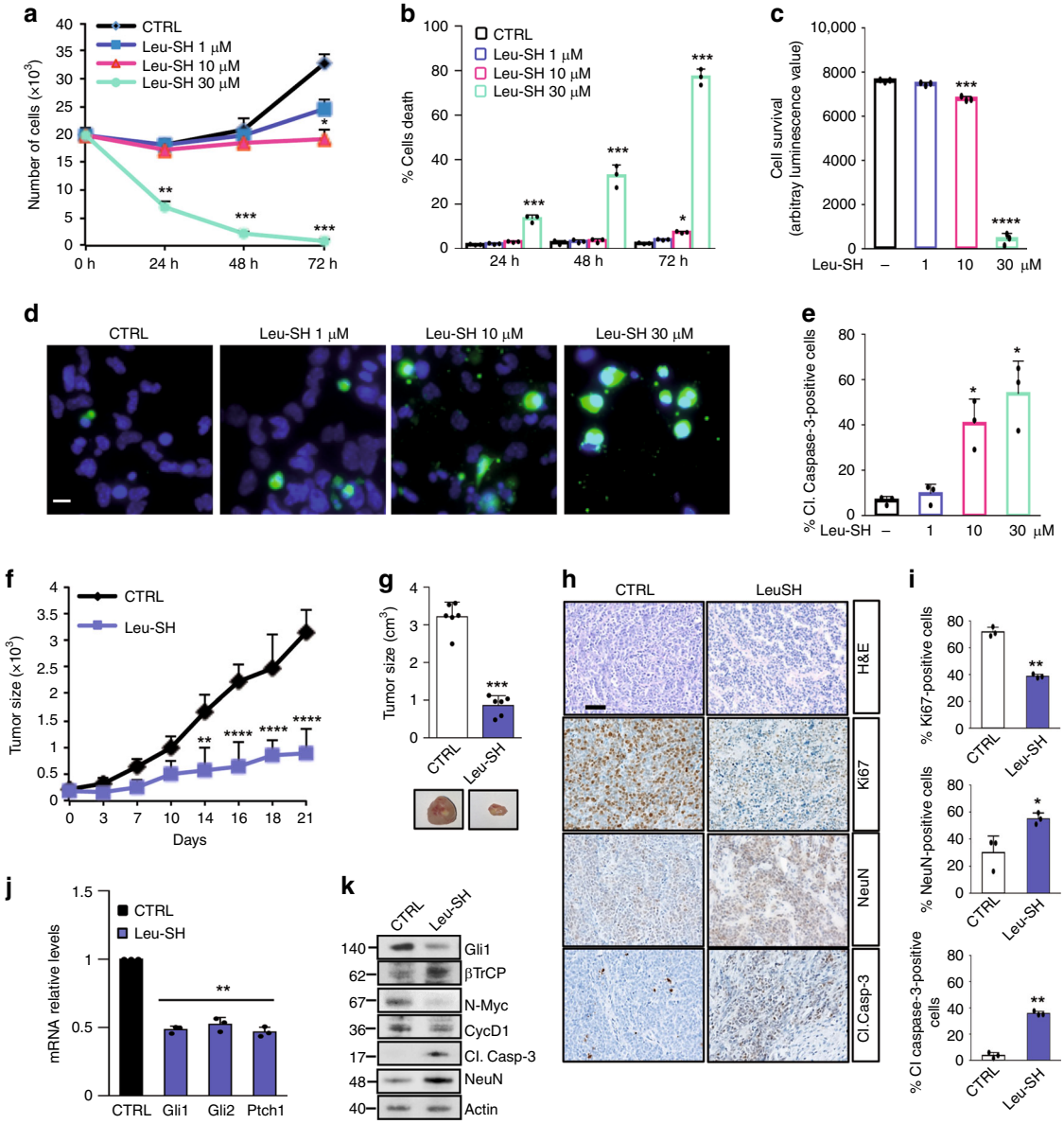

Fig. 7 a–e SHH-MB PDX tumor cells were treated with different amounts of Leu-SH. **a**, **b** Cells were counted with trypan blue at the indicated time points to evaluate the growth rate of viable cells (**a**) and the percentage of cell death (**b**). **c** Cell survival was also assessed by the Cell Titer Glo assay. **d** Immunofluorescent staining of cleaved Caspase 3 (green) of Leu-SH treated cells (48 h). Nuclei were counter stained with Hoechst (Blue). Scale bar 5 μm. **e** Quantification of cleaved Caspase-3 from immunofluorescence stainings in (**d**). (**f**–**k**) NSG mice ($n = 6$ for group) were grafted with SHH-MB PDX tumor cells. Tumor masses (150 mm^3) were intratumorally injected with Leu-SH (0.528 μM/Kg). **f** Tumor growth was monitored every three days. **g** Quantification of the explanted tumor masses (upper panel) and representative flank xenograft average volumes (lower panel). **h** H&E, Ki67, NeuN and cleaved Caspase-3 immunohistochemical staining of PDX tumor samples. **i** Quantification of Ki67, NeuN and cleaved Caspase-3 from immunohistochemical stainings in **h**. Scale bar 100 μm. **j**, **k** mRNA (**j**) and protein (**k**) expression levels of the indicated Hh target genes from the tumor masses assayed in **g**. Mean ± S.D. *$P < 0,05$; **$P < 0,01$; ***$P < 0,001$; ****$P < 0,0001$ determined using two-tailed Student's *t*-test

USP47 is a member of a class of enzymes named Ubiquitin-Specific Proteases (USPs), which are able to catalyze the removal of ubiquitin from substrates counteracting the activity of E3 ubiquitin ligases or protect them from self-ubiquitylation/degradation events.

Previous reports have demonstrated that USP47 is a key player in the regulation of cell viability and maintenance of genome integrity by promoting the stability of DNA polymerase β[52,73]. USP47 has been also described as a βTrCP interactor, although the biological outcome of this interaction is controversial[52,74]. Here, we found that USP47 strongly stabilizes βTrCP preventing its ubiquitin-dependent degradation. Interestingly, this process is inhibited by ERAP1 that, through the binding to USP47, hampers the βTrCP/USP47 interaction and induces βTrCP proteolysis. Consequently, the Hh pathway is triggered by the transcription factors Gli, which promote cell proliferation. These results also provide convincing evidence that USP47 impairs Hh/Gli signaling and the Hh-driven tumorigenesis. Interestingly, no difference in ERAP1 and USP47 expression levels was observed in SHH MB as compared to other molecular subgroup or other brain tumor entities (Supplementary Fig. 9), thus suggesting that the activity, rather than the expression, of ERAP1 could be related to the SHH-MB. This adds more complexity due to the presence of modulators or not yet identified ERAP1 polymorphisms that

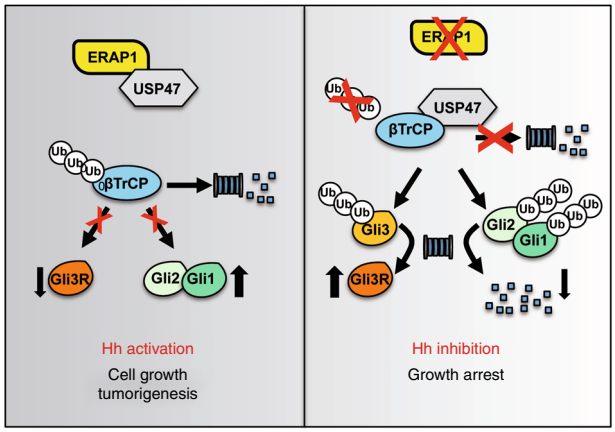

Fig. 8 A representative model showing the role of ERAP1 in Hh-dependent tumorigenesis. ERAP1 promotes ubiquitylation and proteasomal degradation of βTrCP by sequestering USP47. This event leads to increase of Gli1 and Gli2 protein levels and decrease of Gli3R, thus triggering the Hh pathway and favoring cell growth and tumorigenesis. In the absence of ERAP1, USP47 binds and stabilizes βTrCP, which, in turn, promotes ubiquitylation and proteasomal degradation of Gli1 and Gli2, and ubiquitylation and proteolytic cleavage of Gli3 into the repressor form Gli3R. These events lead to the repression of the Hh pathway and inhibition of cell proliferation and tumor growth

could alter its conformational state and induce defects in its open-close transitions[75], thus modifying the activity of ERAP1 or its binding affinity to other proteins (i.e. to favor interaction with USP47 that leads to the degradation of βTrCP and stability of Gli proteins).

In conclusion, our study reveals an unexpected function of ERAP1 in cancer development suggesting that targeting ERAP1 could open innovative perspectives for effective therapeutic approaches in the treatment of Hh-dependent tumors.

Methods

Cell cultures, transfections, and lentiviral infections. NIH3T3 cells, Shh-Light-II cells and MEFs from wild-type (WT) or Ptch$^{-/-}$, SuFu$^{-/-}$, USP47$^{+/+}$ and USP47$^{-/-}$ mice were cultured in Dulbecco's Modified Eagle's Medium (DMEM) plus 10% fetal bovine serum (FBS) or 10% bovine serum (BS) for NIH3T3 cells. Daoy cells were cultured in Eagle's minimum essential medium (MEM) plus 10% FBS. All media contained L-glutamine and antibiotics. HEK293T (CTR-3216^{TM}) and NIH3T3 (CRL-1658^{TM}) cells were obtained from ATCC. SuFu$^{-/-}$ MEFs were gift from Dr. R. Toftgård (Karolinska Institute), Ptch$^{-/-}$ MEFs were gift from Dr. M. P. Scott (Stanford, California, USA). For cerebellar GCPs culture from 4-days-old mice, cerebella were removed aseptically, cut into small pieces, and incubated at room temperature for 15 min in digestion buffer [Dulbecco's PBS (Invitrogen, Gaithersburg, MD) with 0.1% trypsin, 0.2% EDTA, and 10 μg/ml DNase]. Tissues were then triturated with fire-polished Pasteur pipettes to obtain a single-cell suspension. Cells were centrifuged and resuspended in Neurobasal medium supplemented with B27 (2%), penicillin–streptomycin (1%) and L-glutamine (1%) (Invitrogen) and plated at a density of 8×10^5 cells/cm^2. Primary MB cells were freshly isolated from Ptch$^{+/-}$ mice. Briefly, tumor was mechanically disrupted with fire-polished Pasteur pipettes in HBSS with 1% Pen/Strep and treated with DNase (10 μg/ml) for twenty minutes. Cells were centrifuged and resuspended in Neurobasal Media-A with B27 supplement minus vitamin A, penicillin–streptomycin (1%) and L-glutamine (1%). Stable Hh-dependent MB cells were cultured as neurospheres in DMEM/F12 media (2% B27 minus vitamin A; 3% Glucose 10×; 0.2% Insulin 10 mg/ml; 1% Pen/Strep; 0.01% Heparin 2 mg/ml; 0.06% *N*-Acetyl-L-Cysteine).

Mycoplasma contamination in cell cultures was routinely detected by using PCR detection kit (Applied Biological Materials, Richmond, BC, Canada).

Transient transfections were performed using DreamFect^{TM}Gold transfection reagent (Oz Biosciences SAS, Marseille, France), or Lipofectamine$^{®}$ with Plus^{TM} Reagent (Thermo Fisher Scientific, Waltham, MA, USA) in accordance with the manufacturer's protocols.

Lentiviral particles were generated in HEK293T cells by combining packaging plasmids pCMV-dR8.74 and VSV-G/pMD2, with pLKO.1 plasmid (shCTRL SHC002; shERAP1 TRCN0000031119 (#1), TRCN0000031121 (#2), TRCN0000060542 (for Daoy and PDX), Sigma-Aldrich) or TWEEN-ERAP1 and its empty vector, using TransIT-293 transfection reagent (MIRUS Bio LLC, Madison, WI, USA). NIH3T3, MEFs and Daoy cells were infected by spin inoculation method. Primary MB cells were infected with purified lentiviruses for 72 h.

For RNA interference, cells were transfected with scrambled or βTrCP shRNAs (Cat no: D-001810-10-05 and E-044048-00, respectively, Dharmacon, Inc., Lafayette, CO, USA) for 48 h with HiPerFect transfection reagent (Qiagen, Hilden, Germany) according to the manufacturer's instructions.

Plasmids, Antibodies and other reagents. pcDNA3.1-Flag-USP47, pcDNA3-Flag-Gli1, pcDNA3-Flag-Gli2, and pcDNA3-Flag-Gli3 were generated in our lab with standard cloning techniques and verified by sequencing. pCS2HA3hGli1 WT and pCS2HA3hGli1ΔC were kindly provided by A.E. Oro. pCMV6-XL5-ERAP1 (SC311137) was purchased from Origene (Rockville, MD, USA). shCTRL (SHC002) and shERAP1 (TRCN0000031119, TRCN0000031121, TRCN0000060542) in pLKO.1 plasmids were purchased from Sigma-Aldrich. ERAP1 transcript variant 2 was cloned in the lentiviral vector pRRL-CMV-PGK-GFP-WPRE (TWEEN) under the control of the CMV promoter.

Mouse anti-Gli1 (L42B10, 1:500), rabbit anti-βTrCP (D13F10, 1:1000), rabbit anti-cleaved Caspase-3 (Asp175 D3E9, 1:100 for IHC, 1:500 for WB) and rabbit anti-Phospho-PKA Substrate (RRXS*/T*, 100G7E, 1:1,000) were purchased from Cell Signaling (Beverly, MA, USA). Mouse anti-α Tubulin TU-02 (sc-8035, 1:1000), goat anti-Actin I-19 (sc-1616, 1:1,000), mouse anti-βTrCP C-6 (sc-390629, 2 μg), mouse anti-HA-probe F-7 HRP (sc-7392 HRP, 1:1,000), mouse anti-pCAF E-8 (sc-13124, 1:500), rabbit anti-Cyclin D1-20 (sc-717, 1:500), mouse anti-N-Myc B8.4.B (sc-53993, 1:500), rabbit anti-Gli1 H300 (sc-20687, 1:100) and HRP-conjugated secondary antibodies were purchased from Santa Cruz Biotechnology (Santa Cruz, CA, USA). Anti-Flag M2 HRP (A8592, 1:1000) and rabbit anti-Flag (F7425, 2 μg) were purchased from Sigma Aldrich (St Louis, MO, USA). Rabbit anti-USP47 (A301-048A, 1:1000, 2 μg) from Bethyl Laboratories (Montgomery, TX, USA). Mouse anti-SKP2 (323300, 1:500) were purchased from Invitrogen (Thermo Fisher Scientific, Waltham, MA, USA). Goat anti-Gli3 (AF3690, 1:1000) and goat anti-Gli2 (AF3635, 1:1000) were from R&D Systems (Minneapolis, MN, USA). Mouse anti-ERAP1 6H9 (1:1000) and mouse anti-ERAP1 4D2 (2 μg), kindly provided by P. van Endert, recognize denatured and native human ERAP1, respectively. Mouse anti-Itch (611199, 1:1000) antibody was purchased from BD Bioscience (Heidelberg, Germany). Rabbit anti-SPOP (16750-1-AP, 1:1000), Rabbit anti-USP22 (55110-1-AP, 1:2000) and Rabbit anti-USP24 (13126-1-AP, 1:1000) were purchased from Proteintech (Thermo Fisher Scientific, Waltham, MA, USA). Rabbit anti-Ki67 SP6 (MA5-14520, 1:100) was from Thermo Fisher Scientific (Waltham, MA, USA). Anti-rabbit Alexa Fluor 488 (A21206, 1:400 in BSA 3%) and anti-mouse Alexa Fluor 546 (A11003, 1:400 in BSA 5% and Goat Serum 3%) were purchased from Life Technologies (Foster City, CA, USA). Mouse anti-NeuN (clone A60, MAB377, 1:100 for IHC and 1:1000 for WB) was from Millipore (Merk, Darmstadt, Germany).

Where indicated, cells were treated with SAG (200 nM, Alexis Biochemicals Farmingdale, NY, USA) for 24 or 48 h, MG132 (50 μM; Calbiochem, Nottingham, UK) for 4 h, Cycloheximide (CHX 100 μg/ml, Sigma Aldrich), Dihydrochloride (H-89, Calbiochem, Nottingham, UK), L-Leucinethiol (Leu-SH, Sigma Aldrich) or Dithiothreitol (DTT, SERVA, Heidelberg, Germany) as indicated.

Luciferase reporter assay. The Hh-dependent luciferase assay was performed in Shh-Light II cells, stably expressing a Gli-responsive luciferase reporter and the pRL-TK Renilla (normalization control), treated for 48 h with SAG (200 nM) and for 24 h with Leu-SH and/or DTT as control at the indicated concentrations.

AP1/Jun- and WNT/β-Catenin-luciferase assays were carried out in MEFs WT transfected with MMP1-luciferase reporter and Jun- or Top Flash-luciferase reporter and β-Catenin, respectively, and pRL-TK Renilla. After 24 h from transfection, cells were treated with increasing amounts of Leu-SH and/or DTT.

Luciferase and Renilla activities were assayed with a dual-luciferase assay system according to the manufacturer's instructions (Biotium Inc., Hayward, CA, USA). Results were expressed as luciferase/Renilla ratios and represented the mean ± S.D. of three experiments, each performed in triplicate.

Immunoblot analysis and immunoprecipitation. Cells were lysed in a solution containing RIPA buffer (50 mM Tris-HCl at pH 7.6, 150 mM NaCl, 0.5% sodium deoxycholic, 5 mM EDTA, 0.1% SDS, 100 mM NaF, 2 mM NaPPi, 1% NP-40) supplemented with protease and phosphatase inhibitors. The lysates were centrifuged at 13,000 g for 30 min at 4 °C and the resulting supernatants were subjected to immunoblot analysis. Immunoprecipitation was performed using whole-cell extracts obtained by lysing cell pellets with Triton Buffer (50 mM Tris-HCl pH 7.5, 250 mM sodium chloride, 50 mM sodium fluoride, 1 mM EDTA pH 8, 0.1% Triton), supplemented with protease and phosphatase inhibitors. Cell lysates were immunoprecipitated overnight at 4 °C with rotation with specific primary antibodies or IgG used as a control (1–2 μg/ml, Santa Cruz Biotechnology) and then incubated with Protein G- or Protein A-agarose beads (Santa Cruz Biotechnology) for 1 h at 4 °C with rotation. The immunoprecipitates were then washed five times with the lysis buffer described above, resuspended in sample loading buffer, boiled for 5 min, resolved in SDS-PAGE and then subjected to immunoblot analysis.

Uncropped scans of the most important blots are reported in Supplementary Figs. 10 and 11.

In vivo ubiquitylation assay. MEFs were lysed with denaturing buffer (1% SDS, 50 mM Tris-HCl at pH 7.5, 0.5 mM EDTA, 1 mM DTT) to disrupt protein-protein interactions. Lysates were then diluted 10 times with NETN lysis buffer and subjected to immunoprecipitation with anti-βTrCP (Santa Cruz Biotechonology) overnight at 4 °C with rotation. The immunoprecipitated proteins were then washed five times with the NETN lysis buffer, resuspended in sample loading buffer, boiled for 5 min, resolved in SDS-PAGE and then subjected to immunoblot analysis. Polyubiquitylated forms were detected using mouse anti-HA from Santa Cruz Biotechnology.

mRNA expression analysis. Total RNA was extracted using TRIzol reagent (Thermo Fisher Scientific) and reverse-transcribed with SensiFASTcDNA Synthesis Kit (Bioline Reagents Limited, London, UK). Quantitative real time PCR (qPCR) analysis of *ERAP1, βTrCP, Gli1, Gli2, Ptch1, Hip1, CyclinD2, N-Myc, Oct4,* and *Nanog* mRNA expression was performed using the ViiA^{TM} 7 Real-Time PCR System (Life Technologies). Standard qPCR thermal cycler parameters were used to amplify a reaction mixture containing cDNA template, SensiFAST^{TM} Probe Lo-ROX mix (Bioline Reagents Limited) and Taqman Gene Expression Assays (Thermo Fisher Scientific). The average of three threshold cycles was used to calculate the amount of transcript in each sample amplificated in triplicate (using SDS version 2.3 software). mRNA quantification was calculated as the ratio of the sample quantity to the calibrator quantity expressed in arbitrary units. Data were normalized with the endogenous controls (*GAPDH* and *HPRT)* and expressed as the fold change respect to the control sample value.

BrdU incorporation and MB neurosphere-forming assay. Cell proliferation was evaluated by BrdU detection (Roche, Welwyn Garden City, UK). Briefly, cells were pulsed 24 h with BrdU and then fixed and permeabilized with 4% paraformaldehyde and 0.2% Triton X-100, respectively. Nuclei were counterstained with Hoechst reagent and BrdU detection was performed according to the manufacturer's instructions. At least 500 nuclei were counted in triplicate, and the number of BrdU-positive nuclei was recorded. To determine the growth rate of viable cells, a trypan blue count was performed after a treatment period of 24, 48 and 72 h with Leu-SH at the indicated dose.

For the neurosphere-forming assay, cells were plated at clonal density (1–2 cells/mm^2) into 96-well plates and treated with Leu-SH at the indicated concentration.

Cell viability assay in SHH-MB PDX model. Patient-derived xenograft (PDXs)-ICN-MB 12 was generated from primary human SHH- MB sample diagnosed at the Children's Necker Hospital in Paris and transplanted into the subscapular fatpad of immunocompromised NOD/SCID mice[63]. Human sample for xenograft studies was obtained under written informed consent and ethical approved by the Internal Review Board of the Necker Sick Children's Hospital, Paris, France. Tumor cells from PDX model were purified and cultured[63]. For culture experiments, 75,000 tumor cells per well were plated in 96-well plates, pre-coated with poly-D-lysine (EMD Millipore, Billerica, MA) and Matrigel (BD Biosciences, San Jose, CA). Cells were grown in Neurobasal medium with B27 supplement, 2 mM glutamine, penicillin/streptomycin (all from Thermo Fisher Scientific), bovine serum albumin, and 0.45% D-glucose (both from Sigma Aldrich). The next day, cultured tumor cells were treated with different concentrations of Leu-SH plus 0.1 M DTT or water plus 0.1 M DTT for the control. For the Incucyte experiment, cells were treated with 0.3 µg/ml of propidium iodide (PI, Sigma Aldrich). Then, the plates were scanned for phase contrast and PI staining every 3 h during 72 h using the IncuCyte imager with a 4X objective (Essen BioScience). Proliferation was measured using quantitative kinetic processing metrics from time-lapse image acquisition and showed as percentage of culture confluence over time. For the PI staining, which allowed to fluorescently stain the nuclear DNA of cells that have lost plasma membrane integrity, the percentage of PI positive cells (corresponding to red object confluence) was divided by the phase object confluence percentage for each well, thus indicating the level of dead cells in each well. For the CellTiter-Glo® Luminescent Cell Viability Assay the cell viability was examined after 72 h of treatment according to the manufacturer's instructions (Promega Corporation, Madison, WI, USA). Results were expressed as luciferase fluorescence and represented the mean ± S.D. of three experiments, each performed in triplicate.

Animal studies. For allograft experiment, spontaneous MB from Math1-cre/Ptc$^{C/C}$ mice[57] was isolated, minced and pipetted to obtain a single-cell suspension. Equal amounts of cells (2×10^6) were injected s.c. at the posterior flank of NSG (Charles River Laboratories, Lecco, Italy). Tumors were grown until a median size of ~150 mm^3. Animals were randomly divided in two groups ($n = 6$) and intratumorally injected every other day with (0.528 µmol/Kg) Leu-SH and/or 0.1 M DTT for 18 days. Primary cells of spontaneous MB from Math1-cre/Ptc$^{C/C}$ mice were infected for 72 h with purified lentiviral particles encoding short hairpin RNA targeting murine ERAP1 (shERAP1) or a control non-targeting sequence (shCTRL). Equal amounts of cells (2×10^6) were injected s.c. at the posterior flank of NSG mice. GCPs from the cerebella of postnatal (P) day P5-P7 Math1-cre/Ptc$^{C/C}$ mice were infected with purified lentiviral particles encoding ERAP1 or an empty GFP vector. Equal amounts of cells (2×10^6) were injected s.c. at the posterior flank of NSG mice. Cells were resuspended in an equal volume of culture medium and Matrigel (BD Biosciences, Heidelberg, Germany) before the s.c. injection. After the injection, tumor growth was monitored and measured with caliper. Changes in tumor volume were evaluated with the formula (length × width) × 0.5 × (length + width).

For orthotopic allograft model, adult NSG mice were anesthetized by i.p. injection of ketamine (10 mg/kg) and xylazine (100 mg/kg). The posterior cranial region was shaved and placed in a stereotaxic head frame and primary cells of spontaneous MB from Math1-cre/Ptc$^{C/C}$ mice freshly isolated or infected for 72 h with purified lentiviral particles encoding murine shERAP1 or shCTRL were stereotaxically implanted into the cerebellum (2×10^5/3 µl) according to the atlas of Franklin and Paxinos coordinates. After injection, at an infusion rate of 1 µl/min, the cannula was kept in place for 5 min and then the skin was closed using metallic clips. After 10 days following tumor implantation, the animals were randomly divided into two groups ($n = 6$) and treated i.p. every other day with Leu-SH 1 mg/Kg or vehicle only. After 25 days of treatment, animals were sacrificed and brains were fixed in 4% formaldehyde and paraffin embedded. Mice implanted with the tumor cells silenced for ERAP1 were sacrificed after six weeks. Tumor volume calculation was performed on serial 40 coronal sections of 2 µm after H&E staining every 40 µm of brain slice. A microscope (Axio Imager M1 microscope; Leica Microsystems GmbH, Wetzlar, Germany) equipped with a motorized stage and Image Pro Plus 6.2 software was used to evaluate tumor area of each slide and the tumor volume was calculated by the formula: tumor volume = sum of measured area for each slice × slice thickness × sampling frequency[59].

For Gfap-Cre/Ptc$^{fl/fl}$ mice injection, symptomatic Gfap-Cre/Ptc$^{fl/fl}$ mice were randomly divided into two groups ($n = 5$) and injected s.c under the scruff with (0.528 µmol/Kg) Leu-SH and/or 0.1 M DTT for two days. Tumor masses were analyzed by qRT-PCR and immunoblotting.

For survival analysis, P21 Math-cre/Ptc$^{C/C}$ mice were randomized to receive either Leu-SH (1 mg/Kg) or vehicle every other day by i.p. injection. Statistical analysis was performed by MedCalc software.

For xenograft experiment, Daoy cells were infected with lentiviral particles encoding either short hairpin RNA targeting human ERAP1 (shERAP1) or a control non-targeting sequence (shCTRL). Equal amounts (2×10^6) of cells were injected s.c. at the posterior flank of NSG mice.

Patient-derived xenograft (PDXs)-ICN-MB 12 was isolated, minced and purified. Cells (3×10^6) were injected s.c. at the posterior flank of NSG mice. Tumors were grown until a median size of ~150 mm^3. Animals were randomly divided in two groups ($n = 6$) and intratumorally injected with (0.528 µmol/Kg) Leu-SH and/or 0.1 M DTT for 18 days. Cells were resuspended in an equal volume of culture medium and Matrigel before the s.c. injection. Tumor growth was monitored and measured with caliper. Changes in tumor volume were evaluated with the formula (length x width) x 0.5 × (length + width).

All animal protocols were approved by local ethic authorities (Ministry of Health) and conducted in accordance with Italian Governing Law (D.lgs 26/2014).

Immunohistochemistry. Formaldehyde-fixed paraffin-embedded (FFPE) tissues and frozen OCT-embedded tissues were cut into 4µm sections for Gli1, Ki67, cleaved Caspase-3, NeuN, and ERAP1 immunohistochemical staining. FFPE slides were deparaffinized and subjected to heat-induced antigen retrieval at low or high pH buffer, whereas frozen tissues were fixed in 4% paraformaldehyde. Slides were blocked for 30 min with 5% PBS/BSA. FFPE slides were incubated with monoclonal antibodies against Gli1, Ki67, cleaved Caspase-3, NeuN, whereas cryostat sections were incubated with monoclonal antibody ERAP1 (4D2, 50 mg/ml overnight 4 °C). This step was followed by incubation for 20 min with secondary antibodies coupled with peroxidase (Dako). Bound peroxidase was detected with diaminobenzidine (DAB) solution and EnVision FLEX Substrate buffer containing peroxide (Dako). Cell quantification was performed on collected sections using the imaging software NIS-Elements BR 4.00.05 (Nikon Instruments Europe B.V., Italy). Images were captured by HistoFAXS software (TissueGnostics GmbH, Vienna, Austria) at 20x magnification. Tumor regions were analyzed with HistoQuest software (TissueGnostics) for automatic color separation and quantification. Expression levels were evaluated as stained area per mm^2.

Immunofluorescence. After 24 h of transfection, cells were fixed for 15 min in 4% paraformaldehyde, treated with glycine 1 M for 15 min to saturate the residual site of paraformaldehyde, permeabilized for 8 min in 0.2% Triton X-100 and blocked with 3% BSA for 30 min. Cells were then labeled with primary antibody for 1 h, followed by staining with secondary antibodies specific for rabbit or mouse (Alexa Fluor 488, A21206, and Alexa Fluor 546, A11030, respectively, Life Technologies). Single plane confocal images were acquired using an inverted Olympus iX73 microscope equipped with an X-light Nipkow spinning-disk head (Crest Optics, Rome, Italy) and Lumencor Spectra X Led illumination. Images were collected using a CoolSNAP MYO CCD camera (Photometrics, Tucson, AZ, USA) and MetaMorph Software (Molecular Device, Sunnyvale, CA, USA) with a x60 oil objective.

Statistical analysis. Statistical analysis was performed using the StatView 4.1 software (Abacus Concepts, Berkeley, CA, USA). For all experiments, *P* values were determined using two-tailed Student's *t*-test and statistical significance was set at $P < 0.05$. Results are expressed as mean ± S.D. from an appropriate number of experiments (at least three biological replicas). For IncuCyte experiments, statistical significance was determined with GraphPad Prism software (version 6.0, La Jolla, CA, USA). Data were analyzed with the Two-way ANOVA test and given as mean ± SD. For survival analysis statistical significance was calculated with Logrank-test performed by MedCalc software.

Data availability

All data in this study are available within the Article and Supplementary Information or from the corresponding author on reasonable request.

Received: 14 August 2018 Accepted: 18 June 2019
Published online: 24 July 2019

References

1. Ramaswamy, V. & Taylor, M. D. Medulloblastoma: from myth to molecular. *J. Clin. Oncol.: Off. J. Am. Soc. Clin. Oncol.* **35**, 2355–2363 (2017).
2. Briscoe, J. & Therond, P. P. The mechanisms of Hedgehog signalling and its roles in development and disease. *Nat. Rev. Mol. cell Biol.* **14**, 416–429 (2013).
3. Clark, V. E. et al. Genomic analysis of non-NF2 meningiomas reveals mutations in TRAF7, KLF4, AKT1, and SMO. *Science* **339**, 1077–1080 (2013).
4. Jones, S. et al. Core signaling pathways in human pancreatic cancers revealed by global genomic analyses. *Science* **321**, 1801–1806 (2008).
5. Caro, I. & Low, J. A. The role of the hedgehog signaling pathway in the development of basal cell carcinoma and opportunities for treatment. *Clin. Cancer Res.: Off. J. Am. Assoc. Cancer Res.* **16**, 3335–3339 (2010).
6. Raducu, M. et al. SCF (Fbxl17) ubiquitylation of Sufu regulates Hedgehog signaling and medulloblastoma development. *EMBO J.* **35**, 1400–1416 (2016).
7. Ruiz i Altaba, A., Sanchez, P. & Dahmane, N. Gli and hedgehog in cancer: tumours, embryos and stem cells. *Nat. Rev. Cancer* **2**, 361–372 (2002).
8. Bhatia, N. et al. Gli2 is targeted for ubiquitination and degradation by beta-TrCP ubiquitin ligase. *J. Biol. Chem.* **281**, 19320–19326 (2006).
9. Huntzicker, E. G. et al. Dual degradation signals control Gli protein stability and tumor formation. *Genes Dev.* **20**, 276–281 (2006).
10. Pan, Y., Bai, C. B., Joyner, A. L. & Wang, B. Sonic hedgehog signaling regulates Gli2 transcriptional activity by suppressing its processing and degradation. *Mol. Cell. Biol.* **26**, 3365–3377 (2006).
11. Jiang, J. & Struhl, G. Regulation of the Hedgehog and Wingless signalling pathways by the F-box/WD40-repeat protein Slimb. *Nature* **391**, 493–496 (1998).
12. Infante, P. et al. Itch/beta-arrestin2-dependent non-proteolytic ubiquitylation of SuFu controls Hedgehog signalling and medulloblastoma tumorigenesis. *Nat. Commun.* **9**, 976 (2018).
13. Humke, E. W., Dorn, K. V., Milenkovic, L., Scott, M. P. & Rohatgi, R. The output of Hedgehog signaling is controlled by the dynamic association between Suppressor of Fused and the Gli proteins. *Genes Dev.* **24**, 670–682 (2010).
14. Wang, B. & Li, Y. Evidence for the direct involvement of {beta}TrCP in Gli3 protein processing. *Proc. Natl Acad. Sci. USA* **103**, 33–38 (2006).
15. Rusert, J. M., Wu, X., Eberhart, C. G., Taylor, M. D. & Wechsler-Reya, R. J. SnapShot: Medulloblastoma. *Cancer cell* **26**, 940–940 e941 (2014).
16. Pak, E. & Segal, R. A. Hedgehog signal transduction: key players, oncogenic drivers, and cancer therapy. *Dev. cell* **38**, 333–344 (2016).
17. Robbins, D. J., Fei, D. L. & Riobo, N. A. The Hedgehog signal transduction network. *Sci. Signal.* **5**, re6 (2012).
18. Wang, J., Garancher, A., Ramaswamy, V. & Wechsler-Reya, R. J. Medulloblastoma: from molecular subgroups to molecular targeted therapies. *Annu. Rev. Neurosci.* **41**, 207–232 (2018).
19. Pandolfi, S. & Stecca, B. Cooperative integration between HEDGEHOG-GLI signalling and other oncogenic pathways: implications for cancer therapy. *Expert Rev. Mol. Med.* **17**, e5 (2015).
20. Serwold, T., Gaw, S. & Shastri, N. ER aminopeptidases generate a unique pool of peptides for MHC class I molecules. *Nat. Immunol.* **2**, 644–651 (2001).
21. Serwold, T., Gonzalez, F., Kim, J., Jacob, R. & Shastri, N. ERAAP customizes peptides for MHC class I molecules in the endoplasmic reticulum. *Nature* **419**, 480–483 (2002).
22. Saric, T. et al. An IFN-gamma-induced aminopeptidase in the ER, ERAP1, trims precursors to MHC class I-presented peptides. *Nat. Immunol.* **3**, 1169–1176 (2002).
23. Kanaseki, T., Blanchard, N., Hammer, G. E., Gonzalez, F. & Shastri, N. ERAAP synergizes with MHC class I molecules to make the final cut in the antigenic peptide precursors in the endoplasmic reticulum. *Immunity* **25**, 795–806 (2006).
24. Hammer, G. E., Gonzalez, F., James, E., Nolla, H. & Shastri, N. In the absence of aminopeptidase ERAAP, MHC class I molecules present many unstable and highly immunogenic peptides. *Nat. Immunol.* **8**, 101–108 (2007).
25. Parmentier, N. et al. Production of an antigenic peptide by insulin-degrading enzyme. *Nat. Immunol.* **11**, 449–454 (2010).
26. Nagarajan, N. A., Gonzalez, F. & Shastri, N. Nonclassical MHC class Ib-restricted cytotoxic T cells monitor antigen processing in the endoplasmic reticulum. *Nat. Immunol.* **13**, 579–586 (2012).
27. James, E., Bailey, I., Sugiyarto, G. & Elliott, T. Induction of protective antitumor immunity through attenuation of ERAAP function. *J. Immunol.* **190**, 5839–5846 (2013).
28. Cifaldi, L. et al. ERAP1 regulates natural killer cell function by controlling the engagement of inhibitory receptors. *Cancer Res.* **75**, 824–834 (2015).
29. Fruci, D., Romania, P., D'Alicandro, V. & Locatelli, F. Endoplasmic reticulum aminopeptidase 1 function and its pathogenic role in regulating innate and adaptive immunity in cancer and major histocompatibility complex class I-associated autoimmune diseases. *Tissue Antigens* **84**, 177–186 (2014).
30. Stratikos, E., Stamogiannos, A., Zervoudi, E. & Fruci, D. A role for naturally occurring alleles of endoplasmic reticulum aminopeptidases in tumor immunity and cancer pre-disposition. *Front. Oncol.* **4**, 363 (2014).
31. Saveanu, L. et al. Concerted peptide trimming by human ERAP1 and ERAP2 aminopeptidase complexes in the endoplasmic reticulum. *Nat. Immunol.* **6**, 689–697 (2005).
32. York, I. A. et al. The ER aminopeptidase ERAP1 enhances or limits antigen presentation by trimming epitopes to 8-9 residues. *Nat. Immunol.* **3**, 1177–1184 (2002).
33. Fruci, D. et al. Altered expression of endoplasmic reticulum aminopeptidases ERAP1 and ERAP2 in transformed non-lymphoid human tissues. *J. Cell. Physiol.* **216**, 742–749 (2008).
34. Fruci, D. et al. Expression of endoplasmic reticulum aminopeptidases in EBV-B cell lines from healthy donors and in leukemia/lymphoma, carcinoma, and melanoma cell lines. *J. Immunol.* **176**, 4869–4879 (2006).
35. Mehta, A. M., Jordanova, E. S., Kenter, G. G., Ferrone, S. & Fleuren, G. J. Association of antigen processing machinery and HLA class I defects with clinicopathological outcome in cervical carcinoma. *Cancer Immunol., Immunother.: CII* **57**, 197–206 (2008).
36. Cifaldi, L. et al. Natural killer cells efficiently reject lymphoma silenced for the endoplasmic reticulum aminopeptidase associated with antigen processing. *Cancer Res.* **71**, 1597–1606 (2011).
37. Taipale, J. et al. Effects of oncogenic mutations in Smoothened and Patched can be reversed by cyclopamine. *Nature* **406**, 1005–1009 (2000).
38. Chen, J. K., Taipale, J., Cooper, M. K. & Beachy, P. A. Inhibition of Hedgehog signaling by direct binding of cyclopamine to Smoothened. *Genes Dev.* **16**, 2743–2748 (2002).
39. Goodrich, L. V., Milenkovic, L., Higgins, K. M. & Scott, M. P. Altered neural cell fates and medulloblastoma in mouse patched mutants. *Science* **277**, 1109–1113 (1997).
40. Svard, J. et al. Genetic elimination of suppressor of fused reveals an essential repressor function in the mammalian Hedgehog signaling pathway. *Dev. cell* **10**, 187–197 (2006).
41. Tempe, D., Casas, M., Karaz, S., Blanchet-Tournier, M. F. & Concordet, J. P. Multisite protein kinase A and glycogen synthase kinase 3beta phosphorylation leads to Gli3 ubiquitination by SCFbetaTrCP. *Mol. Cell. Biol.* **26**, 4316–4326 (2006).
42. Di Marcotullio, L. et al. Multiple ubiquitin-dependent processing pathways regulate hedgehog/gli signaling: implications for cell development and tumorigenesis. *Cell cycle* **6**, 390–393 (2007).
43. Di Marcotullio, L. et al. Numb activates the E3 ligase Itch to control Gli1 function through a novel degradation signal. *Oncogene* **30**, 65–76 (2011).
44. Di Marcotullio, L. et al. Numb is a suppressor of Hedgehog signalling and targets Gli1 for Itch-dependent ubiquitination. *Nat. cell Biol.* **8**, 1415–1423 (2006).
45. Mazza, D. et al. PCAF ubiquitin ligase activity inhibits Hedgehog/Gli1 signaling in p53-dependent response to genotoxic stress. *Cell death Differ.* **20**, 1688–1697 (2013).
46. Wang, C., Pan, Y. & Wang, B. Suppressor of fused and Spop regulate the stability, processing and function of Gli2 and Gli3 full-length activators but not their repressors. *Development* **137**, 2001–2009 (2010).
47. Uddin, S. et al. Involvement of F-BOX proteins in progression and development of human malignancies. *Semin. cancer Biol.* **36**, 18–32 (2016).
48. Magliozzi, R. et al. Inheritance of the Golgi Apparatus and cytokinesis are controlled by degradation of GBF1. *Cell Rep.* **23**, 3381–3391 e3384 (2018).
49. Pan, Y., Wang, C. & Wang, B. Phosphorylation of Gli2 by protein kinase A is required for Gli2 processing and degradation and the Sonic Hedgehog-regulated mouse development. *Dev. Biol.* **326**, 177–189 (2009).
50. Kotani, T. Protein kinase A activity and Hedgehog signaling pathway. *Vitam. Horm.* **88**, 273–291 (2012).

51. Cohen, M. M. Jr. Hedgehog signaling update. *Am. J. Med. Genet. Part A* **152A**, 1875–1914 (2010).
52. Peschiaroli, A., Skaar, J. R., Pagano, M. & Melino, G. The ubiquitin-specific protease USP47 is a novel beta-TRCP interactor regulating cell survival. *Oncogene* **29**, 1384–1393 (2010).
53. Wang, Y. C. et al. USP24 induces IL-6 in tumor-associated microenvironment by stabilizing p300 and beta-TrCP and promotes cancer malignancy. *Nat. Commun.* **9**, 3996 (2018).
54. Hong, A., Lee, J. E. & Chung, K. C. Ubiquitin-specific protease 22 (USP22) positively regulates RCAN1 protein levels through RCAN1 de-ubiquitination. *J. Cell. Physiol.* **230**, 1651–1660 (2015).
55. Wechsler-Reya, R. J. & Scott, M. P. Control of neuronal precursor proliferation in the cerebellum by Sonic Hedgehog. *Neuron* **22**, 103–114 (1999).
56. Schuller, U. et al. Acquisition of granule neuron precursor identity is a critical determinant of progenitor cell competence to form Shh-induced medulloblastoma. *Cancer cell* **14**, 123–134 (2008).
57. Yang, Z. J. et al. Medulloblastoma can be initiated by deletion of Patched in lineage-restricted progenitors or stem cells. *Cancer cell* **14**, 135–145 (2008).
58. Neumann, J. E., Swartling, F. J. & Schuller, U. Medulloblastoma: experimental models and reality. *Acta Neuropathol.* **134**, 679–689 (2017).
59. Infante, P. et al. Gli1/DNA interaction is a druggable target for Hedgehog-dependent tumors. *EMBO J.* **34**, 200–217 (2015).
60. Kool, M. et al. Genome sequencing of SHH medulloblastoma predicts genotype-related response to smoothened inhibition. *Cancer cell* **25**, 393–405 (2014).
61. Sasai, K. et al. Shh pathway activity is down-regulated in cultured medulloblastoma cells: implications for preclinical studies. *Cancer Res.* **66**, 4215–4222 (2006).
62. Zhao, X. et al. RAS/MAPK activation drives resistance to Smo inhibition, metastasis, and tumor evolution in Shh pathway-dependent tumors. *Cancer Res.* **75**, 3623–3635 (2015).
63. Grausam, K. B. et al. ATOH1 promotes leptomeningeal dissemination and metastasis of sonic hedgehog subgroup medulloblastomas. *Cancer Res.* **77**, 3766–3777 (2017).
64. Cochrane, C. R., Szczepny, A., Watkins, D. N. & Cain, J. E. Hedgehog Signaling in the maintenance of cancer stem cells. *Cancers* **7**, 1554–1585 (2015).
65. Liu K. W., Pajtler K. W., Worst B. C., Pfister S. M., Wechsler-Reya R. J. Molecular mechanisms and therapeutic targets in pediatric brain tumors. *Sci. Signal.* **10**, 1–19 (2017).
66. Rimkus T. K., Carpenter R. L., Qasem S., Chan M., Lo H. W. Targeting the Sonic Hedgehog signaling pathway: review of Smoothened and GLI inhibitors. *Cancers* **8**, 1–23 (2016).
67. Kebenko, M. et al. ErbB2 signaling activates the Hedgehog pathway via PI3K-Akt in human esophageal adenocarcinoma: identification of novel targets for concerted therapy concepts. *Cell. Signal.* **27**, 373–381 (2015).
68. Di Magno, L., Coni, S., Di Marcotullio, L. & Canettieri, G. Digging a hole under Hedgehog: downstream inhibition as an emerging anticancer strategy. *Biochim. et. Biophys. acta* **1856**, 62–72 (2015).
69. Infante, P., Alfonsi, R., Botta, B., Mori, M. & Di Marcotullio, L. Targeting GLI factors to inhibit the Hedgehog pathway. *Trends Pharmacol. Sci.* **36**, 547–558 (2015).
70. Amakye, D., Jagani, Z. & Dorsch, M. Unraveling the therapeutic potential of the Hedgehog pathway in cancer. *Nat. Med.* **19**, 1410–1422 (2013).
71. Onishi, H. & Katano, M. Hedgehog signaling pathway as a therapeutic target in various types of cancer. *Cancer Sci.* **102**, 1756–1760 (2011).
72. Infante, P. et al. Inhibition of Hedgehog-dependent tumors and cancer stem cells by a newly identified naturally occurring chemotype. *Cell death Dis.* **7**, e2376 (2016).
73. Parsons, J. L. et al. USP47 is a deubiquitylating enzyme that regulates base excision repair by controlling steady-state levels of DNA polymerase beta. *Mol. cell* **41**, 609–615 (2011).
74. Shi, J. et al. Deubiquitinase USP47/UBP64E regulates beta-catenin ubiquitination and degradation and plays a positive role in Wnt signaling. *Mol. Cell. Biol.* **35**, 3301–3311 (2015).
75. Kochan, G. et al. Crystal structures of the endoplasmic reticulum aminopeptidase-1 (ERAP1) reveal the molecular basis for N-terminal peptide trimming. *Proc. Natl Acad. Sci. USA* **108**, 7745–7750 (2011).

Acknowledgements

We thank M.P. Scott for the gift of Ptch$^{-/-}$ MEFs, R.Toftgård for SuFu$^{-/-}$ MEFs, Peter van Endert for ERAP1 antibodies, Claire Lovo, from the PICT-IBiSA Orsay Imaging facility of Institut Curie, for IncuCyte imaging assistance, and C. Alberti and E. Belloir for in vivo experiments at the Institut Curie mouse facilities, C. Felici, I. Basili and A. Scipioni for their experimental assistance. This work was supported by Associazione Italiana Ricerca Cancro (AIRC) Grants #IG14723 and #IG20801 to L.D.Mar, #IG18495 to D.F., #IG17575 to G.C. and #IG17734 to G.G., Progetti di Ricerca di Università Sapienza di Roma, Italian Ministry of Health Grant PRIN 2012C5YJSK_002 and PRIN 2017BF3PXZ_003 to L.D.Mar. and #PE-2011-02351866 to D.F., Italian Ministry of Education, Universities and Research - Dipartimenti di Eccellenza - L. 232/2016, Pasteur Institute/Cenci Bolognetti Foundation, Istituto Italiano di Tecnologia (IIT). LLS was supported by PhD Degree Program in Biotechnology in Clinical Medicine, University of Rome La Sapienza.

Author contributions

L.D.Mar. conceived and coordinated the project, designed experiments, analyzed the data, and wrote the paper. F.Bu., P.I. and L.D.Mar. conceived, performed experiments, and analyzed the data. F.Bu., P.I., F.Be. and M.C., performed most of the experiments. P.R., F.Bu. O.M., and L.L.S. generated lentivirus and analyzed data. P.I., M.M., L.L.S., L.D. Mag and M.T. performed the animal experiments, IHC and analysis. J.T., S.Pu. and O.A. provided and performed experiments on SHH-PDX. A.P., L.B., E.D.S., G.C., D.G., D.B., C.C., G.M., F.L., S.Pa., O.A., G.G., A.G. and D.F. discussed the results, and provided critical reagents and comments. F.Bu., D.F. and L.D.Mar. wrote the paper. All authors critically revised and edited the paper.

Additional information

Supplementary Information accompanies this paper at https://doi.org/10.1038/s41467-019-11093-0.

Competing interests: The authors declare no competing interests.

Reprints and permission information is available online at http://npg.nature.com/reprintsandpermissions/

Peer review information: *Nature Communications* thanks the anonymous reviewer(s) for their contribution to the peer review of this work. Peer reviewer reports are available.

Publisher's note: Springer Nature remains neutral with regard to jurisdictional claims in published maps and institutional affiliations.

3.1.3 | *SALL4A/HDAC1/GLI1 axis as a new positive mechanism in Hedgehog signalling regulation*

SALL4 is a stemness marker overexpressed in many cancers and involved in tumorigenesis. However, its function in Hh signalling regulation and MB onset remains unknown.

SALL4, a member of the mammalian homologs of *Drosophila* homeotic gene *spalt* (*sal*), is a zinc finger transcription factor (Al-Baradie et al., 2002) and, in human, its gene has been mapped to chromosome 20.q13.2. Two isoforms of SALL4 exist, SALL4A and SALL4B, as result of different internal splicing patterns in exon 2 (Al-Baradie et al., 2002; Uez et al., 2008; Zhang et al., 2015). Data from literature report that SALL4 is an essential factor for maintenance of the pluripotency and self-renewal of embryonic stem cells (Yang et al., 2008a; Zhang et al., 2006). During early embryogenesis, SALL4A and SALL4B are able to form homodimers or heterodimers with distinct DNA-binding sites and exhibit different roles (Rao et al., 2010).

High expression of SALL4 has been observed in several tumors, confirming that this transcription factor acts as an oncogene involved in tumor initiation and progression. However, there are no reports exploring the role of SALL4 in MB.

We focused our study on SALL4 because it emerged as potential REN^{KCTD11} interactor from a mass spectrometry analysis. REN^{KCTD11} is an adaptor protein of the Cul3 SCF-like E3-ubiquitin ligase complex that works as a specific checkpoint for Hh signalling activity (Di Marcotullio et al., 2004; Gallo et al., 2002). Therefore, REN^{KCTD11} is a negative regulator of Hh signalling and its inactivation, due to chromosome 17p deletion, leads to a deregulation of the tumor promoting Hh pathway.

In this study, we focused on the full length isoform of SALL4 (SALL4A) because data from literature report its involvement in various tumor context. More interestingly, SALL4A regulates gene expression not only through its transcriptional activity, but also by interacting with epigenetic factors; it is known that SALL4A binds the NuRD complex and the histone deacetylases HDAC (Lu et al., 2009; Yuri et al., 2009). This knowledge

was very important in the idealization of my project, since data obtained by our research group shown that HDAC1 is a positive regulator of Hh signalling able to deacetylate GLI1 on K518 and to promote its transcriptional activity (Canettieri et al., 2010), but it is also a substrate of REN^{KCTD11} which induces its poly-ubiquitylation and proteasome-dependent degradation (Canettieri et al., 2010).

These evidences led us to hypothesize that SALL4A can work together with HDAC1 in Hh pathway regulation.

To confirm this hypothesis, we first demonstrated that SALL4A is a substrate of REN^{KCTD11}, and its REN^{KCTD11}-mediated poly-ubiquitylation induces a proteasome-dependent degradation. Through functional assays we demonstrated that SALL4A promotes GLI1 transcriptional activity, and this effect is significantly improved in presence of HDAC1. We observed that SALL4A interacts with both HDAC1 and GLI1, and modulates the acetylation state of GLI1; in particular, GLI1 acetylated form decreases in the presence of SALL4A, similarly to what observed in the presence of HDAC1.

Our findings sustain the hypothesis that the three proteins (SALL4A, HDAC1 and GLI1) form a ternary complex in which, following the activation of the Hh pathway, SALL4A binds HDAC1 and recruits it on GLI1, promoting its deacetylation and enhancing its transcriptional activity; in the absence of the Hh signal, the Cul3/REN^{KCTD11} E3-ubiquitin ligase complex promotes the ubiquitylation and the consequent proteasome-dependent degradation of both SALL4A and HDAC1, thus inhibiting GLI1.

SALL4A activity on Hh signalling is also sustained by i*n vitro* and *in vivo* biological assays that demonstrate how SALL4A modulation affects the proliferation and the migration rate of cultured Hh-dependent MB cells, as well as Hh-dependent tumor growth and progression. Since data are not yet published, a detailed description of obtained results is reported below.

3.1.3.1 | The transcription factor SALL4A is a novel interactor of REN^{KCTD11}

To identify novel interactors of REN^{KCTD11} we performed a mass spectrometry analysis in HEK293T cells transfected with a control (empty) vector or with an expression vector encoding human REN^{KCTD11} N-terminally HA- and Flag-tagged. Before lysis, cells were treated with the proteasome inhibitor MG132 and cell lysates underwent a sequential double co-immunoprecipitation (Co-IP). Co-immunoprecipitated proteins were then analysed by mass spectrometry analysis and polypeptides that were represented with a number of peptides ≥ 3 were selected for further analysis.

Data analysis identified several interactors, including proteins involved in developmental processes, stemness, apoptosis, post-translational modification mechanisms (i.e. ubiquitylation and sumoylation), transcription factors and methyltransferase. Among them, we focused on SALL4.

SALL4 is a transcription factor that plays different roles in embryonic development, stemness and cancer. In human and mouse three isoforms of SALL4 (A, B and C), who share high structural homology, have been identified and derive from alternative splicing events.

SALL4 re-expression in cancer is often related to worse prognosis and lower survival rate (such as in hepatocellular carcinoma) or to a greater tendency to metastasize (as in endometrial cancer and colorectal carcinoma). Given the central role played by SALL4, its presence among REN^{KCTD11} interactors represents an interesting topic for the study and understanding of the molecular mechanisms underlying Hh-dependent tumorigenesis. In particular, we focused on isoform A of SALL4 because it is known that SALL4A, and not SALL4B, associates with NuRD complex and that this association enhances SALL4A-mediated repression of developmental genes (Bode et al., 2016). Therefore, we speculate that REN^{KCTD11}/SALL4A complex could be implicated in Hh regulation during cerebellar development, differentiation and tumorigenesis.

To validate mass spectrometry data, we performed Co-IP experiments following overexpression of HA-tagged SALL4A and Flag-tagged REN^{KCTD11} in HEK293T cells, thus confirming the interaction of the two proteins (**Figure 1**).

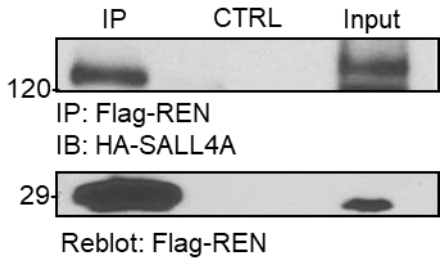

Figure 1 | *SALL4A specifically interacts with REN^{KCTD11}.* Co-IP assay was performed on total lysates from HEK293T cells transfected with expression vectors encoding for the indicated proteins and immunoprecipitated with anti-Flag agarose beads. IP samples and a fraction (5%) of the total lysate (Input) were separated on SDS-PAGE gels. Blots were immunoblotted with anti-SALL4 antibody and reblotted with anti-Flag antibody.

The BTB/Poz is a protein-protein interaction domain involved in oligomerization of many KCTD family members. This family includes adaptor proteins (Pintard et al., 2004); indeed, the KCTD family member REN^{KCTD11} binds Cul3 (a component of the SCF-like E3-ubiquitin ligase complex able to promote the ubiquitylation and proteolytic degradation of its substrates) through its BTB/Poz domain. This interaction allows the recruitment of specific substrates for Cul3.

To identify the domain of REN^{KCTD11} involved in the binding with SALL4A, we transfected HEK293T cells with the full-length REN^{KCTD11} (REN WT), the BTB/Poz-containing N-terminal half of the protein (REN Poz) and the C-terminal half lacking the BTB/Poz domain (REN ΔPoz). We demonstrated by Co-IP experiments that REN^{KCTD11}/SALL4A interaction is mediated by the C-terminal domain (REN ΔPoz) of REN^{KCTD11} (**Figure 2**).

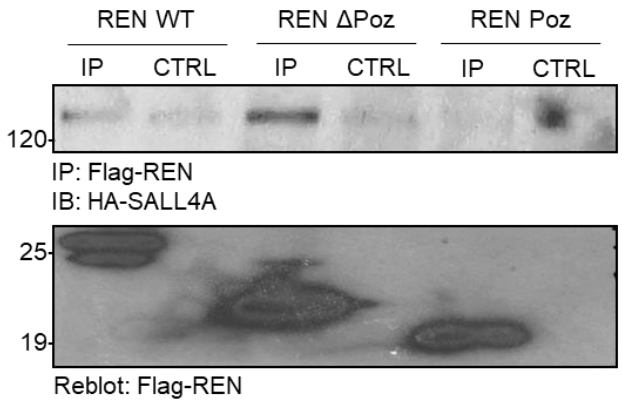

Figure 2 | *REN^{KCTD11}/SALL4A interaction is mediated by the C-terminal domain of REN^{KCTD11}.* Co-IP assay was performed on total lysates from HEK293T cells transfected with expression vectors encoding for the indicated proteins and immunoprecipitated with anti-Flag agarose beads. IP samples were separated on SDS-PAGE gels. Blots were immunoblotted with anti-HA antibody for SALL4A revelation and reblotted with anti-Flag antibody.

3.1.3.2 | The Cul3/REN^{KCTD11} E3-ligase complex promotes SALL4A ubiquitylation

We next investigated the ability of Cul3/REN^{KCTD11} E3-ligase complex to ubiquitylate SALL4A *in vivo*. In HEK293T cells, ectopic expression of REN^{KCTD11} induces the ubiquitylation of endogenous SALL4A; interestingly, REN^{KCTD11} ΔPoz mutant and KCTD21 (or KCASH2, belonging to the KCASH family and known as negative regulators of the Hh signalling (De Smaele et al., 2011)) do not promote SALL4A ubiquitylation (**Figure 3**).

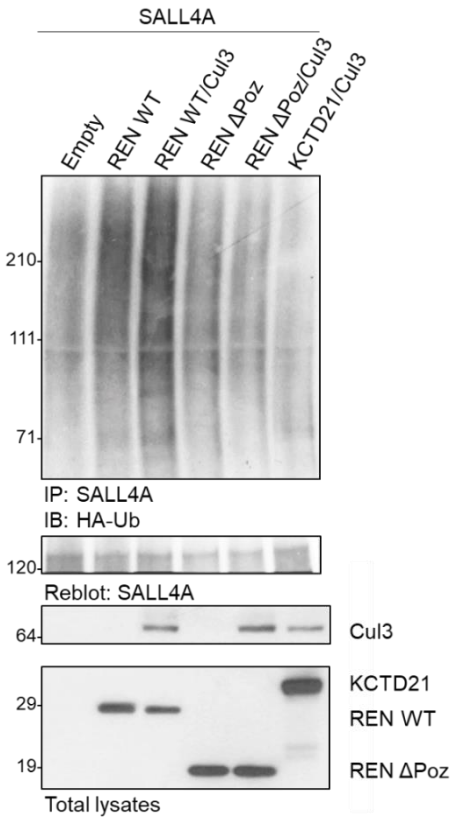

Figure 3 | *Cul3/REN^{KCTD11} complex induces SALL4A ubiquitylation.* HEK293T cells were co-transfected with HA-Ub in the presence of Flag-REN WT (alone or in combination with ectopic Myc-Cul3), Flag-REN ΔPoz mutant or Flag-KCTD21. Cell lysates were immunoprecipitated with anti-SALL4 antibody; IP samples and a fraction (5%) of the total lysate were separated on SDS-PAGE gels followed by immunoblotting with an anti-HA antibody to detect ubiquitylated forms or with an anti-Flag and anti-Myc antibodies to assess the expression of transfected plasmids. IP blots were reblotted with anti-SALL4 antibody.

Accordingly, increasing amounts of REN^{KCTD11} induce a progressive increase in the ubiquitylation levels of ectopic SALL4A (**Figure 4**).

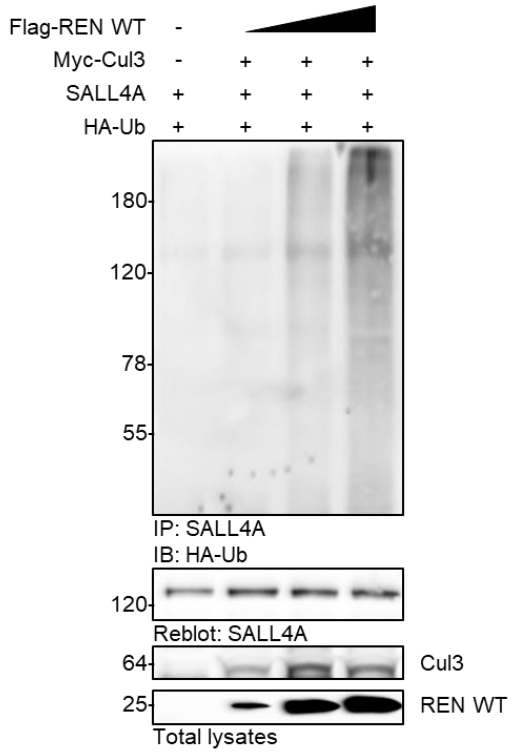

Figure 4 | *SALL4A ubiquitylation in presence of increasing amounts of ectopic REN^{KCTD11}.* HEK293T cells were transfected with plasmids expressing HA-Ub in the presence of increasing amounts of Flag-REN WT. Cell lysates were immunoprecipitated with an anti-SALL4 antibody; IP samples and a fraction (5%) of the total lysate were separated on SDS-PAGE gels followed by immunoblotting with an anti-HA antibody to detect ubiquitylated forms or with anti-Flag and anti-Myc antibodies to assess the expression of transfected plasmids. IP blots were reblotted with anti-SALL4 antibody.

3.1.3.3 | The Cul3/REN^{KCTD11} E3-ligase complex ubiquitylates SALL4A affecting its stability

To investigate if REN^{KCTD11}-induced ubiquitylation primes SALL4A for proteasomal degradation, we treated cells with the proteasome inhibitor MG132. To this purpose, we performed an *in vivo* ubiquitylation assay upon ectopic expression of increasing amounts of REN^{KCTD11} in mouse embryonic fibroblasts (MEFs) treated with solvent only as control (DMSO) or with MG132 [50μM]$_f$ for 4h. High levels of REN^{KCTD11} promote the poly-ubiquitylation of ectopic SALL4A and its subsequent degradation by the proteasome, leading to a significant accumulation of SALL4A ubiquitylated form in cells treated with the proteasome-inhibitor MG132 (**Figure 5**).

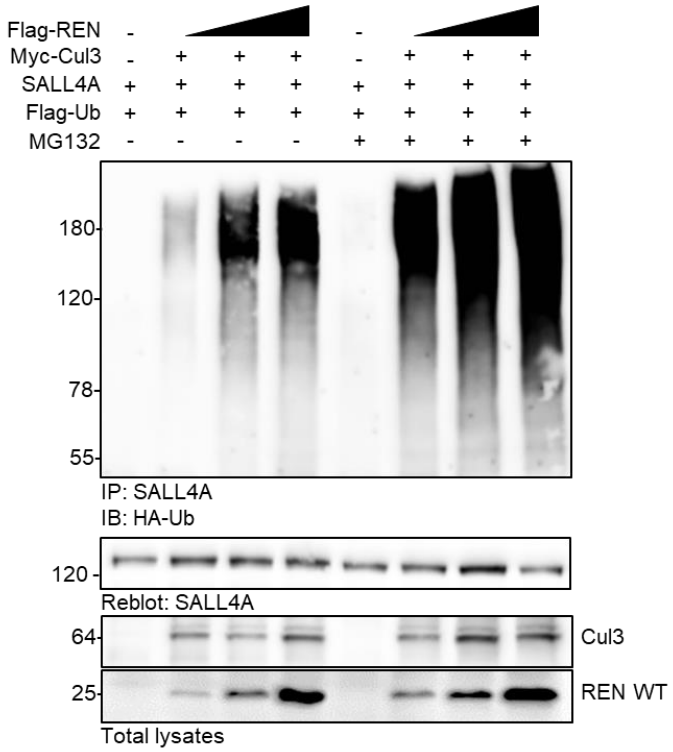

Figure 5 | *REN^{KCTD11}-mediated poly-ubiquitylation of SALL4A induces its proteasome-dependent degradation.* MEFs were transfected with plasmids expressing HA-Ub in the presence of increasing amount of Flag-REN WT. 24 h after transfection, cells were treated with solvent only as control (DMSO) or with the known proteasome inhibitor MG132 [50μM]$_f$ for 4 h. Cell lysates were then immunoprecipitated with an anti-SALL4 antibody; IP samples and a fraction of the total lysate (5%) were separated on SDS-PAGE gels followed by immunoblotting with an anti-HA antibody to detect ubiquitylated forms or with anti-Flag and anti-Myc antibodies to assess the expression of transfected plasmids. IP blots were reblotted with anti-SALL4 antibody.

Moreover, SALL4A half-life was evaluated in MEFs expressing ectopic REN^{KCTD11} and treated with the know inhibitor of protein synthesis Cycloheximide (CHX, 100µg/ml) at different time points. As shown in **Figure 6**, SALL4A half-life is shorter when overexpressing REN^{KCTD11}, confirming that REN^{KCTD11} affects SALL4A protein stability.

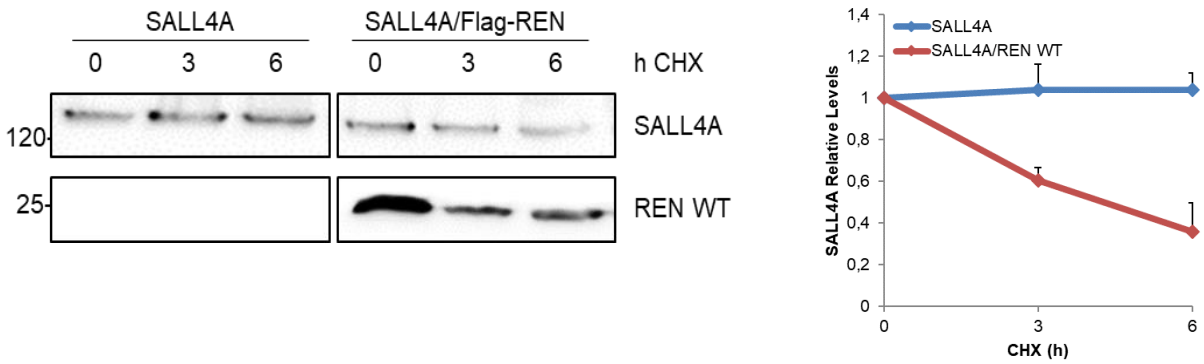

Figure 6 | *REN^{KCTD11} affects SALL4A protein stability.* SALL4A protein levels were evaluated in MEFs transfected with vectors encoding SALL4A alone or in combination with REN^{KCTD11}. 24 h after transfection cells were treated with cycloheximide (CHX, 100µg/mL) at different time points. Total lysate was separated on SDS-PAGE gels followed by immunoblotting with an anti-SALL4 or anti-Flag antibodies. Densitometry analysis of actin-normalized SALL4A protein levels of three independent experiments is shown (right panel).

3.1.3.4 | SALL4A acts as Hedgehog signalling activator enhancing GLI1 transcriptional activity

To investigate the role of SALL4A in Hh signalling, we tested its effect on GLI1 transcriptional activity. To this aim, we transfected MEFs transiently expressing ectopic GLI1 and a Gli-dependent luciferase reporter (12xGliBS-Luc), with increasing amounts of SALL4A and HDAC1 (used as control, Canettieri et al., 2010). Results shown in **Figure 7** report that SALL4A significantly increases the transcriptional activity of GLI1 effector.

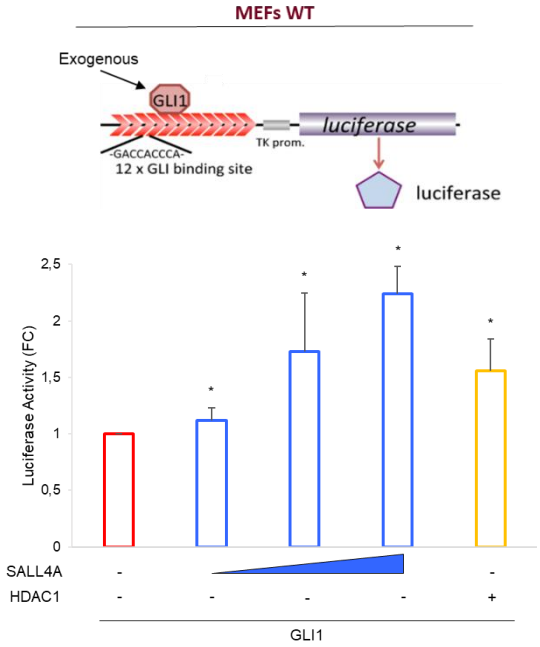

Figure 7 | *SALL4A positively regulates the Hh pathway.* Luciferase activity was evaluated in MEFs transfected with GLI1-luciferase reporter (in which the *Firefly* luciferase gene is under the control of GLI1-promoter containing 12 binding sites (12xBS) for the transcription factor – schematic representation in the upper panel), pRL-TK Renilla used as control and the indicated plasmids. Data are normalized against Renilla activity and indicated as fold change (FC) relative to GLI1-induced activation. Statistical significance was determined with two-tailed Student's t-test. Data show the mean ± standard deviation (S. D.) of three independent experiments. (*) $p < 0.05$ *vs* GLI1-induced activation.

As expected, SALL4A-induced activation of Hh signalling is counteracted by REN^{KCTD11}, but not by ΔPoz mutant (**Figure 8**).

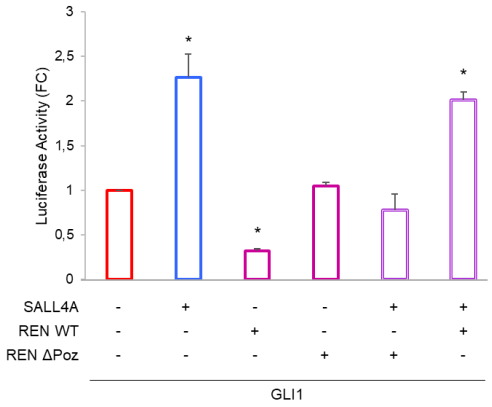

Figure 8 | *SALL4A positive regulation of the Hh pathway is abrogated by REN^{KCTD11}.* Luciferase activity was evaluated in MEFs transfected with GLI1-luciferase reporter, pRL-TK Renilla used as control and indicated plasmids. Data are normalized against Renilla activity and indicated as FC relative to GLI1-induced activation. Statistical significance was determined with two-tailed Student's t-test. Data show the mean ± S. D. of three independent experiments. (*) $p < 0.05$ *vs* GLI1-induced activation.

3.1.3.5 | SALL4A promotes GLI1 transcriptional activity working in complex with HDAC1

SALL4A transcription factor regulates gene expression through the direct interaction of its zinc-finger domains with the regulatory regions of its target gene, but also recruiting complexes involved in chromatin remodeling (Lu et al., 2009).

Data from literature have highlighted the ability of SALL4A to interact with HDAC complex on *Cdx2* gene promoter during trophoectoderm differentiation, thus promoting the deacetylation and subsequent transcriptional repression of this gene in the ICM (Yuri et al., 2009).

Since findings from our laboratory shown that HDAC1 is a positive regulator of Hh signalling which, deacetylating GLI1, promotes its transcriptional activity (Canettieri et al., 2010), we investigated the potential collaboration between SALL4A and HDAC1 in Hh pathway.

To this aim, we tested GLI1 activity in MEFs WT transiently transfected with ectopic SALL4A and HDAC1, alone or in combination. Results obtained show that GLI1 activity is strongly increased in presence of both SALL4A and HDAC1, suggesting that the two proteins could work together in the activation of the Hh signalling (**Figure 9**).

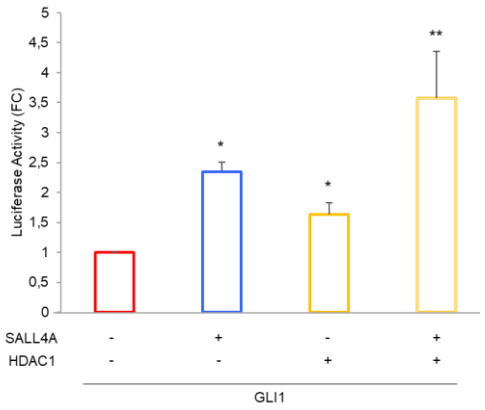

Figure 9 | *SALL4A and HDAC1 induce GLI1 transcriptional activity.* Luciferase activity was evaluated in MEFs transfected with GLI1-luciferase reporter, pRL-TK Renilla used as control and indicated plasmids. Data are normalized against Renilla activity and indicated as FC relative to GLI1-induced activation. Statistical significance was determined with two-tailed Student's t-test. Data show the mean ± S. D. of three independent experiments. (*) $p < 0.05$, (**) $p < 0.01$ *vs* GLI1-induced activation.

Same results were obtained by quantitative real-time PCR (qRT-PCR) in MEFs WT transfected with SALL4A and HDAC1 expression plasmids analysing *Gli1* mRNA levels. **Figure 10** shows that SALL4A and HDAC1 induce an increase of *Gli1* mRNA levels, thus confirming their function as Hh pathways activators, and this effect is stronger co-expressing the two proteins.

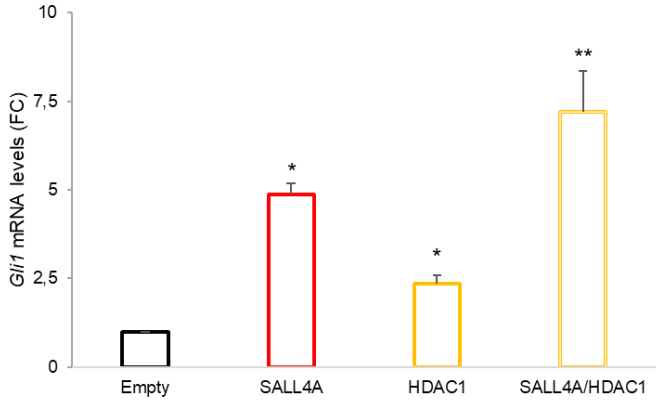

Figure 10 | *Gli1 expression is upregulated by SALL4A and HDAC1.* qRT-PCR analysis of *Gli1* expression in MEFs WT transfected with SALL4A and HDAC1, alone or in combination. Data are normalized to endogenous *Hprt* control and expressed as FC compared to the empty control sample. Statistical significance was determined with two-tailed Student's t-test. Data show the mean ± S. D. of three independent experiments. (*) $p < 0.05$, (**) $p < 0.01$ *vs* empty-transfected cells.

Assuming that SALL4A and HDAC1 form a complex in which SALL4A recruits HDAC1 on GLI1 to induce its deacetylation and to promote its transcriptional activity, we performed an *in vivo* Co-IP assay in HEK293T cells expressing tagged GLI1, SALL4A and HDAC1 in different combinations. As expected, GLI1 co-immunoprecipitates both with SALL4A and HDAC1 (**Figure 11**). Further, the presence of all the three proteins increases the association of both HDAC1/GLI1 and SALL4A/GLI1 binding, suggesting a mechanism of mutual regulation among the three proteins.

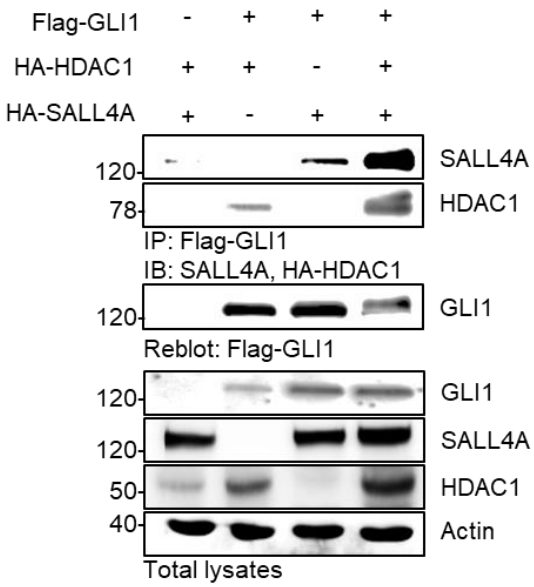

Figure 11 | *GLI1, SALL4A and HDAC1 form a complex.* Co-IP assay was performed on total lysates from HEK293T cells transfected with expression vectors encoding for the indicated proteins and immunoprecipitated with anti-Flag agarose beads. IP samples and a fraction (5%) of total lysate were separated on SDS-PAGE gels. Blots were immunoblotted with anti-HA or anti-SALL4 antibodies, then reblotted with anti-Flag antibody.

We also evaluated the acetylation state of GLI1 in presence of SALL4A. As shown in **Figure 12**, SALL4A alone is able to reduce the acetylation level of GLI1, similarly to HDAC1.

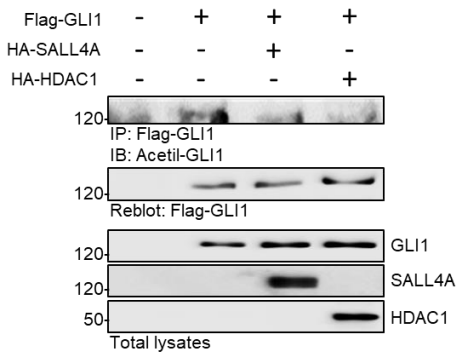

Figure 12 | *SALL4A impairs GLI1 acetylation.* HEK293T cells were transfected with expression vectors encoding for the indicated proteins and immunoprecipitated with anti-Flag agarose beads. IP samples and a fraction (5%) of the total lysate were separated on SDS-PAGE gels followed by immunoblotting with anti-acetylated lysine antibody to detect the acetylated form of GLI1, or with anti-Flag, anti-HA and anti-SALL4 antibodies to assess the expression of transfected plasmids. IP blots were reblotted with anti-Flag antibody.

3.1.3.6 | SALL4A is expressed in Hedgehog-dependent cerebellar granule cell progenitors

Hh signalling crucially regulates cerebellar development by controlling the expansion of a subset of GCPs and the proper development of the granule neuron lineage under Purkinje cell-derived SHH stimuli. Withdrawal of Hh signal causes physiologically GCPs growth arrest after the first post-natal week in mice, inducing their differentiation into mature granules (Wechsler-Reya and Scott, 1999).

Importantly, genetic or epigenetic alterations in the Hh signalling lead GCPs to uncontrolled proliferation and tumorigenic conversion (Schüller et al., 2008; Yang et al., 2008c).

To investigate SALL4A expression in a physiological context, we analysed SALL4A protein levels in GCPs at early post-natal stage (post-natal day 5, P5, when Hh signalling is physiologically maintained) treated with the known SMO agonist, SAG. Similar to GLI1, SALL4A expression is increased under SAG-treatment (**Figure 13**).

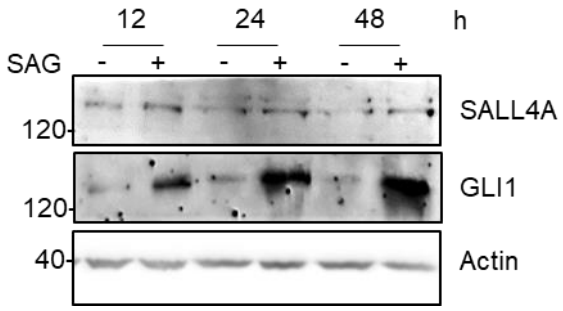

Figure 13 | *SALL4A expression in Hh-dependent cerebellar GCPs.* GCPs were isolated from 5-days-old WT mice and treated with solvent only (DMSO) as control or SAG [200nM] at indicated times. Total lysate was separated on SDS-PAGE gels followed by immunoblotting with anti-SALL4 or anti-GLI1 antibodies.

3.1.3.7 | SALL4A over-expression affects Hedgehog-dependent tumor growth *in vitro*

The relevance of SALL4A on Hh-dependent tumor cell growth was determined by testing *in vitro* cultures of human MB cells (Daoy) belonging to the SHH-MB subgroup (Ivanov et al., 2016; Northcott et al., 2012; Triscott et al., 2013).

We first compared the proliferation rate of human MB Daoy cells expressing SALL4A, GLI1 and REN^{KCTD11}, alone or in combination. As evaluated by bromodeoxyuridine (BrdU) incorporation, SALL4A promotes the proliferation of human MB Daoy cells, similarly to GLI1; this effect is strengthened by the co-expression with GLI1 and counteracted by the presence of REN^{KCTD11} (**Figure 14**, left panel). As expected, the opposite effect is observed in human MB Daoy cells genetically silenced for SALL4A (**Figure 14**, right panel).

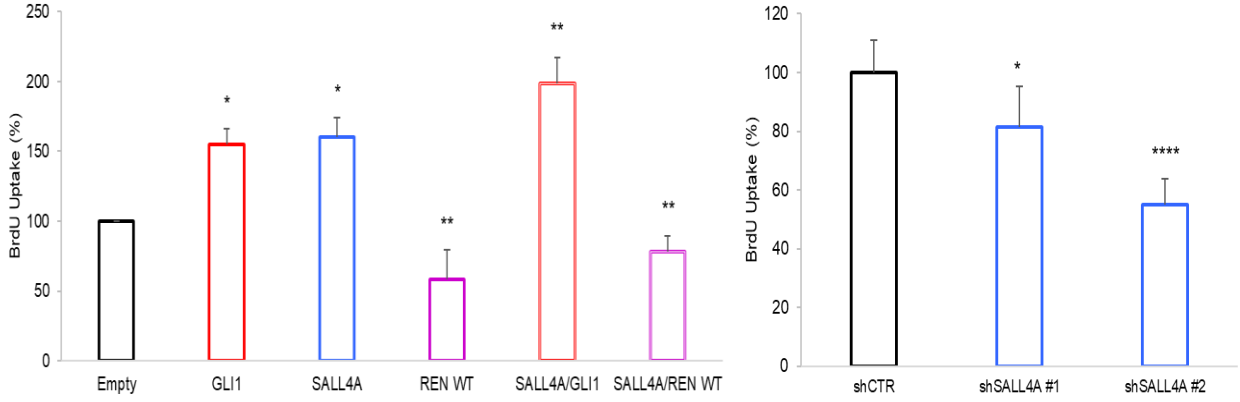

Figure 14 | *Effects of SALL4A modulation on human Hh-dependent MB cells proliferation*. (Left panel) The graph shows the percentage of BrdU incorporation in Daoy cells expressing control plasmid (Empty) or plasmids encoding SALL4A, GLI1 and REN WT, alone or in combination. (Right panel) The graph shows the percentage of BrdU incorporation in Daoy cells transduced with control lentivirus or two different lentiviruses expressing shRNA oligonucleotides targeting SALL4A (shSALL4A #1 and #2). Statistical significance was determined with two-tailed Student's t-test. Data show the mean ± S. D. of three independent experiments. (*) $p < 0.05$, (**) $p < 0.01$ *vs* empty control; (*) $p < 0.05$, (****) $p < 0.001$ *vs* shCTR.

Moreover, we carried out a wound healing assay, using the IncuCyte® Live Cell Analysis System, in human MB Daoy cells infected with two different lentiviruses expressing shRNA oligonucleotides targeting SALL4A to assess the effect of SALL4A genetic

depletion on MB cells migration. Daoy cells lacking of SALL4A display a significant reduction of motility when compared to control cells (**Figure 15**).

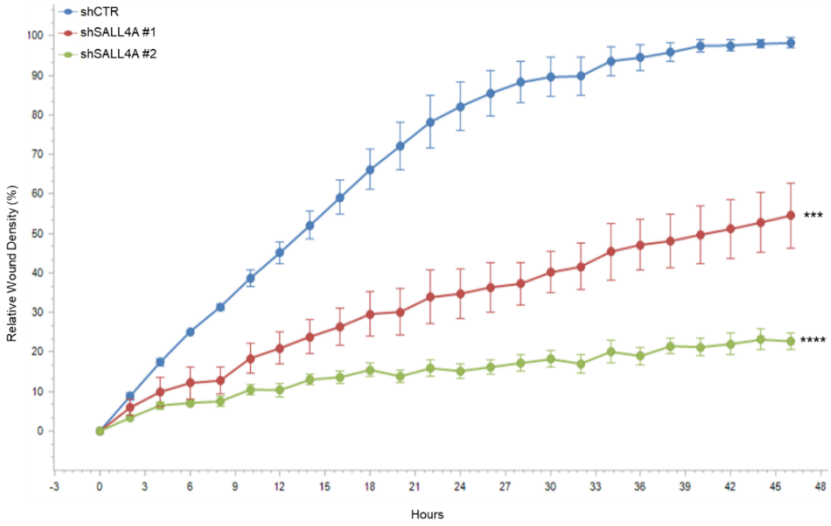

Figure 15 | *SALL4A genetic depletion limits migration of Hh-dependent MB cells*. Daoy cells were first infected with control lentivirus (shCTR) or lentivirus expressing two different shRNA oligonucleotides targeting SALL4A (shSALL4A #1 and #2). Infected cells were then seeded in 96-well tissue culture plates (12 wells for each experimental point) and cultured for 16 h to reach 100% confluence. Daoy cells were scratched and images of wounds were automatically acquired within the CO_2 incubator by IncuCyte zoom software (Essen BioScience). The wound image updates were taken at 2 h intervals. The graph shows data ± S. D. analysed with respect to wound confluence and calculated by using the IncuCyte software package (Essen BioScience). (***) $p < 0.001$, (****) $p < 0.0001$ vs shCTR.

In order to assess that SALL4A activity is restricted to Hh signalling, we tested the effect of SALL4A genetic depletion in non-Hh related MB cell lines using the IncuCyte® Live Cell Analysis System. Human Group 3 MB cells were infected with lentivirus expressing shRNA oligonucleotides that selectively target SALL4A and their proliferation rate was followed over 96 h. As shown in **Figure 16**, Group 3 MB cells proliferation is not affected by SALL4A genetic depletion.

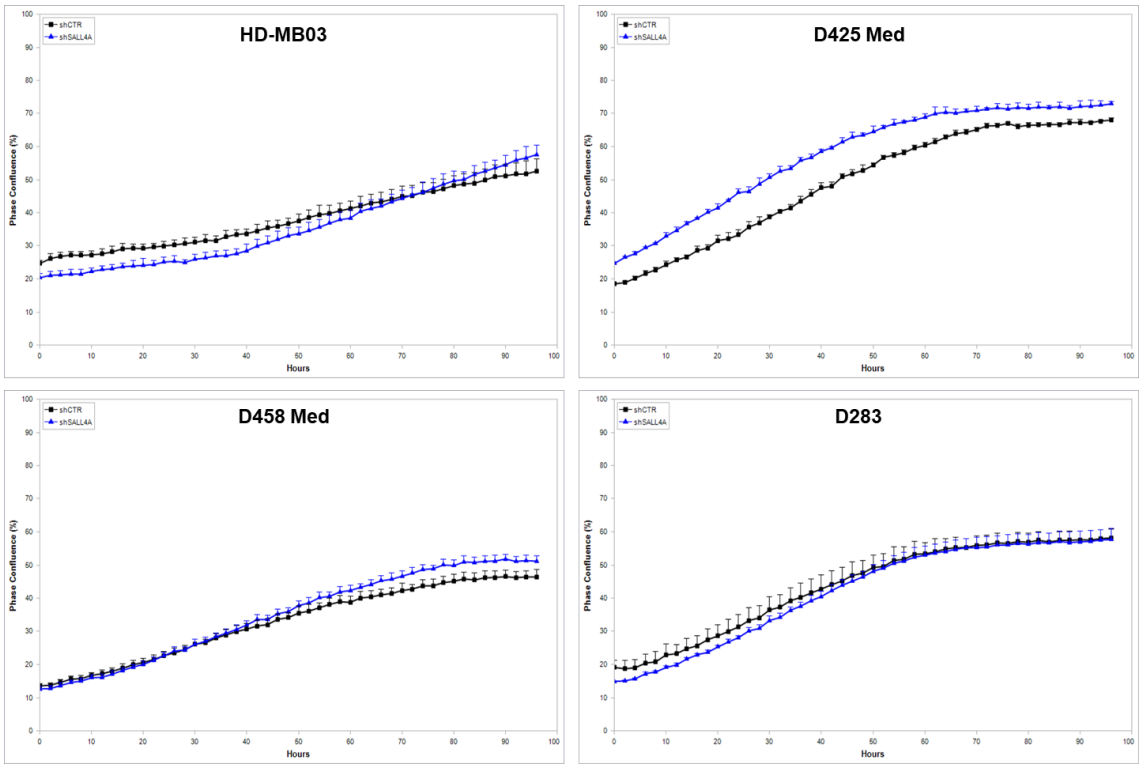

Figure 16 | *Effect of SALL4A depletion on Group 3 MB cells proliferation*. Group 3 MB cells (HD-MB03, D425, D458, D283) were first infected with control lentivirus (shCTR) or lentivirus expressing shRNA oligonucleotide targeting SALL4A (shSALL4A #1 and #2). Infected cells were then seeded in 96-well tissue culture plates (6 wells for each experimental point) and their proliferation was measured as cell confluence (%) calculated using IncuCyte Zoom software by phase-contrast images. Cells were scanned every 2 h up to 96 h after infection.

Overall, these data demonstrate that SALL4A affects Hh-dependent MB cell proliferation and migration *in vitro*.

3.1.3.8 | SALL4A depletion inhibits Hh-dependent MB growth *in vivo*

Based on the *in vitro* studies, we hypothesized that inhibition of SALL4A activity may reduce tumor growth *in vivo*. To address this critical issue, BALB/c nude mice (nu/nu) were grafted with spontaneous primary MB freshly isolated from Math1-cre/Ptc$^{C/C}$ mice and then infected with control lentivirus or shSALL4A lentivirus before implantation on mice flanks. We performed the *in vivo* experiments genetically silencing SALL4A expression only with shSALL4A #2 lentiviruses particles because of their strongest effect in *in vitro* experiments.

Of note, all mice engrafted with MB cells infected with control lentivirus developed progressively enlarging tumors compared to mice engrafted with MB cells lacking of SALL4A (**Figure 17**).

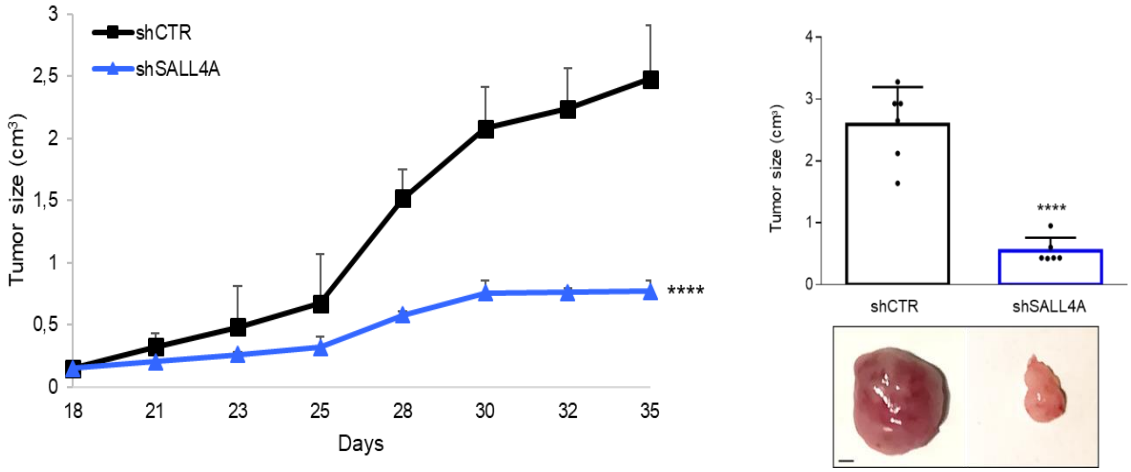

Figure 17 | *SALL4A genetic depletion suppresses Hh-dependent tumor growth in vivo*. nu/nu mice were grafted with spontaneous primary MB from Math1-cre/Ptc$^{C/C}$ mice genetically silenced for SALL4A. (Left) Tumor masses (150 mm^3) were monitored by caliper measurements three times a week until 35 days. (Right) Representative flank allograft tumors (lower panel) and quantification of tumor explants (upper panel). Scale bar: 500µm. All data represent the mean of three independent experiments. Mean ± S.D. of tumor (n = 4) for each treatment. (****) $p < 0.0001$ *vs* shCTR calculated by two-sided Student's t-test.

In agreement with the *in vitro* data, expression of endogenous Hh target genes were reduced both at mRNA and protein levels in tumor masses lacking SALL4A compared to controls (**Figure 18**).

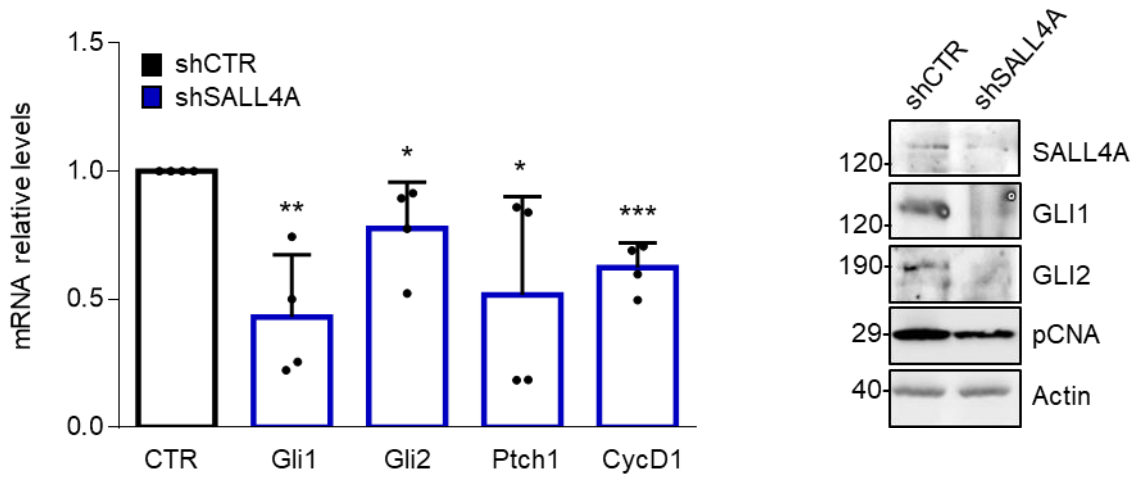

Figure 18 | *SALL4A genetic depletion impairs Hh signature in vivo*. mRNA (left) and protein (right) expression levels of Hh targets from tumors assayed in **Figure 17**.

A robust effect of SALL4A function on MB growth *in vivo* was also observed in an orthotopic allograft model in which spontaneous primary MB cells from Math1-cre/Ptc$^{C/C}$ mice genetically silenced for SALL4A were implanted into the cerebellum of nu/nu mice. As shown in **Figure 19**, only cells infected with the lentiviruses particles encoding for a non-targeting sequence gave rise to detectable tumor masses. These findings demonstrate that inhibition of SALL4A interferes with Hh-dependent MB growth *in vivo*.

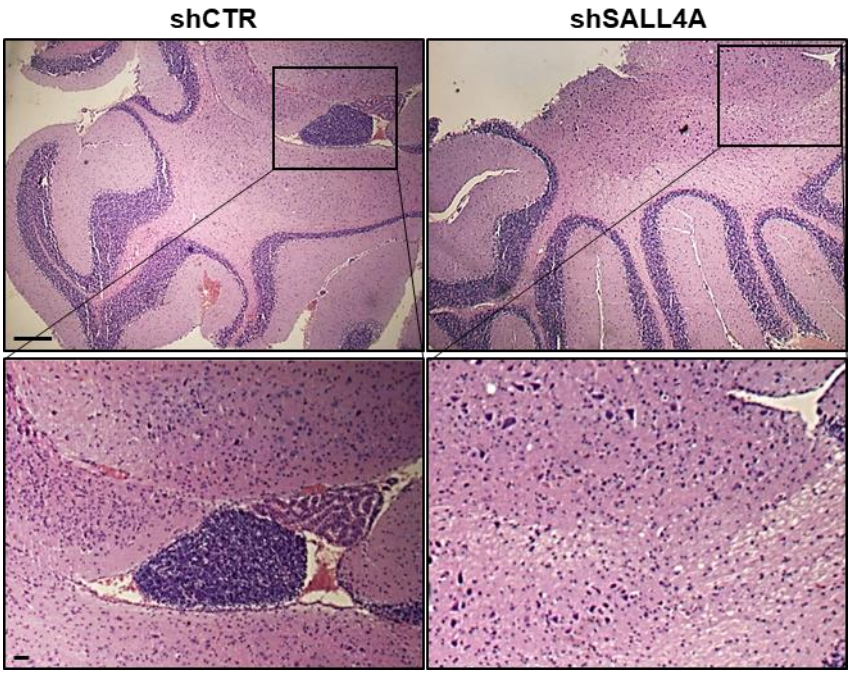

Figure 19 | *SALL4A genetic depletion suppresses Hh-dependent tumor growth in a MB orthotopic allograft animal model.* Representative hematoxylin and eosin staining (H&E) images (low and high magnification) of a murine MB cell-derived orthotopic tumor genetically interfered for SALL4A before the injection in nu/nu mice cerebella. Scale bars: 500 and 200μm (upper and lower panels, respectively).

Together, our findings identify a new player in the regulation of Hh signalling and unveil the relevance of SALL4A in the control of GLI1 activity and Hh-dependent tumor growth.

3.1.3.9 | High SALL4 levels are associated with poor prognosis in human medulloblastoma

To sustain data obtained in *in vivo* murine models, we finally investigated the association between SALL4 gene expression and patients survival in human MB cohorts (Tumor Medulloblastoma Cavalli database, SHH subgroup) from the online R2 genomics analysis and visualization platform (http://r2.amc.nl). **Figure 20** shows that high expression levels of SALL4 are associated with decreased survival in MB cancer patients.

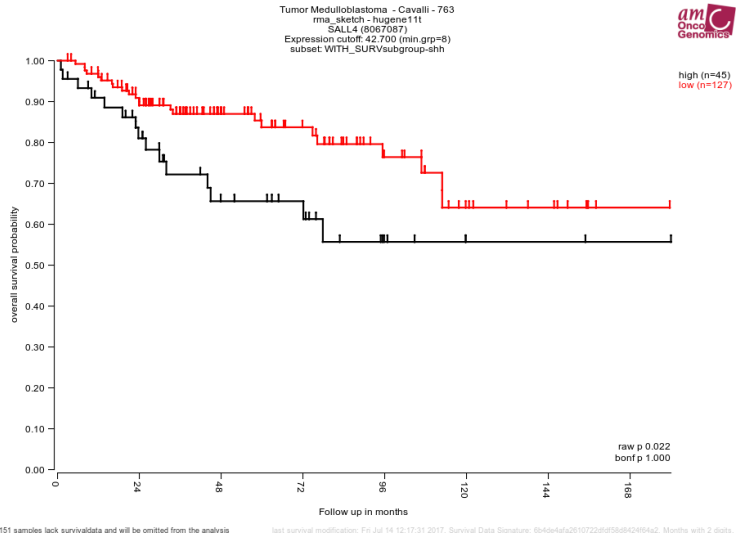

Figure 20 | *Correlation of SALL4A expression with SHH-MB patients survival time.* The correlation of SALL4A expression with patients survival time in the available complete dataset "Tumor Medulloblastoma – Cavalli – 763" in the R2 database was analysed using the R2 software. Survival time was measured from the time of initial diagnosis to the date of death or the date of last follow up. The survival distribution was estimated according to the Kaplan-Meier method using optimal cut-off selection and log-rank statistics. $p < 0.05$ was considered to be statistically significant.

3.2 | Aim 2: Pharmacological targeting of Hedgehog pathway

3.2.1 | Chemical, computational and functional insights into the chemical stability of the Hedgehog pathway inhibitor GANT61

One of the most challenging tasks in drug discovery is the identification of the active species responsible for the observed biological activity of a drug (thereafter referred as the bioactive form). Indeed, any molecular entity may undergo structural modifications and understanding the metabolic or chemical stability of bioactive compounds may help to unravel the mechanism of action and to optimise the pharmacokinetics properties, thus increasing the success rate of a drug discovery campaign (Masimirembwa et al., 2003; Shu et al., 2008).

In the last 10 years, many efforts have been spent on the identification of small molecule inhibitors of the Hh signalling (Infante et al., 2015a; Infante et al., 2016; Infante et al., 2015b; Iovine et al., 2016; Ng and Curran, 2011; Varjosalo and Taipale, 2008) able to target the pathway upstream (acting on SMO receptor) or downstream (acting on GLI transcription factors).

GANT61 is the first small molecule reported to inhibit GLI1 activity in living cells. It was discovered in 2007 by Lauth et al. and a subsequent study highlighted the possible chemical instability of GANT61 by designing a GANT61 diamine derivative (GANT61-D) that showed Hh inhibitory efficacy comparable to the parent prodrug (Lauth et al., 2007). Even though prior works synergistically substantiated that GANT61-D is the bioactive form of GANT61, they fail to provide clear and detailed information on the mechanism and kinetics of GANT61 hydrolysis, thus limiting the further development of GANT61 as anticancer drug.

To fill this gap, and to pursue our scientific interest in developing Hh-targeting small molecules, we combined multiple approaches including chemical synthesis, computational modelling, analytical tools and functional studies to provide additional insights into the chemical stability and Hh inhibitory activity of GANT61.

Our results unequivocally indicate that the bioactive form of GANT61 in cell-based experiments is the diamine derivative GANT61-D. Molecular modelling studies identified the main pharmacophores of GANT61-D relevant for the binding to GLI1-ZFs and suggested some strategies to generate optimised derivatives.

To address this goal, I was involved in the evaluation of the Hh inhibitory properties of GANT61 and GANT61-D in Hh-responsive cells (NIH3T3 SHH-Light II, which stably incorporate a Gli-responsive element; for further information please see the attached paper[3]) and in $SuFu^{-/-}$ MEFs, in which Hh pathway is constitutively active. In both assays, GANT61-D showed the ability to antagonise Hh signalling and to inhibit *Gli1* expression with comparable efficacy as GANT61.

Our findings strongly support that GANT61-D is the bioactive form of GANT61 able to counteract the Hh signalling at downstream level, thus limiting the oncogenic potential of the pathway occurring in a context of SMO-independence or GLI1 hyperactivation by alternative mechanisms.

Since this work has been published, I only provided a brief outline of obtained results. Please refer to the paper attached below[3] for more detailed evaluation.

[3]Calcaterra, A., Iovine, V., Botta, B., Quaglio, D., D'Acquarica, I., ... **Lospinoso Severini, L**., Infante, P., Di Marcotullio, L., Mori, M. & Ghirga, F. (**2018**). Chemical, computational and functional insights into the chemical stability of the Hedgehog pathway inhibitor GANT61**. Journal of enzyme inhibition and medicinal chemistry**, 33(1), 349-358.

JOURNAL OF ENZYME INHIBITION AND MEDICINAL CHEMISTRY
2018, VOL. 33, NO. 1, 349–358
https://doi.org/10.1080/14756366.2017.1419221

Taylor & Francis
Taylor & Francis Group

RESEARCH PAPER

OPEN ACCESS Check for updates

Chemical, computational and functional insights into the chemical stability of the Hedgehog pathway inhibitor GANT61

Andrea Calcaterra[a], Valentina Iovine[a], Bruno Botta[a], Deborah Quaglio[a], Ilaria D'Acquarica[a], Alessia Ciogli[a], Antonia Iazzetti[a], Romina Alfonsi[b], Ludovica Lospinoso Severini[b], Paola Infante[c], Lucia Di Marcotullio[b,d], Mattia Mori[c] and Francesca Ghirga[c]

[a]Department of Chemistry and Technology of Drugs, Sapienza University of Rome, Rome, Italy; [b]Department of Molecular Medicine, Sapienza University of Rome, Rome, Italy; [c]Center for Life Nano Science@Sapienza, Istituto Italiano di Tecnologia, Rome, Italy; [d]Pasteur Institute/Cenci Bolognetti Foundation, Sapienza University of Rome, Rome, Italy

ABSTRACT

This work aims at elucidating the mechanism and kinetics of hydrolysis of GANT61, the first and most-widely used inhibitor of the Hedgehog (Hh) signalling pathway that targets Glioma-associated oncogene homologue (Gli) proteins, and at confirming the chemical nature of its bioactive form. GANT61 is poorly stable under physiological conditions and rapidly hydrolyses into an aldehyde species (GANT61-A), which is devoid of the biological activity against Hh signalling, and a diamine derivative (GANT61-D), which has shown inhibition of Gli-mediated transcription. Here, we combined chemical synthesis, NMR spectroscopy, analytical studies, molecular modelling and functional cell assays to characterise the GANT61 hydrolysis pathway. Our results show that GANT61-D is the bioactive form of GANT61 in NIH3T3 Shh-Light II cells and SuFu$^{-/-}$ mouse embryonic fibroblasts, and clarify the structural requirements for GANT61-D binding to Gli1. This study paves the way to the design of GANT61 derivatives with improved potency and chemical stability.

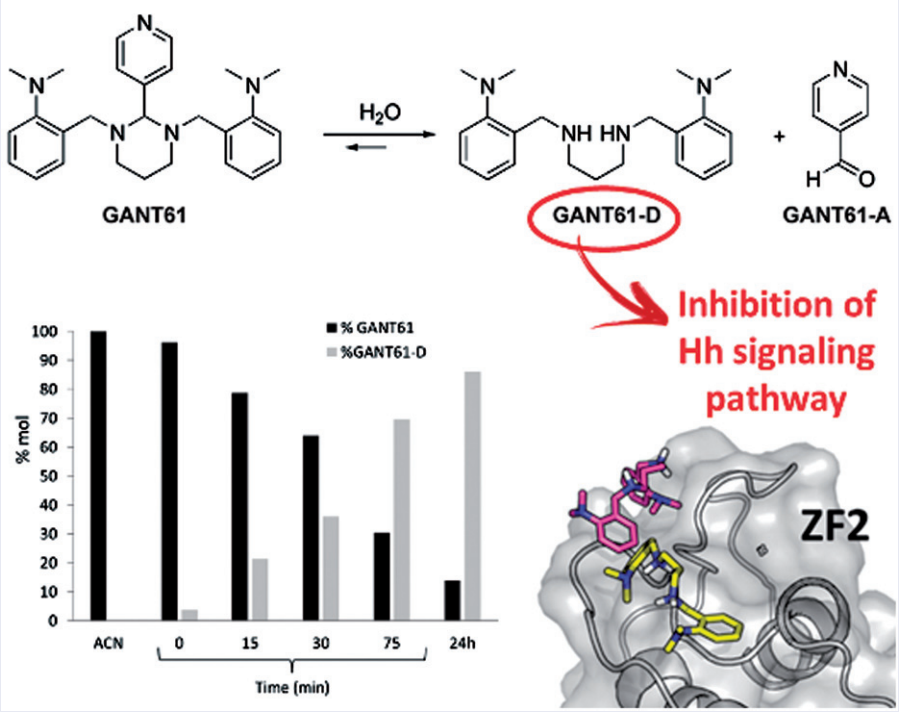

ARTICLE HISTORY
Received 13 November 2017
Revised 14 December 2017
Accepted 15 December 2017

KEYWORDS
GANT61; Hedgehog pathway; Gli inhibitor; chemical stability; bioactive form

CONTACT Mattia Mori mattia.mori@iit.it Center For Life Nano Science@Sapienza, Istituto Italiano di Tecnologia, Viale Regina Elena 291, 00161 Rome, Italy; Lucia Di Marcotullio lucia.dimarcotullio@uniroma1.it Department of Molecular Medicine, Sapienza University of Rome, Viale Regina Elena 291, 00161 Rome, Italy

Supplemental data for this article can be accessed here.

Introduction

One of the most challenging tasks in drug discovery is the identification of the active species responsible for the observed biological activity of a drug or a drug candidate (thereafter referred as the bioactive form). In fact, any molecular entity may undergo structural modifications due to the exposure to different cellular environments, metabolic enzymes, reactions with redox species, and so on. In this regard, understanding the metabolic or chemical stability of a bioactive compound may help to unravel its mechanism of action and to optimise pharmacokinetics properties, which increases the success rate of a drug discovery campaign[1,2].

In the last 10 years, many efforts have been spent by our own and other research groups on the identification of small molecule inhibitors of the Hedgehog (Hh) signalling pathway[3–8], which plays a pivotal role in the initiation, proliferation, invasion and metastasis of a wide variety of cancers including basal cell carcinoma (BCC), medulloblastoma[9–11], rhabdomyosarcoma[12,13], pancreatic[14], colorectal[15], metastatic prostate[16], small-cell lung[17], breast[18] carcinomas, and malignant gliomas. The Hh pathway is also implicated in the regulation and maintenance of cancer stem cells (CSCs), providing a link between the Hh signalling in the regulation of normal stem cells and its role in CSCs maintenance[19–22]. Noteworthy, targeting CSCs has recently emerged as a profitable anticancer strategy endowed with impressive therapeutic implications and challenges[23,24].

Smoothened receptor (Smo) is the most widely appreciated drug target of the Hh signalling pathway. Two small molecule antagonists of Smo have been approved by the FDA (namely, Vismodegib in 2012 and Sonidegib in 2015) for the treatment of metastatic or locally advanced BCC[25,26], while a number of clinical trials are currently running on additional chemotypes of Smo antagonists[27,28]. However, drug-resistant mutations of Smo sequence[29–31], as well as Smo-independent Hh pathway activation have been highlighted during the treatment with Vismodegib or other clinical candidates[32,33], thus raising the need to identify novel leads capable to act on the drug-resistant forms of Smo and/or to block the pathway downstream or independently by Smo[34]. In this regard, the Glioma-associated oncogene homologue 1 (Gli1) is the final effector of the Hh pathway and has emerged as an alternative and more promising target than Smo[6].

By integrating multidisciplinary efforts in a concerted strategy, recently we proved that Gli1/DNA interaction is a druggable target for the treatment of Hh-dependent tumours[8]. We also identified the naturally occurring isoflavone Glabrescione B (GlaB) as the first small molecule capable of impairing Gli1 activity by directly interfering with its binding to DNA[8]. However, for the sake of clarity GANT61 (Figure 1) has been the first small molecule reported to inhibit Gli1 activity in living cells. It was discovered in 2007 by Lauth et al. in a cell-based screen for small molecule inhibitors of Gli-mediated transcription, together with GANT58 (Figure 1)[35]. These two molecules proved to inhibit both Gli1- and Gli2-mediated gene transactivation in a dose-dependent manner, with an IC_{50} value of about 5 μM in cellular assays.

A subsequent study has highlighted the possible chemical instability of GANT61 by designing a GANT61 diamine derivative (GANT61-D, Figure 1) that has shown Hh inhibitory efficacy comparable to the parent prodrug GANT61[36]. The same authors have also underlined the chemical instability of GANT61 in aqueous buffers[37], suggesting that GANT61-D and the pyridine 4-carboxyaldehyde (GANT61-A) are formed according to the pathway shown in Figure 1.

GANT61-D has been the subject of another recent study aimed at investigating its mode and specificity of binding to Gli proteins and to further corroborate the druggability of Gli in cancer[38]. Molecular docking simulations have identified the putative GANT61-D binding site within residues E119 and E167, although the authors have carried out molecular docking on the neutral form of the GANT61-D that is expected to be less abundant than the corresponding mono- and di-protonated forms at physiological pH values.

Even though these prior works[36–38] synergistically substantiated that GANT61-D is the bioactive form of GANT61, they fail to provide clear and detailed information on the mechanism and kinetics of GANT61 hydrolysis, thus limiting the further development of GANT61 as anticancer lead. To fill this gap, and to pursue our scientific interest in developing Hh-targeting small molecules, here we combined multiple approaches including chemical synthesis, computational modelling, analytical tools and functional studies to provide additional insights into the chemical stability and Hh inhibitory activity of GANT61. To this end, we synthesised both GANT61 and GANT61-D in order to provide sufficient amounts of pure compounds for analytical and functional assays. Afterwards, GANT61 chemical stability was monitored by NMR spectroscopy and hydrophilic interaction chromatography (HILIC), whereas molecular modelling was used to evaluate the mode of binding of GANT61-D in its neutral as well as multiple ionisation states to Gli1 zinc finger domain (Gli1ZF). Hh pathway inhibition by

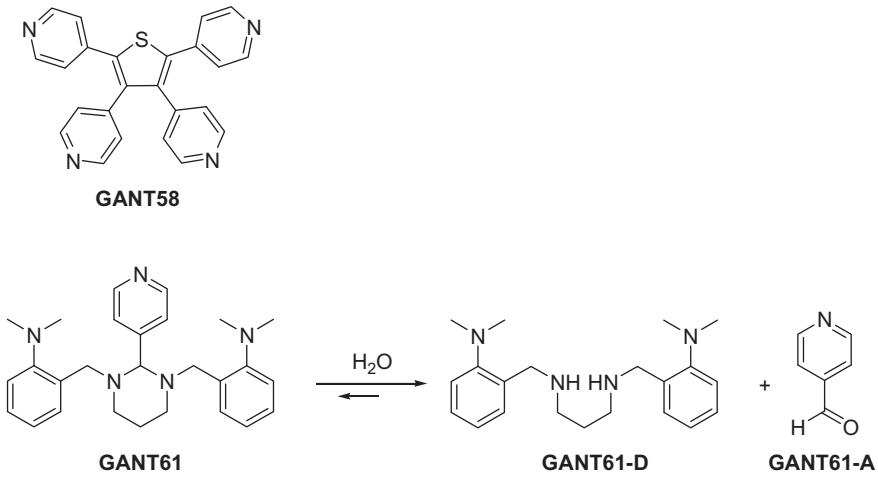

Figure 1. Chemical structures of two Gli antagonists GANT58 and GANT61 discovered in 2007 by Lauth et al. and GANT61 hydrolysis products GANT61-D and GANT61-A.

GANT61 and GANT61-D was finally evaluated in NIH3T3 Shh-Light II cells stably incorporating a Gli-responsive firefly luciferase reporter (Gli-RE), and in $SuFu^{-/-}$ mouse embryonic fibroblasts (MEFs) to monitor effects on the Hh signalling at a downstream level.

Methods

General experimental procedures

Commercially available reagents were supplied by Sigma-Aldrich (St. Louis, MO) and used without further purification. A sample of GANT61 was purchased from Tocris Bioscience (Bristol, UK) for comparison with the newly synthesised sample. Dry solvents were purchased from Sigma-Aldrich except for ethanol, which was dried by distillation from I_2/Mg.

^{1}H and ^{13}C NMR spectra have been acquired with a Bruker Avance 400 spectrometer operating at 400.13 and 100.6 MHz, respectively, at 300 K in $CDCl_3$, MeOD or DMSO-d_6, using 5-mm diameter glass tubes.

^{1}H NMR spectra of GANT61 for kinetic studies were recorded at 310 K in EtOH-d_6/PBS-d(D_2O) at 50:50 ratio (v/v). The deuterated PBS buffer was prepared by mixing 0.066 M stock solution of K_2DPO_4 (98 atom % D) and KD_2PO_4 (98 atom % D) prepared in D_2O to the correct pD = 7.4, diluting the solution to the proper phosphate buffer concentration reported for PBS, and then adding NaCl and KCl to the final solution in order to reach the concentration of 0.137 M and 0.0027 M, respectively. The mixture was thoroughly equilibrated for ~1 h before being used for NMR measurements. The resulting pD was 7.4 (assuming that pD = pH meter reading +0.4)[39], otherwise it was adjusted to 7.4 by addition of 37% w/w DCl or 40% w/w NaOD solutions in D_2O.

Chemical shifts were expressed in ppm and coupling constants (J) in Hertz (Hz), approximated to 0.1 Hz. Residual solvent peak was used as an internal reference for ^{1}H NMR and ^{13}C NMR spectra. Data for ^{1}H NMR are reported as follows: chemical shift, multiplicity (ovrlp = overlapped, s = singlet, d = doublet, t = triplet, p = pentuplet, m = multiplet, dd = doublet of doublets, dt = doublet of triplets, td = triplet of doublets, ABq = AB quartet), coupling constant, integral. Spectra were processed with the program MestReNova version 6.0.2–5475, FT and zero filling at 64 K.

Mass spectra were obtained using a Thermo Finnigan LCQ Deca XP Plus mass spectrometer equipped with an electrospray ionisation (ESI) source and a Fleet ion-trapanalyser; capillary temperature 275 °C, spray voltage 5.0 kV (positive mode), sheath gas (N_2) 25 arbitrary units, capillary voltage 40 V, tube lens 15 V.

Analytical liquid chromatography was performed using a Waters-1525 HPLC system equipped with an UV detector (Waters 2487) and an evaporative light scattering detector (ELSD) (SEDEX) detector. The column used was the Acclaim HILIC-10, 3 μm (150 × 4.6 mm I.D.), purchased from Thermo Scientific (Waltham, MA). Eluent: CH_3CN/NH_4OAc 100 mM (pH = 4.5) at 95:5 ratio (v/v). Flow-rate: 1.0 ml/min, room temperature. Detection: UV at 254 nm, and ELSD (P = 3.0 bar, T = 60 °C). The crude product purifications were carried out on silica column chromatography using Silica Gel Fluka 60 Å (0.063–0.200 mm, 70–230 mesh). GANT61 was purified by column chromatography on aluminium oxide active basic EMD Millipore (0.063–0.200 mm, 70–230 mesh, pH = 9–10.5).

Synthesis of 2-(dimethylamino)benzaldehyde (2)

Commercially available 2-fluorobenzaldehyde (1) (0.45 g, 0.38 ml, 3.62 mmol) and K_2CO_3 (1.0 g, 7.24 mmol) were introduced in a sealed tube under an argon atmosphere. Anhydrous DMSO (0.38 ml) and a 2 M solution of $(CH_3)_2NH$ in THF (2.0 ml, 4.0 mmol) were added and the mixture was heated to reflux temperature (about 100 °C) for 3 h. Then, after cooling, another aliquot (2.0 ml, 4.0 mmol) of 2 M solution of $(CH_3)_2NH$ in THF was added and the mixture was refluxed for other 3 h. The last addition of the $(CH_3)_2NH$ solution (2.0 ml, 4.0 mmol) was made before refluxing the mixture overnight. The reaction mixture was poured into water and extracted with CH_2Cl_2. Organic layers were collected, dried over Na_2SO_4 and concentrated *in vacuo* to give a pale yellow oil. The crude product was purified by column chromatography using silica gel and 5% ethyl acetate/*n*-hexane as eluent to obtain 2-(dimethylamino)benzaldehyde (2) in 65% yield (0.35 g, 2.35 mmol). Pale yellow oil; ^{1}H NMR (400.13 MHz, $CDCl_3$) δ 10.20 (s, 1H), 7.74 (dd, J_1 = 7.6 Hz, J_2 = 1.6 Hz, 1H), 7.46–7.41 (m, 1H), 7.02 (d, J = 8.0 Hz, 1H), 6.97 (t, J = 7.6 Hz, 1H), 2.89 (s, 6H); ^{13}C NMR (100.6 MHz, $CDCl_3$) δ 191.2, 155.9, 134.6, 131.1, 127.1, 120.8, 117.7, 45.5; ESI-MS (pos.) m/z = 150 ($[M+H]^+$).

Synthesis of N^1,N^3-(bis-2-isopropylbenzyl)propane-1,3-diamine (GANT61-D)

In a three-necked round bottom flask, equipped with a Dean–Stark separator fulfilled with molecular sieves (pore size 3 Å) and anhydrous benzene, were introduced benzaldehyde **2** (0.166 g, 1.11 mmol), anhydrous benzene (15 ml) and 1,3-diaminopropane (0.041 g, 46 μl, 0.556 mmol), freshly distilled from molecular sieves. The mixture was heated at reflux temperature and stirred overnight. The reaction mixture, monitored by TLC (eluent: *n*-hexane/ethyl acetate = 90:10), showed the partial disappearance of the starting material after 12 h. After that time, the solvent was removed under reduced pressure and the residue was dissolved in 10 ml of dry ethanol. After cooling the solution to 0 °C, $NaBH_4$ (0.083 g, 2.226 mmol) was added and the mixture was stirred for 30 min. Then, the reaction was quenched with a saturated aqueous NH_4Cl solution and most of the solvent (ethanol) was removed under reduced pressure. The aqueous residue was washed with ethyl acetate (3 × 15 ml) and the organic layers were discarded. 2 M NaOH was added to the aqueous solution until pH 14 and a white precipitate rapidly appeared. The mixture was thus extracted with ethyl acetate (4 × 15 ml) and the collected organic layers were dried over Na_2SO_4 and concentrated *in vacuo* to give a yellow oil. The crude product was purified by column chromatography using silica gel and the mixture MeOH/Et_3N/CH_2Cl_2 10:5:85 as eluent to obtain the pure GANT61-D in 60% yield (0.11 g, 0.34 mmol). Oily transparent or yellowish liquid; ^{1}H NMR (400.13 MHz, MeOD) δ 7.28–7.17 (m, 6H), 7.04 (td, J_1 = 7.2 Hz, J_2 = 1.2 Hz, 2H), 3.86 (s, 4H), 2.65 (ovrlp s, 12H), 2.68–2.60 (ovrlp m, 4H), 1.75 (p, J = 7.1 Hz, 2H). ^{13}C NMR (100.6 MHz, MeOD) δ 154.3, 134.4, 131.0, 129.4, 125.0, 121.0, 51.0, 48.2, 45.4, 29.5. ESI-MS (pos.) m/z = 341 ($[M+H]^+$), 171 ($[M+2H]^{2+}$).

Synthesis of GANT61

In a three-necked round bottom flask were introduced GANT61-D (0.051 g, 0.15 mmol) in anhydrous THF (0.5 ml) and commercially available pyridine 4-carboxyaldehyde (GANT61-A; 0.016 g, 0.15 mmol) in anhydrous THF (1.0 ml). The reaction mixture was heated at reflux temperature and stirred for 18 h. The solvent was removed under reduced pressure and the crude residue was purified by column chromatography using basic alumina and ethyl acetate/*n*-hexane as eluent to obtain GANT61 in 90% yield

(0.058 g, 0.135 mmol). White solid; ^{1}H NMR (400.13 MHz, DMSO-d$_6$) δ 8.55 (dd, J = 4.5, 1.3 Hz, 2H), 7.67 (dd, J = 4.5, 1.3 Hz, 2H), 7.47 (dd, J = 4.5, 1.3 Hz, 2H), 7.15 (m, 2H), 7.06–6.98 (m, 4H), 4.01 (s, 1H), 3.40, 3.51 (ABq, J_{AB} = 14.2 Hz, 4H), 2.81 (td, J = 11.5, 3.7 Hz, 2H), 2.50 (ovrlp s, 12H), 2.18 (p, J = 6.3 Hz, 2H), 1.62–1.54 (m, 2H). ^{13}C NMR (100.6 MHz, DMSO-d$_6$) δ 152.5, 150.6, 149.5, 132.9, 128.8, 127.1, 124.4, 122.8, 118.8, 85.3, 52.00, 49.9, 44.7, 22.51. ESI-MS (pos.) m/z = 431 ([M + H]$^+$), 215.7 ([M + 2H]$^{2+}$).

Molecular modelling

The crystallographic structure of Gli1ZF in complex with DNA (PDB ID: 2GLI)[40] was used as a rigid receptor in molecular docking simulations performed with AutoDock4.2[41]. Before doing docking, DNA atoms and water molecules were manually removed, whereas cobalt ions present in the X-ray structure were substituted with Zn(II) ions as in the physiologically relevant human Gli1. For grid generation, a box of 80 × 70 × 80 points with a grid spacing of 0.5 Å that covered the whole Gli1ZF accessible surface was centred on the mass centre of the protein. An arbitrary +1 charge was set to Zn(II) ions within each ZF, taking into consideration that coordination by amino acids decreases the total point charge of a metal ion as observed in prior studies[42–45]. Docking calculations were performed with AutoDock using the Lamarckian Genetic Algorithm by running 100 GA_RUNS for each molecule and keeping all other parameters at their default value. Electrostatic properties of Gli1ZF were evaluated by solving the Poisson–Boltzmann equation using APBS[46].

Docking complexes were further relaxed by energy minimisation in explicit water solvent (TIP3P type) with Amber12[47]. The ff12 and the GAFF force fields were used for simulating proteins and ligands, respectively. As in docking simulations, an arbitrary charge of +1 and was assigned to Zn(II) ions, which were treated by a non-bonded approach (harmonic restraint of 10 kcal/(mol·Å^2)). Energy minimisation was performed as follows, in agreement with prior works[42,48–51]: (i) water molecules were energy minimised for 100 steps with a steepest-descent algorithm (SD) and subsequent 300 steps with a conjugate gradient algorithm (CG) while keeping the solute as frozen; (ii) the solvated solute was energy minimised for 1000 steps SD and 9000 steps CG. After energy minimisation, ligand theoretical affinity was calculated by means of the Molecular Mechanics Generalised Born Surface Area (MM-GBSA) method[52,53] and the XSCORE function[54]. Prediction of pKa of GANT61-D was performed by MoKa (Molecular Discovery Ltd.)[55].

Hh-dependent luciferase reporter assay

The luciferase assay was performed in NIH3T3 Shh-Light II cells, stably incorporating a Gli-responsive luciferase reporter and the pRL-TK Renilla (normalisation control). The Shh-Light II cells were cultured in DMEM plus 10% FBS and then treated for 48 h with SAG alone (200 nM, Alexis Biochemicals, Farmingdale, NY) or in combination with GANT61 or GANT61-D.

Luciferase and *Renilla* activity were assayed with a dual-luciferase assay system according to the manufacturer's instruction (Biotium Inc., Hayward, CA). Results are expressed as luciferase/*Renilla* ratios and represent the mean ± SD of three independent experiments, each performed in triplicate.

mRNA expression analysis

Total RNA was isolated with Trizol (Invitrogen/Life Technologies, Carlsbad, CA) from SuFu$^{-/-}$ MEFs cultured in DMEM plus 10% FBS and then treated for 24 h with GANT61 or GANT61-D. RNA was then reverse transcribed with SensiFAST cDNA Synthesis Kit (Bioline Reagents Limited, London, UK). Quantitative real-time PCR (Q-PCR) analysis of Gli1, β-2 microglobulin and HPRT mRNA expression was performed on each cDNA sample using the VIIA7 Real-Time PCR System employing Assay-on-Demand Reagents (Life Technologies, Carlsbad, CA). A reaction mixture containing cDNA template, SensiFAST Probe Lo-ROX Kit (Bioline Reagents Limited) and primer-probe mixture was amplified using FAST Q-PCR thermal cycler parameters. Each amplification reaction was performed in triplicate and the average of the three threshold cycles was used to calculate the amount of transcript in the sample (using SDS version 2.3 software). mRNA quantification was expressed, in arbitrary units, as the ratio of the sample quantity to the quantity of the calibrator. All values were normalised with two endogenous controls, β-2 microglobulin and HPRT, which yielded similar results.

Results

Chemical synthesis of GANT61 and GANT61-D

As recently disclosed by Chenna et al., GANT61-D (Figure 1) is an intermediate in the synthetic pathway to GANT61[56]. Therefore, here we applied a similar chemical synthesis protocol with slight modifications (see Scheme 1) to obtain both compounds in good yields for analytical and functional studies.

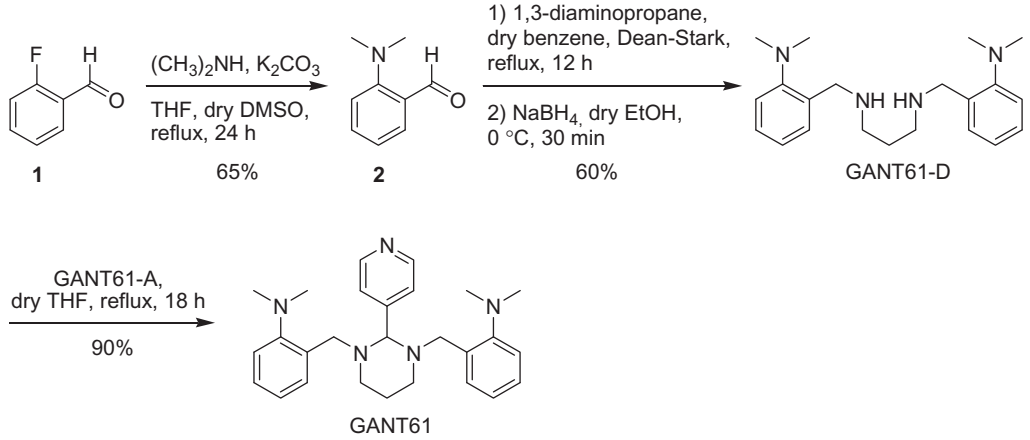

Scheme 1. Synthetic pathway to obtain both GANT61-D and GANT61.

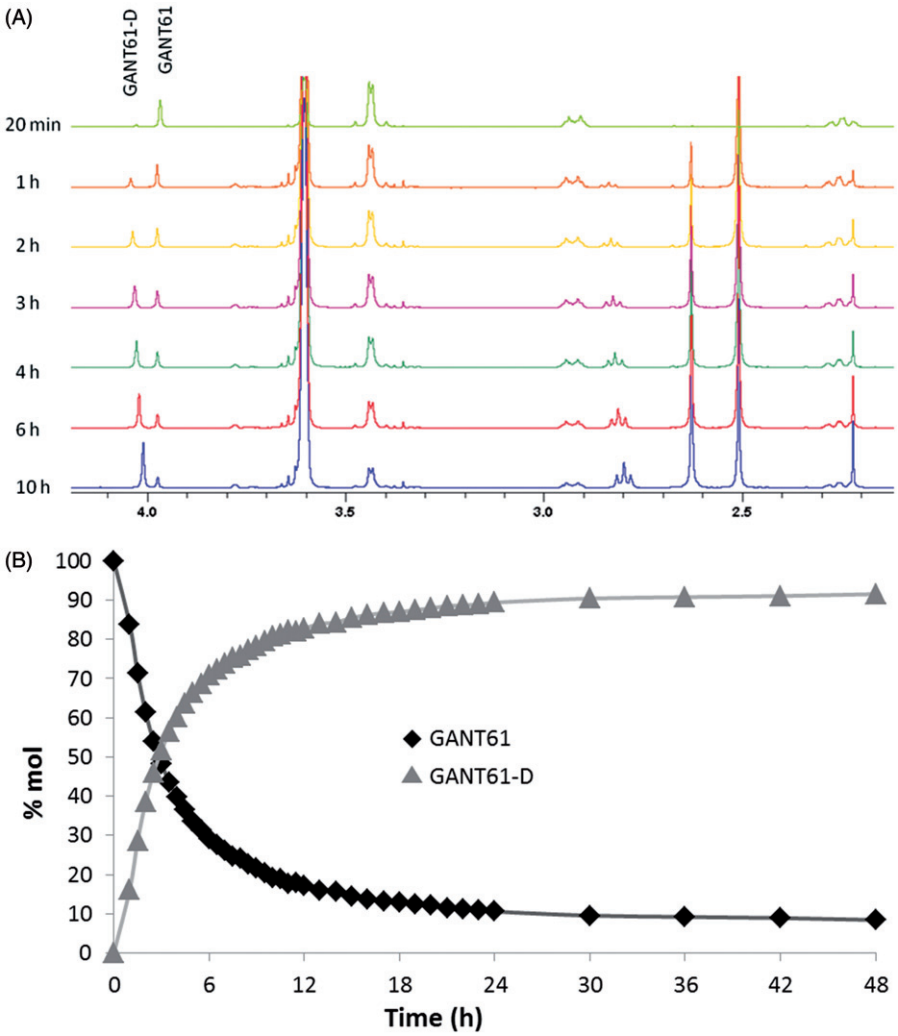

Figure 2. GANT61 hydrolysis in EtOH-d_6/PBS-d(D_2O) 50:50 v/v at 37 °C monitored by ^{1}H NMR spectroscopy. **(A)** Time evolution of the ^{1}H NMR spectrum in the aliphatic signals region (2–4.2 ppm); peaks corresponding to the monitored proton of GANT61 and GANT61-D are labelled. **(B)** Evolution of the normalised areas of the selected ^{1}H NMR signals for GANT61 and GANT61-D monitored up to 48 h incubation.

Briefly, nucleophilic aromatic substitution of commercially available 2-fluorobenzaldehyde (**1**) with dimethylamine led to 2-(dimethylamino)benzaldehyde (**2**) in 65% yield. Afterwards, **2** was converted into the intermediate diimine by treatment with 1,3-diaminopropane. Reduction *in situ* with sodium borohydride afforded GANT61-D in 39% overall yield from 2-fluorobenzaldehyde (**1**). To obtain GANT61, GANT61-D was condensed with commercially available GANT61-A (see Scheme 1), thus yielding the target compound in 35% overall yield. The structures of GANT61, GANT61-D and **2** were confirmed by ^{1}H and ^{13}C NMR spectroscopy and by ESI mass spectrometry (ESI-MS). The NMR spectra of chemically synthesised GANT61 were superimposable with those of a sample of GANT61 purchased from Tocris Bioscience and used for comparison (data not shown).

Chemical stability of GANT61 checked by NMR spectroscopy

NMR is a powerful tool to monitor the chemical stability of bioactive substances in solution and to clarify their possible degradation pathway[57]. Due to limited water solubility, NMR-based kinetic studies of GANT61 were performed in a 1:1 mixture of EtOH-d_6 and deuterated PBS buffer prepared by mixing Na_2DPO_4 and KD_2PO_4 in D_2O and adding proper amounts of NaCl and KCl (pD = 7.4). In addition, and with the aim to reproduce as much as possible the physiological pathway of GANT61 hydrolysis in living cells, NMR experiments were performed at 310 K (37 °C). The singlet centred at $\delta = 3.97$ ppm in the ^{1}H NMR spectrum of a freshly prepared solution of GANT61 was attributed to the aminalic proton (N-CH-N) and was selected as a probe to monitor the kinetics of hydrolysis of GANT61 (Figure 2(A)). In fact, this proton resonates in a rather clean and empty region of the NMR spectrum and is thought to be included in GANT61-A upon hydrolysis of GANT61 based on the pathway described in Figure 1. The intensity of this signal (normalised with respect to the adjacent increasing signal) proved to decrease during the time (Figure 2(A)), which indicates GANT61 degradation. In parallel, a new singlet peak is formed at 4.04 ppm, which was attributed to the Ph-CH_2-NH protons of the newly formed hydrolysis product GANT61-D. Notably, the chemical shift of the new peak from GANT61-D was shown to vary in time as the result of H-bond interactions with the buffer, in agreement with literature data[58,59]. Based on NMR data acquired up to 48 h of incubation, a kinetic plot was built to show the hydrolysis of GANT61 (Figure 2(B)).

The data shown in Figure 2(B) clearly highlights the fast kinetics of GANT61 hydrolysis. After 6 h, around 70% of the initial product is hydrolysed into the corresponding GANT61-D, while the plateau is reached at 24 h when around 90% of initial GANT61 is hydrolysed to GANT61-D. From this time point, the reaction is at

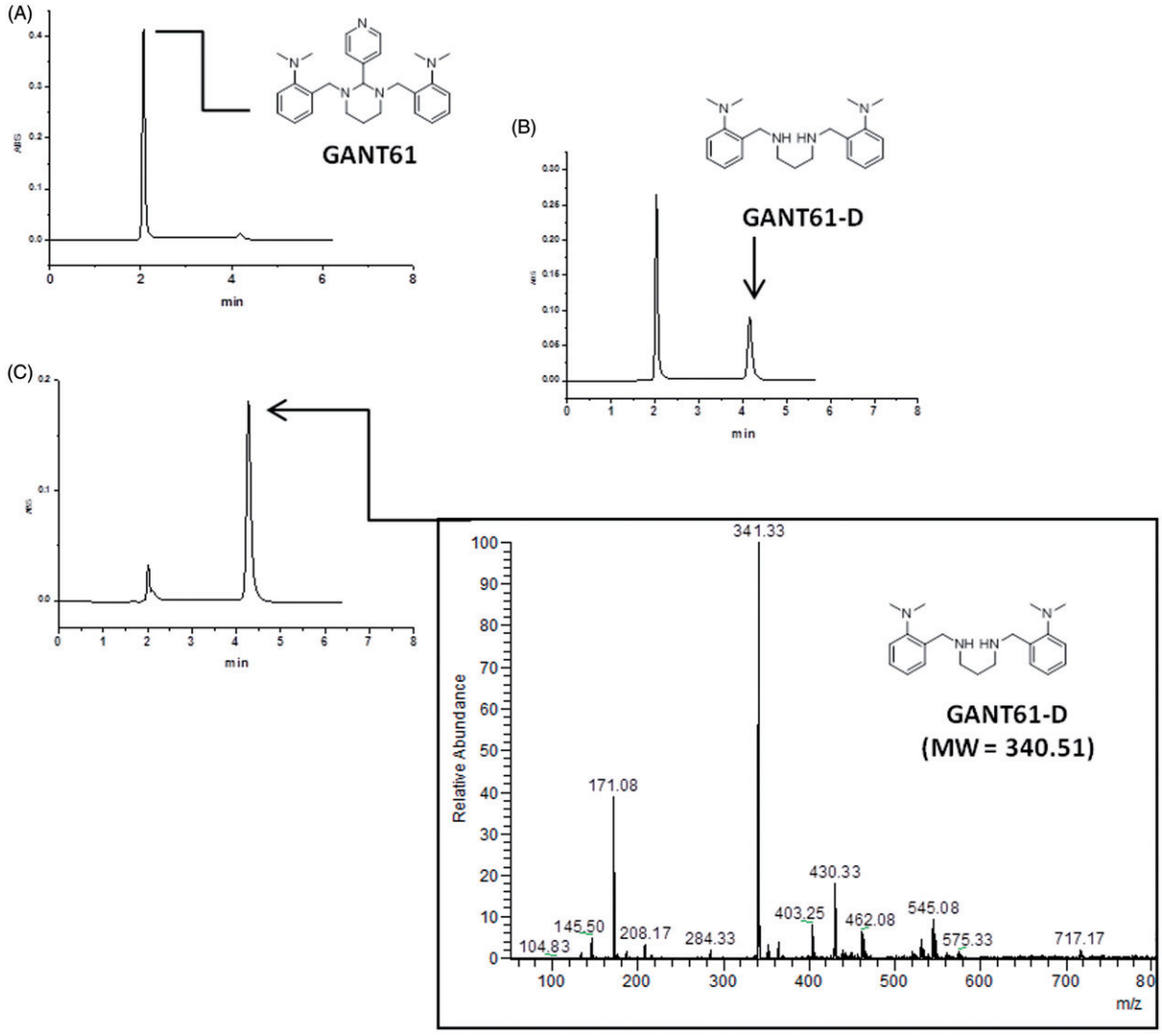

Figure 3. HPLC-UV chromatograms acquired during the time showing the disappearance of GANT61 and the formation of GANT61-D. Sample: GANT61 in CH_3CN/100 mM NH_4OAc (pH 4.5) = 95/5 (v/v) (1 mg/ml), column: Acclaim HILIC-10, 3 μm (150 × 4.6 mm I.D.), mobile phase: CH_3CN/100 mM NH_4OAc (pH 4.5) = 95/5 (v/v), flow-rate: 1.0 ml/min, detection: UV at 254 nm. (A) t = 0 min; (B) t = 30 min; (C) t = 24 h. The ESI-MS (pos.) spectrum of GANT61-D is included in the box for unequivocal identification.

the equilibrium and no further increase in the relative abundance of GANT61-D is observed up to 48 h incubation.

Chemical stability of GANT61 checked by HPLC

For the HPLC monitoring of the chemical stability of GANT61, we chose to resort to HILIC, which is nowadays accepted as a common separation mode[60–62], essentially dedicated to the separation of very polar compounds, such as carbohydrates, amino acids, oligonucleotides, and highly polar natural products. One of the major advantages of HILIC is the easy coupling with MS which extends its applicability to impurity detection[63]. In fact, the use of a low aqueous/high acetonitrile mobile phase significantly improves detection sensitivity for compounds analysed by liquid chromatography (LC)/ESI-MS, thus overcoming the mismatch between normal-phase LC and ESI-MS[64]. Also, ELSD has been widely used in the detection of chromophores-lacking compounds, and thus it proved to be particularly suitable to HILIC applications.

After an initial step of investigation for the most suitable chromatographic column operating in the HILIC mode, chromatographic studies were performed on the commercially available Acclaim HILIC-10, 3 μm (150 × 4.6 mm I.D.) column, which was operated under different combinations of aqueous/organic mobile phases. The best mobile phase, consisting of acetonitrile/ammonium acetate 100 mM (pH 4.5) = 95:5 (v/v), yielded the GANT61 peak at about 2 min of retention time (see Figure 3 and Supporting Information Figure S1 for HPLC-UV traces and Supporting Information Figure S2 for the corresponding ELSD chromatograms). When the sample was dissolved in pure acetonitrile (1 mg/ml), the GANT61 peak was the only peak detected for at least 1 h, but when we dissolved GANT61 in the mobile phase (at the same above-mentioned concentration), a new peak attributed to GANT61-D was immediately detected ($t = 0$ in Figure 4) with a retention time equal to 4.20 min. Such a peak proved to increase during the time, to become the main peak after 24 h (Figure 3(C)).

The identity of the two peaks was confirmed by flow injection analysis into an ESI-MS of the above-mentioned solutions (positive ions mode). In particular, the injection of the acetonitrile solution yielded a peak at $m/z = 430.33$ (monoisotopic mass), corresponding to the protonated form of GANT61 (MW = 429.61), i.e. $[M + H]^+$, while replicated analyses of the GANT61 solution in

mobile phase gave a signal at $m/z = 341.33$, which was attributed to the mono-protonated form of GANT61-D (MW = 340.51), i.e. $[M + H]^+$.

By plotting the HPLC-UV areas measured from the chromatograms acquired during the monitoring against the time (Figure 4) it was pointed out that the GANT61 molecule undergoes the same hydrolytic dissociation described above by NMR analysis, although at lower pH values and hence more rapidly. However, similar to the NMR study, about 90% of GANT61 is converted in GANT61-D after 24 h.

Taken together, NMR and HILIC experiments clearly suggest that GANT61 hydrolyses quickly into GANT61-D, this latter becoming the most abundant species – and hence the bioactive form of GANT61 – in physiological conditions and for incubation time equal or higher than 6 h. Notably, at 24 h, around 90% of GANT61 is converted in GANT61-D.

Molecular modelling

In order to check whether the bioactive form of GANT61, namely GANT61-D, could bind the Gli1ZF, we performed structure-based molecular modelling studies. It is worth mentioning that a similar computational study has been performed earlier by Agyeman et al.[38] by means of molecular docking simulations on the neutral form of GANT61-D. Different from this prior work, pK_a predictions clearly indicated that the secondary amino group of GANT61-D is protonated under physiological conditions, with a prevalence of the di-protonated form over the mono-protonated form of the molecule in the pH range 7–7.5[55]. Therefore, to explore the possible binding mode of GANT61-D to Gli1ZF in a physiological context and to compare our results with previous findings, we performed molecular docking of GANT61-D in its neutral, mono- and di-protonated forms by using the same computational settings described by Agyeman et al.[38] The lowest energy pose of the most populated cluster of each GANT61-D form was visually inspected and used for theoretical affinity studies (see below). Notably, the neutral form of GANT61-D was docked within the groove between ZF2 and ZF3 (Figure 5(A)) in H-bond contacts to Glu250 and Glu298, in excellent agreement with the results published previously (see also the Supporting Information Figure S3)[38]. For the sake of clarity, here we use the numbering scheme of the full-length Gli1 (Glu250 and Glu298 used in this work correspond to Glu119 and Glu167 of the X-ray structure, respectively)[40]. In contrast, protonated forms of GANT61-D were docked preferentially within ZF1 and ZF2 (Figure 5(A)) in a negatively charged surface region of Gli1ZF (Figure 5(B)). Accordingly, we hypothesised that the binding of GANT61-D to Gli1ZF in the most abundant protonation forms is mainly driven by electrostatic forces (detailed binding modes of GANT61-D are showed in Supporting Information Figure S3). Based on molecular docking, GANT61-D is not able to bind within the DNA-binding site of Gli1 that is located within ZF4 and ZF5 as highlighted by X-ray and computational studies (Figure 5(B))[40]. Therefore, it is unlikely that GANT61-D may directly interfere with Gli1 binding to DNA, as instead observed for the direct Gli1/DNA interaction inhibitor GlaB[8], although we cannot rule out indirect mechanisms leading to alteration in DNA interaction.

Finally, the theoretical affinity of the three protonation forms of GANT61-D towards Gli1ZF was predicted by means of the MM-GBSA method and the XSCORE function[53,54], upon energy minimisation of docking-based binding complexes in explicit water solvent. Results reported in Table 1 unequivocally show that the di-protonated form of GANT61-D holds the strongest affinity for Gli1ZF, whereas the neutral form was predicted to be the lowest

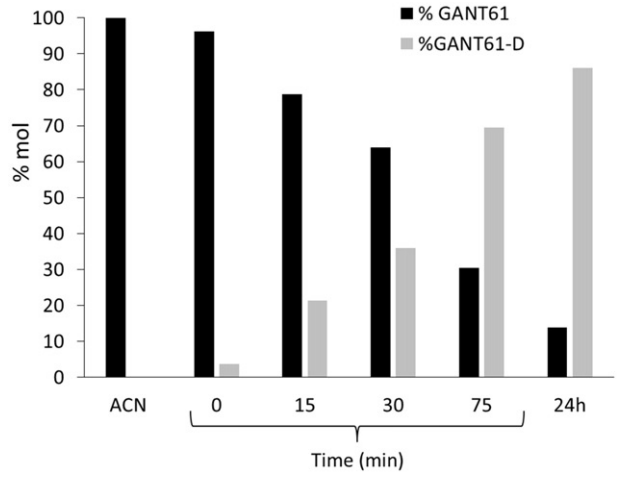

Figure 4. Chemical stability of GANT61 monitored by HPLC as a function of time. The acetonitrile (ACN) solution has been plotted on the left as a control.

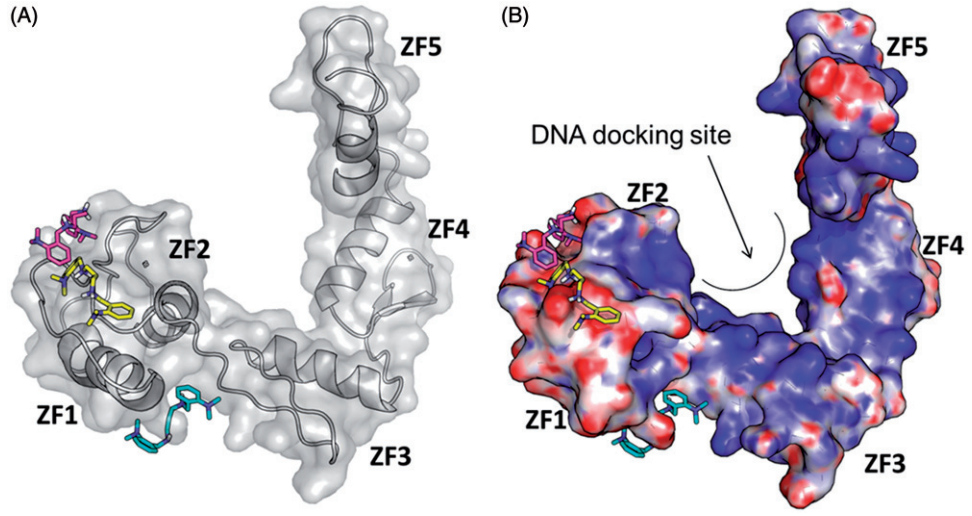

Figure 5. Predicted binding mode of GANT61-D in its three different protonation states: neutral (cyan sticks), mono-protonated (magenta sticks) and di-protonated (yellow sticks). The Gli1ZF crystallographic structure is showed as (A) cartoon and grey transparent surface and (B) surface coloured according to the electrostatic potential calculated by APBS. Red = negatively charged surface; blue = positively charged surface. The positively charged DNA docking site on Gli1ZF is highlighted.

affinity species. These results further support the hypothesis of an electrostatic-driven binding of GANT61-D to Gli1ZF that may target the surface region within ZF1 and ZF2 of Gli1ZF, as well as that GANT61-D binds with the highest affinity as protonated species compared to the neutral form. Finally, a good correlation between pK_d values predicted by XSCORE and experimental affinity measured previously was found[38].

Biological activity

To investigate whether GANT61-D carried the ability to inhibit the Hh signalling, we performed a luciferase functional assay and compared the Hh inhibitory activity of GANT61 with that exerted by GANT61-D. To this end, we treated NIH3T3 Shh-Light II cells, which stably incorporate a Gli-RE[65], with the synthetic Smo agonist SAG[66] alone or in combination with different concentrations of the tested compounds. As shown in Figure 6(A), GANT61-D antagonised the SAG-induced Hh pathway in a dose-dependent manner and with comparable efficacy as the parent GANT61. Next, we analysed the effect of GANT61-D in SuFu$^{-/-}$ MEFs, in which the constitutive activation of the pathway is a consequence of the deletion of the negative regulator *SuFu* gene. GANT61-D at 10 μM concentration significantly reduced the expression of Gli1, the final and most powerful effector of the Hh signalling (Figure 6(B)), already after 24 h, in agreement with the concept that the bioactive form of GANT61 to mediate Hh inhibition is its diamine derivative GANT61-D.

Discussion

The Hh signalling pathway is involved in many different types of cancer and its inhibition by small molecules is nowadays considered an effective anticancer strategy[4,6,65]. Although the initial enthusiasm for the approval by the FDA of two antagonists of the Smo receptor[25,26], drug-resistant Smo mutations and aberrant activation of Hh signalling downstream of Smo have been identified in clinical patients, which pointed to the serious need of alternative approaches[29–33]. Besides Smo, one of the most profitable Hh targets is Gli1, the final and most powerful effector of Hh signalling[6,8]. GANT61 has been identified as the first small molecule inhibitor of Gli1 and to date, it is used as a reference control in multiple studies focusing on Hh signalling transduction and modulation by small molecules[35]. The chemical instability of GANT61 was first highlighted in 2010 by Lauth et al.[36,37], and further addressed in 2014 by Agyeman et al.[38]. Besides these reports, here we aim to provide additional insights into the mechanism and kinetics of GANT61 hydrolysis and to complement the knowledge on the mechanism of actions of this reference Hh signalling inhibitor. To these aims, GANT61 and its diamine derivative GANT61-D were obtained by chemical synthesis, while the kinetics of GANT61 hydrolysis was monitored by high-resolution analytical tools such as NMR spectroscopy and HILIC. Results of our study show that GANT61 hydrolysed to the diamine GANT61-D and the aldehyde GANT61-A. This process is endowed with a rather fast kinetics, as a plateau is reached in 24 h when about 90% of GANT61 is converted in GANT61-D. These results unequivocally indicate that the bioactive form of GANT61 in cell-based experiments is the diamine derivative GANT61-D, particularly when incubation time is equal or higher than 6 h.

To corroborate this hypothesis, and to further support NMR and HILIC data, we performed molecular modelling and functional studies. Multiple protonation states of GANT61-D were considered in molecular docking simulations against Gli1ZF, including the neutral form that – although being endowed with a very low probability to exist in physiological conditions – has been the subject of a recent modelling study[38]. Results of the present computational analysis show that the protonated forms are most affine to Gli1ZF compared to the neutral form, and bind in a negatively charged region of the protein in correspondence of ZF1 and ZF2 thus suggesting that electrostatic forces may be crucial for intermolecular recognition and binding.

Finally, the Hh inhibitory properties of GANT61 and GANT61-D were evaluated in NIH3T3 Shh-Light II cells, which stably incorporate a Gli-RE, and in SuFu$^{-/-}$ MEFs, in which the pathway is constitutively active. In both assays, GANT61-D showed its ability to antagonise Hh signalling and to inhibit Gli1 expression with

Table 1. Theoretical affinity of GANT61-D to Gli1ZF.

Protonation form of GANT61-D	ΔG binding MM-GBSA (kcal/mol)	XSCORE (pK_d)
Neutral	−25.982 ± 0.008	4.50
Mono-protonated	−28.217 ± 0.006	4.60
Di-protonated	−31.972 ± 0.002	4.65

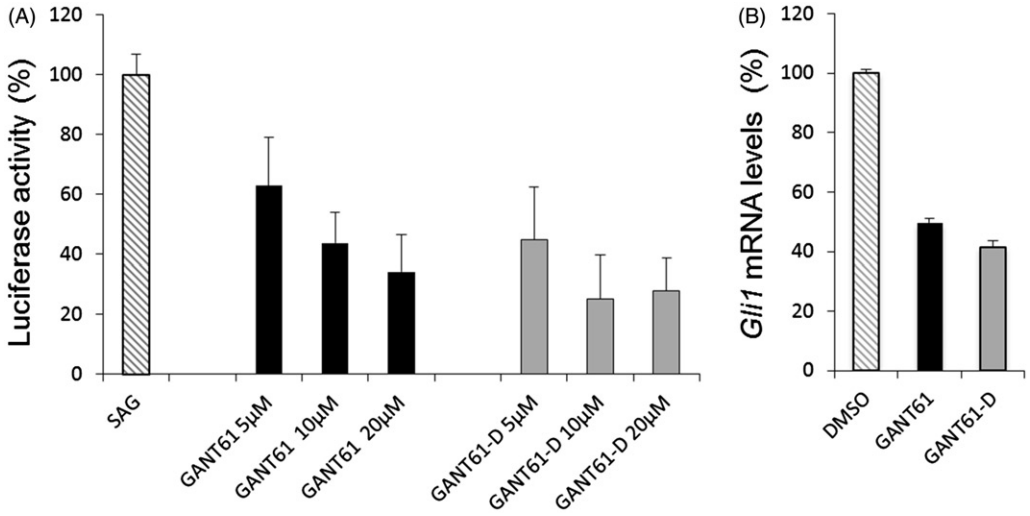

Figure 6. (A) Luciferase reporter assay in NIH3T3 Shh-Light II cells, which shows the dose-dependent inhibition of Hh signalling by GANT61 and GANT61-D after 48 h of treatment. (B) SuFu$^{-/-}$ MEFs were treated for 24 h with GANT61 or GANT61-D (10 μM) or DMSO as a control. *Gli1* mRNA levels were determined by qRT-PCR normalised to β2-microglobulin and *HPRT* expression.

comparable efficacy as GANT61. Our findings strongly support that GANT61-D is the bioactive form of GANT61 able to counteract the Hh signalling at downstream level, thus limiting the oncogenic potential of the pathway occurring in a context of Smo-independent or Gli1 hyperactivation by alternative mechanisms.

Conclusion

In this work, we shed light on the mechanism and kinetics of GANT61 hydrolysis, and further complement previous works in substantiating that GANT61-D is the bioactive form of GANT61 in Hh inhibition. Molecular modelling studies identified the main pharmacophores of GANT61-D that are relevant for the binding to Gli1ZF and suggested some strategies to generate optimised derivatives. For example, molecular rigidification and the design of GANT61-D analogues with constrained diamine linker may be undertaken to limit the conformational freedom of the molecule; phenyl rings may be decorated with functional groups that improve the interaction with Gli1ZF, or with chemical moieties that may ameliorate the pharmacokinetics profile of the lead; the aryl-dimethylamino group may be also replaced by different chemotypes, as it seems not particularly relevant for the interaction with Gli1ZF that we found to be driven mostly by electrostatic forces. Besides these suggestions, we hope that results of our integrated and multidisciplinary effort will inspire additional routes to design more potent and effective Hh inhibitors based on the scaffold of GANT61-D.

Disclosure statement

The authors report no conflicts of interest.

Funding

Authors gratefully acknowledge Professor Francesco Gasparrini from Sapienza University of Rome for his precious support with HILIC measurements. We thank the financial support from Associazione Italiana Ricerca Cancro (AIRC) Grant #IG14723 and #IG20801, PRIN 2012–2013 (2012C5YJSK002), Progetti di Ricerca di Università Sapienza di Roma, Pasteur Institute/Cenci Bolognetti Foundation. We would like to acknowledge networking contribution by the COST Action CM-1407 "Challenging organic syntheses inspired by nature – from natural products chemistry to drug discovery".

References

1. Masimirembwa CM, Bredberg U, Andersson TB. Metabolic stability for drug discovery and development: pharmacokinetic and biochemical challenges. Clin Pharmacokinet 2003;42:515–28.
2. Shu YZ, Johnson BM, Yang TJ. Role of biotransformation studies in minimizing metabolism-related liabilities in drug discovery. AAPS J 2008;10:178–92.
3. Varjosalo M, Taipale J. Hedgehog: functions and mechanisms. Genes Dev 2008;22:2454–72.
4. Ng JM, Curran T. The Hedgehog's tale: developing strategies for targeting cancer. Nat Rev Cancer 2011;11:493–501.
5. Iovine V, Mori M, Calcaterra A, et al. One hundred faces of cyclopamine. Curr Pharm Des 2016;22:1658–81.
6. Infante P, Alfonsi R, Botta B, et al. Targeting GLI factors to inhibit the Hedgehog pathway. Trends Pharmacol Sci 2015;36:547–58.
7. Infante P, Alfonsi R, Ingallina C, et al. Inhibition of Hedgehog-dependent tumors and cancer stem cells by a newly identified naturally occurring chemotype. Cell Death Dis 2016;7:e2376.
8. Infante P, Mori M, Alfonsi R, et al. Gli1/DNA interaction is a druggable target for Hedgehog-dependent tumors. EMBO J 2015;34:200–17.
9. Berman DM, Karhadkar SS, Hallahan AR, et al. Medulloblastoma growth inhibition by hedgehog pathway blockade. Science 2002;297:1559–61.
10. De Smaele E, Fragomeli C, Ferretti E, et al. An integrated approach identifies Nhlh1 and Insm1 as Sonic Hedgehog-regulated genes in developing cerebellum and medulloblastoma. Neoplasia 2008;10:89–98.
11. Di Magno L, Manzi D, D'Amico D, et al. Druggable glycolytic requirement for Hedgehog-dependent neuronal and medulloblastoma growth. Cell Cycle 2014;13:3404–13.
12. Ridzewski R, Rettberg D, Dittmann K, et al. Hedgehog inhibitors in rhabdomyosarcoma: a comparison of four compounds and responsiveness of four cell lines. Front Oncol 2015;5:130.
13. Oue T, Uehara S, Yamanaka H, et al. Hedgehog signal inhibitors suppress the invasion of human rhabdomyosarcoma cells. Pediatr Surg Int 2013;29:1153–8.
14. Feldmann G, Dhara S, Fendrich V, et al. Blockade of hedgehog signaling inhibits pancreatic cancer invasion and metastases: a new paradigm for combination therapy in solid cancers. Cancer Res 2007;67:2187–96.
15. Varnat F, Duquet A, Malerba M, et al. Human colon cancer epithelial cells harbour active HEDGEHOG-GLI signalling that is essential for tumour growth, recurrence, metastasis and stem cell survival and expansion. EMBO Mol Med 2009;1:338–51.
16. Karhadkar SS, Bova GS, Abdallah N, et al. Hedgehog signalling in prostate regeneration, neoplasia and metastasis. Nature 2004;431:707–12.
17. Watkins DN, Berman DM, Burkholder SG, et al. Hedgehog signalling within airway epithelial progenitors and in small-cell lung cancer. Nature 2003;422:313–17
18. Clement V, Sanchez P, de Tribolet N, et al. HEDGEHOG-GLI1 signaling regulates human glioma growth, cancer stem cell self-renewal, and tumorigenicity. Curr Biol 2007;17:165–172
19. Zhao C, Chen A, Jamieson CH, et al. Hedgehog signalling is essential for maintenance of cancer stem cells in myeloid leukaemia. Nature 2009;458:776–9.
20. Reya T, Morrison SJ, Clarke MF, Weissman IL. Stem cells, cancer, and cancer stem cells. Nature 2001;414:105–11.
21. Pardal R, Clarke MF, Morrison SJ. Applying the principles of stem-cell biology to cancer. Nat Rev Cancer 2003;3:895–902.
22. Coni S, Infante P, Gulino A. Control of stem cells and cancer stem cells by Hedgehog signaling: pharmacologic clues from pathway dissection. Biochem Pharmacol 2013;85:623–8.
23. Chen K, Huang YH, Chen JL. Understanding and targeting cancer stem cells: therapeutic implications and challenges. Acta Pharmacol Sin 2013;34:732–40.
24. Ismail F, Winkler DA. Getting to the source: selective drug targeting of cancer stem cells. ChemMedChem 2014;9:885–98.
25. Dlugosz A, Agrawal S, Kirkpatrick P. Vismodegib. Nat Rev Drug Discov 2012;11:437–8.
26. Mullard A. 2015 FDA drug approvals. Nat Rev Drug Discov 2016;15:73–6.
27. Ruat M, Hoch L, Faure H, Rognan D. Targeting of smoothened for therapeutic gain. Trends Pharmacol Sci 2014;35:237–46.

28. Rimkus TK, Carpenter RL, Qasem S, et al. Targeting the sonic hedgehog signaling pathway: review of smoothened and GLI inhibitors. Cancers (Basel) 2016;8:22.
29. Yauch RL, Dijkgraaf GJ, Alicke B, et al. Smoothened mutation confers resistance to a Hedgehog pathway inhibitor in medulloblastoma. Science 2009;326:572–4.
30. Atwood SX, Sarin KY, Whitson RJ, et al. Smoothened variants explain the majority of drug resistance in basal cell carcinoma. Cancer Cell 2015;27:342–53.
31. Sharpe HJ, Pau G, Dijkgraaf GJ, et al. Genomic analysis of smoothened inhibitor resistance in basal cell carcinoma. Cancer Cell 2015;27:327.
32. Buonamici S, Williams J, Morrissey M, et al. Interfering with resistance to smoothened antagonists by inhibition of the PI3K pathway in medulloblastoma. Sci Transl Med 2010;2:51ra70.
33. Metcalfe C, de Sauvage FJ. Hedgehog fights back: mechanisms of acquired resistance against smoothened antagonists. Cancer Res 2011;71:5057–61.
34. Gonnissen A, Isebaert S, Haustermans K. Targeting the Hedgehog signaling pathway in cancer: beyond smoothened. Oncotarget 2015;6:13899–913.
35. Lauth M, Bergström A, Shimokawa T, Toftgård R. Inhibition of GLI-mediated transcription and tumor cell growth by small-molecule antagonists. Proc Natl Acad Sci USA 2007;104:8455–60.
36. Lauth M, Rohnalter V, Bergstrom A, et al. Correction to "Antipsychotic drugs regulate hedgehog signaling by modulation of 7-dehydrocholesterol reductase levels". Mol Pharmacol 2011;79:793.
37. Lauth M, Rohnalter V, Bergström A, et al. Antipsychotic drugs regulate hedgehog signaling by modulation of 7-dehydrocholesterol reductase levels. Mol Pharmacol 2010;78:486–96.
38. Agyeman A, Jha BK, Mazumdar T, Houghton JA. Mode and specificity of binding of the small molecule GANT61 to GLI determines inhibition of GLI-DNA binding. Oncotarget 2014;5:4492–503.
39. Glasoe PK, Long FA. Use of glass electrodes to measure acidities in deuterium oxide. J Phys Chem 1960;64:188–90.
40. Pavletich NP, Pabo CO. Crystal structure of a five-finger GLI-DNA complex: new perspectives on zinc fingers. Science 1993;261:1701–7.
41. Morris GM, Huey R, Lindstrom W, et al. AutoDock4 and AutoDockTools4: automated docking with selective receptor flexibility. J Comput Chem 2009;30:2785–91.
42. Cirigliano A, Menta S, Mori M, et al. *S. cerevisiae* as a tool to select inhibitors of the deneddylating activity of the COP9 signalosome. Yeast 2015;32:S175
43. Mori M, Dietrich U, Manetti F, Botta M. Molecular dynamics and DFT study on HIV-1 nucleocapsid protein-7 in complex with viral genome. J Chem Inf Model 2010;50:638–50.
44. Mori M, Massaro A, Calderone V, et al. Discovery of a new class of potent MMP inhibitors by structure-based optimization of the arylsulfonamide scaffold. ACS Med Chem Lett 2013;4:565–9.
45. Mori M, Moraca F, Deodato D, et al. Discovery of the first potent and selective *Mycobacterium tuberculosis* Zmp1 inhibitor. Bioorg Med Chem Lett 2014;24:2508–11.
46. Baker NA, Sept D, Joseph S, et al. Electrostatics of nanosystems: application to microtubules and the ribosome. Proc Natl Acad Sci USA 2001;98:10037–41.
47. Case DA, Darden TA, Cheatham TE, et al. AMBER 12. San Francisco, CA: University of California; 2012.
48. Cau Y, Fiorillo A, Mori M, et al. Molecular dynamics simulations and structural analysis of Giardia duodenalis 14-3-3 protein-protein interactions. J Chem Inf Model 2015;55:2611–22.
49. Cau Y, Mori M, Supuran CT, Botta M. Mycobacterial carbonic anhydrase inhibition with phenolic acids and esters: kinetic and computational investigations. Org Biomol Chem 2016;14:8322–30.
50. Mori M, Nucci A, Lang MC, et al. Functional and structural characterization of 2-amino-4-phenylthiazole inhibitors of the HIV-1 nucleocapsid protein with antiviral activity. ACS Chem Biol 2014;9:1950–5.
51. Sholokh M, Improta R, Mori M, et al. Tautomers of a fluorescent G surrogate and their distinct photophysics provide additional information channels. Angew Chem Int Ed Engl 2016;55:7974–8.
52. Mori M, Manetti F, Botta M. Predicting the binding mode of known NCp7 inhibitors to facilitate the design of novel modulators. J Chem Inf Model 2011;51:446–54.
53. Miller BR 3rd, McGee TD Jr, Swails JM, et al. MMPBSA.py: an efficient program for end-state free energy calculations. J Chem Theory Comput 2012;8:3314–21.
54. Wang R, Lai L, Wang S. Further development and validation of empirical scoring functions for structure-based binding affinity prediction. J Comput-Aided Mol Des 2002;16:11–26.
55. Milletti F, Storchi L, Sforna G, Cruciani G. New and original pKa prediction method using grid molecular interaction fields. J Chem Inf Model 2007;47:2172–81.
56. Chenna V, Hu C, Khan SR. Synthesis and cytotoxicity studies of Hedgehog enzyme inhibitors SANT-1 and GANT-61 as anticancer agents. J Environ Sci Health A Tox Hazard Subst Environ Eng 2014;49:641–7.
57. Valensin D, Cau Y, Calandro P, et al. Molecular insights to the bioactive form of BV02, a reference inhibitor of 14-3-3sigma protein-protein interactions. Bioorg Med Chem Lett 2016;26:894–8.
58. Mitra A, Seaton PJ, Ali Assarpour R, Williamson T. Unprecedented concentration dependent chemical shift variation in 1H-NMR studies: a caveat in the investigations of molecular recognition and structure elucidation. Tetrahedron 1998;54:15489–98.
59. D'Acquarica I, Calcaterra A, Sacco F, et al. Stereochemical preference of 2′-deoxycytidine for chiral bis(diamido)-bridged basket resorcin[4]arenes. Chirality 2013;25:840–51.
60. Alpert AJ. Hydrophilic-interaction chromatography for the separation of peptides, nucleic acids and other polar compounds. J Chromatogr 1990;499:177–96.
61. Hemstrom P, Irgum K. Hydrophilic interaction chromatography. J Sep Sci 2006;29:1784–821.
62. Nguyen HP, Schug KA. The advantages of ESI-MS detection in conjunction with HILIC mode separations: fundamentals and applications. J Sep Sci 2008;31:1465–80.
63. Dejaegher B, Vander Heyden Y. HILIC methods in pharmaceutical analysis. J Sep Sci 2010;33:698–715.
64. Lammerhofer M. HILIC and mixed-mode chromatography: the rising stars in separation science. J Sep Sci 2010;33:679–80.
65. Taipale J, Chen JK, Cooper MK, et al. Effects of oncogenic mutations in Smoothened and Patched can be reversed by cyclopamine. Nature 2000;406:1005–9.
66. Chen JK, Taipale J, Cooper MK, Beachy PA. Inhibition of Hedgehog signaling by direct binding of cyclopamine to smoothened. Genes Dev 2002;16:2743–8.

3.2.2 | *A Smo/Gli Multitarget Hedgehog Pathway Inhibitor Impairs Tumor Growth*

Starting from a previous project developed by our team which identified the isoflavone GlaB as a potent and direct inhibitor of GLI1/DNA interaction, with strong anticancer efficacy against the Hh-dependent tumorigenesis of BCC and MB (Infante et al., 2015b), we recently exploited the high versatility of the isoflavone scaffold for targeting the Hh signalling pathway at multiple levels (Berardozzi et al., 2018). In particular, we designed and synthesized isoflavones bearing bulky chemical groups in the *para* position of ring B, with the aim to enhance the targeting at the level of the SMO receptor. Similarly, the introduction of bulky substitutions in the *meta* position of the same ring promoted the targeting of the downstream GLI effectors.

Notably, the simultaneous administration of newly designed isoflavones targeting SMO and GLI1 provided synergistic Hh pathway inhibition, which might become relevant to increase the barrier to drug resistance, particularly at the level of SMO (Berardozzi et al., 2018). The aim of my project was the synthesis of the first multitarget Hh pathway inhibitor (Compound 22, c22) which combines the most promising pharmacophores targeting SMO and GLI1 in a single and individual isoflavone.

Compound 22 is able to inhibit Hh-dependent tumor growth in human and murine MB cells at sub-micromolar concentration as a consequence of the reduction in *Gli1* expression levels. Despite the limitations of intratumoral administration (i.e., the invasive nature of the injection itself, the rapid clearance of drugs directly applied to the tumor and the development of dose-limiting toxicities in the area surrounding the site of injection), c22 remarkably shows a strong anti-tumor effect also *in vivo* by suppressing cell proliferation and promoting apoptosis. Molecular modeling further corroborates the multitarget mechanism of action of c22, showing that the molecule is able to fit the ligand-binding site in both SMO and GLI1.

Overall, these results reveal a valuable form of targeted therapy to increase the efficacy and to decrease the toxicity of individual anticancer agents. Our findings discover the

first multitarget Hh inhibitor that impinges Hh-dependent tumor growth and stands as new potential weapons against Hh-driven cancer, like MB.

Since this work has been published, I only provided a brief outline of obtained results. Please refer to the paper attached below[4] for more detailed evaluation.

[4]**Lospinoso Severini, L**.*, Quaglio, D.*, Basili, I., Ghirga, F., Bufalieri, F., Caimano, M., ... & Maroder, M. (**2019**). A Smo/Gli Multitarget Hedgehog Pathway Inhibitor Impairs Tumor Growth. ***Cancers***, *11*(10), 1518.

cancers

MDPI

Article

A Smo/Gli Multitarget Hedgehog Pathway Inhibitor Impairs Tumor Growth

Ludovica Lospinoso Severini [1,†], Deborah Quaglio [2,†], Irene Basili [1], Francesca Ghirga [3], Francesca Bufalieri [1], Miriam Caimano [1], Silvia Balducci [2], Marta Moretti [4], Isabella Romeo [2], Elena Loricchio [1], Marella Maroder [1], Bruno Botta [2], Mattia Mori [5,*,†], Paola Infante [3,*,†] and Lucia Di Marcotullio [1,6,*,†]

[1] Department of Molecular Medicine, Sapienza University, Viale Regina Elena 291, 00161 Rome, Italy; ludovica.lospinososeverini@uniroma1.it (L.L.S.); irenebasili.ib@gmail.com (I.B.); francesca.bufalieri@uniroma1.it (F.B.); miriam.caimano@uniroma1.it (M.C.); elena.loricchio@uniroma1.it (E.L.); marella.maroder@uniroma1.it (M.M.)

[2] Department of Chemistry and Technology of Drugs, Sapienza University, Piazzale A. Moro 5, 00161 Rome, Italy; deborah.quaglio@uniroma1.it (D.Q.); silvia.balducci@uniroma1.it (S.B.); isabella.romeo1988@gmail.com (I.R.); bruno.botta@uniroma1.it (B.B.)

[3] CLNS@Sapienza, Istituto Italiano di Tecnologia, Viale Regina Elena 291, 00161 Rome, Italy; francesca.ghirga@iit.it

[4] Department of Experimental Medicine, Sapienza University, Viale Regina Elena 324, 00161 Rome, Italy; marta.moretti@uniroma1.it

[5] Department of Biotechnology, Chemistry and Pharmacy, University of Siena, via Aldo Moro 2, 53100 Siena, Italy

[6] Laboratory Affiliated to Istituto Pasteur Italia-Fondazione Cenci Bolognetti—Department of Molecular Medicine, Sapienza University, Viale Regina Elena 291, 00161 Rome, Italy

* Correspondence: mattia.mori@unisi.it (M.M.); paola.infante@iit.it (P.I.); lucia.dimarcotullio@uniroma1.it (L.D.M.); Tel.: +39-06-49255132 (P.I.); +39-06-49255657 (L.D.M.); Fax: +39-06-49255660 (L.D.M.)

† These authors equally contributed to the work.

Received: 11 July 2019; Accepted: 2 October 2019; Published: 9 October 2019

Abstract: Pharmacological Hedgehog (Hh) pathway inhibition has emerged as a valuable anticancer strategy. A number of small molecules able to block the pathway at the upstream receptor Smoothened (Smo) or the downstream effector glioma-associated oncogene 1 (Gli1) has been designed and developed. In a recent study, we exploited the high versatility of the natural isoflavone scaffold for targeting the Hh signaling pathway at multiple levels showing that the simultaneous targeting of Smo and Gli1 provided synergistic Hh pathway inhibition stronger than single administration. This approach seems to effectively overcome the drug resistance, particularly at the level of Smo. Here, we combined the pharmacophores targeting Smo and Gli1 into a single and individual isoflavone, compound **22**, which inhibits the Hh pathway at both upstream and downstream level. We demonstrate that this multitarget agent suppresses medulloblastoma growth in vitro and in vivo through antagonism of Smo and Gli1, which is a novel mechanism of action in Hh inhibition.

Keywords: Hedgehog; cancer; multitarget; Smo; Gli1

1. Introduction

Hedgehog (Hh) signaling is a developmental pathway involved in tissue homeostasis, cell stemness and tumorigenesis [1–4]. The Hh pathway activity is controlled by Hh ligands and the transmembrane receptors, Patched1 (Ptch1) and Smoothened (Smo), that are endowed with inhibitory and activator function, respectively. In the absence of Hh ligand, Ptch1 represses Smo keeping the pathway off. In the presence of ligand, Ptch1 relieves Smo-derived signals that activate Gli transcription factors, thus, promoting proliferation, survival and cell migration. Aberrant activation of the Hh pathway has been found in a wide spectrum of tumors, such as basal cell carcinoma (BCC) and medulloblastoma (MB) [5], and its deregulation can alter cancer stem cells features (i.e., self-renewal, survival, neoangiogenesis, metastatic spread) [6–9]. For this reason, Hh pathway represents an attractive target for anticancer therapy nowadays [10–12].

Many Hh-dependent human cancers are driven by an inappropriate upstream pathway activation (i.e., loss-of-function mutations of Ptch1 receptor, gain-of-function mutations involving Smo receptor, Hh ligand overproduction) [13,14]; that is why most of the Hh inhibitors developed to date act at an upstream level on the Smo receptor [15,16]. Unfortunately, these agents have shown many limits [17,18], such as low pharmacokinetic properties and severe side effects, including nausea, diarrhea, muscle cramping dysgeusia, fatigue, alopecia, hyponatremia, weight loss [19–21]. Vismodegib (Erivedge®, Genentech) and Sonidegib (Odomzo®, Novartis) are two Smo-antagonists approved by the Food and Drug Administration (FDA) for the treatment of metastatic and/or locally advanced BCC [22]. Despite some promising clinical response, treatments with Vismodegib or Sonidegib have resulted in aggressive tumor relapse, due to the development of resistant tumor clones [14,21,23,24].

Vismodegib resistance is prevalently associated with Smo mutation and to a lesser extent with alterations of downstream Hh pathway components (SuFu and Gli2) or induction of alternative signaling pathways leading to Gli1 activation, such as phosphatidylinositol 3-kinase (PI3K) and atypical protein kinase C ι/λ (aPKC-ι/λ) [24].

It is known that the Hh pathway can also be activated by Smo-independent mechanisms (i.e., gene amplification of Gli factors, mutation of the tumor suppressor SuFu, post-synthetic modifications like decreased ubiquitination-mediated degradation or acetylation of the Gli proteins or increased PI3K/mTOR/S6K1 kinase-dependent phosphorylation) [25–33] that lead to an increased activity of downstream Gli effectors. All mechanisms that act downstream of Smo are alternative causes of drug-resistance to the treatment of Hh-driven cancers [34,35].

One of the most relevant Hh-dependent tumors is MB, a highly aggressive and heterogeneous pediatric brain tumor with a poor clinical outcome [36]. MB has been classified in four major molecular subgroups (WNT, SHH, Group 3 and Group 4), each one presenting distinct genetic alterations, gene expression landscape and prognosis. Current treatments of MB consist of maximal surgical removal of tumor followed by radio- and chemo-therapy that have long-term toxicity effects, including delays in physical and cognitive development, a high frequency of relapse and increased cardiac risk of diseases [37–39].

These issues raise the need to develop new therapeutic strategies, especially focusing on the targeting of Hh-signaling. Indeed, the SHH-MB subgroup comprises 25–30% of all MB cases and is the best genetically characterized. The use of the Smo-antagonist Vismodegib to treat metastatic MB caused tumor relapse in one patient within three months, due to D473H point mutation that rendered Smo insensitive to the drug [14,19]. Although two phase II studies suggest the efficacy of Vismodegib in recurrent MB [40], the most effective strategy to overcome the drug-resistance appears the development of new Hh-inhibitors that counteract this pathway downstream of Smo or independently by Smo, as well as to combine different drugs, in a multitargeting approachable to inhibit Hh-signaling at multiple levels.

In this scenario, particular interest has emerged for the development of small molecules as inhibitors of Gli1 transcription factor, the final and most powerful positive effector of Hh signaling [41]. We have identified and characterized the isoflavone Glabrescione B (GlaB) as a potent and direct inhibitor of Gli1/DNA interaction, with strong anticancer efficacy against the Hh-dependent

tumorigenesis of BCC and MB [42]. Recently, we exploited the high versatility of the isoflavone scaffold for targeting the Hh signaling pathway at multiple levels [43]. In particular, we designed and synthesized isoflavones bearing bulky chemical groups in the *para* position of ring B, with the aim to enhance the targeting at the level of the Smo receptor. Similarly, the introduction of bulky substitutions in the *meta* position of the same ring promoted the targeting of the downstream Gli effectors. Notably, the simultaneous administration of newly designed isoflavones targeting Smo and Gli1 provided synergistic Hh pathway inhibition, which might become relevant to increase the barrier to drug resistance, particularly at the level of Smo [43]. In this work, we have designed multitarget Hh pathway inhibitors through the combination of the most promising pharmacophores targeting Smo and Gli1 in a single and individual isoflavone. Organic synthesis and in vitro testing led to the identification of compound **22** as the most efficient multitarget Hh inhibitor that antagonizes both Smo and Gli1. This molecule showed strong inhibitory properties on Hh signaling as tested in functional and biological in vitro assays and in an in vivo model of Hh-dependent MB, thus, becoming the first small molecule able to target Hh signaling at multiple levels.

2. Results

2.1. Design, Synthesis and Functional Screening of Hh Inhibition by Isoflavones **20**, **21** *and* **22**

In a previous study, we demonstrated that the introduction of a bulky substituent in *meta* or in the *para* position of the isoflavone's ring B enhanced the specific affinity of these compounds for Gli or Smo, respectively, and that their simultaneous administration provided synergistic Hh pathway inhibition [43]. In order to develop a multitarget Hh inhibitor, we selected the most promising GlaB-ring B derivatives [43] as specific Smo and Gli pharmacophores and combined them in a single and individual isoflavone, compound **20** (Figure 1). The ability of this newly synthesized isoflavone to inhibit Hh signaling was investigated by a luciferase reporter assay in which NIH3T3 Shh-Light II cells, stably incorporating a Gli-responsive firefly luciferase reporter (Gli-RE) and the pRL-TK Renilla as normalization control, were activated following the treatment with the synthetic Smo agonist SAG alone or in combination with compound **20**. However, **20** was inactive to suppress Hh signaling (Figure S1), probably due to the physicochemical features of the trifluoromethyl group. Based on these findings, we designed and synthetized two bioisosters featuring methyl (**21**) and chlororine (**22**) groups, respectively (Figure 1). For the synthesis of compounds **20–22** (Figure S2), we performed the deoxybenzoin approach, a mild and cost-effective method that allows the preparation of isoflavones [43]. Compounds **21** and **22** were tested for their inhibitory properties on Hh signaling by functional luciferase assay in NIH3T3 Shh-Light II cells as described above. Notably, **21** and **22** showed strong Hh pathway inhibition, with **22** being the most potent Hh inhibitor of this series with an IC_{50} of 0.79 μM (Figure 2A,B).

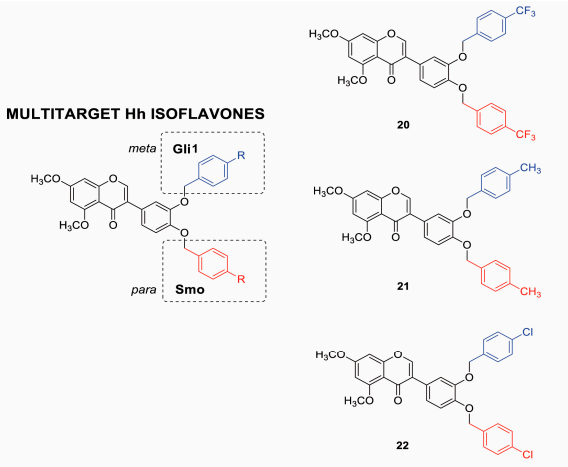

Figure 1. Chemical structure of isoflavones **20–22**. GlaB-ring B derivatives were designed as multitarget Hh inhibitors and synthesized via deoxybenzoin route. O-substitution at *meta* position of ring B (blue) is preferred to interact with Gli, whereas, O-substitution at *para* position (red) is preferred for the interaction with Smo.

Afterwards, to prove the inhibitory activity of the two newly synthesized isoflavones **21** and **22** on Hh signaling at the downstream level, we verified their effects on Gli1 transcription activity in a Smo-independent condition. To this aim, we treated mouse embryonic fibroblasts (MEFs) transiently expressing ectopic Gli1 and a Gli-dependent luciferase reporter, with increasing amounts of the two compounds. Both molecules impinge Gli1 function directly, but not Gli1 exogenous protein levels, with **22** demonstrating a stronger effect (IC_{50} of 7.00 μM) (Figure 2C,D and Figure S3). These results clearly suggest that physicochemical features of substituents to isoflavone's ring B might play a key role in binding to Smo, as well as to Gli1.

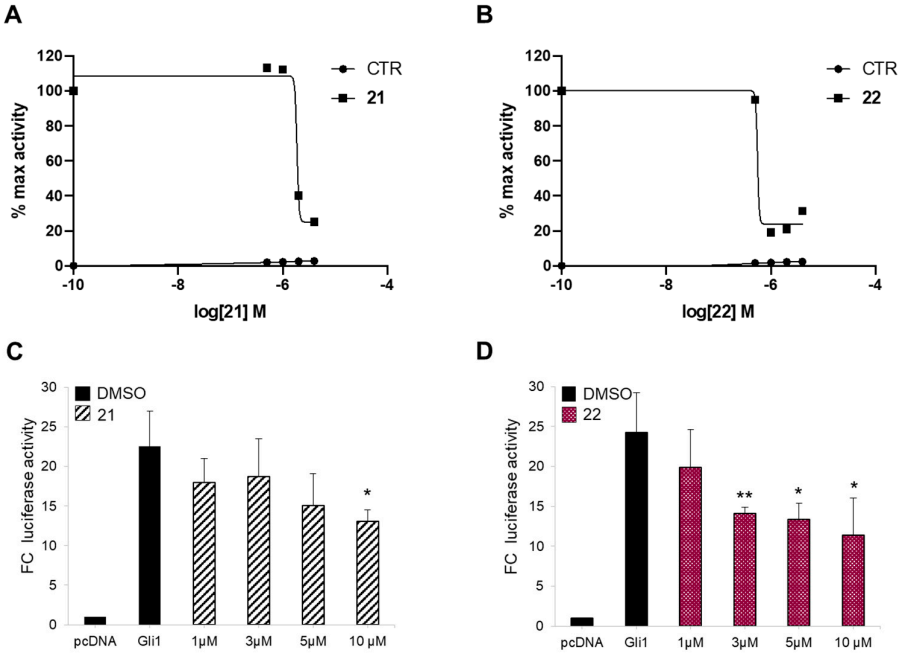

Figure 2. Hh inhibition by compounds **21** and **22**. The dose-response curve in SAG-treated NIH3T3 Shh-Light II cells (**A**,**B**) or mouse embryonic fibroblasts (MEFs) transfected with 12XGliBS-Luc and pRL-TK Renilla (normalization control) plus control (empty) or Gli1 vector (**C**,**D**). Cells were treated with increasing concentrations of compounds **21** (**A**,**C**) and **22** (**B**,**D**). Treatment time was 48 h and 24 h for NIH3T3 Shh-Light II cells and transfected MEFs, respectively. Data were normalized against Renilla luciferase. Data show the mean ± SD of three independent experiments. (*) $p < 0.05$ vs. SAG or Dimethyl sulfoxide (DMSO); (**) $p < 0.01$ vs. SAG or DMSO.

2.2. *Inhibitory Effect of Compounds* **21** *and* **22** *on Hh-Active Cell Models*

In order to demonstrate the capability of compounds **21** and **22** to target Hh signaling both at upstream and downstream level by acting on Smo and Gli respectively, we used Hh-active cell models, in which the loss of the main regulators of Hh signaling determines the constitutive activation of this pathway. At first, we treated with compounds **21** and **22** Ptch1$^{-/-}$ mouse embryonic fibroblasts (Ptch1$^{-/-}$ MEFs), in which the loss of repressive receptor *Ptch1* gene constitutively induces the activation of Hh signaling, thus, determining high expression levels of Hh target genes, including *Gli1*. The treatment with compound **22** at 1 and 2 μM for 48 h reduced the mRNA levels of *Gli1* in this cell model stronger than compound **21** used at the same concentrations (Figure 3A). Next, to verify the ability of the two isoflavones to inhibit Hh signaling independently of Smo, we tested their activity in mouse embryonic fibroblasts lacking the receptor Smoothened (Smo$^{-/-}$ MEFs).

Also in this cellular context, compounds **21** and **22**, as well as GANT61 and ATO (two well-known Gli1 inhibitors), but not the Smo antagonist Vismodegib, were able to reduce the mRNA expression levels of *Gli1*, with an increased effect of **22** compared to **21** (Figure 3B, Figure S4 and Table S1). To confirm the inhibitory properties of the two compounds on Hh signaling at Smo downstream level, we tested compounds **21** and **22** in SuFu$^{-/-}$ MEFs, in which the loss of the Gli negative regulator *SuFu* leads to the constitutive activation of the pathway. The endogenous expression of *Gli1* was significantly reduced in these cells after treatment with the two compounds showing, also in this case, a stronger efficacy of compound **22** (Figure 3C). These data sustain the ability of the two isoflavones to inhibit the Hh signaling both at upstream and downstream levels and identify compound **22** as the most effective Hh-inhibitor among the ones we have tested. Moreover, compound **22** did not affect WNT or Jun/AP-1 activity supporting its specificity of action for Hh/Gli signaling (Figure S5).

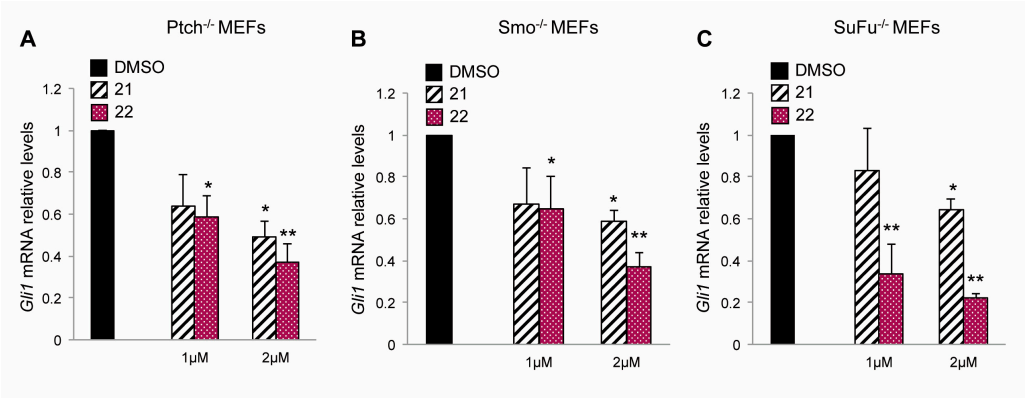

Figure 3. Inhibitory effect of compounds **21** and **22** on Hh-active cell models. The graphs show mRNA expression levels of *Gli1* in Ptch1$^{-/-}$ (**A**), Smo $^{-/-}$ (**B**) and SuFu$^{-/-}$ (**C**) MEFs treated for 48 h with DMSO as a control, or compounds **21** or **22** at 1 or 2 μM concentrations. *Gli1* mRNA levels were normalized to endogenous controls *β2-microglobulin* and *Hprt*. Data show the mean ± SD of three independent experiments. (*) $p < 0.05$ vs. DMSO; (**) $p < 0.01$ vs. DMSO.

2.3. Molecular Modeling Study on the Interaction between Compound **22** *and Smo and Gli1*

To further support the ability of compound **22** to interact with the respective targets Smo and Gli1, we performed molecular modeling simulations by using the computational protocols already described previously [42–44]. Results clearly show that compound **22** is able to fit the well-known antagonists' site located within the heptahelical bundle of Smo, as well as the isoflavones' binding site located within zinc-finger 4 and zinc-finger 5 of Gli1. In detail, docking of compound **22** to Smo by FRED docking program (OpenEye) highlighted a number of H-bond interactions between the molecule and Smo key residues, such as Asn219, Gln477, and Arg400 (Figure 4A). The aromatic core of the isoflavone's ring B of 22 is π-π stacked to the side chain of Tyr394, while the *p*-chlorophenyl ring substituted in position -*para* of the isoflavone's ring B is π-π stacked to His470 in a T-shaped configuration (Figure 4A). It is worth noting that this interaction is similar to the predicted binding mode of other isoflavones within the Smo antagonists' site [43]. Molecular docking of compound **22** to Gli1 zinc finger was carried out by the GOLD docking program, showing that the compound is able to establish a H-bond interaction with Lys350, which has been already highlighted in a previous mutagenesis study [42], as well as with the well-known Thr374 from the nuclear localization signal [45] (Figure 4B). Additional H-bonds are established by compound **22** with Thr355 and the Zn-binding His351 (Figure 4B). Further, the binding mode of this molecule is highly comparable to that of other isoflavones [42,43].

To verify the direct action of compound **22** on Smo receptor we performed a Bodipy-Cyclopamine (BC) displacement assay using a fluorescent derivate of Cyclopamine that interacts with Smo at the level of its heptahelical bundle [46]. To this end, HEK293T cells were transfected

with a vector expressing Smo WT or Smo D473H mutant, which confers resistance following Vismodegib treatment, and incubated with BC at increasing concentrations of compound **22**. As shown in Figure 4C, compound **22** displayed similar dose-dependent effects on both WT and D473H Smo, indicating its direct binding within the Cyclopamine site of Smo and suggesting its potential use for the treatment of Vismodegib-resistant tumors.

To further confirm molecular modeling results on compound **22** to Gli1 zinc finger domain, we verified the effect on Gli1 mutated in Lys340 (K340A), a residue involved in DNA binding and transcriptional function of Gli1 [41,42]. As expected, different doses of compound **22** induced a moderated reduction of Gli1-dependent transcriptional activation in MEFs WT expressing ectopic Gli1 K340A and Gli1-dependent luciferase reporter compared to cells expressing Gli1 WT (Figure 4D). Of note, by ChIP assay in Gli1-overexpressing MEFs, we observed a significant reduction of the Gli1 recruitment into the *Ptch1* promoter following the treatment with compound **22** compared to control (Figure 4E). According to the high homology degree between the zinc finger domain of Gli1 and Gli2, compound **22** also inhibits Gli2-mediated transcription (Figure S6).

In summary, molecular modeling and biological assays further substantiate the multitarget effect of compound **22** by showing that the small molecule is able to fit the ligand-binding site in Smo and Gli1, and to interact with residues that are crucial for Hh signaling transduction, without affecting ciliogenesis processes or Gli1 subcellular localization (Figure S7A–D, respectively).

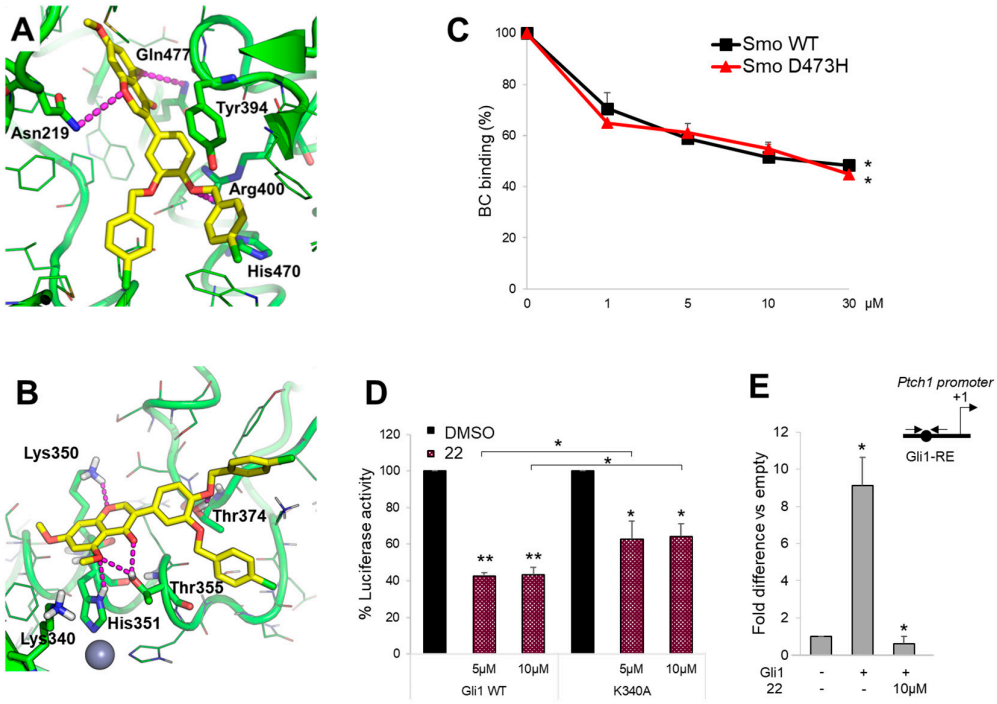

Figure 4. Compound **22** directly binds Smo and Gli1. (**A**,**B**) Predicted binding mode of compound **22** to Smo and Gli1. The small molecule is shown as yellow sticks, the proteins as a green cartoon; residues within 5 Å from the ligand are shown as lines. Residues contacted by compound **22** are shown as sticks and are labeled. Lys340 is shown as sticks as well. H-bond interactions are highlighted by magenta dashed lines. (**C**) The concentration-response curves show the percentage of BC binding to WT or D473H Smo mutant after compound **22** treatment. (*) $p < 0.05$ vs. CTR. (**D**) MEFs WT were transfected with 12XGliBS-Luc and pRL-TK Renilla (as normalization control) plus empty vector or WT or K340A Gli1 mutant; 24 h after transfection cells were treated with DMSO only or increasing concentrations of compound **22**. Luciferase activity was analyzed 24 h after treatment. (*) $p < 0.05$ vs. DMSO, (**) $p < 0.01$ vs. DMSO; (*) $p < 0.05$ K340A vs. WT Gli1. (**E**) MEFs WT were transfected with Flag-tagged Gli1 or empty vector and then treated with compound **22** at 10 μM. Chromatin immunoprecipitation (ChIP) and qRT–PCR using primers surrounding the Gli1-

binding site (BS) of mouse *Ptch1* promoter (schematic representation on the right) were performed. Results are indicated as fold difference to empty control. All data show the mean ± S.D. of three independent experiments. (*) $p < 0.05$ vs. empty control.

2.4. Compound **22** Inhibits the Hh-Dependent Tumor Growth In Vitro

The aberrant activation of Hh signaling is strongly involved in the onset of several tumors, such as medulloblastoma (MB). In order to test the efficacy of isoflavone **22** to suppress the Hh-dependent tumor growth, we used primary MB cells freshly isolated from Math1-cre/Ptch$^{C/C}$ mice that spontaneously developed MB and tested in short-term cultures to keep Hh sensitivity in vitro. As shown in Figure 5A, compound **22** used at final concentrations of 0.5, 1 and 5 μM, significantly inhibits the proliferation of primary MB cells in a dose- and time-dependent manner. This was consistent with increased cell death (Figure 5B). Of note, this effect was not observed in Hh-independent MB cell lines following treatment with compound **22** (Figure S8) [47], indicating its selectivity to impair the growth of Hh-MB cells. Consistent with above data, compound **22** reduced *Gli1* and other Hh pathway target genes (Figure 5C,D) and the endogenous protein levels of Gli1 and Gli2, but not those of other Hh pathway regulators, such as ERAP1 [48], Itch [49], HDAC1 [30] and β-Catenin [50] (Figure 5E,F).

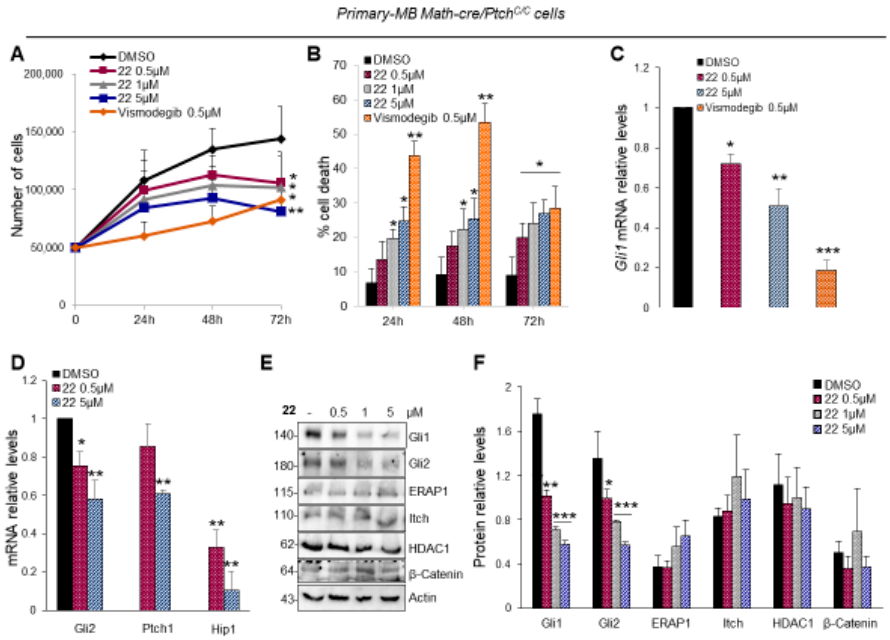

Figure 5. Hh-dependent tumor growth inhibition in vitro by compound **22**. (**A,B**) Primary cell cultures from Math1-cre/Ptch$^{C/C}$ mice medulloblastoma (MBs) were treated with compound **22** (0.5, 1 and 5 μM), Vismodegib (0.5 μM) or DMSO only. After the indicated times, a trypan blue count was performed to determine the growth rate of viable cells and the percentage of cell death. (**C,D**) *Gli1* and Hh target genes mRNA levels of primary MB cells treated with compound **22** determined by qRT–PCR and normalized to endogenous control *β2-microglobulin* and *Hprt*. (**E**,**F**) Representative immunoblotting and densitometric analyses of the indicated proteins in primary MB cells after the treatment with compound **22**. Data show the mean ± SD of three independent experiments. (*) $p < 0.05$ vs. DMSO; (**) $p < 0.01$ vs. DMSO; (***) $p < 0.001$ vs. DMSO.

The ability of compound **22** to inhibit tumor cells proliferation and promote cell death was confirmed in Med1-MB cell line generated from a spontaneous tumor arisen in a *Ptch1*$^{+/-}$; *lacZ mouse* [51,52] (Figure 6A,B). As expected, the treatment with compound **22** significantly reduced mRNA expression of Hh target genes and endogenous Gli1 protein levels (Figure 6C,D). To elucidate the

anti-proliferative effect of isoflavone **22** also in human cancer cells we used MB Daoy cells, belonging to the SHH-MB subgroup [47,53,54]. Compound **22** showed marked activity in inhibiting cell proliferation and promoting cell death also at the lower concentration (Figure 6E,F) as a consequence of the reduction of the Hh pathway activity (Figure 6G,H).

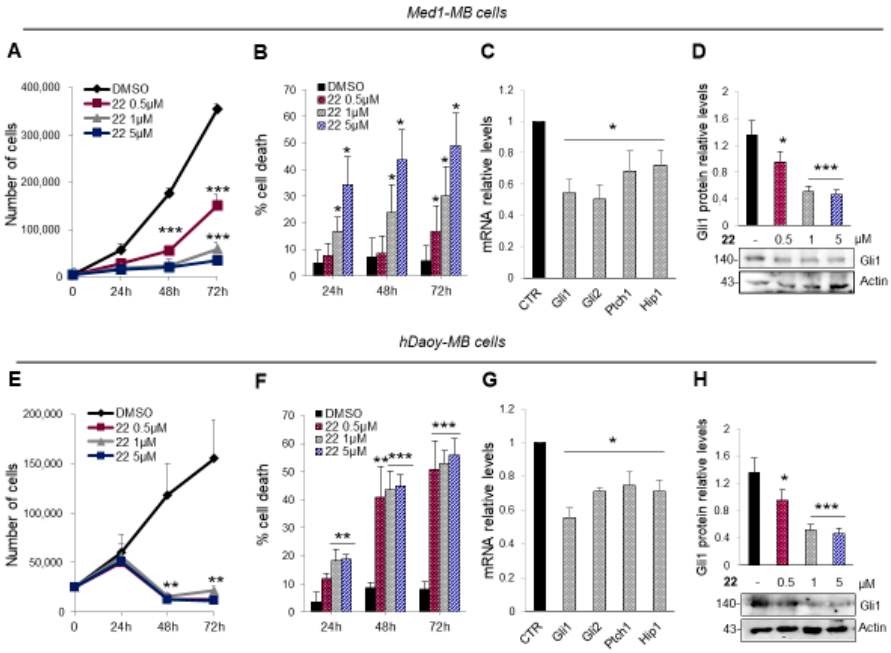

Figure 6. Mouse Med1-MB (**A**–**D**) and human Daoy MB (**E**–**H**). Cells were treated with compound **22** (0.5, 1 and 5 μM) or DMSO only. After the indicated times, a trypan blue count was performed to determine the growth rate of viable cells and the percentage of cell death (**A**,**B** and **E**,**F**). mRNA expression levels of the Hh target genes (**C**,**G**) and Gli1 protein levels with the corresponding densitometric analysis (**D**,**H**) were shown. Data show the mean ± SD of three independent experiments. (*) $p < 0.05$ vs. DMSO; (**) $p < 0.01$ vs. DMSO; (***) $p < 0.001$ vs. DMSO.

2.5. Compound **22** *Inhibits the Hh-Dependent Tumor Growth In Vivo*

These promising results prompted us to test the ability of isoflavone **22** to inhibit the Hh-driven tumor growth also in an in vivo allograft model of MB. To this aim, nude mice were grafted with spontaneous primary MB cells from Math1-cre/Ptch$^{C/C}$ mice and treated every second day with s.c. injections of compound **22** at a concentration of 5 mg/kg or solvent only. The tumor growth was monitored by caliper during the treatment period, and the tumor mass volumes were measured after explant appearing significantly reduced in compound **22**-treated mice compare to controls (Figure 7A,B). These data correlate with the inhibition of both mRNA and protein expression levels of endogenous Hh target genes in treated masses, whereas, protein levels of cleaved PARP are increased suggesting apoptotic cell death (Figure 7C–E). Moreover, compound **22**-treated tumor masses showed reduced cellularity with few MB cells dispersed in a large amount of Masson's staining-mediated blue-labeled connective tissue (Figure 7F), associated with a decreased amount of Ki67 positive cells (Figure 7F,G). These findings support the strong anti-tumor activity of compound **22** in Hh-dependent MB and underline as the use of one molecule with multitargeting properties represents a promising therapeutic strategy to antagonize Hh-signaling and the tumor growth driven by this oncogenic pathway.

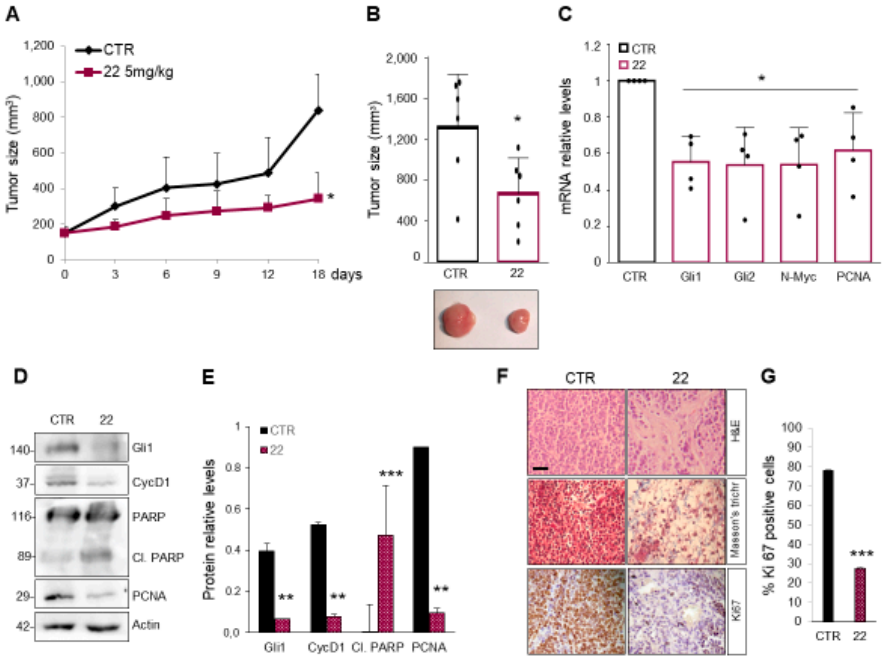

Figure 7. Compound **22** impairs Hh-dependent tumor growth in vivo. (**A**) BALB/c nude mice (*nu/nu*) were grafted with spontaneous primary MB from Math1-cre/Ptc$^{C/C}$ mice. Tumor masses (150 mm^3) were injected with compound **22** or solvent only. Tumor growth was monitored during the treatment period. (**B**) Representative flank allograft average volumes (lower panel) and quantification of tumor explants (upper panel). (**C**) The graphs show mRNA expression levels of *Gli1*, *Gli2*, *N-Myc* and *PCNA* determined by qRT–PCR and normalized to endogenous control *β2-microglobulin* and *Hprt*. (**D**,**E**) Western blot and densitometric analysis show Hh target protein and proliferation marker expression levels from the tumor masses assayed in **B**. (**F**) Hematoxylin/Eosin (H&E), Masson's trichrome and Ki67 staining of representative tumor masses. Scale bar 100 μm. (**G**) Quantification of Ki67 immunohistochemical staining, shown in **F**. Data show the mean ± S.D. of tumor (n = 6) for each treatment. (*) $p < 0.05$ vs. CTR; (**) $p < 0.01$ vs. CTR; (***) $p < 0.001$ vs. CTR.

3. Discussion

In this study, we propose a novel mechanism of action for targeting Hh signaling pathway. Specifically, taking advantage from our previous work, we have designed an isoflavone with the aim to target simultaneously the Hh pathway at both upstream and downstream level, i.e., Smo and Gli1 respectively, and identify an innovative approach to limit tumor growth.

Abnormal Hh reactivation is a hallmark of many cancers, and several germline or somatic mutations in the Hh pathway components have been documented in BCC, MB, rhabdomyosarcoma (RMS), meningioma and many other tumors. For this reason, Hh signaling has emerged in recent years as an attractive target for anticancer therapy [55], and small molecules of both natural and synthetic origin have emerged as profitable drugs that target key components of the pathway. The majority of Hh modulators developed so far act as antagonists of the upstream Smo receptor, and two Smo antagonists (Vismodegib and Sonidegib) have been approved by the FDA for the treatment of advanced or metastatic BCC. However, the use of these drugs is strongly limited by the emergence of drug-resistance and the occurrence of aberrant Hh activation downstream of Smo [56]. Hence, the most efficacy strategy to block Hh signaling in cancer appears to be the pharmacological inhibition of the final and most powerful effector Gli1 [41]. However, only the Gli antagonist Arsenic trioxide (ATO) has entered clinical evaluation so far. For these reasons, innovative, efficacy and less toxic Hh antagonists are urgently needed as therapeutic candidates for the treatment of Hh-dependent tumors. Natural compounds represent a significant resource for the discovery and development of new Hh inhibitors, as demonstrated in the case of isoflavones,

derived from plants of the *Leguminosae* family [57]. In a recent study, we have exploited the high versatility of the isoflavone scaffold, and we demonstrated that the introduction of bulky chemical groups in the *para* position of the isoflavone's ring B enhances the targeting at the level of the Smo receptor. In contrast, bulky substitutions introduced in the *meta* position of the same ring promote the targeting of the downstream Gli effectors. Simultaneous administration of isoflavones targeting Smo and Gli provided synergistic Hh pathway inhibition with a reduction of around 20 folds of the administered dose, which might be relevant to limit toxic side effects and overcome the Smo-drug resistance [43].

Here, by combining the most profitable pharmacophores for targeting Smo and Gli1 by synthetic isoflavones, we have designed and synthesized the isoflavone **22** acting as a multitarget Hh inhibitor that targets both Smo and Gli1 at the same time. Compound **22** was able to inhibit Hh-dependent tumor growth in human and murine MB cells at sub-micromolar concentration, as a consequence of the reduction in *Gli1* expression levels. Despite the limitations of intratumoral administration (i. e. the invasive nature of the injection itself, the rapid clearance of drugs directly applied to the tumor and the development of dose-limiting toxicities in the area surrounding the site of injection) isoflavone **22** remarkably showed a strong anti-tumor effect also in vivo by suppressing cell proliferation and promoting apoptosis. Molecular modeling further corroborated the multitarget mechanism of action of **22**, showing that the molecule is able to fit the ligand-binding site in both Smo and Gli1.

Overall, these results reveal a valuable form of targeted therapy to increase efficacy and to decrease the toxicity of individual anticancer agents. Our findings discover the first multitarget Hh inhibitor that impinges the Hh-dependent tumor growth and stands as new potential weapons against Hh-driven cancer, such as medulloblastoma, the most malignant childhood brain tumor for which poor therapeutic options exist.

4. Material and Methods

4.1. General Experimental Methods for the Preparation of Compounds **20–22**

All reagents were commercial and were used without further purification. Chromatography was carried out on silica gel (230–400 mesh). All reactions were monitored by thin-layer chromatography (TLC), and silica gel plates with fluorescence F254 were used. Melting points were taken in open capillaries on a Büchi Melting Point B-545 apparatus and are presented uncorrected. ^{1}H NMR and ^{13}C NMR spectra were recorded using a Bruker 400 Ultra ShieldTM spectrometer (operating at 400 MHz for ^{1}H and 100 MHz for ^{13}C) using tetramethylsilane (TMS) as an internal standard. Chemical shifts (d) are reported in parts per million (ppm) and are referenced to $CHCl_3$ (⊚⊚7.26 ppm for ^{1}H, ⊚⊚77.16 ppm for ^{13}C). All ^{13}CNMR spectra were measured with complete proton decoupling. Data for NMR spectra are reported, as follows—s (singlet), d (doublet), t (triplet), q (quartet), m (multiplet), br (broad) signal, J coupling constant in Hz. Electron spray ionization mass spectra (ESI-MS) were recorded on Bruker BioApex Fourier transform ion cyclotron resonance (FT-ICR) mass spectrometer. HPLC analysis was performed on a Waters 2690 Separation Module, equipped with a Rheodyne Model 8125 20 mL injector and a Model M486 programmable multi-wavelength detector (PDA). The purity of the sample used in this study was higher than 95% by HPLC. HPLC conditions, % and Retention times (Rt) were as follows. Column: Phenomenex Luna C18, 5.0 μm (250 × 4.6 mm). Eluent A) water/acetonitrile = 95:5 (*v*/*v*). Eluent B) water/acetonitrile = 5:95 (*v*/*v*). Gradient elution: For 0–5 min A: B = 50:50; 5–20 min up to 100% B; 20–25 min to 100% B. Flow rate: 1.0 mL/min. PDA detection at 200–400 nm.

4.2. General Procedure for the Synthesis of Compounds **20–22**

The procedure for the synthesis of isoflavone 4d has been already described in Berardozzi et al. [43]. To a solution of the isoflavone (4d) (0.18 mmol, 1.00 equiv.) in acetone (5 mL), K_2CO_3 (1.8 mmol, 10.00 equiv.) was added. After stirring for 15 min the corresponding benzyl bromide (0.9 mmol, 5.00 equiv.) was added drop wise to the mixture and stirred at 45 °C overnight. After

removing the acetone in a vacuum, H_2O (10 mL) and EtOAc (20 mL) were added, and the aqueous phase was extracted with EtOAc (3 × 20 mL). The combined organic layers were dried over Na_2SO_4, and finally concentrated under reduced pressure. The residue was purified by Flash Chromatography using Petroleum Ether/ EtOAc as eluent to give the corresponding substituted-isoflavone (**20**-**22**). The characterization for all compounds is reported in the SI.

4.3. Luciferase Reporter Assay

The Hh-dependent luciferase assay was performed in NIH3T3 Shh-Light II cells, stably expressing a Gli-responsive luciferase reporter and the pRL-TK Renilla (normalization control), treated for 48 h with SAG (200 nM) and the tested compounds at the indicated concentrations. Luciferase and Renilla activities were assayed with a dual-luciferase assay system according to the manufacturer's instructions (Biotium Inc., Hayward, CA, USA). Results were expressed as Luciferase/Renilla ratios and represented the mean ± S.D. of three experiments, each performed in triplicate.

4.4. Cell Cultures, Transfection and Treatments

NIH3T3 Shh-Light II, MEFs WT, Ptch1$^{-/-}$ (kindly provided by M.P. Scott), SuFu$^{-/-}$ and Smo$^{-/-}$ (kindly provided by R. Toftgard) MEFs and Med1-MB cells (kindly provided by Yoon-Jae Cho), D425 and HDMB03 (kindly provided by V. D'Angiolella) were cultured in DMEM plus 10% FBS. Daoy cells (obtained from the American Type Culture Condition, ATCC) were cultured in Eagle's minimum essential medium (MEM) plus 10% FBS. D458, D283 (kindly provided by V. D'Angiolella) and D341 (obtained from the American Type Culture Condition, ATCC) were maintained in Eagle's minimum essential medium (MEM) plus 20% FBS. All media contained 1% Penicillin-Streptomycin and 1% Glutamine. Primary MB cells were freshly isolated from Math1-cre/Ptch$^{C/C}$ mice. Tumors were collected and mechanically disrupted with fire-polished Pasteur pipettes in HBSS with 1% Pen/Strep and treated with DNase (10 μg/mL) for twenty minutes to obtain a single-cell suspension. Cells were centrifuged and resuspended in Neurobasal Media-A with B27 supplement minus vitamin A, penicillin–streptomycin (1%) and L-glutamine (1%) and used for short-term to keep Hh-sensitivity in vitro. Mycoplasma contamination in cell cultures was routinely detected by using PCR detection kit (Applied Biological Materials, Richmond, BC, Canada). Transient transfections were performed using DreamFect™ Gold transfection reagent (Oz Biosciences SAS, Marseille, France). NIH3T3 Shh-Light II cells were treated with SAG (200 nM, Alexis Biochemicals Farmingdale, NY, USA) for 48 h. Where indicated, cells were treated with Vismodegib (Selleckchem), Arsenic (III) oxide (ATO, Sigma Aldrich, St. Louis, MO, USA) and GANT61 (Enzo Life Sciences, Exeter, UK) at the indicated concentrations.

4.5. Bodipy-Cyclopamine (BC) Binding Assay

Human Myc-DDK-tagged Smo WT or human Myc-DDK-tagged Smo D473H was transfected in HEK293T cells. Cells were washed in PBS supplemented with 0.5% fetal bovine serum, fixed in 4% paraformaldehyde in phosphate-buffered saline (PBS) for 10 min, and incubated for 2 h at 37 °C both in the same medium supplemented with Bodipy-Cyclopamine (5 nM) and the studied compounds at indicated concentrations. The cells were permeabilized with 0.2% Triton X100 (Sigma) 0.2%. Dako Fluorescent mounting (Dako, Carpinteria, CA, USA) was used as a mounting medium and Hoechst reagent for staining of the cell nuclei. Bodipy (green) and Hoechst (blue) signals were analyzed.

4.6. mRNA Expression Analysis

Trizol reagent (Invitrogen/Life Technologies, Carlsbad, CA, USA) was used to isolate total RNA from cells and tissues and reverse transcribed with SensiFAST cDNA Synthesis Kit (Bioline Reagents Limited, London, UK). Quantitative real-time PCR (Q-PCR) analysis of *Gli1*, *Gli2*, *Ptch1*, *Hip1*, *N-Myc*, *PCNA*, *β-2 microglobulin* and *Hprt* mRNA expression was performed on each cDNA

sample using the VIIA7 Real Time PCR System employing Assay-on-Demand Reagents (Life Technologies). FAST Q-PCR thermal cycler parameters were used to amplify the reaction mixtures containing cDNA template, SensiFAST Probe Lo-ROX Kit (Bioline Reagents Limited, London, UK) and primer probe. Each amplification reaction was performed in triplicate, and the average of the three threshold cycles was used to calculate the amount of transcript in the sample (using SDS version 2.3 software). mRNA quantification was expressed as the ratio of the genes of interest quantity to the housekeeping genes quantity. All values were normalized with two endogenous controls, *β-2 microglobulin* and *Hprt*.

4.7. Cell Proliferation Assay

To determine the growth rate of viable MB cells, a trypan blue count was performed after a treatment period of 24–48–72 h with the studied compounds or solvent only used as control.

4.8. Immunoblot Analysis

Tissues were lysed in a solution containing RIPA buffer (50 mM Tris-HCl at pH 7.6, 150 mM NaCl, 0.5% sodium deoxycholic, 5 mM EDTA, 0.1% SDS, 100 mM NaF, 2 mM NaPPi, 1% NP-40) supplemented with protease and phosphatase inhibitors. Lysates were centrifuged at 13,000 × *g* for 30 min at 4 °C and the resulting supernatants were subjected to immunoblot analysis with the following antibodies: mouse anti-Gli1 (L42B10, 1:500) and rabbit anti-PARP (9542, 1:1000) purchased from Cell Signaling (Beverly, MA, USA); rabbit anti-Cyclin D1-20 (sc-717, 1:500), rabbit anti-β-Catenin (sc-7199, 1:1000) and goat anti-Actin (sc-1616, 1:1000) were purchased from Santa Cruz Biotechnology (Santa Cruz, CA, USA); mouse anti-ERAP1 6H9 (1:1000) kindly provided by P. van Endert; goat anti-Gli2 (AF3635, 1:1000) was purchased from R&D Systems; mouse anti-Itch (611199, 1:1000) antibody was purchased from BD Bioscience (Heidelberg, Germany); rabbit anti-HDAC1 (H3284, 1:1000) was purchased from Sigma Aldrich (St. Louis, MO, USA).

4.9. Chromatin Immunoprecipitation

MEFs WT transfected with Flag-tagged Gli1 plasmid or pcDNA3.1 were crosslinked, and chromatin immunoprecipitation was carried out with (1:200) mouse anti Flag-M2 antibody (Sigma Aldrich, St. Louis, MO, USA). Eluted DNA was analyzed by qRT-PCR as previously described [42].

4.10. Subcellular Fractionation

Freshly harvested cells were lysed in Buffer A (10 mM HEPES at pH 7.4, 10 mM KCl, 10 mM NaCl, 0.1 mM EDTA, 0.1 mM EGTA, 1 mM DTT, 0.5 mM PMSF) and centrifuged at 11,000 × g for 20 min to obtain the cytoplasmic fraction. The nuclear pellet was washed in Buffer B (20 mM HEPES at pH 7.4, 20% glycerol, 100 mM KCl, 1 mM EDTA, 1 mM DTT, 0.5 mM PMSF, 10 ng ml^{-1} Leupeptin) and centrifuged at 11,000 × g for 10 s to remove the supernatant. Nuclei were extracted with Buffer C (20 mM HEPES at pH 7.4, 20% glycerol, 400 mM NaCl, 1 mM EDTA, 1 mM EGTA, 1 mM DTT, 0.5 mM PMSF, 10 ng ml^{-1}Leupeptin) by centrifugation at 13,000 × g for 10 min. Lysates were analyzed by western blotting assay.

4.11. Immunofluorescence

For the analysis of ciliogenesis, MEFs WT were treated with compound **22** at several concentrations for 24 h in 0.05% FBS and then fixed 10 min in 4% paraformaldehyde. The primary antibody for the cilium marker IFT88 (Rabbit Polyclonal 13967-1-AP, from ProteinTech, Manchester, UK) was incubated overnight at the dilution (1:200) in blocking solution (2% FBS, 2% BSA, 0.2% fish gelatin in PBS1X). A secondary antibody conjugated to Alexa-488 (ThermoFisher Scientific, MA, USA) and DAPI for the staining of nuclei, were diluted in blocking solution (1:1000) and incubated 1 h at room temperature. Images were acquired through 60X oil objective lens (Olympus IX81) coupled to a monochrome CCD camera (Sensicam QE; Cooke Corporation, ME, USA). For

quantification of IFT88 positive cells and the length of cilia expressed in μm was used ImageJ Measure function to count the number of objects and their length.

4.12. Immunohistochemistry

For immunohistochemical staining tissues were fixed in formalin and paraffin embedded. Sections were incubated with rabbit monoclonal Ki67 antibody (Thermo Fisher Scientific, MA, USA) (1:100) diluted in PBS. Detection was carried out with the mouse-to-mouse HRP (DAB) staining system (ScyTek Laboratories, Logan, UT, USA) accordingly to the manufacturer's instructions.

4.13. Molecular Modeling

The predicted binding mode of compound **22** to Smo and Gli1 was investigated as described previously [43]. Briefly, molecular docking to Smo was carried out with FRED version 3.3.0.3 (OpenEye) (OpenEye Scientific Software, Santa Fe, NM, USA. http://www.eyesopen.com) [58,59], using the highest docking resolution, while other parameters were used at their default values. Ligand conformational analysis was carried out with OMEGA version 3.1.0.3 (OpenEye) (OpenEye Scientific Software, Santa Fe, NM, USA. http://www.eyesopen.com) [46] by storing up to 600 conformations of the molecule. The crystallographic structure of Smo in complex with cyclopamine coded by PDB-ID 4O9R was used as a rigid receptor in docking towards Smo [46]. Docking to Gli1 zinc finger domain was carried out by GOLD version 5.7.1 (The Cambridge Crystallographic Data Centre, Cambridge, UK) [60] using the Goldscore docking function. The crystallographic structure of Gli1 in complex with DNA coded by PDB-ID 2GLI was used as a rigid receptor in docking towards Gli1 zinc finger domain [61].

4.14. Animal Studies

For allograft experiment**,** spontaneous MB from Math1-cre/Ptch$^{C/C}$ mice was collected, minced and pipetted to obtain a single-cell suspension. Equal amounts of cells (2×10^6) were injected s.c. at the posterior flank of BALB/c nude mice (*nu*/*nu*) (Charles River Laboratories, Lecco, Italy). When tumors reached a median size of ~150 mm^3, animals were randomly divided into two groups ($n = 6$) and intratumorally injected every second day with compound **22** or solvent only (2-hydroxypropyl-b-cyclodextrin:DMSO) for 18 days. Tumor growth was monitored and measured with caliper. Changes in tumor volume were evaluated with the formula (length × width) × 0.5 × (length + width). All animal protocols were approved by local ethic authority (Ministry of Health) and conducted in accordance with Italian Governing Law (D.lgs 26/2014).

4.15. Statistical Analysis

Statistical analysis was performed using the StatView 4.1 software (Abacus Concepts, Berkeley, CA, USA). For in vivo studies, statistical differences were analyzed by Mann-Whitney *U*-test for non-parametric values, and a p value < 0.05 was considered significant. For all other experiments, p values were determined using two-tailed Student's *t*-test, and statistical significance was set at $p < 0.05$. Results are expressed as mean ± S.D. from an appropriate number of experiments (at least three biological replicas).

5. Conclusions

We designed a modified isoflavone bearing specific substitutions at *para* or *meta* position of ring B that are preferred for the interaction with Smo or Gli1, respectively. We demonstrated that this small molecule, compound **22**, is able to target the Hh pathway at both upstream and downstream level simultaneously, leading to a marked tumor growth inhibition in a model of Hh-dependent cancer. Our study provides significant support in oncology research for the development of new clinically relevant Hh inhibitors, and encourages the use of a multitargeting approach for the treatment of Hh-driven tumors.

Supplementary Materials: The following are available online at www.mdpi.com/xxx/s1. Figure S1: Hh inhibition by compound 20. Dose-response curve in SAG-treated NIH3T3 Shh-Light II cells, Figure S2: General procedure for the synthesis of compounds 20-22. Characterization of compounds 20–22, Figure S3: Effect of compounds 21 and 22 on overexpressed Gli1 protein, Figure S4: Effect of ATO, GANT61 and Vismodegib on Gli1 mRNA levels in $Smo^{-/-}$ MEFs, Figure S5: Compound 22 does not affect Jun and WNT pathways, Figure S6: Inhibition of Gli2-induced transcription in MEFs WT treated with increasing concentrations of compound 22, Figure S7: Effect of compound 22 on ciliogenesis and Gli1 localization, Figure S8: Effect of compound 22 on non-Hedgehog-dependent MB cell lines, Table S1: Effect of compounds 21 and 22 on Gli1 mRNA levels in $Smo^{-/-}$ MEFs.

Author Contributions: L.D.M. conceived and coordinated the project, designed the experiments, analyzed the data, and wrote the paper. L.L.S., D.Q. conceived, performed experiments and analyzed the data. F.G., S.B. and I.R. isolated, purified and characterized organic molecules, performed analytic studies and analyzed data. I.B, M.C. performed experiments on cell lines. F.B. and P.I. performed the animal experiments. M.M. (Marta Moretti) performed IHC and western blot analysis. E.L. performed the real-time experiments. M.M. (Mattia Mori) performed molecular modeling. B.B. and M.M. (Marella Maroder). helped to interpret data. M.M. (Mattia Mori), P.I. and L.D.M. designed experiments, interpreted data and wrote the manuscript. All authors critically revised and edited the manuscript.

Funding: This work was supported by Associazione Italiana Ricerca Cancro (AIRC) Grant #IG20801, Ministry of University and Research (PRIN 2012C5YJSK002), (PRIN 2017BF3PXZ003), Progetti di Ricerca di Università Sapienza di Roma, Universities and Research—Dipartimenti di Eccellenza—L.232/2016, Pasteur Institute/Cenci Bolognetti Foundation and Istituto Italiano di Tecnologia (IIT).

Acknowledgments: We thank F. Bartolini and A. Kumar for their experimental assistance in immunofluorescence. L. Lospinoso Severini is the recipient of a fellowship of the PhD Programme in Tecnologie Biomediche in Medicina Clinica, University La Sapienza. The authors wish to thank the OpenEye Free Academic Licensing Program for providing a free academic license for molecular modeling and chemoinformatics software.

Conflicts of Interest: The authors declare no conflict of interest.

References

1. Pak, E.; Segal, R.A. Hedgehog Signal Transduction: Key Players, Oncogenic Drivers, and Cancer Therapy. *Dev. Cell* **2016**, *38*, 333–344, doi:10.1016/j.devcel.2016.07.026.
2. Varjosalo, M.; Taipale, J. Hedgehog: Functions and mechanisms. *Genes Dev.* **2008**, *22*, 2454–2472, doi:10.1101/gad.1693608.
3. Ruiz, I.; Altaba, A.; Mas, C.; Stecca, B. The Gli code: An information nexus regulating cell fate, stemness and cancer. *Trends. Cell Biol.* **2007**, *17*, 438–447, doi:10.1016/j.tcb.2007.06.007.
4. Robbins, D.J.; Fei, D.L.; Riobo, N.A. The Hedgehog signal transduction network. *Sci. Signal* **2012**, *5*, re6, doi:10.1126/scisignal.2002906.
5. Meiss, F.; Zeiser, R. Vismodegib. *Recent. Results Cancer Res.* **2014**, *201*, 405–417, doi:10.1007/978-3-642-54490-3_25.
6. Gulino, A.; Di Marcotullio, L.; Canettieri, G.; De Smaele, E.; Screpanti, I. Hedgehog/Gli control by ubiquitination/acetylation interplay. *Vitam. Horm.* **2012**, *88*, 211–227, doi:10.1016/B978-0-12-394622-5.00009-2.
7. Amakye, D.; Jagani, Z.; Dorsch, M. Unraveling the therapeutic potential of the Hedgehog pathway in cancer. *Nat. Med.* **2013**, *19*, 1410–1422, doi:10.1038/nm.3389.
8. Briscoe, J.; Thérond, P.P. The mechanisms of Hedgehog signalling and its roles in development and disease. *Nat. Rev. Mol. Cell Biol.* **2013**, *14*, 416–429, doi:10.1038/nrm3598.
9. Aberger, F.; Ruiz, I.; Altaba, A. Context-dependent signal integration by the GLI code: The oncogenic load, pathways, modifiers and implications for cancer therapy. *Semin. Cell. Dev. Biol.* **2014**, *33*, 93–104, doi:10.1016/j.semcdb.2014.05.003.
10. Ghirga, F.; Mori, M.; Infante, P. Current trends in Hedgehog signaling pathway inhibition by small molecules. *Bioorg. Med. Chem. Lett.* **2018**, *28*, 3131–3140, doi:10.1016/j.bmcl.2018.08.033.
11. Xin, M.; Ji, X.; De La Cruz, L.K.; Thareja, S.; Wang, B. Strategies to target the Hedgehog signaling pathway for cancer therapy. *Med. Res. Rev.* **2018**, *38*, 870–913, doi:10.1002/med.21482.

12. Palermo, R.; Ghirga, F.; Piccioni, M.G.; Bernardi, F.; Zhdanovskaya, N.; Infante, P.; Mori, M. Natural Products Inspired Modulators of Cancer Stem Cells-specific Signaling Pathways Notch and Hedgehog. *Curr. Pharm. Des.* **2018**, *24*, 4251–4269, doi:10.2174/1381612825666190111124822.
13. Goodrich, L.V.; Milenković, L.; Higgins, K.M.; Scott, M.P. Altered neural cell fates and medulloblastoma in mouse patched mutants. *Science* **1997**, *277*, 1109–1113.
14. Yauch, R.L.; Dijkgraaf, G.J.; Alicke, B.; Januario, T.; Ahn, C.P.; Holcomb, T.; Pujara, K.; Stinson, J.; Callahan, C.A.; Tang, T.; et al. Smoothened mutation confers resistance to a Hedgehog pathway inhibitor in medulloblastoma. *Science* **2009**, *326*, 572–574, doi:10.1126/science.1179386.
15. Infante, P.; Alfonsi, R.; Ingallina, C.; Quaglio, D.; Ghirga, F.; D'Acquarica, I.; Bernardi, F.; Di Magno, L.; Canettieri, G.; Screpanti, I.; et al. Inhibition of Hedgehog-dependent tumors and cancer stem cells by a newly identified naturally occurring chemotype. *Cell Death Dis.* **2016**, *7*, e2376, doi:10.1038/cddis.2016.195.
16. Pietrobono, S.; Stecca, B. Targeting the Oncoprotein Smoothened by Small Molecules: Focus on Novel Acylguanidine Derivatives as Potent Smoothened Inhibitors. *Cells* **2018**, *7*, doi:10.3390/cells7120272.
17. Huang, S.Y.; Yang, J.Y. Targeting the Hedgehog Pathway in Pediatric Medulloblastoma. *Cancers* **2015**, *7*, 2110–2123, doi:10.3390/cancers7040880.
18. Pandolfi, S.; Stecca, B. Cooperative integration between HEDGEHOG-GLI signalling and other oncogenic pathways: Implications for cancer therapy. *Expert Rev. Mol. Med.* **2015**, *17*, e5, doi:10.1017/erm.2015.3.
19. Rudin, C.M.; Hann, C.L.; Laterra, J.; Yauch, R.L.; Callahan, C.A.; Fu, L.; Holcomb, T.; Stinson, J.; Gould, S.E.; Coleman, B.; et al. Treatment of medulloblastoma with hedgehog pathway inhibitor GDC-0449. *N. Engl. J. Med.* **2009**, *361*, 1173–1178, doi:10.1056/NEJMoa0902903.
20. Tang, J.Y.; Mackay-Wiggan, J.M.; Aszterbaum, M.; Yauch, R.L.; Lindgren, J.; Chang, K.; Coppola, C.; Chanana, A.M.; Marji, J.; Bickers, D.R.; et al. Inhibiting the hedgehog pathway in patients with the basal-cell nevus syndrome. *N. Engl. J. Med.* **2012**, *366*, 2180–2188, doi:10.1056/NEJMoa1113538.
21. Metcalfe, C.; de Sauvage, F.J. Hedgehog fights back: Mechanisms of acquired resistance against Smoothened antagonists. *Cancer Res.* **2011**, *71*, 5057–5061, doi:10.1158/0008-5472.CAN-11-0923.
22. Dlugosz, A.; Agrawal, S.; Kirkpatrick, P. Vismodegib. *Nat. Rev. Drug Discov.* **2012**, *11*, 437–438, doi:10.1038/nrd3753.
23. Atwood, S.X.; Sarin, K.Y.; Whitson, R.J.; Li, J.R.; Kim, G.; Rezaee, M.; Ally, M.S.; Kim, J.; Yao, C.; Chang, A.L.; et al. Smoothened variants explain the majority of drug resistance in basal cell carcinoma. *Cancer Cell* **2015**, *27*, 342–353, doi:10.1016/j.ccell.2015.02.002.
24. Sharpe, H.J.; Pau, G.; Dijkgraaf, G.J.; Basset-Seguin, N.; Modrusan, Z.; Januario, T.; Tsui, V.; Durham, A.B.; Dlugosz, A.A.; Haverty, P.M.; et al. Genomic analysis of smoothened inhibitor resistance in basal cell carcinoma. *Cancer Cell* **2015**, *27*, 327–341, doi:10.1016/j.ccell.2015.02.001.
25. Kinzler, K.W.; Bigner, S.H.; Bigner, D.D.; Trent, J.M.; Law, M.L.; O'Brien, S.J.; Wong, A.J.; Vogelstein, B. Identification of an amplified, highly expressed gene in a human glioma. *Science* **1987**, *236*, 70–73.
26. Taylor, M.D.; Liu, L.; Raffel, C.; Hui, C.C.; Mainprize, T.G.; Zhang, X.; Agatep, R.; Chiappa, S.; Gao, L.; Lowrance, A.; et al. Mutations in SUFU predispose to medulloblastoma. *Nat. Genet.* **2002**, *31*, 306–310, doi:10.1038/ng916.
27. Infante, P.; Faedda, R.; Bernardi, F.; Bufalieri, F.; Lospinoso Severini, L.; Alfonsi, R.; Mazzà, D.; Siler, M.; Coni, S.; Po, A.; et al. Itch/β-arrestin2-dependent non-proteolytic ubiquitylation of SuFu controls Hedgehog signalling and medulloblastoma tumorigenesis. *Nat. Commun.* **2018**, *9*, 976, doi:10.1038/s41467-018-03339-0.
28. Di Marcotullio, L.; Ferretti, E.; Greco, A.; De Smaele, E.; Po, A.; Sico, M.A.; Alimandi, M.; Giannini, G.; Maroder, M.; Screpanti, I.; et al. Numb is a suppressor of Hedgehog signalling and targets Gli1 for Itch-dependent ubiquitination. *Nat. Cell. Biol.* **2006**, *8*, 1415–1423, doi:10.1038/ncb1510.
29. Di Marcotullio, L.; Greco, A.; Mazzà, D.; Canettieri, G.; Pietrosanti, L.; Infante, P.; Coni, S.; Moretti, M.; De Smaele, E.; Ferretti, E.; et al. Numb activates the E3 ligase Itch to control Gli1 function through a novel degradation signal. *Oncogene* **2011**, *30*, 65–76, doi:10.1038/onc.2010.394.
30. Canettieri, G.; Di Marcotullio, L.; Greco, A.; Coni, S.; Antonucci, L.; Infante, P.; Pietrosanti, L.; De Smaele, E.; Ferretti, E.; Miele, E.; et al. Histone deacetylase and Cullin3-REN(KCTD11) ubiquitin ligase interplay regulates Hedgehog signalling through Gli acetylation. *Nat. Cell. Biol.* **2010**, *12*, 132–142, doi:10.1038/ncb2013.

31. Wang, Y.; Ding, Q.; Yen, C.J.; Xia, W.; Izzo, J.G.; Lang, J.Y.; Li, C.W.; Hsu, J.L.; Miller, S.A.; Wang, X.; et al. The crosstalk of mTOR/S6K1 and Hedgehog pathways. *Cancer Cell* **2012**, *21*, 374–387, doi:10.1016/j.ccr.2011.12.028.
32. Mazzà, D.; Infante, P.; Colicchia, V.; Greco, A.; Alfonsi, R.; Siler, M.; Antonucci, L.; Po, A.; De Smaele, E.; Ferretti, E.; et al. PCAF ubiquitin ligase activity inhibits Hedgehog/Gli1 signaling in p53-dependent response to genotoxic stress. *Cell Death Differ.* **2013**, *20*, 1688–1697, doi:10.1038/cdd.2013.120.
33. Pietrobono, S.; Gagliardi, S.; Stecca, B. Non-canonical Hedgehog Signaling Pathway in Cancer: Activation of GLI Transcription Factors Beyond Smoothened. *Front. Genet.* **2019**, *10*, 556, doi:10.3389/fgene.2019.00556.
34. Gu, D.; Xie, J. Non-Canonical Hh Signaling in Cancer-Current Understanding and Future Directions. *Cancers* **2015**, *7*, 1684–1698, doi:10.3390/cancers7030857.
35. Buonamici, S.; Williams, J.; Morrissey, M.; Wang, A.; Guo, R.; Vattay, A.; Hsiao, K.; Yuan, J.; Green, J.; Ospina, B.; et al. Interfering with resistance to smoothened antagonists by inhibition of the PI3K pathway in medulloblastoma. *Sci. Transl. Med.* **2010**, *2*, 51ra70, doi:10.1126/scitranslmed.3001599.
36. Northcott, P.A.; Robinson, G.W.; Kratz, C.P.; Mabbott, D.J.; Pomeroy, S.L.; Clifford, S.C.; Rutkowski, S.; Ellison, D.W.; Malkin, D.; Taylor, M.D.; et al. Medulloblastoma. *Nat. Rev. Dis. Primers.* **2019**, *5*, 11, doi:10.1038/s41572-019-0063-6.
37. Fossati, P.; Ricardi, U.; Orecchia, R. Pediatric medulloblastoma: Toxicity of current treatment and potential role of protontherapy. *Cancer Treat. Rev.* **2009**, *35*, 79–96, doi:10.1016/j.ctrv.2008.09.002.
38. Crawford, J.R.; MacDonald, T.J.; Packer, R.J. Medulloblastoma in childhood: New biological advances. *Lancet Neurol.* **2007**, *6*, 1073–1085, doi:10.1016/S1474-4422(07)70289-2.
39. Wechsler-Reya, R.; Scott, M.P. The developmental biology of brain tumors. *Annu. Rev. Neurosci.* **2001**, *24*, 385–428, doi:10.1146/annurev.neuro.24.1.385.
40. Robinson, G.W.; Orr, B.A.; Wu, G.; Gururangan, S.; Lin, T.; Qaddoumi, I.; Packer, R.J.; Goldman, S.; Prados, M.D.; Desjardins, A.; et al. Vismodegib Exerts Targeted Efficacy Against Recurrent Sonic Hedgehog-Subgroup Medulloblastoma: Results From Phase II Pediatric Brain Tumor Consortium Studies PBTC-025B and PBTC-032. *J. Clin. Oncol.* **2015**, *33*, 2646–2654, doi:10.1200/JCO.2014.60.1591.
41. Infante, P.; Alfonsi, R.; Botta, B.; Mori, M.; Di Marcotullio, L. Targeting GLI factors to inhibit the Hedgehog pathway. *Trends. Pharmacol. Sci.* **2015**, *36*, 547–558, doi:10.1016/j.tips.2015.05.006.
42. Infante, P.; Mori, M.; Alfonsi, R.; Ghirga, F.; Aiello, F.; Toscano, S.; Ingallina, C.; Siler, M.; Cucchi, D.; Po, A.; et al. Gli1/DNA interaction is a druggable target for Hedgehog-dependent tumors. *EMBO J.* **2015**, *34*, 200–217, doi:10.15252/embj.201489213.
43. Berardozzi, S.; Bernardi, F.; Infante, P.; Ingallina, C.; Toscano, S.; De Paolis, E.; Alfonsi, R.; Caimano, M.; Botta, B.; Mori, M.; et al. Synergistic inhibition of the Hedgehog pathway by newly designed Smo and Gli antagonists bearing the isoflavone scaffold. *Eur. J. Med. Chem.* **2018**, *156*, 554–562, doi:10.1016/j.ejmech.2018.07.017.
44. Calcaterra, A.; Iovine, V.; Botta, B.; Quaglio, D.; D'Acquarica, I.; Ciogli, A.; Iazzetti, A.; Alfonsi, R.; Lospinoso Severini, L.; Infante, P.; et al. Chemical, computational and functional insights into the chemical stability of the Hedgehog pathway inhibitor GANT61. *J. Enzyme. Inhib. Med. Chem.* **2018**, *33*, 349–358, doi:10.1080/14756366.2017.1419221.
45. Sheng, T.; Chi, S.; Zhang, X.; Xie, J. Regulation of Gli1 localization by the cAMP/protein kinase a signaling axis through a site near the nuclear localization signal. *J. Biol. Chem.* **2006**, *281*, 9–12, doi:10.1074/jbc.C500300200.
46. Weierstall, U.; James, D.; Wang, C.; White, T.A.; Wang, D.; Liu, W.; Spence, J.C.; Bruce Doak, R.; Nelson, G.; Fromme, P.; et al. Lipidic cubic phase injector facilitates membrane protein serial femtosecond crystallography. *Nat. Commun.* **2014**, *5*, 3309, doi:10.1038/ncomms4309.
47. Ivanov, D.P.; Coyle, B.; Walker, D.A.; Grabowska, A.M. In vitro models of medulloblastoma: Choosing the right tool for the job. *J. Biotechnol.* **2016**, *236*, 10–25, doi:10.1016/j.jbiotec.2016.07.028.
48. Bufalieri, F.; Infante, P.; Bernardi, F.; Caimano, M.; Romania, P.; Moretti, M.; Lospinoso Severini, L.; Talbot, J.; Melaiu, O.; Tanori, M.; et al. ERAP1 promotes Hedgehog-dependent tumorigenesis by controlling USP47-mediated degradation of βTrCP. *Nat. Commun.* **2019**, *10*, 3304, doi:10.1038/s41467-019-11093-0.

49. Infante, P.; Lospinoso Severini, L.; Bernardi, F.; Bufalieri, F.; Di Marcotullio, L. Targeting Hedgehog Signalling through the Ubiquitylation Process: The Multiple Roles of the HECT-E3 Ligase Itch. *Cells* **2019**, *8*, doi:10.3390/cells8020098.
50. Zinke, J.; Schneider, F.T.; Harter, P.N.; Thom, S.; Ziegler, N.; Toftgård, R.; Plate, K.H.; Liebner, S. β-Catenin-Gli1 interaction regulates proliferation and tumor growth in medulloblastoma. *Mol. Cancer* **2015**, *14*, 17, doi:10.1186/s12943-015-0294-4.
51. Tang, Y.; Gholamin, S.; Schubert, S.; Willardson, M.I.; Lee, A.; Bandopadhayay, P.; Bergthold, G.; Masoud, S.; Nguyen, B.; Vue, N.; et al. Epigenetic targeting of Hedgehog pathway transcriptional output through BET bromodomain inhibition. *Nat. Med.* **2014**, *20*, 732–740, doi:10.1038/nm.3613.
52. Hayden Gephart, M.G.; Su, Y.S.; Bandara, S.; Tsai, F.C.; Hong, J.; Conley, N.; Rayburn, H.; Milenkovic, L.; Meyer, T.; Scott, M.P. Neuropilin-2 contributes to tumorigenicity in a mouse model of Hedgehog pathway medulloblastoma. *J. Neurooncol.* **2013**, *115*, 161–168, doi:10.1007/s11060-013-1216-1.
53. Triscott, J.; Lee, C.; Foster, C.; Manoranjan, B.; Pambid, M.R.; Berns, R.; Fotovati, A.; Venugopal, C.; O'Halloran, K.; Narendran, A.; et al. Personalizing the treatment of pediatric medulloblastoma: Polo-like kinase 1 as a molecular target in high-risk children. *Cancer Res.* **2013**, *73*, 6734–6744, doi:10.1158/0008-5472.CAN-12-4331.
54. Northcott, P.A.; Shih, D.J.; Remke, M.; Cho, Y.J.; Kool, M.; Hawkins, C.; Eberhart, C.G.; Dubuc, A.; Guettouche, T.; Cardentey, Y.; et al. Rapid, reliable, and reproducible molecular sub-grouping of clinical medulloblastoma samples. *Acta Neuropathol.* **2012**, *123*, 615–626, doi:10.1007/s00401-011-0899-7.
55. Zhang, X.; Tian, Y.; Yang, Y.; Hao, J. Development of anticancer agents targeting the Hedgehog signaling. *Cell Mol. Life Sci.* **2017**, *74*, 2773–2782, doi:10.1007/s00018-017-2497-x.
56. Ruat, M.; Hoch, L.; Faure, H.; Rognan, D. Targeting of Smoothened for therapeutic gain. *Trends. Pharmacol. Sci.* **2014**, *35*, 237–246, doi:10.1016/j.tips.2014.03.002.
57. Ko, K.P. Isoflavones: Chemistry, analysis, functions and effects on health and cancer. *Asian Pac. J. Cancer Prev.* **2014**, *15*, 7001–7010, doi:10.7314/apjcp.2014.15.17.7001.
58. McGann, M. FRED pose prediction and virtual screening accuracy. *J. Chem. Inf. Model.* **2011**, *51*, 578–596, doi:10.1021/ci100436p.
59. McGann, M. FRED and HYBRID docking performance on standardized datasets. *J. Comput. Aided. Mol. Des.* **2012**, *26*, 897–906, doi:10.1007/s10822-012-9584-8.
60. Verdonk, M.L.; Cole, J.C.; Hartshorn, M.J.; Murray, C.W.; Taylor, R.D. Improved protein-ligand docking using GOLD. *Proteins* **2003**, *52*, 609–623, doi:10.1002/prot.10465.
61. Pavletich, N.P.; Pabo, C.O. Crystal structure of a five-finger GLI-DNA complex: New perspectives on zinc fingers. *Science* **1993**, *261*, 1701–1707, doi:10.1126/science.8378770.

Supplementary Materials: A Smo/Gli Multitarget Hedgehog Pathway Inhibitor Impairs Tumor Growth

Ludovica Lospinoso Severini, Deborah Quaglio, Irene Basili, Francesca Ghirga, Francesca Bufalieri, Miriam Caimano, Silvia Balducci, Marta Moretti, Isabella Romeo, Elena Loricchio, Marella Maroder, Bruno Botta, Mattia Mori, Paola Infante, Lucia Di Marcotullio

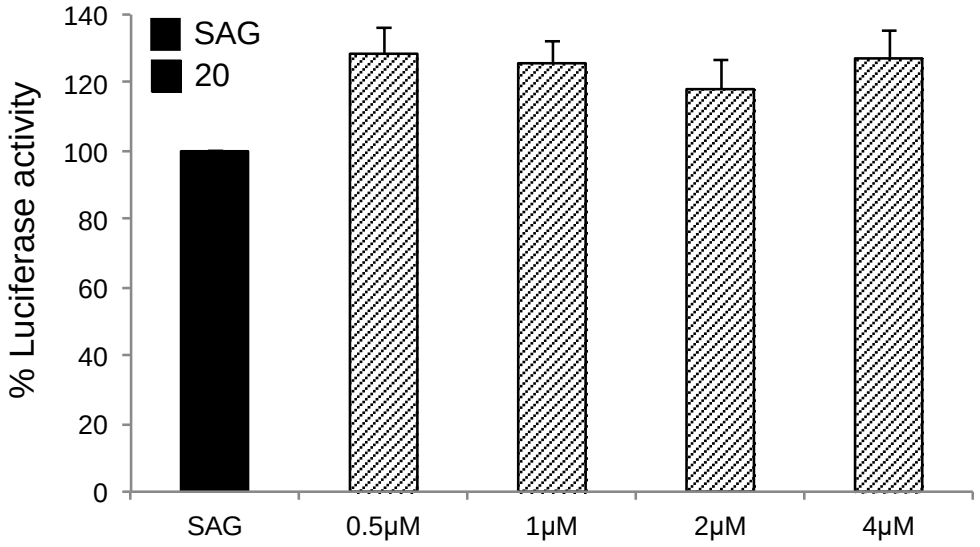

Figure S1. Hh inhibition by compound **20**. Dose-response curve in SAG-treated NIH3T3 Shh-Light II cells. Cells were treated for 48 h with increasing concentrations of compounds **20**. Data were normalized against Renilla luciferase. Data show the mean ± SD of three independent experiments.

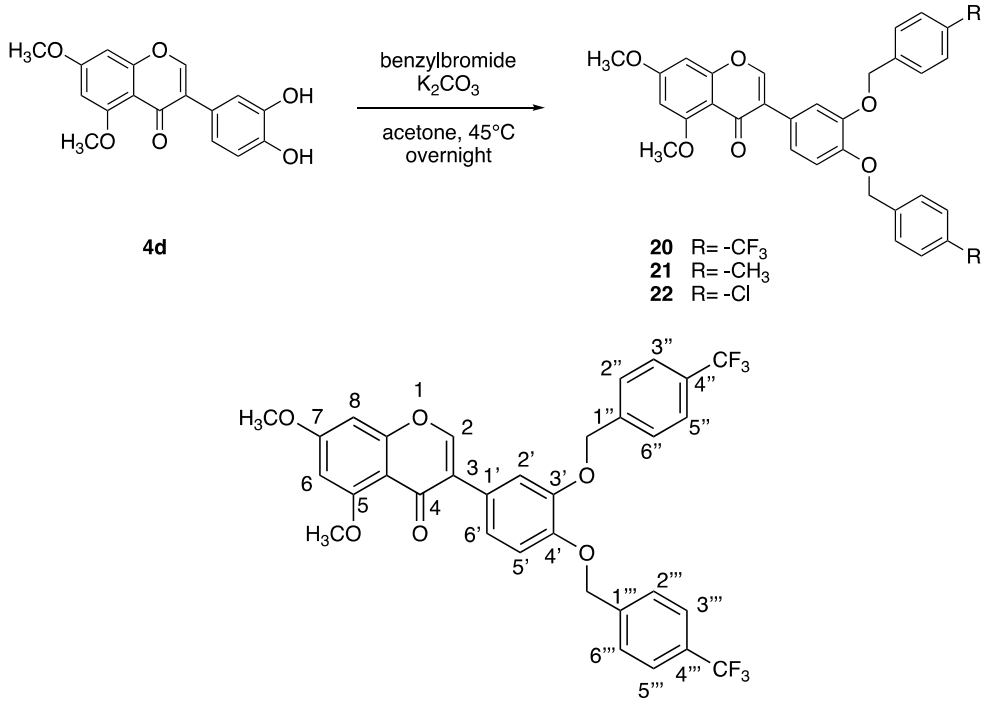

3-(3,4-bis((4-(trifluoromethyl)benzyl)oxy)phenyl)-5,7-dimethoxy-4H-chromen-4-one (**20**)

White solid (Yield 65%) mp: 182-184°C ^{1}H NMR (400 MHz, $CDCl_3$) δ 7.74 (s, 1H, H-2), 7.65-7.52 (m, 8H, H-2′′, H-2′′′, H-3′′, H-3′′′, H-5′′, H-5′′′, H-6′′, H-6′′′), 7.38 (d, *J* = 1.7 Hz, 1H, H-2′), 7.00 (dd, *J* = 8.3, 1.8 Hz, 1H, H-6′), 6.93 (d, *J* = 8.3 Hz, 1H, H-5′), 6.43 (d, *J* = 2.2 Hz, 1H, H-6), 6.37 (d, *J* = 2.2 Hz, 1H, H-8), 5.23 (s, 2H, CH_2), 5.22 (s, 2H, CH_2), 3.95 (s, 3H, OCH_3), 3.89 (s, 3H, OCH_3). ^{13}C NMR (100 MHz, $CDCl_3$): δC 173.42, 164.73, 161.07, 157.91, 149.01, 147.98, 140.93, 132.25, 128.85, 127.68, 125.45, 125.19, 124.94, 122.82, 121.45, 120.38, 116.09, 116.40, 113.40, 109.21, 96.65,94.94,71.53,56.52, 55.96. ESI-MS(*m*/*z*): $[M+H]^+$calcd. for $C_{33}H_{25}F_6O_6$, 631.1; found, 631.3.

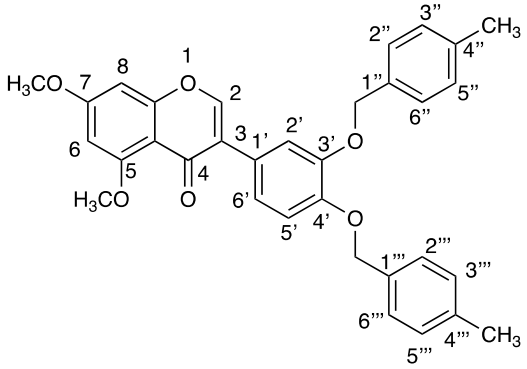

3-(3,4-bis((4-methylbenzyl)oxy)phenyl)-5,7-dimethoxy-4H-chromen-4-one (**21**)

Pale Brown Solid (Yield 70%); mp: 148.0-153.8 °C; ^{1}H NMR (400 MHz, $CDCl_3$): δH 7.70 (s, 1H, H-2), 7.38-7.28 (m, 5H, H-2′, H-2″, H-2‴, H-6″ and H-6‴), 7.16 (d, *J*=7.9 Hz, 4H, H-3″, H-3‴, H-5″, H-5‴),, 6.98 (dd, *J* = 8.3 Hz, *J* = 2.0 Hz, 1H, H-6′), 6.93 (d, *J* = 8.3 Hz, 1H, H-5′), 6.43 (d, *J* = 2.3 Hz, 1H, H-6), 6.37 (d, *J* = 2.3 Hz, 1H, H-8), 5.14 (s, 2H, CH_2), 5.3 (s, 2H, CH_2), 3.94 (s, 3H, OCH_3), 3.88 (s, 3H, OCH_3), 2.35 (s, 6H, CH_3); ^{13}C NMR (100 MHz, $CDCl_3$): δC 175.45, 163.98, 161.60, 159.96, 150.37, 149.07, 148.84, 137.51, 137.48, 134.47, 129.24, 129.20, 127.71, 127.49, 125.97, 125.55, 122.14, 116.50, 115.02, 110.06, 96.31, 92.64, 71.39, 71.33, 56.52, 55.85, 21.34. ESI-MS (m/z): $[M+H]^+$calcd. for $C_{33}H_{31}O_6$, 523.59; found, 523.60

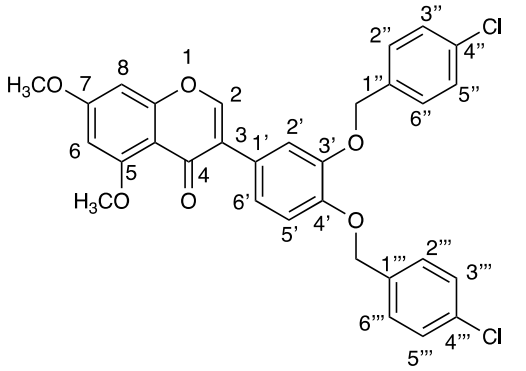

3-(3,4-bis((4-chlorobenzyl)oxy)phenyl)-5,7-dimethoxy-4H-chromen-4-one (**21**)

Pale Yellow Solid (Yield 90%); mp: 158.0-160.0 °C; ^{1}H NMR (400 MHz, $CDCl_3$): δH 7.73 (s, 1H, H-2), 7.42-7.29 (m, 9H, H-2′, H-2″, H-2‴, H-3″, H-3‴, H-5″, H-5‴, H-6″ and H-6‴), 6.98 (dd, *J* = 8.0 Hz, *J* = 1.2 Hz, 1H, H-6′), 6.93 (d, *J* = 8.3 Hz, 1H, H-5′), 6.44 (d, *J* = 2.0 Hz, 1H, H-6), 6.37 (d, *J* = 2.0 Hz, 1H, H-8), 5.13 (s, 2H, CH_2), 5.11 (s, 2H, CH_2), 3.94 (s, 3H, OCH_3), 3.89 (s, 3H, OCH_3); ^{13}C NMR (101 MHz, $CDCl_3$) δ 175.41, 164.09, 161.62, 159.99, 150.45, 148.71, 148.54, 135.90, 135.88, 133.73, 133.70, 128.93, 128.79, 128.75, 126.04, 125.77, 122.27, 116.61, 114.99, 110.04, 96.40, 92.72, 70.75, 70.73, 56.57, 55.88. ESI-MS(m/z): $[M+H]^+$calcd. for$C_{31}H_{25}Cl_2O_6$, 563.42; found, 563.43

Compound 20

^{1}H NMR (400 MHz, $CDCl_3$)

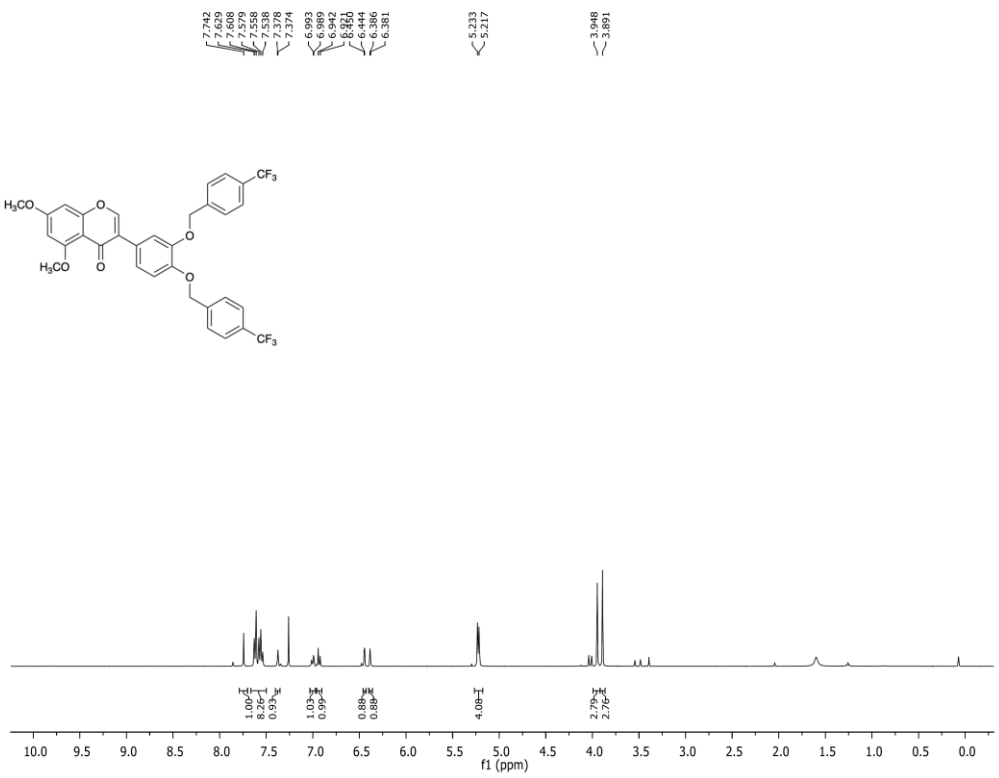

Compound 21

^{1}H NMR (400 MHz, $CDCl_3$)

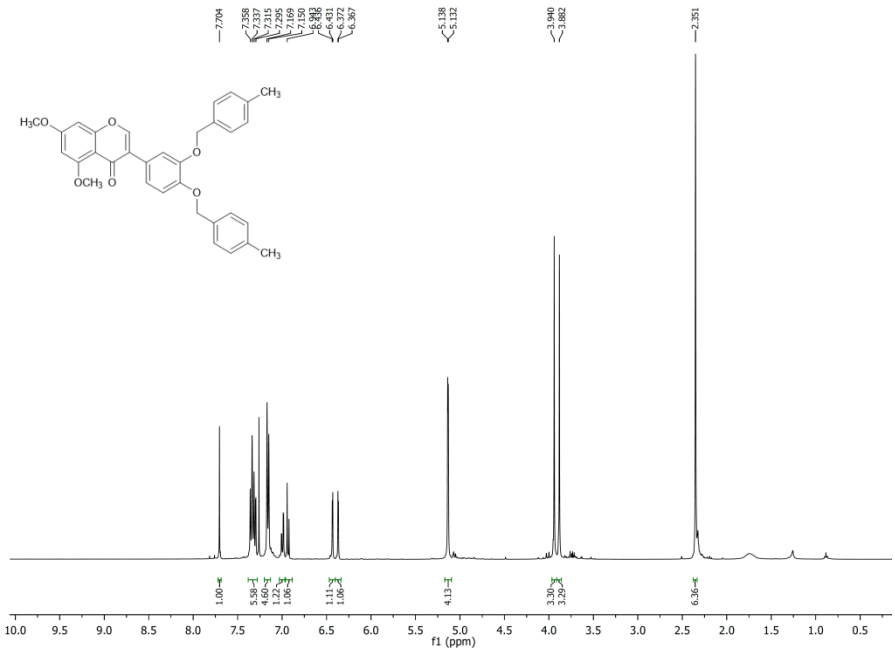

Compound 22

^{1}H NMR (400 MHz, $CDCl_3$)

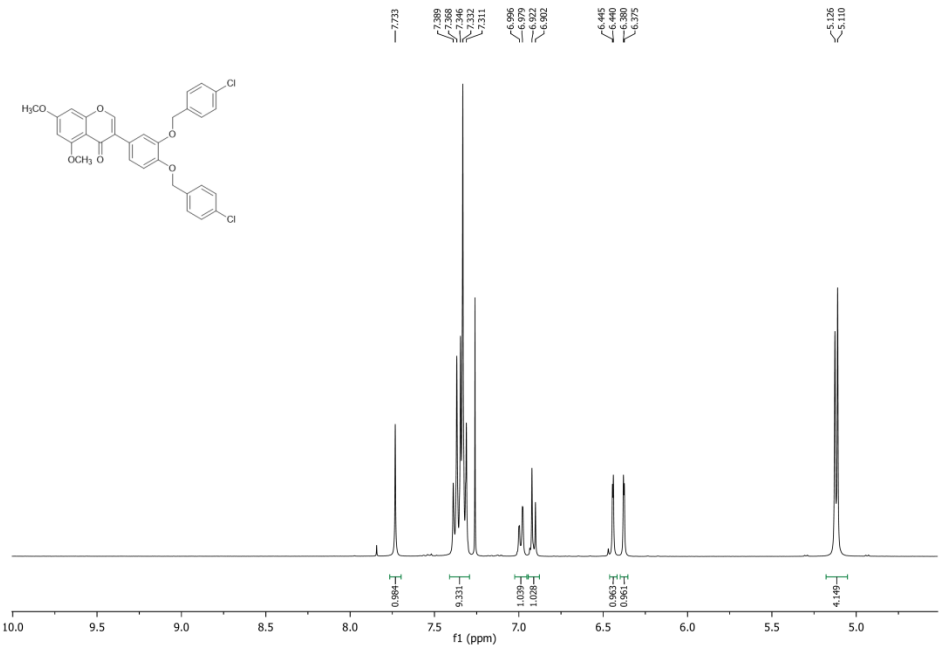

Figure S2. General procedure for the synthesis of compounds 20-22. Characterization of compounds 20-22.

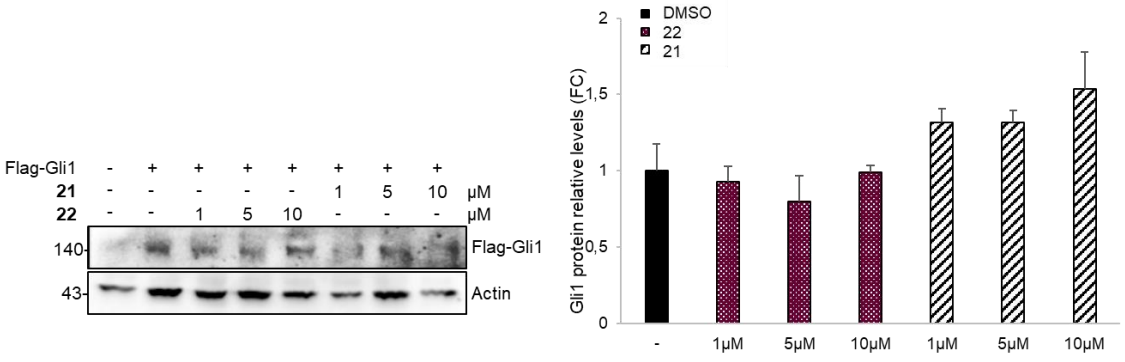

Figure S3. Effect of compounds **21** and **22** on overexpressed Gli1 protein. MEFs WT were transfected with Flag-tagged Gli1 or empty vector, then treated with DMSO only or increasing concentrations of compounds **21** and **22**. The graph shows densitometric analysis ± S.D.

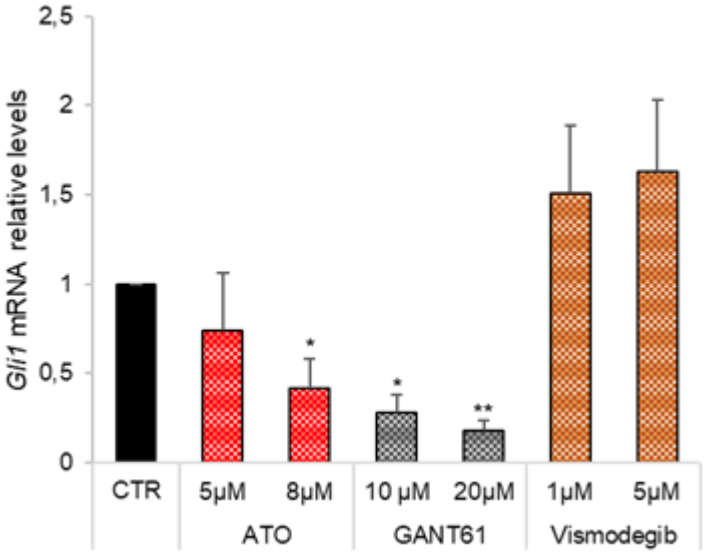

Figure S4. Effect of ATO, GANT61 and Vismodegib on *Gli1* mRNA levels in $Smo^{-/-}$ MEFs. Data show means ± S.D of three independent experiments. (*) $p < 0.05$, (**) $p < 0.01$ vs. CTR.

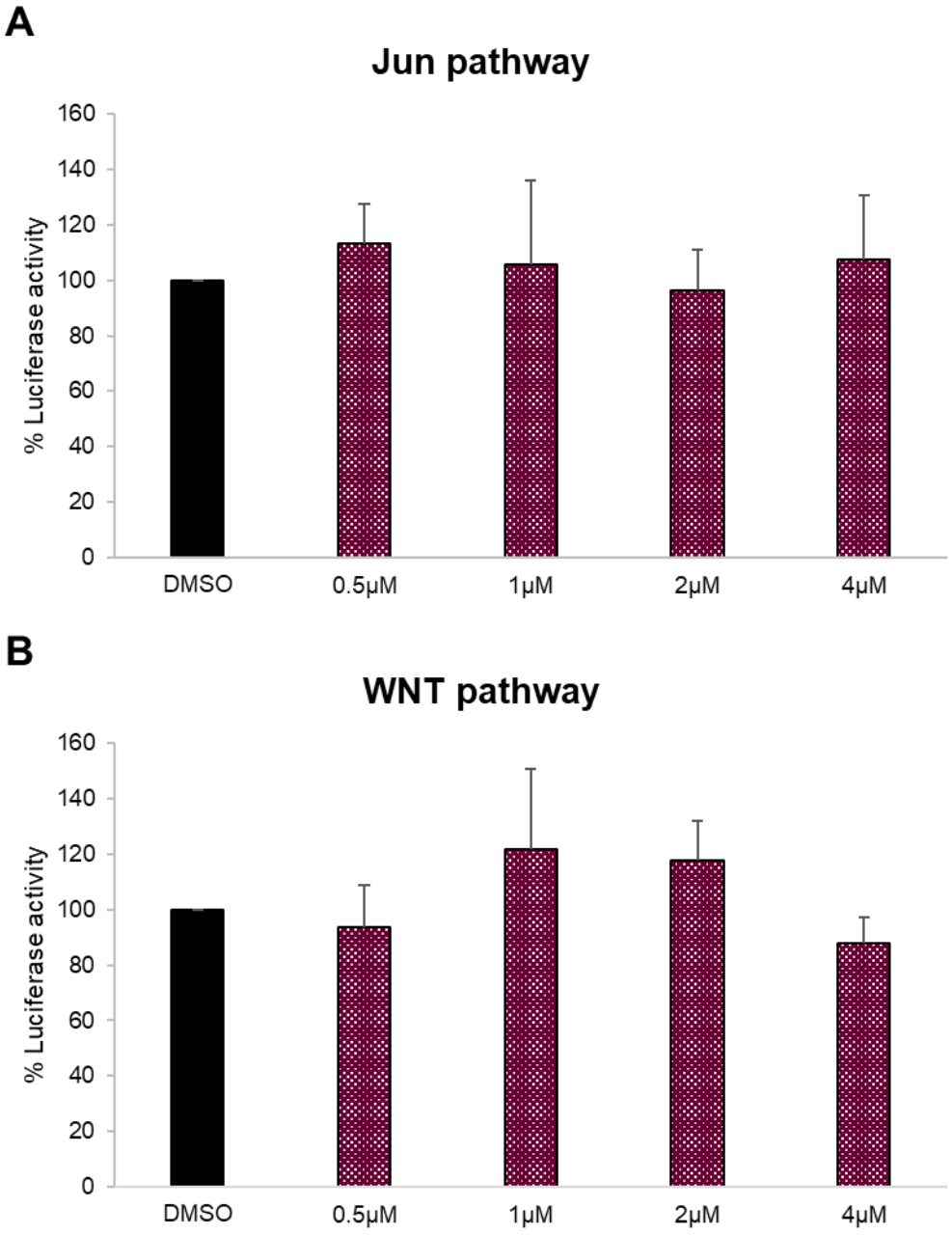

Figure S5. Compound **22** does not affect Jun and WNT pathways. Luciferase assays were performed in MEFs WT co-transfected with MMP1- or TopFlash-luciferase reporter and c-Jun or β-catenin to assay Jun and WNT pathway activity, respectively. 24 h after transfection cells were treated with DMSO only or increasing concentrations of compound **22**. Specific luciferase activities were normalized to Renilla luciferase reporter. Data show means ± S.D of three independent experiments.

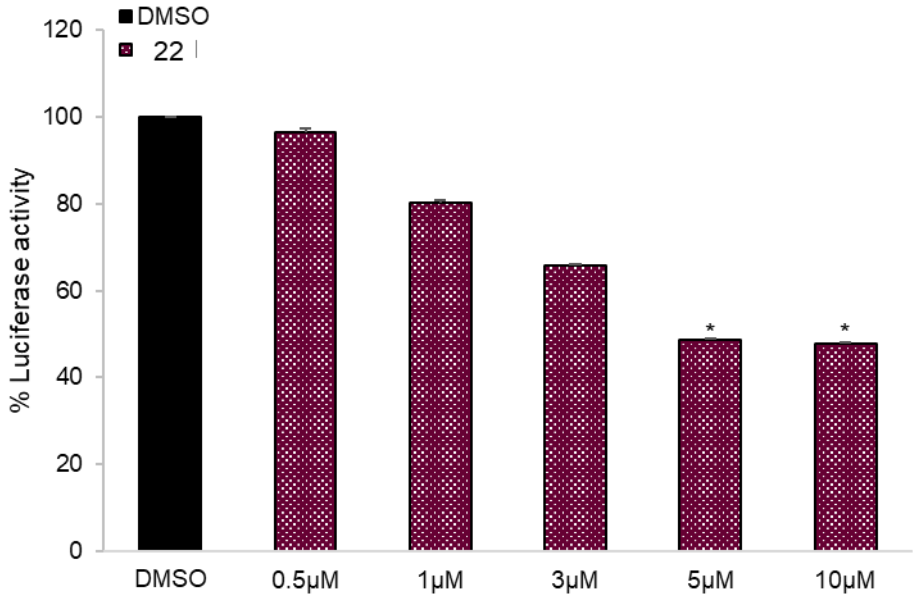

Figure S6. Inhibition of Gli2-induced transcription in MEFs WT treated with increasing concentrations of compound **22**. Luciferase assay was performed in MEFs WT transfected with 12XGliBS-Luc and pRL-TK Renilla (as normalization control) plus empty vector or Gli2 WT; 24 h after transfection cells were treated with DMSO only or increasing concentrations of compound **22**. Luciferase activity was analyzed 24 h after treatment. Data show the mean ± SD of three independent experiments. (*) $p < 0.05$ vs. DMSO.

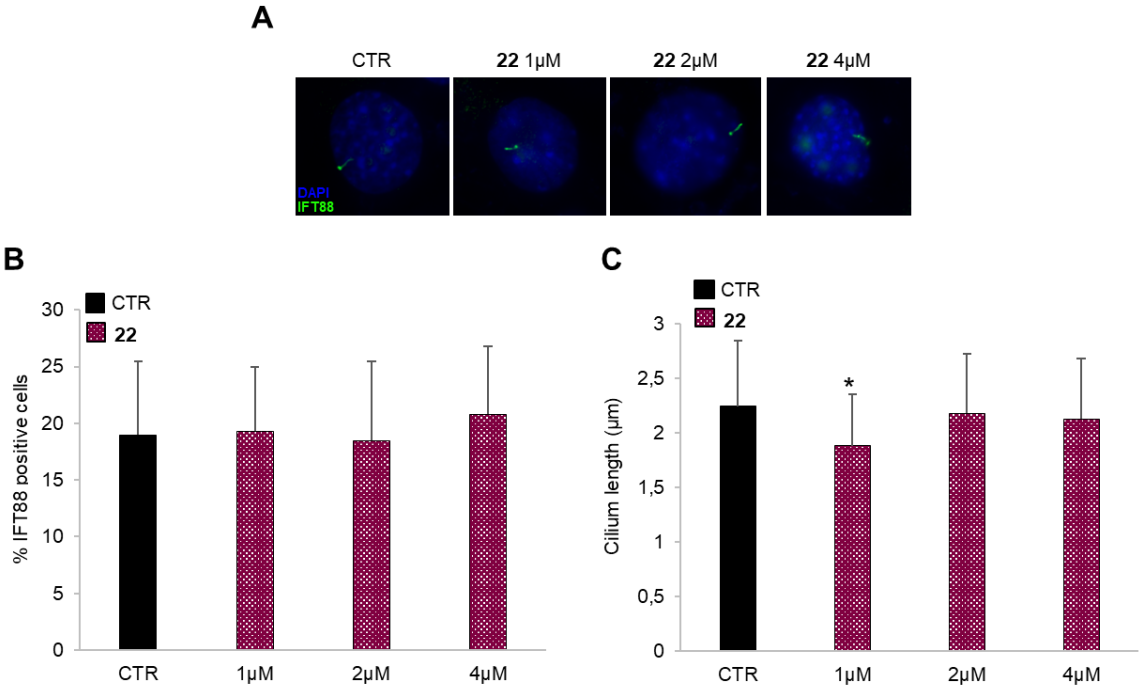

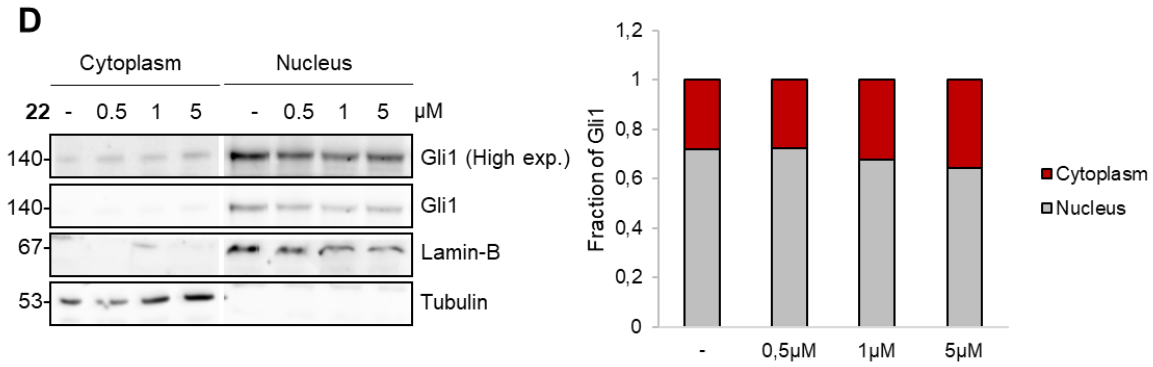

Figure S7. Effect of compound **22** on ciliogenesis and Gli1 localization. (**A-C**) Compound **22** does not affect ciliogenesis. MEFs WT were incubated in the presence or absence of **22** at different concentrations for 24 h, as indicated. Cells were stained for the cilium marker IFT88 and DAPI (**A**), and the number (**B**) and length of cilia (**C**) were quantified from immunofluorescence images. Data shown mean ± S.D. of three independent experiments. (*) $p < 0.05$ vs. CTR. (**D**) Compound **22** does not affect Gli1 subcellular localization. Subcellular fractions were obtained from murine Med-1 MB cells treated with DMSO or increasing concentrations of compound **22**. Lamin-B and Tubulin were used as nuclear and cytoplasmic markers, respectively. The fraction of Gli1 in the cytoplasm or nucleus for each concentration is plotted on the right.

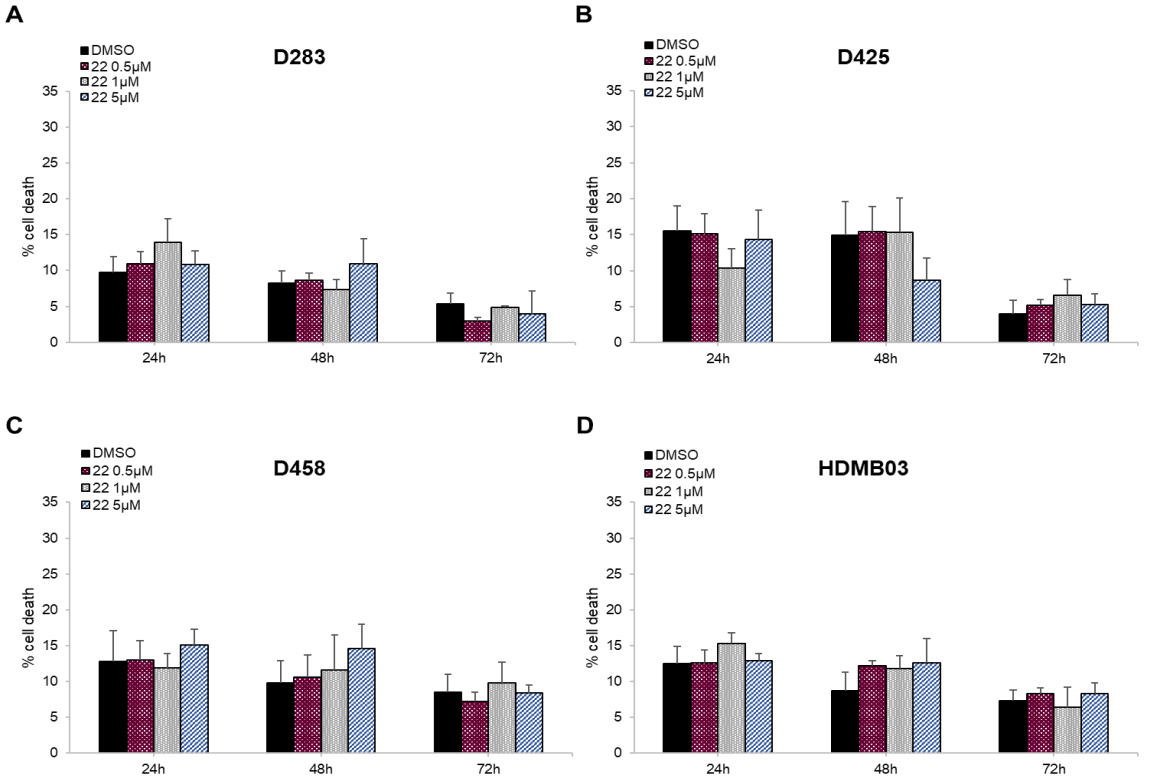

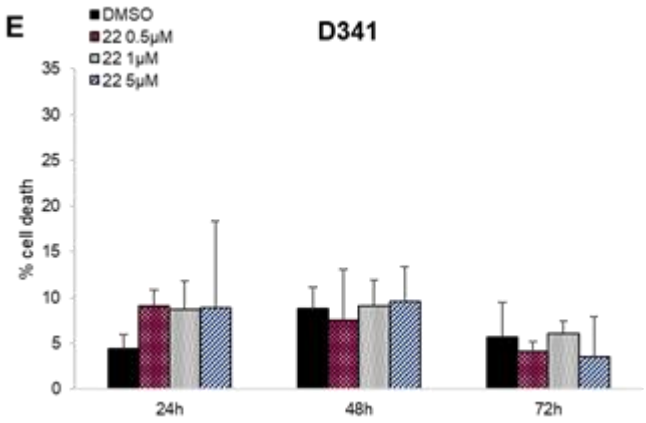

Figure S8. Effect of compound **22** on Hedgehog-independent MB cell lines. MB cells belonging to Group3 (D425, D458, HDMB03, D341) and Gropu3/4 (D283) were treated with DMSO only or increasing concentrations of compound **22**. A trypan blue count was performed after 24–48–72 h of treatment to determine the cytotoxic effects of compound **22**. Data shown mean ± S.D. of three independent experiments.

Table S1. Effect of compounds **21** and **22** on *Gli1* mRNA levels in $Smo^{-/-}$ MEFs. Fold change ($2^{-\Delta Ct}$) is normalized to *Hprt* gene expression.

Treatment	Gli1 Ct Mean	ΔCt Mean	Mean Fold change
DMSO	28.82	7.91	1 ± S. D.
21 1 μM	29.22	8.55	0.68 ± S. D.
21 2 μM	29.64	8.74	0.58 ± S. D.
22 1 μM	29.42	8.51	0.67 ± S. D.
22 2 μM	30.34	9.33	0.37 ± S. D.

4 | DISCUSSION AND CONCLUSIONS

I hadn't been aware that there were doors closed to me
until I started knocking on them.
[Gertrude B. Elion, Nobel Prize in Physiology or Medicine]

Paediatric tumours have long been known to be distinct from adult cancers in terms of epidemiology, cellular origins, response to therapy, etc. However, it is only in the era of widespread genome-wide profiling that we are now approaching a full realization of just how heterogeneous and distinct these childhood cancers are at molecular and genetic level. Large-scale analyses of paediatric malignancies have demonstrated differences in mutation frequencies and signatures as well as in classes of driving events (Gröbner et al., 2018). The contribution of genetic predisposition is also particularly important in this patient population, likely being involved in at least 10% of cases (Brodeur et al., 2017), slightly higher than the ~8% estimated for adult cancers (Huang et al., 2018). However, it must be acknowledged that the number of potentially "druggable" targets that can be acted upon at present remains disappointingly low. The tumor-intrinsic drug targets in paediatric solid tumours can be grouped largely according to some of the hallmarks of cancer (Hanahan and Weinberg, 2011). Developmental pathways and epigenetic modifiers are of specific interest in paediatric tumors since several embryonal cancers originate from precursor cells arrested in an early developmental stage by aberrations in genes that regulate transcriptional networks. MB is a clear example, because subsets of this tumor are dependent by activating events in Hh or WNT pathways.

MB is the most common malignant solid tumor in childhood. Current therapies, even if have improved the overall survival of patients, consist of aggressive treatments with short- and long-term adverse side effects devastating for children. Improved knowledge of MB has given rise to a new and detailed classification of MB subgroups which may lead, in the future, to a better stratification of the patients based on the molecular characteristics of their tumor, thus moving towards a personalized therapy. To achieve this goal, a deeper molecular profiling of each tumor becomes necessary after the biopsy or surgery.

Signalling pathways whose deregulations are implicated in the onset of different subgroups of MB, such as the Hh signalling, have been identified and represent an attractive "druggable" target in MB treatment.

For this reason, the elucidation of regulatory events that modulates Hh activity, the identification of new molecular players involved in Hh pathway regulation, as well as the synthesis of new drugs able to impair signalling activation are fields of clinical importance and represent dramatic challenges in tumor biology.

In this work, we addressed all this relevant points. First, we started from what is known but still needs to be clarified.

SuFu is a tumour suppressor gene and negative regulator of Hh signalling; it is localised in both the cytoplasm and the nucleus and controls the Hh pathway by binding directly to GLI transcription factors (Pearse et al., 1999; Stone et al., 1999). SuFu-GLI3 complex has emerged as a major control node in Hh signalling in the last years; however, how the integrity of this complex is maintained and how SuFu is regulated is still poorly understood.

We revealed the non-proteolytic ubiquitylation of the tumor suppressor SuFu, mediated by the HECT E3-ubiquitin ligase Itch in complex with the adaptor protein β-arrestin2, as a novel mechanism that inhibits the Hh signalling pathway. Itch/β-arrestin2-dependent K63-linked poly-ubiquitylation of SuFu on K321 and K457 does not trigger SuFu degradation; instead, it increases the association of SuFu-GLI3 complex driving the synthesis of GLI3R, which in turn inhibits signal transduction. Alterations of this process, caused by SuFu mutations that make it insensitive to Itch-mediated ubiquitylation, contribute to the pathogenesis of MB (**Figure 21**).

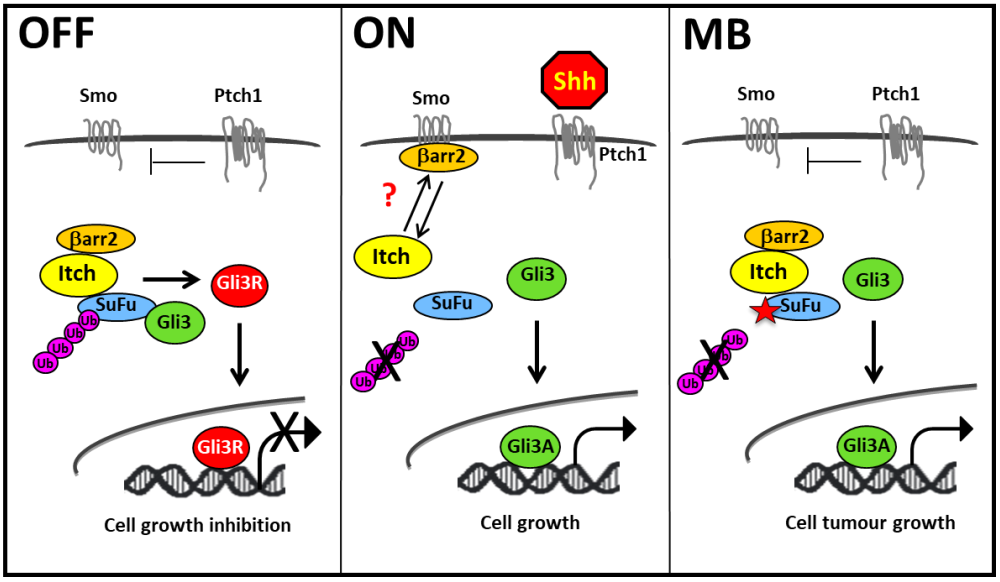

Figure 21 | *Model showing the Itch/β-arrestin2-dependent regulation of the SuFu/Gli3 complex function.* When Hh pathway is off, Itch, coadjuvated by the protein adaptor β-arrestin2, ubiquitylates SuFu. This event does not lead to SuFu degradation but increases the association between SuFu and GLI3. In this way GLI3 is protected from SPOP-dependent degradation and is cleaved into a repressor form (GLI3R) that inhibits Hh target gene transcription and cell growth. When Hh pathway is switched on, β-arrestin2 dissociates from the SuFu/Itch complex, thus abrogating Itch-dependent SuFu ubiquitylation. This process induces the dissociation of SuFu-GLI3 complex and impairs GLI3R formation, thereby leading to Hh pathway activation and sustaining cell growth. Alterations in this mechanism, caused by SuFu mutations that make it insensitive to Itch-dependent ubiquitylation, are responsible for MB tumorigenesis (Infante et al., 2018).

Furthermore, we directed our study toward a more challenging goal: to expand the list of key components and regulators of Hh pathway that could represent new targets for Hh-driven tumor treatment. In particular, we characterized the oncogenic property of ERAP1 and SALL4A in regulating Hh-dependent tumorigenesis.

ERAP1 is known and well studied for its immunological functions: it has been described to shape the peptide repertoire presented by MHC class I molecules, playing a role in immunity, inflammation or blood pressure. The role of ERAP1 in tumorigenesis is still controversial: while its loss is a frequent event and is associated with the lack of detectable MHC class I surface expression, potentially contributing to tumor immunoescape, analysis of ERAP1 expression in human neoplastic lesions has revealed

that this enzyme can be lost, acquired or retained as compared to the normal counterparts, depending on the tumor type (Fruci et al., 2008).

Our data demonstrate that ERAP1 has a positive role in Hh signalling regulation by sequestering the deubiquitylase USP47 and promoting βTrCP ubiquitylation and degradation. Of note, all GLI transcription factors undergo ubiquitylation processes and deregulations of these events result in uncontrolled cell proliferation and tumorigenesis (Huntzicker et al., 2006). The $SCF^{\beta TrCP}$-ubiquitin ligase complex is a RING E3-ubiquitin ligase important in the regulation of GLIs; indeed, βTrCP degradation leads to an accumulation of GLI1 and GLI2 proteins and a reduction of the GLI3R form, thus activating the Hh pathway.

Our study reveals an unexpected function of ERAP1 in cancer development suggesting that targeting this aminopeptidase could open innovative perspectives for effective therapeutic approaches in the treatment of Hh-dependent tumors (**Figure 22**).

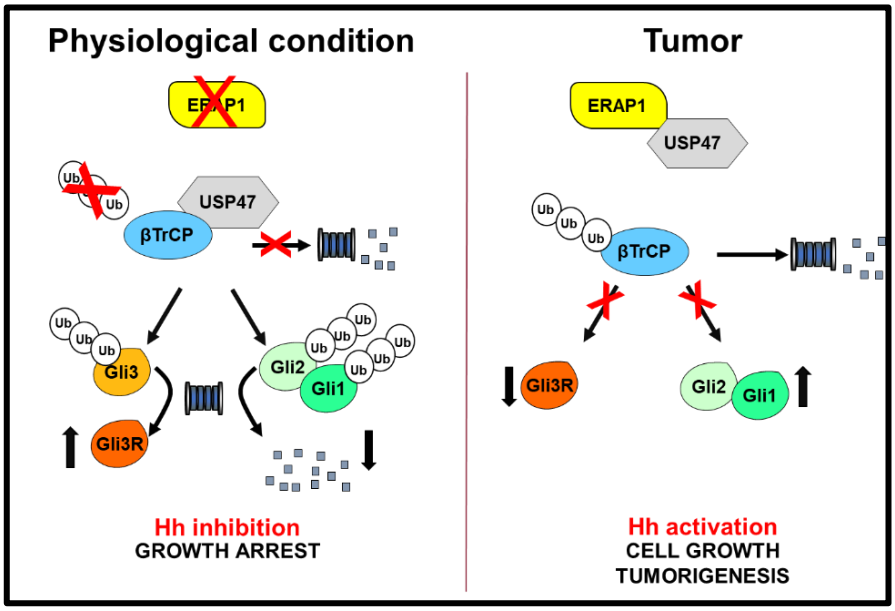

Figure 22 | *Model showing the role of ERAP1 in Hh-dependent tumorigenesis.* ERAP1 promotes ubiquitylation and proteasomal degradation of βTrCP by sequestering USP47. This event leads to increase of GLI1 and GLI2 protein levels and decrease of GLI3R, thus triggering the Hh pathway and favouring cell growth and tumorigenesis. In the absence of ERAP1, USP47 binds and stabilizes βTrCP, which in turn promotes ubiquitylation and proteasomal degradation of GLI1 and GLI2, and ubiquitylation and proteolytic cleavage of GLI3 into the repressor form GLI3R. These events lead to the repression of the Hh pathway and inhibition of cell proliferation and tumor growth (Bufalieri et al., 2019).

Transcription factors are generally considered as challenging targets in drug discovery for different reasons, including the lack of deep hydrophobic pockets that accommodate small molecules and the highly charged surface. Nevertheless, big pharmaceutical companies are currently running Phase I clinical trials with small molecules targeting transcription factors such as Notch (BristolMyers Squibb and Ely Lilly) and p53 (Roche and Sanofi), although no drugs have been approved yet by the FDA.

The main focus of my research activity concerned the study of the transcription factor SALL4A. The driving aim was to identify new interactors of REN^{KCTD11}, a tumor suppressor and negative regulator of Hh signalling that resides on chromosome 17p, a region that is frequently deleted in human MBs. REN^{KCTD11} is an adaptor protein of Cul3, a component of the SCF-like E3-ubiquitin ligase complex, able to recruit substrates and to promote Cul3-dependent ubiquitylation.

Starting from mass spectrometry analysis performed in HEK293T cells, we identified SALL4A as a new interactor of REN^{KCTD11} and we investigated how this interaction could affect Hh signalling activity.

SALL4A is a zinc finger transcription factor that maintains the self-renewal and pluripotency of embryonic stem cells (Zhang et al., 2006). Its expression gradually decreases during development and is even absent in most adult tissues (Oikawa et al., 2013). However, recent findings show that SALL4A is re-expressed in cancer; the current state-of-the-art makes this transcription factor a very appealing target for our research.

Confirming SALL4A/REN^{KCTD11} binding and identifying that the C-terminal domain of REN^{KCTD11} (but not the N-terminal BTB/Poz domain required for Cul3-binding) is involved in this interaction, we next demonstrated through *in vivo* ubiquitylation assays that the Cul3/REN^{KCTD11} E3-ubiquitin ligase complex promotes the ubiquitylation of SALL4A, that is then directed to a proteasome-mediated degradation.

Investigating the biological role of SALL4A in Hh pathway, we observed that it induces GLI1 transcriptional activity. Data from literature report the ability of SALL4A to interact

with the NuRD complex, which includes HDAC1 deacetylase (Zhang et al., 2014); this notion gave us an important hint in the design and development of our research plan. Indeed, we previously demonstrated that HDAC1 is a powerful Hh signalling activator (Canettieri et al., 2010) because able to deacetylate GLI1 thus enhancing its transcriptional activity.

So, we hypothesized that HDAC1 could require SALL4A to carry out its function. We interestingly observed that SALL4A binds both HDAC1 (thus confirming data from literature) and GLI1, and the presence of all the three proteins significatively strengthens their binding affinity. Moreover, the positive effect of SALL4A on GLI1 activity increases in presence of HDAC1, whereas the acetylation state of GLI1 decreases in presence of SALL4A, similarly to HDAC1-induced effect.

Biochemical and biological data sustain our idea that SALL4A/HDAC1/GLI1 axis is a novel and important mechanism in Hh signalling regulation: we hypothesize that, following the activation of the Hh pathway, SALL4A binds HDAC1 and recruits it on GLI1, promoting its deacetylation and transcriptional activity; conversely, in absence of the Hh signal, the Cul3/REN^{KCTD11} E3 ubiquitin-ligase complex induces the ubiquitylation and proteasome-dependent degradation of both SALL4A and HDAC1 (Canettieri et al., 2010), thereby strongly suppressing the Hh pathway (**Figure 23**).

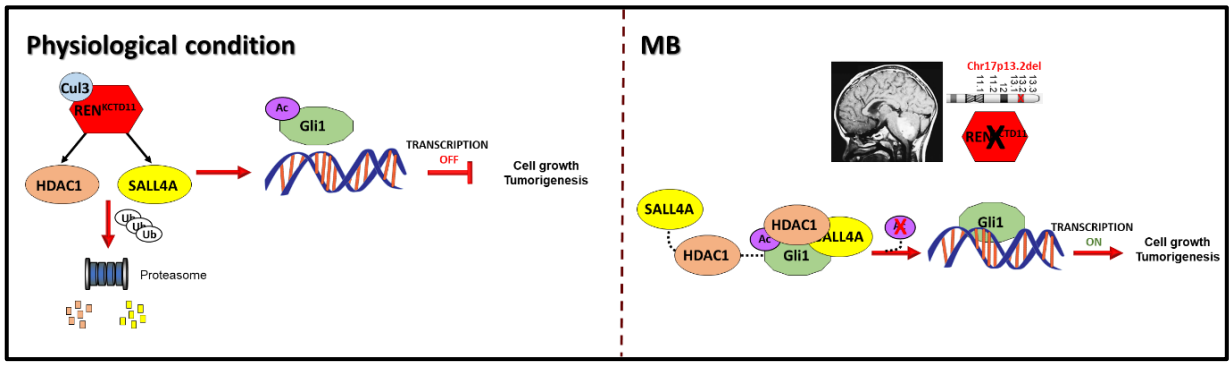

Figure 23 | *Model showing the role of SALL4A/HDAC1/GLI1 axis in Hh-dependent tumorigenesis.* Under physiological condition, SALL4A and HDAC1 are bound by the Cul3/E3-ubiquitin ligase REN^{KCTD11}, and their proteasome-dependent degradation is induced. In this context, GLI1 maintains its acetylation state and its transcriptional activity is abrogated. These post-translational events lead to the repression of the Hh pathway and inhibition of cell proliferation. In MB, loss of REN^{KCTD11}, occurring with chromosome 17p deletion (the most frequent genetic

lesion observed in this tumor), leads to an accumulation of SALL4A and HDAC1. In this context, SALL4A works as carrier protein able to bring HDAC1 close to GLI1; HDAC1 deacetylates GLI1, thus triggering the Hh pathway. Abrogation of GLI1 acetylation sustains cellular proliferation and transformation (Lospinoso Severini et al., manuscript in preparation).

Of note, *in vivo* experiments support the new role identified for SALL4A and its relevance as new molecular target in MB treatment. We demonstrated that SALL4A over-expression enhances the proliferation ability of human MB cell lines, while its depletion impairs their migration. Also in allograft and orthotopic MB mouse models, we observed that SALL4A genetic depletion strongly inhibits tumor growth.

In conclusion, the developmental processes that are hijacked by the tumor cells might represent novel classes of potential vulnerabilities specific to paediatric solid tumors that deserve further exploration (Lin et al., 2016). The information gathered from these projects increase our knowledge about the critical nodes that can be targeted for the treatment of Hh-driven tumors, i.e. MB.

Hh regulation is certainly relevant to propose new key components that can be targeted in clinic, but in childhood brain tumors treatment a second critical challenge is the discovery of drugs able to block Hh pathway at a downstream level. The rationale for the development of these pharmacological agents is based on (i) the heterogeneity of molecular defects sustaining Hh signalling activation; and (ii) the need to overcome the resistance to clinically available SMO antagonists.

Vismodegib is a direct, cyclopamine-competitive antagonist of SMO. A recent analysis of pooled data from patients with advanced-stage BCC, included in the pivotal phase II that led to FDA approval and phase I studies, indicates that a median overall survival duration of 2.8 years was achieved in patients with metastatic BCC who received Vismodegib monotherapy, compared with 2.0 years estimated from the literature for standard treatments. However, in contrast to data observed in BCC, studies in glioblastoma did not show compelling clinical efficacy of Vismodegib as a single agent, because the median progression-free survival (PFS) and overall survival durations of

patients were comparable to the control groups of historical studies (Sachs and Clevers, 2014).

To date, clinical efficacy of SMO inhibitors has not been demonstrated in trials, except in patients with tumors driven by mutations in components of the Hh signalling cascade, such as SMO and PTCH1 (Von Hoff et al., 2009). Possible reasons for primary resistance to Hh inhibitor monotherapy and the lack of additional efficacy or benefit in combination with chemotherapy, compared with the outcomes of chemotherapy alone, may be due to compensatory upregulation mechanism of Hh signalling. For example, primary resistance to SMO inhibitors can be due to non-canonical activation of GLI transcription factors through pathways that bypass SMO and, therefore, the effects of SMO inhibitors (Ramaswamy et al., 2012).

However, only the GLI antagonist Arsenic trioxide (ATO) has entered clinical evaluation so far; that's why innovative, more effective and less toxic Hh antagonists are urgently needed.

Good premises are hold by small molecules having a direct action on GLI1/DNA interaction, which showed remarkable efficacy *in vivo*, as well as by the combination of multiple agents in a multitarget strategy. In this respect, a single compound able to target simultaneously SMO and GLI1 is expected to provide extraordinary clinical outcomes compared to single-agent treatments.

Natural compounds represent a significant resource for the discovery and development of new Hh inhibitors, as demonstrated for isoflavones, derived from plants of the *Leguminosae* family (Ko, 2014). In a recent study, our team exploited the high versatility of the isoflavone scaffold demonstrating that the introduction of bulky chemical groups in the *para* position of the isoflavone's ring B enhances the targeting at the level of the SMO receptor. In contrast, bulky substitutions introduced in the *meta* position of the same ring promote the targeting of the downstream GLI effectors. Simultaneous administration of isoflavones targeting SMO and GLI1 provided synergistic Hh pathway inhibition with a reduction of around 20 folds of the administered dose, which might be

relevant to limit toxic side effects and overcome the SMO-drug resistance (Berardozzi et al., 2018).

I used these data as starting point to achieve the second goal of my research activity: the synthesis and validation of a single multitarget molecule able to inhibit Hh signalling acting both upstream and downstream of the oncogenic pathway at the same time. By combining the most profitable pharmacophores for targeting SMO and GLI1 by synthetic isoflavones, we designed and synthesized the isoflavone 22 acting as a multitarget Hh inhibitor. Compound 22 is able to inhibit Hh-dependent tumor growth in human and murine MB cells at sub-micromolar concentration, as a consequence of the reduction in GLI1 expression levels, and to suppress tumor progression *in vivo* by hindering cell proliferation and promoting apoptosis (**Figure 24**). Overall, these results reveal a valuable form of targeted therapy to increase efficacy and to decrease the toxicity of individual anticancer agents.

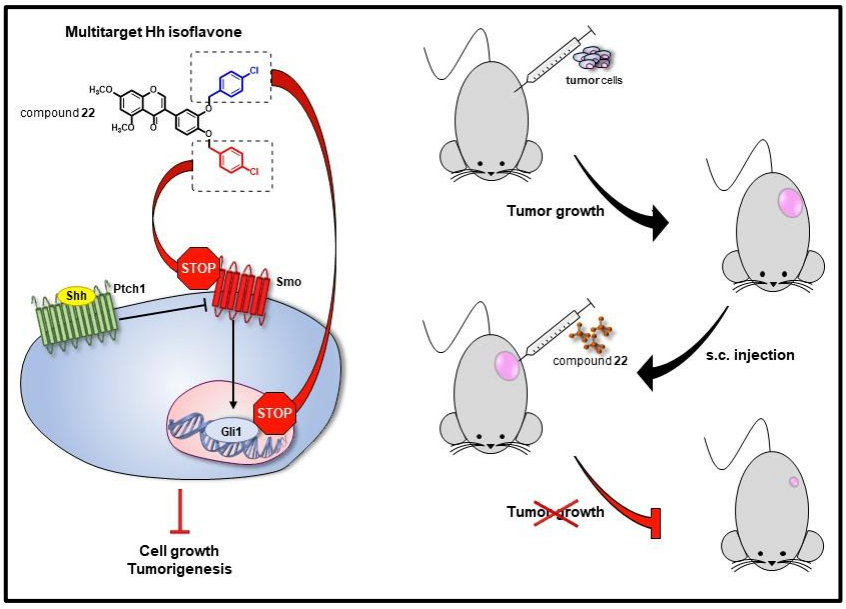

Figure 24 | *Model showing the chemical structure of isoflavone 22 and its capability to impair Hh-dependent tumor growth in vivo.* We designed a modified isoflavone bearing specific substitutions at *para* or *meta* position of ring B that are preferred for the interaction with SMO or GLI1, respectively. We demonstrated that this small molecule, compound 22, is able to target the Hh pathway at both upstream and downstream level simultaneously, leading to a marked tumor growth inhibition in a model of Hh-dependent cancer (Lospinoso Severini et al., 2019).

In conclusion, results obtained from this study provide a significant support in oncology research for the identification of novel therapeutic target and the development of new clinically relevant Hh inhibitors for the treatment of Hh-driven tumors.

5 | MATERIALS AND METHODS

5.1 | Cell cultures, transfections and lentiviral infections

HEK293T (CTR-3216TM, obtained from the American Type Culture Condition, ATCC), MEFs from wild-type (WT) mice, D425 and HD-MB03 (kindly provided by V. D'Angiolella) were cultured in Dulbecco's Modified Eagle's Medium (DMEM) plus 10 % fetal bovine serum (FBS). Daoy cells (obtained from ATCC) were cultured in Eagle's minimum essential medium (MEM) plus 10% FBS. D458 and D283 (kindly provided by V. D'Angiolella) were maintained in Eagle's minimum essential medium (MEM) plus 20 % FBS. All media contained 1% L-glutamine and 1% antibiotics (penicillin–streptomycin). For cerebellar GCPs culture from 5-days old mice, cerebella were removed aseptically, cut into small pieces, and incubated at room temperature for 15 minutes in digestion buffer [Dulbecco's PBS (Invitrogen, Gaithersburg, MD) with 0.1% trypsin, 0.2% EDTA, and 10μg/ml DNase]. Tissues were then triturated with fire-polished Pasteur pipettes to obtain a single-cell suspension. Cells were centrifuged and resuspended in Neurobasal medium supplemented with B27 (2%), penicillin–streptomycin (1%) and L-glutamine (1%) (Invitrogen) and plated at a density of 8×10^5 cells/cm^2. Primary MB cells were freshly isolated from Ptch$^{+/-}$ mice. Briefly, tumor was mechanically disrupted with fire-polished Pasteur pipettes in HBSS with 1% penicillin–streptomycin and treated with DNase (10μg/ml) for 20 minutes. Cells were centrifuged and resuspended in Neurobasal Media-A with B27 supplement minus vitamin A, 1% penicillin–streptomycin and 1% L-glutamine. Mycoplasma contamination in cell cultures was routinely detected by using PCR detection kit (Applied Biological Materials, Richmond, BC, Canada). Transient transfections were performed using DreamFect™ Gold transfection reagent (Oz Biosciences SAS, Marseille, France) or Lipofectamine® with Plus™ Reagent (Thermo Fisher Scientific, Waltham, MA, USA) in accordance with the manufacturer's protocols. Lentiviral particles were generated in HEK293 cells by combining packaging plasmids pCMV-dR8.74 and VSV-G/pMD2, with pLKO.1 plasmids (shCTR SHC002; shSALL4 TRCN0000097823 (#1), TRCN0000097824 (#2)) using calcium phosphate transfection

method. Daoy cells were infected with purified lentiviruses for 72 h in the presence of 8μg/ml polybrene (Sigma Aldrich, St Louis, MO); primary MB cells were infected with purified lentiviruses for 72 h in the presence of 4μg/ml polybrene.

5.2 | Plasmids, antibodies and other reagents

pcDNA3.1 Flag-Gli1, Flag-HDAC1 and Flag-REN^{KCTD11} expressing vectors were generated in our lab with standard cloning techniques and verified by sequencing. pCDNA3.1 Flag-HDAC1 was subcloned from pBJ5-HDAC1 (S.L. Schreiber, Huntsman Cancer Institute, Salt Lake City, UT). pCDNA3.1 Flag-REN^{KCTD11} ΔPoz or Flag-REN^{KCTD11} ΔC mutants were constructed by deleting amino acids 18–80 or 196–232, respectively.

The following plasmids were kindly provided by other labs: pcDNA3.1 Myc-Cul3 (M. Pagano, New York University School of Medicine, USA), 12 × Gli–RE TKO-Luc (R. Toftgård, Karolinska Institutet, Sweden), pcDNA3.1 HA-Ub (I. Dikic, Institute of Biochemistry Goethe University, Germany), pcDNA3.1 HA-Sall4A (W. Dai, New York University Langone Medical Center, USA). shCTR (SHC002) and shSALL4 (TRCN0000097823, TRCN0000097824) in pLKO.1 plasmids were purchased from Sigma-Aldrich.

Mouse anti-Gli1 (L42B10, 1:500) and rabbit anti-cleaved Caspase-3 (Asp175 D3E9, 1:500) were purchased from Cell Signaling (Beverly, MA, USA). Goat anti-Actin I-19 (sc-1616, 1:1,000), mouse anti-HA-probe F-7 HRP (sc-7392 HRP, 1:1000), mouse anti-Myc 9E10 (sc-40, 1:500), mouse anti-Sall4 G-3 (sc-166033, 2μg), mouse anti-PCNA PC10 (sc-56, 1:1000) and HRP-conjugated secondary antibodies were purchased from Santa Cruz Biotechnology (Santa Cruz, CA, USA). Anti-Flag M2 HRP (A8592, 1:1000) and rabbit anti-Flag (F7425, 2μg) were purchased from Sigma Aldrich (St Louis, MO, USA). Goat anti-Gli2 (AF3635, 1:1000) was purchased from R&D Systems (Minneapolis, MN, USA). Rabbit anti-Sall4 (ab29112, 1:1000) was purchased from Abcam (Cambridge, UK).

Where indicated, cells were treated with SAG (200 nM, Alexis Biochemicals Farmingdale, NY, USA) for 12, 24 or 48 h, MG132 (50μM; Calbiochem, Nottingham, UK) for 4 h, Cycloheximide (CHX 100μg/ml, Sigma Aldrich) for 3 or 6 h.

5.3 | Luciferase reporter assay

The Hh-dependent luciferase assay was performed in MEFs WT transfected with 12 × Gli–Luc luciferase reporter, pRL-TK Renilla and indicated plasmids. 24 h after transfection, Luciferase and Renilla activities were assayed with a dual-luciferase assay system according to the manufacturer's instructions (Biotium Inc., Hayward, CA, USA). Results were expressed as Luciferase/Renilla ratios and represented the mean ± S. D. of three experiments, each performed in triplicate.

5.4 | Immunoblot analysis and immunoprecipitation

Cells were lysed in a solution containing RIPA buffer (50mM Tris-HCl at pH 7.6, 150mM NaCl, 0.5% sodium deoxycholic, 5mM EDTA, 0.1% SDS, 100mM NaF, 2mM NaPPi, 1% NP-40) supplemented with protease and phosphatase inhibitors. The lysates were centrifuged at 13,000 g for 30 minutes at 4 °C and the resulting supernatants were subjected to immunoblot analysis.

Immunoprecipitation was performed using whole cell extracts obtained by lysing cell pellets with Triton Buffer (50mM Tris-HCl pH 7.5, 250mM sodium chloride, 50mM sodium fluoride, 1mM EDTA pH 8, 0.1% Triton), supplemented with protease and phosphatase inhibitors. Cell lysates were immunoprecipitated overnight at 4 °C with rotation with specific primary antibodies or IgG used as a control (1–2µg/ml, Santa Cruz Biotechnology, CA, USA) and then incubated with Protein G- or Protein A-agarose beads (Santa Cruz Biotechnology, CA, USA) for 1 h at 4 °C with rotation. The immunoprecipitates were then washed five times with the lysis buffer described above, resuspended in sample loading buffer, boiled for 5 minutes, resolved in SDS-PAGE and then subjected to immunoblot analysis.

5.5 | *In vivo* ubiquitylation assay

MEFs WT were lysed with denaturing buffer (1% SDS, 50 mM Tris-HCl at pH 7.5, 0.5 mM EDTA, 1 mM DTT) to disrupt protein-protein interactions. Lysates were then diluted 10 times with NETN lysis buffer (100 mM NaCl, 20 mM Tris-Cl pH 8.0, 0.5 mM EDTA, 0.5% (v/v) NP-40) and subjected to immunoprecipitation with anti-Sall4 antibody (Santa Cruz

Biotechonology, CA, USA) overnight at 4 °C with rotation. The immunoprecipitated proteins were then washed five times with the NETN lysis buffer, resuspended in sample loading buffer, boiled for 5 minutes, resolved in SDS-PAGE and then subjected to immunoblot analysis. Poly-ubiquitylated forms were detected using mouse anti-HA from Santa Cruz Biotechnology (CA, USA).

5.6 | mRNA expression analysis

Total RNA was extracted using TRIzol reagent (Thermo Fisher Scientific) and reverse-transcribed with SensiFAST cDNA Synthesis Kit (Bioline Reagents Limited, London, UK). Quantitative real time PCR (qPCR) analysis of Gli1, Gli2, Ptch1, CyclinD1 mRNA expression was performed using the ViiA™ 7 Real-Time PCR System (Life Technologies). Standard qPCR thermal cycler parameters were used to amplify a reaction mixture containing cDNA template, SensiFAST™ Probe Lo-ROX mix (Bioline Reagents Limited) and Taqman Gene Expression Assays (Thermo Fisher Scientific). The average of three threshold cycles was used to calculate the amount of transcript in each sample amplificated in triplicate (using SDS version 2.3 software). mRNA quantification was calculated as the ratio of the sample quantity to the calibrator quantity expressed in arbitrary units. Data were normalized with the endogenous control *Hprt* and expressed as the fold change respect to the control sample value.

5.7 | Proliferation assays

Daoy proliferation was evaluated by BrdU detection (Roche, Welwyn Garden City, UK). Cells were transfected with indicated plasmids for 24 h or infected for 72 h with purified lentiviral particles encoding short hairpin RNA targeting SALL4A (shSALL4A) or a control non-targeting sequence (shCTR). Then, cells were pulsed 24 h with BrdU, fixed and permeabilized with 4% paraformaldehyde and 0.2% Triton X-100, respectively. Nuclei were counterstained with Hoechst reagent and BrdU detection was performed according to the manufacturer's instructions. At least 500 nuclei were counted in triplicate and the number of BrdU-positive nuclei was recorded.

Group 3 MB cells (HD-MB03, D425, D458, D283) were infected for 72 h with purified lentiviral particles encoding short hairpin RNA targeting SALL4A (shSALL4A) or a control non-targeting sequence (shCTR). 2×10^4 cells/well were seeded onto a 96-well tissue culture plate (Falcon) in 100µl complete medium (6 wells for each experimental point) and their proliferation was measured as cell confluence (%) calculated using IncuCyte Zoom software by phase-contrast images. Cells were scanned every two hours up to 96 h after infection.

5.8 | *In vitro* scratch assay

Daoy cells were infected for 72 h with purified lentiviral particles encoding short hairpin RNA targeting SALL4A (shSALL4A) or a control non-targeting sequence (shCTR). 2×10^4 cells/well were seeded onto a 96-well ImageLock tissue culture plate (Essen BioScience) (12 wells for each experimental point) and incubated at 37 °C with 5% CO_2 for 24 h until they reach 100% confluence. Wounds were made by the 96-well WoundMaker (Essen BioScience). The wounded cells were washed twice with culture medium to remove the debris. Image of the wounds were automatically acquired within the incubator by IncuCyte zoom software (Essen BioScience). The wound closure updates were taken at 2 h intervals; data were analysed with respect to wound confluence and calculated by using the IncuCyte software package (Essen BioScience).

5.9 | Animal studies

For allograft experiment, spontaneous MB from Math1-cre/$Ptc^{C/C}$ mice were isolated, minced and pipetted to obtain a single-cell suspension. Primary cells were infected for 72 h with purified lentiviral particles encoding short hairpin RNA targeting SALL4A (shSALL4A) or a control non-targeting sequence (shCTR). Equal amounts of cells (2.5×10^6) were injected subcutaneously (s.c.) on both posterior flanks of nu/nu mice (Charles River Laboratories, Lecco, Italy) randomly divided in two groups (n = 4). Cells were resuspended in an equal volume of culture medium and Matrigel (BD Biosciences, Heidelberg, Germany) before the s.c. injection. Tumors were grown until a median size of ~150 mm^3. Tumor growth was monitored and measured with caliper. Changes in tumor volume were evaluated with the formula (length × width) × 0.5 × (length + width).

For orthotopic allograft model, nu/nu mice were anesthetized by intraperitoneal (i.p.) injection of ketamine (10mg/kg) and xylazine (100mg/kg). The posterior cranial region was placed in a stereotaxic head frame and primary cells of spontaneous MB from Math1-cre/$Ptc^{C/C}$ mice infected for 72 h with purified lentiviral particles encoding shSALL4A or shCTR were stereotaxically implanted into the cerebellum (2×10^5/3µl) according to the atlas of Franklin and Paxinos coordinates (n=6 mice for each experimental group). After injection, at an infusion rate of 1µl/min, the cannula was kept in place for 5 minutes and then the skin was closed using metallic clips. 45 days after tumor implantation, animals were sacrificed and brains were fixed in 4% formaldehyde and paraffin embedded. Tumor volume calculation was performed on serial 40 coronal sections of 2µm after H&E staining every 40µm of brain slice. A microscope (Axio Imager M1 microscope; Leica Microsystems GmbH, Wetzlar, Germany) equipped with a motorized stage and Image Pro Plus 6.2 software was used to evaluate tumor area of each slide. All animal protocols were approved by local ethic authorities (Ministry of Health) and conducted in accordance with Italian Governing Law (D.lgs 26/2014).

5.10 | Datasets and data analyses

Using the R2: Genomics Analysis and Visualization Platform (http://r2.amc.nl), we analysed the expression levels of SALL4 in MB using the previously generated dataset "Tumor Medulloblastoma – Cavalli – 763 – rma_sketch – hugene11t", SHH subgroup. The survival distribution was estimated according to the Kaplan-Meier method and the significance was determined using log-rank statistics. The log-rank test was used for comparison of patient survival between high and low expression groups for each selected gene. Statistical significance was defined as $p < 0.05$.

5.11 | Statistical analysis

Statistical analysis was performed using the StatView 4.1 software (Abacus Concepts, Berkeley, CA, USA). For all experiments, p values were determined using two-tailed Student's t-test and statistical significance was set at $p < 0.05$. Results are expressed as mean ± S. D. from an appropriate number of experiments (at least three biological replicas). For IncuCyte experiments, statistical significance was determined with the

IncuCyte software package (Essen BioScience). For animal studies, statistical significance was determined with GraphPad Prism software (version 6.0, La Jolla, CA, USA). Data were analysed with the Two-way ANOVA test and given as mean ± S. D.

6 | ABBREVIATIONS

Abbreviation	*Meaning*
AML	Acute Myeloid Leukemia
ATCC	American Type Culture Condition
ATO	Arsenic trioxide
BCC	Basal Cell Carcinoma
BCNS	Basal Cell Nevus Syndrome
BMP	Bone Morphogenetic Protein
BrdU	Bromodeoxyuridine
BTB/Poz	Bric-a-brack, Tram-track, Broad complex
c22	Compound 22
C2H2-ZF	Cys2His2 Zinc Finger domain
CBP	CREB-binding protein
CHX	Cycloheximide
Ci	Cubitus Interruptus
CkIα	Casein kinase Iα
CML	Chronic Myeloid Leukemia
CNS	Central Nervous System
CNS	Central Nervous System
Co-IP	Co-immunoprecipitation
Cul3	Cullin 3
DHH	Desert Hedgehog
DNMTs	DNA methyltransferases
EGL	External Granule Layer
ERAP1	Endoplasmic reticulum aminopeptidase 1
ESCs	Embryonic Stem Cells
FC	Fold Change
GANT61	Gli-ANTagonist 61
GANT61-D	GANT61 Diamine derivative
GlaB	Glabrescione B
GLI	Glioma-associated oncogene
GNPs	Granule Neuron Progenitors
GPCR	G Protein-Coupled Receptor
GSK3β	Glycogen synthase kinase 3β
H&E	Hematoxylin and eosin
HAT	Histone acetyltransferase
HDAC	Histone deacetylase
HECT	Homologous E6-AP Carboxy Terminus
HEK293T	Human Embryonic Kidney 293 contains SV40 T-antigen cells
HGNC	HUGO Gene Nomenclature Committee
Hh	Hedgehog

HHIP	Hedgehog interacting protein
HPCs	Hematopoietic Progenitor Cells
HSCs	Hematopoietic Stem Cells
i. p.	Intraperitoneal
IB	Immunoblotting
ICM	Inner Cell Mass
IGF	Insulin-like Growth Gactor
IGL	Internal Granule cell Layer
IHH	Indian Hedgehog
IL-6	Interleukin-6
IP	Immunoprecipitation
KCASH	KCTD containing, Cullin3 Adaptors, Suppressors of Hh
KCTD	Potassium – K – Channel Tetramerization Domain
LCA	Large cell/anaplastic
Leu-SH	Leucinethiol
LOH	Loss of heterozygosity
LSCs	Leukemic Stem Cells
LSD1	Histone lysine-specific demethylase 1
MB	Medulloblastoma
MBEN	Medulloblastoma with extensive nodularity
MDS	Myelodysplastic syndromes
MEF	Mouse embryonic fibroblast
ML	Molecular Layer
NLS	Nuclear Localization Signal
NuRD	Nucleosome Remodeling and Histone Deacetylase
PCAF	p300/CREB-binding protein-associated factor
PDGF	Platelet-derived Growth Factor
PFS	Progression-Free Survival
PKA	Protein kinase A
PL	Purkinje cell Layer
PRC	Polycomb-Repressive Complexes
PTCH1	Patched1
qPCR	Quantitative real-time Polymerase Chain Reaction
RING	Really Interesting New Gene
RMS	Rhabdomyosarcoma
s. c.	Subcutaneously
SAG	Smoothened agonist
SAID	SMO Auto Inhibitor Domain
SAR	Structure-Activity Relationships
SHH	Sonic Hedgehog
SHH-MB	Sonic Hedgehog Medulloblastoma
SMO	Smoothened
SNVs	Single-nucleotide variants

SuFu	Suppressor of Fused
Ub	Ubiquitin
UBCs	Ubiquitin Carrier Proteins
USP47	Ubiquitin Specific Proteases 47
VEGF	Vascular Endothelial Growth Factor
WHO	World Health Organization
WM	White Matter
WNT-MB	Wingless Medulloblastoma
βTrCP	β-transducing repeat-containing protein

7 | LIST OF TABLES AND FIGURES

INTRODUCTION

RESULTS

DISCUSSION AND CONCLUSIONS

8 | BIBLIOGRAPHY

Aberger, F., and Ruiz I Altaba, A. (2014). Context-dependent signal integration by the GLI code: the oncogenic load, pathways, modifiers and implications for cancer therapy. Semin Cell Dev Biol *33*, 93-104.

Al-Baradie, R., Yamada, K., St Hilaire, C., Chan, W. M., Andrews, C., McIntosh, N., Nakano, M., Martonyi, E. J., Raymond, W. R., Okumura, S., *et al.* (2002). Duane radial ray syndrome (Okihiro syndrome) maps to 20q13 and results from mutations in SALL4, a new member of the SAL family. Am J Hum Genet *71*, 1195-1199.

Amakye, D., Jagani, Z., and Dorsch, M. (2013). Unraveling the therapeutic potential of the Hedgehog pathway in cancer. Nat Med *19*, 1410-1422.

Argenti, B., Gallo, R., Di Marcotullio, L., Ferretti, E., Napolitano, M., Canterini, S., De Smaele, E., Greco, A., Fiorenza, M. T., Maroder, M., *et al.* (2005). Hedgehog antagonist REN(KCTD11) regulates proliferation and apoptosis of developing granule cell progenitors. J Neurosci *25*, 8338-8346.

Atwood, S. X., Sarin, K. Y., Whitson, R. J., Li, J. R., Kim, G., Rezaee, M., Ally, M. S., Kim, J., Yao, C., Chang, A. L., *et al.* (2015). Smoothened variants explain the majority of drug resistance in basal cell carcinoma. Cancer Cell *27*, 342-353.

Bao, C., Kramata, P., Lee, H. J., and Suh, N. (2018). Regulation of Hedgehog Signaling in Cancer by Natural and Dietary Compounds. Mol Nutr Food Res *62*.

Bao, C., Namgung, H., Lee, J., Park, H. C., Ko, J., Moon, H., Ko, H. W., and Lee, H. J. (2014). Daidzein suppresses tumor necrosis factor-α induced migration and invasion by inhibiting hedgehog/Gli1 signaling in human breast cancer cells. J Agric Food Chem *62*, 3759-3767.

Bard, J. D., Gelebart, P., Amin, H. M., Young, L. C., Ma, Y., and Lai, R. (2009). Signal transducer and activator of transcription 3 is a transcriptional factor regulating the gene expression of SALL4. FASEB J *23*, 1405-1414.

Bardwell, V. J., and Treisman, R. (1994). The POZ domain: a conserved protein-protein interaction motif. Genes Dev *8*, 1664-1677.

Basset-Seguin, N., Sharpe, H. J., and de Sauvage, F. J. (2015). Efficacy of Hedgehog pathway inhibitors in Basal cell carcinoma. Mol Cancer Ther *14*, 633-641.

Basson, M. A., and Wingate, R. J. (2013). Congenital hypoplasia of the cerebellum: developmental causes and behavioral consequences. Front Neuroanat *7*, 29.

Bautista, F., Fioravantti, V., de Rojas, T., Carceller, F., Madero, L., Lassaletta, A., and Moreno, L. (2017). Medulloblastoma in children and adolescents: a systematic review of contemporary phase I and II clinical trials and biology update. Cancer Med *6*, 2606-2624.

Becher, O. J., Hambardzumyan, D., Fomchenko, E. I., Momota, H., Mainwaring, L., Bleau, A. M., Katz, A. M., Edgar, M., Kenney, A. M., Cordon-Cardo, C., *et al.* (2008). Gli activity correlates with tumor grade in platelet-derived growth factor-induced gliomas. Cancer Res *68*, 2241-2249.

Bennett, E. J., Shaler, T. A., Woodman, B., Ryu, K. Y., Zaitseva, T. S., Becker, C. H., Bates, G. P., Schulman, H., and Kopito, R. R. (2007). Global changes to the ubiquitin system in Huntington's disease. Nature *448*, 704-708.

Berardozzi, S., Bernardi, F., Infante, P., Ingallina, C., Toscano, S., De Paolis, E., Alfonsi, R., Caimano, M., Botta, B., Mori, M., *et al.* (2018). Synergistic inhibition of the Hedgehog pathway by newly designed Smo and Gli antagonists bearing the isoflavone scaffold. Eur J Med Chem *156*, 554-562.

Berman, D. M., Karhadkar, S. S., Maitra, A., Montes De Oca, R., Gerstenblith, M. R., Briggs, K., Parker, A. R., Shimada, Y., Eshleman, J. R., Watkins, D. N., and Beachy, P. A. (2003). Widespread requirement for Hedgehog ligand stimulation in growth of digestive tract tumours. Nature *425*, 846-851.

Bernassola, F., Karin, M., Ciechanover, A., and Melino, G. (2008). The HECT family of E3 ubiquitin ligases: multiple players in cancer development. Cancer Cell *14*, 10-21.

Bhatia, N., Thiyagarajan, S., Elcheva, I., Saleem, M., Dlugosz, A., Mukhtar, H., and Spiegelman, V. S. (2006). Gli2 is targeted for ubiquitination and degradation by beta-TrCP ubiquitin ligase. J Biol Chem *281*, 19320-19326.

Bode, D., Yu, L., Tate, P., Pardo, M., and Choudhary, J. (2016). Characterization of Two Distinct Nucleosome Remodeling and Deacetylase (NuRD) Complex Assemblies in Embryonic Stem Cells. Mol Cell Proteomics *15*, 878-891.

Briscoe, J., and Thérond, P. P. (2013). The mechanisms of Hedgehog signalling and its roles in development and disease. Nat Rev Mol Cell Biol *14*, 416-429.

Brodeur, G. M., Nichols, K. E., Plon, S. E., Schiffman, J. D., and Malkin, D. (2017). Pediatric Cancer Predisposition and Surveillance: An Overview, and a Tribute to Alfred G. Knudson Jr. Clin Cancer Res *23*, e1-e5.

Brugières, L., Pierron, G., Chompret, A., Paillerets, B. B., Di Rocco, F., Varlet, P., Pierre-Kahn, A., Caron, O., Grill, J., and Delattre, O. (2010). Incomplete penetrance of

the predisposition to medulloblastoma associated with germ-line SUFU mutations. J Med Genet *47*, 142-144.

Bufalieri, F., Infante, P., Bernardi, F., Caimano, M., Romania, P., Moretti, M., Lospinoso Severini, L., Talbot, J., Melaiu, O., Tanori, M., *et al.* (2019). ERAP1 promotes Hedgehog-dependent tumorigenesis by controlling USP47-mediated degradation of βTrCP. Nat Commun *10*, 3304.

Burness, C. B. (2015). Sonidegib: First Global Approval. Drugs *75*, 1559-1566.

Böhm, J., Sustmann, C., Wilhelm, C., and Kohlhase, J. (2006). SALL4 is directly activated by TCF/LEF in the canonical Wnt signaling pathway. Biochem Biophys Res Commun *348*, 898-907.

Canettieri, G., Di Marcotullio, L., Greco, A., Coni, S., Antonucci, L., Infante, P., Pietrosanti, L., De Smaele, E., Ferretti, E., Miele, E., *et al.* (2010). Histone deacetylase and Cullin3-REN(KCTD11) ubiquitin ligase interplay regulates Hedgehog signalling through Gli acetylation. Nat Cell Biol *12*, 132-142.

Cao, D., Guo, S., Allan, R. W., Molberg, K. H., and Peng, Y. (2009). SALL4 is a novel sensitive and specific marker of ovarian primitive germ cell tumors and is particularly useful in distinguishing yolk sac tumor from clear cell carcinoma. Am J Surg Pathol *33*, 894-904.

Caro, I., and Low, J. A. (2010). The role of the hedgehog signaling pathway in the development of basal cell carcinoma and opportunities for treatment. Clin Cancer Res *16*, 3335-3339.

Cavalli, F. M. G., Remke, M., Rampasek, L., Peacock, J., Shih, D. J. H., Luu, B., Garzia, L., Torchia, J., Nor, C., Morrissy, A. S., *et al.* (2017). Intertumoral Heterogeneity within Medulloblastoma Subgroups. Cancer Cell *31*, 737-754.e736.

Chen, J. K., Taipale, J., Cooper, M. K., and Beachy, P. A. (2002). Inhibition of Hedgehog signaling by direct binding of cyclopamine to Smoothened. Genes Dev *16*, 2743-2748.

Chen, M. H., Wilson, C. W., Li, Y. J., Law, K. K., Lu, C. S., Gacayan, R., Zhang, X., Hui, C. C., and Chuang, P. T. (2009). Cilium-independent regulation of Gli protein function by Sufu in Hedgehog signaling is evolutionarily conserved. Genes Dev *23*, 1910-1928.

Choudhry, Z., Rikani, A. A., Choudhry, A. M., Tariq, S., Zakaria, F., Asghar, M. W., Sarfraz, M. K., Haider, K., Shafiq, A. A., and Mobassarah, N. J. (2014). Sonic hedgehog signalling pathway: a complex network. Ann Neurosci *21*, 28-31.

Chuang, P. T., and McMahon, A. P. (1999). Vertebrate Hedgehog signalling modulated by induction of a Hedgehog-binding protein. Nature *397*, 617-621.

Ciechanover, A., Orian, A., and Schwartz, A. L. (2000). Ubiquitin-mediated proteolysis: biological regulation via destruction. Bioessays *22*, 442-451.

Coni, S., Antonucci, L., D'Amico, D., Di Magno, L., Infante, P., De Smaele, E., Giannini, G., Di Marcotullio, L., Screpanti, I., Gulino, A., and Canettieri, G. (2013a). Gli2 acetylation at lysine 757 regulates hedgehog-dependent transcriptional output by preventing its promoter occupancy. PLoS One *8*, e65718.

Coni, S., Infante, P., and Gulino, A. (2013b). Control of stem cells and cancer stem cells by Hedgehog signaling: pharmacologic clues from pathway dissection. Biochem Pharmacol *85*, 623-628.

Cooper, A. F., Yu, K. P., Brueckner, M., Brailey, L. L., Johnson, L., McGrath, J. M., and Bale, A. E. (2005). Cardiac and CNS defects in a mouse with targeted disruption of suppressor of fused. Development *132*, 4407-4417.

Correale, S., Pirone, L., Di Marcotullio, L., De Smaele, E., Greco, A., Mazzà, D., Moretti, M., Alterio, V., Vitagliano, L., Di Gaetano, S., *et al.* (2011). Molecular organization of the cullin E3 ligase adaptor KCTD11. Biochimie *93*, 715-724.

Cortes, J. E., Gutzmer, R., Kieran, M. W., and Solomon, J. A. (2019). Hedgehog signaling inhibitors in solid and hematological cancers. Cancer Treat Rev *76*, 41-50.

Cripps, D., Thomas, S. N., Jeng, Y., Yang, F., Davies, P., and Yang, A. J. (2006). Alzheimer disease-specific conformation of hyperphosphorylated paired helical filament-Tau is polyubiquitinated through Lys-48, Lys-11, and Lys-6 ubiquitin conjugation. J Biol Chem *281*, 10825-10838.

Dahlén, A., Fletcher, C. D., Mertens, F., Fletcher, J. A., Perez-Atayde, A. R., Hicks, M. J., Debiec-Rychter, M., Sciot, R., Wejde, J., Wedin, R., *et al.* (2004). Activation of the GLI oncogene through fusion with the beta-actin gene (ACTB) in a group of distinctive pericytic neoplasms: pericytoma with t(7;12). Am J Pathol *164*, 1645-1653.

Dahmane, N., Lee, J., Robins, P., Heller, P., and Ruiz i Altaba, A. (1997). Activation of the transcription factor Gli1 and the Sonic hedgehog signalling pathway in skin tumours. Nature *389*, 876-881.

de Celis, J. F., and Barrio, R. (2009). Regulation and function of Spalt proteins during animal development. Int J Dev Biol *53*, 1385-1398.

De Smaele, E., Di Marcotullio, L., Moretti, M., Pelloni, M., Occhione, M. A., Infante, P., Cucchi, D., Greco, A., Pietrosanti, L., Todorovic, J., *et al.* (2011). Identification

and characterization of KCASH2 and KCASH3, 2 novel Cullin3 adaptors suppressing histone deacetylase and Hedgehog activity in medulloblastoma. Neoplasia *13*, 374-385.

del Charco, J. O., Bolek, T. W., McCollough, W. M., Maria, B. L., Kedar, A., Braylan, R. C., Mickle, J. P., Buatti, J. M., Mendenhall, N. P., and Marcus, R. B. (1998). Medulloblastoma: time-dose relationship based on a 30-year review. Int J Radiat Oncol Biol Phys *42*, 147-154.

Dementieva, I. S., Tereshko, V., McCrossan, Z. A., Solomaha, E., Araki, D., Xu, C., Grigorieff, N., and Goldstein, S. A. (2009). Pentameric assembly of potassium channel tetramerization domain-containing protein 5. J Mol Biol *387*, 175-191.

Di Magno, L., Coni, S., Di Marcotullio, L., and Canettieri, G. (2015). Digging a hole under Hedgehog: downstream inhibition as an emerging anticancer strategy. Biochim Biophys Acta *1856*, 62-72.

Di Marcotullio, L., Canettieri, G., Infante, P., Greco, A., and Gulino, A. (2011a). Protected from the inside: endogenous histone deacetylase inhibitors and the road to cancer. Biochim Biophys Acta *1815*, 241-252.

Di Marcotullio, L., Ferretti, E., De Smaele, E., Argenti, B., Mincione, C., Zazzeroni, F., Gallo, R., Masuelli, L., Napolitano, M., Maroder, M., *et al.* (2004). REN(KCTD11) is a suppressor of Hedgehog signaling and is deleted in human medulloblastoma. Proc Natl Acad Sci U S A *101*, 10833-10838.

Di Marcotullio, L., Ferretti, E., Greco, A., De Smaele, E., Screpanti, I., and Gulino, A. (2007). Multiple ubiquitin-dependent processing pathways regulate hedgehog/gli signaling: implications for cell development and tumorigenesis. Cell Cycle *6*, 390-393.

Di Marcotullio, L., Greco, A., Mazzà, D., Canettieri, G., Pietrosanti, L., Infante, P., Coni, S., Moretti, M., De Smaele, E., Ferretti, E., *et al.* (2011b). Numb activates the E3 ligase Itch to control Gli1 function through a novel degradation signal. Oncogene *30*, 65-76.

Dierks, C., Grbic, J., Zirlik, K., Beigi, R., Englund, N. P., Guo, G. R., Veelken, H., Engelhardt, M., Mertelsmann, R., Kelleher, J. F., *et al.* (2007). Essential role of stromally induced hedgehog signaling in B-cell malignancies. Nat Med *13*, 944-951.

Ding, Q., Fukami, S., Meng, X., Nishizaki, Y., Zhang, X., Sasaki, H., Dlugosz, A., Nakafuku, M., and Hui, C. (1999). Mouse suppressor of fused is a negative regulator of sonic hedgehog signaling and alters the subcellular distribution of Gli1. Curr Biol *9*, 1119-1122.

Dlugosz, A., Agrawal, S., and Kirkpatrick, P. (2012). Vismodegib. Nat Rev Drug Discov *11*, 437-438.

Eildermann, K., Aeckerle, N., Debowski, K., Godmann, M., Christiansen, H., Heistermann, M., Schweyer, S., Bergmann, M., Kliesch, S., Gromoll, J., *et al.* (2012). Developmental expression of the pluripotency factor sal-like protein 4 in the monkey, human and mouse testis: restriction to premeiotic germ cells. Cells Tissues Organs *196*, 206-220.

Elling, U., Klasen, C., Eisenberger, T., Anlag, K., and Treier, M. (2006). Murine inner cell mass-derived lineages depend on Sall4 function. Proc Natl Acad Sci U S A *103*, 16319-16324.

Ellison, D. (2002). Classifying the medulloblastoma: insights from morphology and molecular genetics. Neuropathol Appl Neurobiol *28*, 257-282.

Ellison, D. W., Dalton, J., Kocak, M., Nicholson, S. L., Fraga, C., Neale, G., Kenney, A. M., Brat, D. J., Perry, A., Yong, W. H., *et al.* (2011). Medulloblastoma: clinicopathological correlates of SHH, WNT, and non-SHH/WNT molecular subgroups. Acta Neuropathol *121*, 381-396.

Fan, L., Pepicelli, C. V., Dibble, C. C., Catbagan, W., Zarycki, J. L., Laciak, R., Gipp, J., Shaw, A., Lamm, M. L., Munoz, A., *et al.* (2004). Hedgehog signaling promotes prostate xenograft tumor growth. Endocrinology *145*, 3961-3970.

Ferretti, E., De Smaele, E., Di Marcotullio, L., Screpanti, I., and Gulino, A. (2005). Hedgehog checkpoints in medulloblastoma: the chromosome 17p deletion paradigm. Trends Mol Med *11*, 537-545.

Fruci, D., Ferracuti, S., Limongi, M. Z., Cunsolo, V., Giorda, E., Fraioli, R., Sibilio, L., Carroll, O., Hattori, A., van Endert, P. M., and Giacomini, P. (2006). Expression of endoplasmic reticulum aminopeptidases in EBV-B cell lines from healthy donors and in leukemia/lymphoma, carcinoma, and melanoma cell lines. J Immunol *176*, 4869-4879.

Fruci, D., Giacomini, P., Nicotra, M. R., Forloni, M., Fraioli, R., Saveanu, L., van Endert, P., and Natali, P. G. (2008). Altered expression of endoplasmic reticulum aminopeptidases ERAP1 and ERAP2 in transformed non-lymphoid human tissues. J Cell Physiol *216*, 742-749.

Fruci, D., Romania, P., D'Alicandro, V., and Locatelli, F. (2014). Endoplasmic reticulum aminopeptidase 1 function and its pathogenic role in regulating innate and adaptive immunity in cancer and major histocompatibility complex class I-associated autoimmune diseases. Tissue Antigens *84*, 177-186.

Gallo, R., Zazzeroni, F., Alesse, E., Mincione, C., Borello, U., Buanne, P., D'Eugenio, R., Mackay, A. R., Argenti, B., Gradini, R., *et al.* (2002). REN: a novel, developmentally regulated gene that promotes neural cell differentiation. J Cell Biol *158*, 731-740.

Ghirga, F., Mori, M., and Infante, P. (2018). Current trends in Hedgehog signaling pathway inhibition by small molecules. Bioorg Med Chem Lett *28*, 3131-3140.

Goldowitz, D., and Hamre, K. (1998). The cells and molecules that make a cerebellum. Trends Neurosci *21*, 375-382.

Gonnissen, A., Isebaert, S., and Haustermans, K. (2015). Targeting the Hedgehog signaling pathway in cancer: beyond Smoothened. Oncotarget *6*, 13899-13913.

Goodrich, L. V., Milenković, L., Higgins, K. M., and Scott, M. P. (1997). Altered neural cell fates and medulloblastoma in mouse patched mutants. Science *277*, 1109-1113.

Gröbner, S. N., Worst, B. C., Weischenfeldt, J., Buchhalter, I., Kleinheinz, K., Rudneva, V. A., Johann, P. D., Balasubramanian, G. P., Segura-Wang, M., Brabetz, S., *et al.* (2018). The landscape of genomic alterations across childhood cancers. Nature *555*, 321-327.

Gulino, A., Di Marcotullio, L., Canettieri, G., De Smaele, E., and Screpanti, I. (2012). Hedgehog/Gli control by ubiquitination/acetylation interplay. Vitam Horm *88*, 211-227.

Hadden, M. K. (2013). Hedgehog pathway inhibitors: a patent review (2009--present). Expert Opin Ther Pat *23*, 345-361.

Haglund, K., Sigismund, S., Polo, S., Szymkiewicz, I., Di Fiore, P. P., and Dikic, I. (2003). Multiple monoubiquitination of RTKs is sufficient for their endocytosis and degradation. Nat Cell Biol *5*, 461-466.

Hanahan, D., and Weinberg, R. A. (2011). Hallmarks of cancer: the next generation. Cell *144*, 646-674.

Harper, J. W., and Tan, M. K. (2012). Understanding cullin-RING E3 biology through proteomics-based substrate identification. Mol Cell Proteomics *11*, 1541-1550.

Haycraft, C. J., Banizs, B., Aydin-Son, Y., Zhang, Q., Michaud, E. J., and Yoder, B. K. (2005). Gli2 and Gli3 localize to cilia and require the intraflagellar transport protein polaris for processing and function. PLoS Genet *1*, e53.

He, J., Zhang, W., Zhou, Q., Zhao, T., Song, Y., Chai, L., and Li, Y. (2013). Low-expression of microRNA-107 inhibits cell apoptosis in glioma by upregulation of SALL4. Int J Biochem Cell Biol *45*, 1962-1973.

Hershko, A., and Ciechanover, A. (1998). The ubiquitin system. Annu Rev Biochem *67*, 425-479.

Hoshino, M., Nakamura, S., Mori, K., Kawauchi, T., Terao, M., Nishimura, Y. V., Fukuda, A., Fuse, T., Matsuo, N., Sone, M., *et al.* (2005). Ptf1a, a bHLH transcriptional gene, defines GABAergic neuronal fates in cerebellum. Neuron *47*, 201-213.

Hu, S., Wang, D., Wu, J., Jin, J., Wei, W., and Sun, W. (2013). Involvement of β-arrestins in cancer progression. Mol Biol Rep *40*, 1065-1071.

Huang, K. L., Mashl, R. J., Wu, Y., Ritter, D. I., Wang, J., Oh, C., Paczkowska, M., Reynolds, S., Wyczalkowski, M. A., Oak, N., *et al.* (2018). Pathogenic Germline Variants in 10,389 Adult Cancers. Cell *173*, 355-370.e314.

Humke, E. W., Dorn, K. V., Milenkovic, L., Scott, M. P., and Rohatgi, R. (2010). The output of Hedgehog signaling is controlled by the dynamic association between Suppressor of Fused and the Gli proteins. Genes Dev *24*, 670-682.

Huntzicker, E. G., Estay, I. S., Zhen, H., Lokteva, L. A., Jackson, P. K., and Oro, A. E. (2006). Dual degradation signals control Gli protein stability and tumor formation. Genes Dev *20*, 276-281.

Infante, P., Alfonsi, R., Botta, B., Mori, M., and Di Marcotullio, L. (2015a). Targeting GLI factors to inhibit the Hedgehog pathway. Trends Pharmacol Sci *36*, 547-558.

Infante, P., Alfonsi, R., Ingallina, C., Quaglio, D., Ghirga, F., D'Acquarica, I., Bernardi, F., Di Magno, L., Canettieri, G., Screpanti, I., *et al.* (2016). Inhibition of Hedgehog-dependent tumors and cancer stem cells by a newly identified naturally occurring chemotype. Cell Death Dis *7*, e2376.

Infante, P., Faedda, R., Bernardi, F., Bufalieri, F., Lospinoso Severini, L., Alfonsi, R., Mazzà, D., Siler, M., Coni, S., Po, A., *et al.* (2018). Itch/β-arrestin2-dependent non-proteolytic ubiquitylation of SuFu controls Hedgehog signalling and medulloblastoma tumorigenesis. Nat Commun *9*, 976.

Infante, P., Lospinoso Severini, L., Bernardi, F., Bufalieri, F., and Di Marcotullio, L. (2019). Targeting Hedgehog Signalling through the Ubiquitylation Process: The Multiple Roles of the HECT-E3 Ligase Itch. Cells *8*.

Infante, P., Mori, M., Alfonsi, R., Ghirga, F., Aiello, F., Toscano, S., Ingallina, C., Siler, M., Cucchi, D., Po, A., *et al.* (2015b). Gli1/DNA interaction is a druggable target for Hedgehog-dependent tumors. EMBO J *34*, 200-217.

Ingham, P. W., and McMahon, A. P. (2001). Hedgehog signaling in animal development: paradigms and principles. Genes Dev *15*, 3059-3087.

Ingham, P. W., Nakano, Y., and Seger, C. (2011). Mechanisms and functions of Hedgehog signalling across the metazoa. Nat Rev Genet *12*, 393-406.

Iovine, V., Mori, M., Calcaterra, A., Berardozzi, S., and Botta, B. (2016). One Hundred Faces of Cyclopamine. Curr Pharm Des *22*, 1658-1681.

Ito, M. (2008). Control of mental activities by internal models in the cerebellum. Nat Rev Neurosci *9*, 304-313.

Iulianella, A., Wingate, R. J., Moens, C. B., and Capaldo, E. (2019). The generation of granule cells during the development and evolution of the cerebellum. Dev Dyn *248*, 506-513.

Ivanov, D. P., Coyle, B., Walker, D. A., and Grabowska, A. M. (2016). In vitro models of medulloblastoma: Choosing the right tool for the job. J Biotechnol *236*, 10-25.

Jia, J., Tong, C., Wang, B., Luo, L., and Jiang, J. (2004). Hedgehog signalling activity of Smoothened requires phosphorylation by protein kinase A and casein kinase I. Nature *432*, 1045-1050.

Johnson, R. L., Rothman, A. L., Xie, J., Goodrich, L. V., Bare, J. W., Bonifas, J. M., Quinn, A. G., Myers, R. M., Cox, D. R., Epstein, E. H., and Scott, M. P. (1996). Human homolog of patched, a candidate gene for the basal cell nevus syndrome. Science *272*, 1668-1671.

Juraschka, K., and Taylor, M. D. (2019). Medulloblastoma in the age of molecular subgroups: a review. J Neurosurg Pediatr *24*, 353-363.

Kijima, C., Miyashita, T., Suzuki, M., Oka, H., and Fujii, K. (2012). Two cases of nevoid basal cell carcinoma syndrome associated with meningioma caused by a PTCH1 or SUFU germline mutation. Fam Cancer *11*, 565-570.

Ko, K. P. (2014). Isoflavones: chemistry, analysis, functions and effects on health and cancer. Asian Pac J Cancer Prev *15*, 7001-7010.

Kobayashi, D., Kuribayashi, K., Tanaka, M., and Watanabe, N. (2011a). Overexpression of SALL4 in lung cancer and its importance in cell proliferation. Oncol Rep *26*, 965-970.

Kobayashi, D., Kuribayshi, K., Tanaka, M., and Watanabe, N. (2011b). SALL4 is essential for cancer cell proliferation and is overexpressed at early clinical stages in breast cancer. Int J Oncol *38*, 933-939.

Kogerman, P., Grimm, T., Kogerman, L., Krause, D., Undén, A. B., Sandstedt, B., Toftgård, R., and Zaphiropoulos, P. G. (1999). Mammalian suppressor-of-fused modulates nuclear-cytoplasmic shuttling of Gli-1. Nat Cell Biol *1*, 312-319.

Kohlhase, J., Chitayat, D., Kotzot, D., Ceylaner, S., Froster, U. G., Fuchs, S., Montgomery, T., and Rösler, B. (2005). SALL4 mutations in Okihiro syndrome (Duane-

radial ray syndrome), acro-renal-ocular syndrome, and related disorders. Hum Mutat *26*, 176-183.

Kohlhase, J., Heinrich, M., Liebers, M., Fröhlich Archangelo, L., Reardon, W., and Kispert, A. (2002a). Cloning and expression analysis of SALL4, the murine homologue of the gene mutated in Okihiro syndrome. Cytogenet Genome Res *98*, 274-277.

Kohlhase, J., Heinrich, M., Schubert, L., Liebers, M., Kispert, A., Laccone, F., Turnpenny, P., Winter, R. M., and Reardon, W. (2002b). Okihiro syndrome is caused by SALL4 mutations. Hum Mol Genet *11*, 2979-2987.

Kohlhase, J., Schubert, L., Liebers, M., Rauch, A., Becker, K., Mohammed, S. N., Newbury-Ecob, R., and Reardon, W. (2003). Mutations at the SALL4 locus on chromosome 20 result in a range of clinically overlapping phenotypes, including Okihiro syndrome, Holt-Oram syndrome, acro-renal-ocular syndrome, and patients previously reported to represent thalidomide embryopathy. J Med Genet *40*, 473-478.

Kohlhase, J., Schuh, R., Dowe, G., Kühnlein, R. P., Jäckle, H., Schroeder, B., Schulz-Schaeffer, W., Kretzschmar, H. A., Köhler, A., Müller, U., *et al.* (1996). Isolation, characterization, and organ-specific expression of two novel human zinc finger genes related to the Drosophila gene spalt. Genomics *38*, 291-298.

Kohout, T. A., and Lefkowitz, R. J. (2003). Regulation of G protein-coupled receptor kinases and arrestins during receptor desensitization. Mol Pharmacol *63*, 9-18.

Kool, M., Jones, D. T., Jäger, N., Northcott, P. A., Pugh, T. J., Hovestadt, V., Piro, R. M., Esparza, L. A., Markant, S. L., Remke, M., *et al.* (2014). Genome sequencing of SHH medulloblastoma predicts genotype-related response to smoothened inhibition. Cancer Cell *25*, 393-405.

Koshiba-Takeuchi, K., Takeuchi, J. K., Arruda, E. P., Kathiriya, I. S., Mo, R., Hui, C. C., Srivastava, D., and Bruneau, B. G. (2006). Cooperative and antagonistic interactions between Sall4 and Tbx5 pattern the mouse limb and heart. Nat Genet *38*, 175-183.

Kovacs, J. J., Whalen, E. J., Liu, R., Xiao, K., Kim, J., Chen, M., Wang, J., Chen, W., and Lefkowitz, R. J. (2008). Beta-arrestin-mediated localization of smoothened to the primary cilium. Science *320*, 1777-1781.

Lauth, M., Bergström, A., Shimokawa, T., and Toftgård, R. (2007). Inhibition of GLI-mediated transcription and tumor cell growth by small-molecule antagonists. Proc Natl Acad Sci U S A *104*, 8455-8460.

Le, H., Kleinerman, R., Lerman, O. Z., Brown, D., Galiano, R., Gurtner, G. C., Warren, S. M., Levine, J. P., and Saadeh, P. B. (2008). Hedgehog signaling is essential for normal wound healing. Wound Repair Regen *16*, 768-773.

Lee, R. T., Zhao, Z., and Ingham, P. W. (2016). Hedgehog signalling. Development *143*, 367-372.

Lee, T. L., Shyu, Y. C., Hsu, T. Y., and Shen, C. K. (2008). Itch regulates p45/NF-E2 in vivo by Lys63-linked ubiquitination. Biochem Biophys Res Commun *375*, 326-330.

Li, A., Yang, Y., Gao, C., Lu, J., Jeong, H. W., Liu, B. H., Tang, P., Yao, X., Neuberg, D., Huang, G., *et al.* (2013). A SALL4/MLL/HOXA9 pathway in murine and human myeloid leukemogenesis. J Clin Invest *123*, 4195-4207.

Lin, C. Y., Erkek, S., Tong, Y., Yin, L., Federation, A. J., Zapatka, M., Haldipur, P., Kawauchi, D., Risch, T., Warnatz, H. J., *et al.* (2016). Active medulloblastoma enhancers reveal subgroup-specific cellular origins. Nature *530*, 57-62.

Lipinski, R. J., Hutson, P. R., Hannam, P. W., Nydza, R. J., Washington, I. M., Moore, R. W., Girdaukas, G. G., Peterson, R. E., and Bushman, W. (2008). Dose- and route-dependent teratogenicity, toxicity, and pharmacokinetic profiles of the hedgehog signaling antagonist cyclopamine in the mouse. Toxicol Sci *104*, 189-197.

Lo Muzio, L. (2008). Nevoid basal cell carcinoma syndrome (Gorlin syndrome). Orphanet J Rare Dis *3*, 32.

Lorick, K. L., Jensen, J. P., Fang, S., Ong, A. M., Hatakeyama, S., and Weissman, A. M. (1999). RING fingers mediate ubiquitin-conjugating enzyme (E2)-dependent ubiquitination. Proc Natl Acad Sci U S A *96*, 11364-11369.

Lospinoso Severini, L., Quaglio, D., Basili, I., Ghirga, F., Bufalieri, F., Caimano, M., Balducci, S., Moretti, M., Romeo, I., Loricchio, E., *et al.* (2019). A Smo/Gli Multitarget Hedgehog Pathway Inhibitor Impairs Tumor Growth. Cancers (Basel) *11*.

Louis, D. N., Perry, A., Reifenberger, G., von Deimling, A., Figarella-Branger, D., Cavenee, W. K., Ohgaki, H., Wiestler, O. D., Kleihues, P., and Ellison, D. W. (2016). The 2016 World Health Organization Classification of Tumors of the Central Nervous System: a summary. Acta Neuropathol *131*, 803-820.

Lu, J., Jeong, H. W., Jeong, H., Kong, N., Yang, Y., Carroll, J., Luo, H. R., Silberstein, L. E., Yupoma, and Chai, L. (2009). Stem cell factor SALL4 represses the transcriptions of PTEN and SALL1 through an epigenetic repressor complex. PLoS One *4*, e5577.

Lu, J., Ma, Y., Kong, N., Alipio, Z., Gao, C., Krause, D. S., Silberstein, L. E., and Chai, L. (2011). Dissecting the role of SALL4, a newly identified stem cell factor, in chronic myelogenous leukemia. Leukemia *25*, 1211-1213.

Ma, X., Sheng, T., Zhang, Y., Zhang, X., He, J., Huang, S., Chen, K., Sultz, J., Adegboyega, P. A., Zhang, H., and Xie, J. (2006a). Hedgehog signaling is activated in subsets of esophageal cancers. Int J Cancer *118*, 139-148.

Ma, Y., Cui, W., Yang, J., Qu, J., Di, C., Amin, H. M., Lai, R., Ritz, J., Krause, D. S., and Chai, L. (2006b). SALL4, a novel oncogene, is constitutively expressed in human acute myeloid leukemia (AML) and induces AML in transgenic mice. Blood *108*, 2726-2735.

Machold, R., and Fishell, G. (2005). Math1 is expressed in temporally discrete pools of cerebellar rhombic-lip neural progenitors. Neuron *48*, 17-24.

Maesawa, C., Tamura, G., Iwaya, T., Ogasawara, S., Ishida, K., Sato, N., Nishizuka, S., Suzuki, Y., Ikeda, K., Aoki, K., *et al.* (1998). Mutations in the human homologue of the Drosophila patched gene in esophageal squamous cell carcinoma. Genes Chromosomes Cancer *21*, 276-279.

Masimirembwa, C. M., Bredberg, U., and Andersson, T. B. (2003). Metabolic stability for drug discovery and development: pharmacokinetic and biochemical challenges. Clin Pharmacokinet *42*, 515-528.

Mazzà, D., Infante, P., Colicchia, V., Greco, A., Alfonsi, R., Siler, M., Antonucci, L., Po, A., De Smaele, E., Ferretti, E., *et al.* (2013). PCAF ubiquitin ligase activity inhibits Hedgehog/Gli1 signaling in p53-dependent response to genotoxic stress. Cell Death Differ *20*, 1688-1697.

McGarvey, T. W., Maruta, Y., Tomaszewski, J. E., Linnenbach, A. J., and Malkowicz, S. B. (1998). PTCH gene mutations in invasive transitional cell carcinoma of the bladder. Oncogene *17*, 1167-1172.

Metzger, M. B., Hristova, V. A., and Weissman, A. M. (2012). HECT and RING finger families of E3 ubiquitin ligases at a glance. J Cell Sci *125*, 531-537.

Mukherjee, S., Frolova, N., Sadlonova, A., Novak, Z., Steg, A., Page, G. P., Welch, D. R., Lobo-Ruppert, S. M., Ruppert, J. M., Johnson, M. R., and Frost, A. R. (2006). Hedgehog signaling and response to cyclopamine differ in epithelial and stromal cells in benign breast and breast cancer. Cancer Biol Ther *5*, 674-683.

Méthot, N., and Basler, K. (2000). Suppressor of fused opposes hedgehog signal transduction by impeding nuclear accumulation of the activator form of Cubitus interruptus. Development *127*, 4001-4010.

Ng, J. M., and Curran, T. (2011). The Hedgehog's tale: developing strategies for targeting cancer. Nat Rev Cancer *11*, 493-501.

Niwa, H., Burdon, T., Chambers, I., and Smith, A. (1998). Self-renewal of pluripotent embryonic stem cells is mediated via activation of STAT3. Genes Dev *12*, 2048-2060.

Northcott, P. A., Buchhalter, I., Morrissy, A. S., Hovestadt, V., Weischenfeldt, J., Ehrenberger, T., Gröbner, S., Segura-Wang, M., Zichner, T., Rudneva, V. A., *et al.* (2017). The whole-genome landscape of medulloblastoma subtypes. Nature *547*, 311-317.

Northcott, P. A., Korshunov, A., Witt, H., Hielscher, T., Eberhart, C. G., Mack, S., Bouffet, E., Clifford, S. C., Hawkins, C. E., French, P., *et al.* (2011). Medulloblastoma comprises four distinct molecular variants. J Clin Oncol *29*, 1408-1414.

Northcott, P. A., Robinson, G. W., Kratz, C. P., Mabbott, D. J., Pomeroy, S. L., Clifford, S. C., Rutkowski, S., Ellison, D. W., Malkin, D., Taylor, M. D., *et al.* (2019). Medulloblastoma. Nat Rev Dis Primers *5*, 11.

Northcott, P. A., Shih, D. J., Remke, M., Cho, Y. J., Kool, M., Hawkins, C., Eberhart, C. G., Dubuc, A., Guettouche, T., Cardentey, Y., *et al.* (2012). Rapid, reliable, and reproducible molecular sub-grouping of clinical medulloblastoma samples. Acta Neuropathol *123*, 615-626.

Nowacka-Zawisza, M., and Krajewska, W. M. (2013). [Triple-negative breast cancer: molecular characteristics and potential therapeutic approaches]. Postepy Hig Med Dosw (Online) *67*, 1090-1097.

Nozawa, Y. I., Lin, C., and Chuang, P. T. (2013). Hedgehog signaling from the primary cilium to the nucleus: an emerging picture of ciliary localization, trafficking and transduction. Curr Opin Genet Dev *23*, 429-437.

Nüsslein-Volhard, C., and Wieschaus, E. (1980). Mutations affecting segment number and polarity in Drosophila. Nature *287*, 795-801.

Oikawa, T., Kamiya, A., Zeniya, M., Chikada, H., Hyuck, A. D., Yamazaki, Y., Wauthier, E., Tajiri, H., Miller, L. D., Wang, X. W., *et al.* (2013). Sal-like protein 4 (SALL4), a stem cell biomarker in liver cancers. Hepatology *57*, 1469-1483.

Oro, A. E. (2007). The primary cilia, a 'Rab-id' transit system for hedgehog signaling. Curr Opin Cell Biol *19*, 691-696.

Pan, Y., Bai, C. B., Joyner, A. L., and Wang, B. (2006). Sonic hedgehog signaling regulates Gli2 transcriptional activity by suppressing its processing and degradation. Mol Cell Biol *26*, 3365-3377.

Paradisi, I., and Arias, S. (2007). IVIC syndrome is caused by a c.2607delA mutation in the SALL4 locus. Am J Med Genet A *143*, 326-332.

Pastorino, L., Ghiorzo, P., Nasti, S., Battistuzzi, L., Cusano, R., Marzocchi, C., Garrè, M. L., Clementi, M., and Scarrà, G. B. (2009). Identification of a SUFU germline mutation in a family with Gorlin syndrome. Am J Med Genet A *149A*, 1539-1543.

Pearse, R. V., Collier, L. S., Scott, M. P., and Tabin, C. J. (1999). Vertebrate homologs of Drosophila suppressor of fused interact with the gli family of transcriptional regulators. Dev Biol *212*, 323-336.

Perreault, S., Ramaswamy, V., Achrol, A. S., Chao, K., Liu, T. T., Shih, D., Remke, M., Schubert, S., Bouffet, E., Fisher, P. G., *et al.* (2014). MRI surrogates for molecular subgroups of medulloblastoma. AJNR Am J Neuroradiol *35*, 1263-1269.

Philipp, M., Evron, T., and Caron, M. G. (2013). The role of arrestins in development. Prog Mol Biol Transl Sci *118*, 225-242.

Pickart, C. M. (2001). Mechanisms underlying ubiquitination. Annu Rev Biochem *70*, 503-533.

Pickart, C. M., and Eddins, M. J. (2004). Ubiquitin: structures, functions, mechanisms. Biochim Biophys Acta *1695*, 55-72.

Pintard, L., Willems, A., and Peter, M. (2004). Cullin-based ubiquitin ligases: Cul3-BTB complexes join the family. EMBO J *23*, 1681-1687.

Raffel, C., Jenkins, R. B., Frederick, L., Hebrink, D., Alderete, B., Fults, D. W., and James, C. D. (1997). Sporadic medulloblastomas contain PTCH mutations. Cancer Res *57*, 842-845.

Ramaswamy, B., Lu, Y., Teng, K. Y., Nuovo, G., Li, X., Shapiro, C. L., and Majumder, S. (2012). Hedgehog signaling is a novel therapeutic target in tamoxifen-resistant breast cancer aberrantly activated by PI3K/AKT pathway. Cancer Res *72*, 5048-5059.

Ramaswamy, V., Remke, M., Bouffet, E., Bailey, S., Clifford, S. C., Doz, F., Kool, M., Dufour, C., Vassal, G., Milde, T., *et al.* (2016). Risk stratification of childhood medulloblastoma in the molecular era: the current consensus. Acta Neuropathol *131*, 821-831.

Ramaswamy, V., and Taylor, M. D. (2017). Medulloblastoma: From Myth to Molecular. J Clin Oncol *35*, 2355-2363.

Ramsbottom, S. A., and Pownall, M. E. (2016). Regulation of Hedgehog Signalling Inside and Outside the Cell. J Dev Biol *4*, 23.

Rao, S., Zhen, S., Roumiantsev, S., McDonald, L. T., Yuan, G. C., and Orkin, S. H. (2010). Differential roles of Sall4 isoforms in embryonic stem cell pluripotency. Mol Cell Biol *30*, 5364-5380.

Reifenberger, J., Wolter, M., Weber, R. G., Megahed, M., Ruzicka, T., Lichter, P., and Reifenberger, G. (1998). Missense mutations in SMOH in sporadic basal cell carcinomas of the skin and primitive neuroectodermal tumors of the central nervous system. Cancer Res *58*, 1798-1803.

Rimkus, T. K., Carpenter, R. L., Qasem, S., Chan, M., and Lo, H. W. (2016). Targeting the Sonic Hedgehog Signaling Pathway: Review of Smoothened and GLI Inhibitors. Cancers (Basel) *8*.

Robinson, G., Parker, M., Kranenburg, T. A., Lu, C., Chen, X., Ding, L., Phoenix, T. N., Hedlund, E., Wei, L., Zhu, X.*, et al.* (2012). Novel mutations target distinct subgroups of medulloblastoma. Nature *488*, 43-48.

Rohatgi, R., Milenkovic, L., and Scott, M. P. (2007). Patched1 regulates hedgehog signaling at the primary cilium. Science *317*, 372-376.

Romer, J., and Curran, T. (2005). Targeting medulloblastoma: small-molecule inhibitors of the Sonic Hedgehog pathway as potential cancer therapeutics. Cancer Res *65*, 4975-4978.

Ruat, M., Hoch, L., Faure, H., and Rognan, D. (2014). Targeting of Smoothened for therapeutic gain. Trends Pharmacol Sci *35*, 237-246.

Rubin, J. B., and Rowitch, D. H. (2002). Medulloblastoma: a problem of developmental biology. Cancer Cell *2*, 7-8.

Rubin, L. L., and de Sauvage, F. J. (2006). Targeting the Hedgehog pathway in cancer. Nat Rev Drug Discov *5*, 1026-1033.

Ruiz i Altaba, A. (1999). Gli proteins encode context-dependent positive and negative functions: implications for development and disease. Development *126*, 3205-3216.

Ruiz i Altaba, A., Mas, C., and Stecca, B. (2007). The Gli code: an information nexus regulating cell fate, stemness and cancer. Trends Cell Biol *17*, 438-447.

Ruiz i Altaba, A., Sánchez, P., and Dahmane, N. (2002). Gli and hedgehog in cancer: tumours, embryos and stem cells. Nat Rev Cancer *2*, 361-372.

Rutka, J. T., and Hoffman, H. J. (1996). Medulloblastoma: a historical perspective and overview. J Neurooncol *29*, 1-7.

Sachs, N., and Clevers, H. (2014). Organoid cultures for the analysis of cancer phenotypes. Curr Opin Genet Dev *24*, 68-73.

Sakaki-Yumoto, M., Kobayashi, C., Sato, A., Fujimura, S., Matsumoto, Y., Takasato, M., Kodama, T., Aburatani, H., Asashima, M., Yoshida, N., and Nishinakamura, R. (2006). The murine homolog of SALL4, a causative gene in Okihiro syndrome, is essential for embryonic stem cell proliferation, and cooperates with Sall1 in anorectal, heart, brain and kidney development. Development *133*, 3005-3013.

Sari, I. N., Phi, L. T. H., Jun, N., Wijaya, Y. T., Lee, S., and Kwon, H. Y. (2018). Hedgehog Signaling in Cancer: A Prospective Therapeutic Target for Eradicating Cancer Stem Cells. Cells *7*.

Sato, N., Meijer, L., Skaltsounis, L., Greengard, P., and Brivanlou, A. H. (2004). Maintenance of pluripotency in human and mouse embryonic stem cells through activation of Wnt signaling by a pharmacological GSK-3-specific inhibitor. Nat Med *10*, 55-63.

Scheffner, M., Werness, B. A., Huibregtse, J. M., Levine, A. J., and Howley, P. M. (1990). The E6 oncoprotein encoded by human papillomavirus types 16 and 18 promotes the degradation of p53. Cell *63*, 1129-1136.

Schmahmann, J. D. (2004). Disorders of the cerebellum: ataxia, dysmetria of thought, and the cerebellar cognitive affective syndrome. J Neuropsychiatry Clin Neurosci *16*, 367-378.

Schmahmann, J. D., and Caplan, D. (2006). Cognition, emotion and the cerebellum. Brain *129*, 290-292.

Schwalbe, E. C., Lindsey, J. C., Nakjang, S., Crosier, S., Smith, A. J., Hicks, D., Rafiee, G., Hill, R. M., Iliasova, A., Stone, T., *et al.* (2017). Novel molecular subgroups for clinical classification and outcome prediction in childhood medulloblastoma: a cohort study. Lancet Oncol *18*, 958-971.

Schüller, U., Heine, V. M., Mao, J., Kho, A. T., Dillon, A. K., Han, Y. G., Huillard, E., Sun, T., Ligon, A. H., Qian, Y., *et al.* (2008). Acquisition of granule neuron precursor identity is a critical determinant of progenitor cell competence to form Shh-induced medulloblastoma. Cancer Cell *14*, 123-134.

Scialpi, F., Malatesta, M., Peschiaroli, A., Rossi, M., Melino, G., and Bernassola, F. (2008). Itch self-polyubiquitylation occurs through lysine-63 linkages. Biochem Pharmacol *76*, 1515-1521.

Sekulic, A., Migden, M. R., Oro, A. E., Dirix, L., Lewis, K. D., Hainsworth, J. D., Solomon, J. A., Yoo, S., Arron, S. T., Friedlander, P. A., *et al.* (2012). Efficacy and safety of vismodegib in advanced basal-cell carcinoma. N Engl J Med *366*, 2171-2179.

Shahbazian, M. D., and Grunstein, M. (2007). Functions of site-specific histone acetylation and deacetylation. Annu Rev Biochem *76*, 75-100.

Sharpe, H. J., Pau, G., Dijkgraaf, G. J., Basset-Seguin, N., Modrusan, Z., Januario, T., Tsui, V., Durham, A. B., Dlugosz, A. A., Haverty, P. M., *et al.* (2015). Genomic analysis of smoothened inhibitor resistance in basal cell carcinoma. Cancer Cell *27*, 327-341.

Shu, Y. Z., Johnson, B. M., and Yang, T. J. (2008). Role of biotransformation studies in minimizing metabolism-related liabilities in drug discovery. AAPS J *10*, 178-192.

Skaar, J. R., Pagan, J. K., and Pagano, M. (2013). Mechanisms and function of substrate recruitment by F-box proteins. Nat Rev Mol Cell Biol *14*, 369-381.

Skoda, A. M., Simovic, D., Karin, V., Kardum, V., Vranic, S., and Serman, L. (2018). The role of the Hedgehog signaling pathway in cancer: A comprehensive review. Bosn J Basic Med Sci *18*, 8-20.

Smelkinson, M. G., Zhou, Q., and Kalderon, D. (2007). Regulation of Ci-SCFSlimb binding, Ci proteolysis, and hedgehog pathway activity by Ci phosphorylation. Dev Cell *13*, 481-495.

Stone, D. M., Murone, M., Luoh, S., Ye, W., Armanini, M. P., Gurney, A., Phillips, H., Brush, J., Goddard, A., de Sauvage, F. J., and Rosenthal, A. (1999). Characterization of the human suppressor of fused, a negative regulator of the zinc-finger transcription factor Gli. J Cell Sci *112 (Pt 23)*, 4437-4448.

Stratikos, E., Stamogiannos, A., Zervoudi, E., and Fruci, D. (2014). A role for naturally occurring alleles of endoplasmic reticulum aminopeptidases in tumor immunity and cancer pre-disposition. Front Oncol *4*, 363.

Strick, P. L., Dum, R. P., and Fiez, J. A. (2009). Cerebellum and nonmotor function. Annu Rev Neurosci *32*, 413-434.

Svärd, J., Heby-Henricson, K., Henricson, K. H., Persson-Lek, M., Rozell, B., Lauth, M., Bergström, A., Ericson, J., Toftgård, R., and Teglund, S. (2006). Genetic elimination of Suppressor of fused reveals an essential repressor function in the mammalian Hedgehog signaling pathway. Dev Cell *10*, 187-197.

Sweetman, D., and Münsterberg, A. (2006). The vertebrate spalt genes in development and disease. Dev Biol *293*, 285-293.

Sweetman, D., Smith, T., Farrell, E. R., Chantry, A., and Munsterberg, A. (2003). The conserved glutamine-rich region of chick csal1 and csal3 mediates protein interactions with other spalt family members. Implications for Townes-Brocks syndrome. J Biol Chem *278*, 6560-6566.

Tan, M. H., Au, K. F., Leong, D. E., Foygel, K., Wong, W. H., and Yao, M. W. (2013). An Oct4-Sall4-Nanog network controls developmental progression in the pre-implantation mouse embryo. Mol Syst Biol *9*, 632.

Tang, J. Y., Mackay-Wiggan, J. M., Aszterbaum, M., Yauch, R. L., Lindgren, J., Chang, K., Coppola, C., Chanana, A. M., Marji, J., Bickers, D. R., and Epstein, E. H. (2012). Inhibiting the hedgehog pathway in patients with the basal-cell nevus syndrome. N Engl J Med *366*, 2180-2188.

Tatetsu, H., Kong, N. R., Chong, G., Amabile, G., Tenen, D. G., and Chai, L. (2016). SALL4, the missing link between stem cells, development and cancer. Gene *584*, 111-119.

Taylor, M. D., Liu, L., Raffel, C., Hui, C. C., Mainprize, T. G., Zhang, X., Agatep, R., Chiappa, S., Gao, L., Lowrance, A., *et al.* (2002). Mutations in SUFU predispose to medulloblastoma. Nat Genet *31*, 306-310.

Taylor, M. D., Northcott, P. A., Korshunov, A., Remke, M., Cho, Y. J., Clifford, S. C., Eberhart, C. G., Parsons, D. W., Rutkowski, S., Gajjar, A., *et al.* (2012). Molecular subgroups of medulloblastoma: the current consensus. Acta Neuropathol *123*, 465-472.

Tempé, D., Casas, M., Karaz, S., Blanchet-Tournier, M. F., and Concordet, J. P. (2006). Multisite protein kinase A and glycogen synthase kinase 3beta phosphorylation leads to Gli3 ubiquitination by SCFbetaTrCP. Mol Cell Biol *26*, 4316-4326.

Teperino, R., Amann, S., Bayer, M., McGee, S. L., Loipetzberger, A., Connor, T., Jaeger, C., Kammerer, B., Winter, L., Wiche, G., *et al.* (2012). Hedgehog partial agonism drives Warburg-like metabolism in muscle and brown fat. Cell *151*, 414-426.

Thayer, S. P., di Magliano, M. P., Heiser, P. W., Nielsen, C. M., Roberts, D. J., Lauwers, G. Y., Qi, Y. P., Gysin, S., Fernández-del Castillo, C., Yajnik, V., *et al.* (2003). Hedgehog is an early and late mediator of pancreatic cancer tumorigenesis. Nature *425*, 851-856.

Timmann, D., Drepper, J., Frings, M., Maschke, M., Richter, S., Gerwig, M., and Kolb, F. P. (2010). The human cerebellum contributes to motor, emotional and cognitive associative learning. A review. Cortex *46*, 845-857.

Tostar, U., Malm, C. J., Meis-Kindblom, J. M., Kindblom, L. G., Toftgård, R., and Undén, A. B. (2006). Deregulation of the hedgehog signalling pathway: a possible role for the PTCH and SUFU genes in human rhabdomyoma and rhabdomyosarcoma development. J Pathol *208*, 17-25.

Triscott, J., Lee, C., Foster, C., Manoranjan, B., Pambid, M. R., Berns, R., Fotovati, A., Venugopal, C., O'Halloran, K., Narendran, A., *et al.* (2013). Personalizing the

treatment of pediatric medulloblastoma: Polo-like kinase 1 as a molecular target in high-risk children. Cancer Res *73*, 6734-6744.

Uez, N., Lickert, H., Kohlhase, J., de Angelis, M. H., Kühn, R., Wurst, W., and Floss, T. (2008). Sall4 isoforms act during proximal-distal and anterior-posterior axis formation in the mouse embryo. Genesis *46*, 463-477.

Varjosalo, M., and Taipale, J. (2008). Hedgehog: functions and mechanisms. Genes Dev *22*, 2454-2472.

Varnat, F., Duquet, A., Malerba, M., Zbinden, M., Mas, C., Gervaz, P., and Ruiz i Altaba, A. (2009). Human colon cancer epithelial cells harbour active HEDGEHOG-GLI signalling that is essential for tumour growth, recurrence, metastasis and stem cell survival and expansion. EMBO Mol Med *1*, 338-351.

Veneroni, L., Boschetti, L., Barretta, F., Clerici, C. A., Simonetti, F., Schiavello, E., Biassoni, V., Spreafico, F., Gandola, L., Pecori, E., *et al.* (2017). Quality of life in long-term survivors treated for metastatic medulloblastoma with a hyperfractionated accelerated radiotherapy (HART) strategy. Childs Nerv Syst *33*, 1969-1976.

Vladoiu, M. C., El-Hamamy, I., Donovan, L. K., Farooq, H., Holgado, B. L., Sundaravadanam, Y., Ramaswamy, V., Hendrikse, L. D., Kumar, S., Mack, S. C., *et al.* (2019). Childhood cerebellar tumours mirror conserved fetal transcriptional programs. Nature *572*, 67-73.

Von Hoff, D. D., LoRusso, P. M., Rudin, C. M., Reddy, J. C., Yauch, R. L., Tibes, R., Weiss, G. J., Borad, M. J., Hann, C. L., Brahmer, J. R., *et al.* (2009). Inhibition of the hedgehog pathway in advanced basal-cell carcinoma. N Engl J Med *361*, 1164-1172.

Vorechovský, I., Undén, A. B., Sandstedt, B., Toftgård, R., and Ståhle-Bäckdahl, M. (1997). Trichoepitheliomas contain somatic mutations in the overexpressed PTCH gene: support for a gatekeeper mechanism in skin tumorigenesis. Cancer Res *57*, 4677-4681.

Wang, B., and Li, Y. (2006). Evidence for the direct involvement of {beta}TrCP in Gli3 protein processing. Proc Natl Acad Sci U S A *103*, 33-38.

Wang, F., Zhao, W., Kong, N., Cui, W., and Chai, L. (2014). The next new target in leukemia: The embryonic stem cell gene. Mol Cell Oncol *1*, e969169.

Wang, V. Y., Rose, M. F., and Zoghbi, H. Y. (2005). Math1 expression redefines the rhombic lip derivatives and reveals novel lineages within the brainstem and cerebellum. Neuron *48*, 31-43.

Warren, M., Wang, W., Spiden, S., Chen-Murchie, D., Tannahill, D., Steel, K. P., and Bradley, A. (2007). A Sall4 mutant mouse model useful for studying the role of Sall4 in early embryonic development and organogenesis. Genesis *45*, 51-58.

Wechsler-Reya, R. J., and Scott, M. P. (1999). Control of neuronal precursor proliferation in the cerebellum by Sonic Hedgehog. Neuron *22*, 103-114.

Wong, C. C., Gaspar-Maia, A., Ramalho-Santos, M., and Reijo Pera, R. A. (2008). High-efficiency stem cell fusion-mediated assay reveals Sall4 as an enhancer of reprogramming. PLoS One *3*, e1955.

Wu, M., Yang, F., Ren, Z., Jiang, Y., Ma, Y., Chen, Y., and Dai, W. (2014). Identification of the nuclear localization signal of SALL4B, a stem cell transcription factor. Cell Cycle *13*, 1456-1462.

Wu, Q., Chen, X., Zhang, J., Loh, Y. H., Low, T. Y., Zhang, W., Sze, S. K., Lim, B., and Ng, H. H. (2006). Sall4 interacts with Nanog and co-occupies Nanog genomic sites in embryonic stem cells. J Biol Chem *281*, 24090-24094.

Xiong, J. (2014). SALL4: engine of cell stemness. Curr Gene Ther *14*, 400-411.

Yang, F., Yao, Y., Jiang, Y., Lu, L., Ma, Y., and Dai, W. (2012a). Sumoylation is important for stability, subcellular localization, and transcriptional activity of SALL4, an essential stem cell transcription factor. J Biol Chem *287*, 38600-38608.

Yang, J., Chai, L., Fowles, T. C., Alipio, Z., Xu, D., Fink, L. M., Ward, D. C., and Ma, Y. (2008a). Genome-wide analysis reveals Sall4 to be a major regulator of pluripotency in murine-embryonic stem cells. Proc Natl Acad Sci U S A *105*, 19756-19761.

Yang, J., Chai, L., Gao, C., Fowles, T. C., Alipio, Z., Dang, H., Xu, D., Fink, L. M., Ward, D. C., and Ma, Y. (2008b). SALL4 is a key regulator of survival and apoptosis in human leukemic cells. Blood *112*, 805-813.

Yang, J., Chai, L., Liu, F., Fink, L. M., Lin, P., Silberstein, L. E., Amin, H. M., Ward, D. C., and Ma, Y. (2007). Bmi-1 is a target gene for SALL4 in hematopoietic and leukemic cells. Proc Natl Acad Sci U S A *104*, 10494-10499.

Yang, J., Corsello, T. R., and Ma, Y. (2012b). Stem cell gene SALL4 suppresses transcription through recruitment of DNA methyltransferases. J Biol Chem *287*, 1996-2005.

Yang, J., Gao, C., Chai, L., and Ma, Y. (2010). A novel SALL4/OCT4 transcriptional feedback network for pluripotency of embryonic stem cells. PLoS One *5*, e10766.

Yang, X. J., and Seto, E. (2007). HATs and HDACs: from structure, function and regulation to novel strategies for therapy and prevention. Oncogene *26*, 5310-5318.

Yang, Z. J., Ellis, T., Markant, S. L., Read, T. A., Kessler, J. D., Bourboulas, M., Schüller, U., Machold, R., Fishell, G., Rowitch, D. H., *et al.* (2008c). Medulloblastoma can

be initiated by deletion of Patched in lineage-restricted progenitors or stem cells. Cancer Cell *14*, 135-145.

Yauch, R. L., Dijkgraaf, G. J., Alicke, B., Januario, T., Ahn, C. P., Holcomb, T., Pujara, K., Stinson, J., Callahan, C. A., Tang, T., *et al.* (2009). Smoothened mutation confers resistance to a Hedgehog pathway inhibitor in medulloblastoma. Science *326*, 572-574.

Yue, S., Chen, Y., and Cheng, S. Y. (2009). Hedgehog signaling promotes the degradation of tumor suppressor Sufu through the ubiquitin-proteasome pathway. Oncogene *28*, 492-499.

Yuri, S., Fujimura, S., Nimura, K., Takeda, N., Toyooka, Y., Fujimura, Y., Aburatani, H., Ura, K., Koseki, H., Niwa, H., and Nishinakamura, R. (2009). Sall4 is essential for stabilization, but not for pluripotency, of embryonic stem cells by repressing aberrant trophectoderm gene expression. Stem Cells *27*, 796-805.

Zhang, C., Kang, Y., Ma, R., Chen, F., and Dong, X. (2018). Expression of Numb and Gli1 in malignant pleural mesothelioma and their clinical significance. J Cancer Res Ther *14*, 970-976.

Zhang, J., Tam, W. L., Tong, G. Q., Wu, Q., Chan, H. Y., Soh, B. S., Lou, Y., Yang, J., Ma, Y., Chai, L., *et al.* (2006). Sall4 modulates embryonic stem cell pluripotency and early embryonic development by the transcriptional regulation of Pou5f1. Nat Cell Biol *8*, 1114-1123.

Zhang, L., Xu, Z., Xu, X., Zhang, B., Wu, H., Wang, M., Zhang, X., Yang, T., Cai, J., Yan, Y., *et al.* (2014). SALL4, a novel marker for human gastric carcinogenesis and metastasis. Oncogene *33*, 5491-5500.

Zhang, X., Yuan, X., Zhu, W., Qian, H., and Xu, W. (2015). SALL4: an emerging cancer biomarker and target. Cancer Lett *357*, 55-62.